Advances in Meteorology

# Marine Aerosol-Cloud-Climate Interaction

Guest Editors: Nicholas Meskhidze, Charles R. McClain, Markus D. Petters, Elisabetta Vignati, Olaf Stetzer, Chris Osburn, and David J. Kieber

# Marine Aerosol-Cloud-Climate Interaction

Advances in Meteorology

# Marine Aerosol-Cloud-Climate Interaction

Guest Editors: Nicholas Meskhidze, Charles R. McClain, Markus D. Petters, Elisabetta Vignati, Olaf Stetzer, Chris Osburn, and David J. Kieber

# Editorial Board

# Contents

Hindawi Publishing Corporation
Advances in Meteorology
Volume 2010, Article ID 250896, 2 pages
doi:10.1155/2010/250896

# *Editorial*
# Marine Aerosol-Cloud-Climate Interaction

**Nicholas Meskhidze,[1] Charles R. McClain,[2] Markus D. Petters,[1] Elisabetta Vignati,[3] Olaf Stetzer,[4] Chris Osburn,[1] and David J. Kieber[5]**

[1] *Department of Marine Earth and Atmospheric Sciences, North Carolina State University, Raleigh, NC, USA*
[2] *NASA/Goddard Space Flight Center, Greenbelt, MD, USA*
[3] *Joint Research Centre Institute for Environment and Sustainability Climate Change Unit, Ispra, VA, Italy*
[4] *Institut f. Atmosphäre und Klima, Zürich, Switzerland*
[5] *Department of Chemistry, State University of New York, College of Environmental Science and Forestry, New York, USA*

Correspondence should be addressed to Nicholas Meskhidze, nmeskhidze@ncsu.edu

Received 8 December 2010; Accepted 8 December 2010



Concerns over the role of atmospheric aerosols in masking observed climate change have sparked renewed interest in the natural emissions of trace gases (functioning as aerosol precursors) and aerosols. Understanding the aerosol budget in the absence of anthropogenic influence is necessary to establish a baseline aerosol forcing and provide a framework for models to properly interpret the historical climate record. Marine aerosol emissions, their composition, and their effects on clouds and radiation budget remain poorly characterized due to the large areal extent of the oceans and resulting scarcity of observational data. It is therefore not surprising that marine aerosols and associated cloud processes play a major role and present a large uncertainty, in predictions of future climate.

This special issue was motivated by our perceived need to provide a platform for current discussions regarding marine aerosol-cloud-climate interactions. Much research had been performed in the 1950s–1970s following the discovery and initial characterization of the bubble burst process by Woodcock, Blanchard, McIntyre, Duce, and coworkers. A special issue appeared in the Journal of Geophysical Research in 1972 and research continued at a modest level over the next decades. Renewed interest in the subject appeared in the early 2000s, when a number of new studies identified large fractions of organic material in ambient marine aerosol in different locations, sparking an upsurge in laboratory, field, satellite, and modeling studies. These studies aimed to better characterize marine primary and secondary organic aerosol production mechanisms, aerosol mass and number fluxes, size-dependent sea spray enrichment factors, the split between water soluble and insoluble organic fractions, the chemical composition of organic aerosol, as well as to determine the effect of marine organics on cloud microphysical properties. This special issue presents a snapshot of current research topics in this study area. It comprises twelve peer-reviewed open access articles spanning the full spectrum of atmospheric science research on this subject.

A number of contributions address the chemical composition of marine aerosols. Rinaldi et al. present a reviews and some innovative results on the chemical composition of primary and secondary marine aerosol, showing seasonal differences in nascent submicron sea spray particle chemical composition collected at the Mace Head Atmospheric Research Station. During low biological activity, submicron marine aerosols were primarily composed of sea salt, while particles collected during high biological activity largely contained nonsea salt sulfate and organics. *Rinaldi* et al. report distinct seasonal difference even in the organic composition of submicron marine aerosol. During low biological activity soluble and insoluble organic compounds were comparable in abundance, while during high biological activity submicron organics were dominated by water soluble organic matter. Hawkins and Russell use scanning Transmission X-ray Microscopy with Near-Edge X-ray Absorption Fine Structure (STXM-NEXAFS) analysis to classify marine primary organic aerosols collected in the Arctic and southeastern Pacific marine boundary layers into four major chemical types: carboxylic acid-containing

polysaccharides, low-solubility polysaccharides, calcareous phytoplankton fragments, and proteinaceous particles. Indirect composition measurements are contributed by Wex et al. who report on the hygroscopic behavior of aerosol generated from laboratory bubble-bursting experiments with seawater solutions containing algae exudates. These types of studies provide semiquantitative estimates of the amounts of organics that can be expected from certain processes.

The sea-to-atmosphere exchange of reactive volatile organic compounds (VOCs) and their reaction with oxidants presents a potential source for secondary organic aerosol formation. McVeigh et al. present new data on the turbulent exchange of $O_3$ between open waters and the atmosphere in the absence of phytoplankton blooms. Under these conditions the net exchange rate is generally small, is bidirectional but skewed towards deposition, and deposition rates appear to decrease with increasing wind speed. Coleman et al. use a regional climate model to evaluate dry deposition of ozone over the North East Atlantic and estimate the magnitude of the ozone deposition-driven upward flux of iodine from the ocean. Results of this study show that iodide reactions alone cannot account for observed deposition velocities, suggesting a missing chemical sink due to reactions of ozone with organic matter and chlorophyll at the air-sea interface. In addition to iodine, the ocean is a source for large number of biogenic nonmethane hydrocarbons such as dimethylsulfide (DMS), isoprene, monoterpenes, and derived secondary organic aerosol (SOA) precursors. Shaw et al. present a topical review of about 70 articles on the subject and provide recommendations towards better characterizing and constraining emissions.

A number of studies are devoted to investigating the effect of ocean emissions on aerosol optical depth (AOD) and aerosol-cloud interactions using remotely sensed data. O'Dowd et al. show that sea spray contribution to marine AOD can approach or even exceed values of 0.3, suggesting that under moderately high wind speed regimes marine emissions can rival those of anthropogenic plumes advecting out into marine environment. By combining data from satellite and field measurement (ground and airborne), Sorooshian and Duong reveal a direct link between ocean emissions and aerosol physiochemical properties during periods of enhanced ocean productivity and low wind speed. However, due to complex cloud microphysical response to aerosol perturbations, the effect of ocean biota on cloud microphysical properties could not be identified with high confidence. To address the difficulties associated with the connection of ocean biological productivity, submicron aerosols, and clouds, Meskhidze and Nenes propose some guidelines for selection of time periods, oceanic regions and statistical methods in remotely-sensed studies. Using the differences in satellite-retrieved total AOD and predicted sea salt AOD at different wavelengths, Meskhidze and Nenesoffer proposed a new approach for exploring causal links between ocean physical and biological systems and abundance of CCN over the oceans.

A number of modeling studies address global and regional sources of marine primary organic aerosol (POA), ocean-derived SOA and potential effects of marine biogenic emissions on a new particle formation and growth over the open ocean. Myriokefalitakis et al. investigate global marine organic aerosol budget using a 3-dimensional chemistry-transport model TM4-ECPL. In this study ocean-derived SOA and submicron POA sources were estimated at about $1.5\,\mathrm{Tg\,C\,yr^{-1}}$ and $4\,\mathrm{Tg\,C\,yr^{-1}}$, respectively. Marine submicron POA was considered to be emitted as water insoluble, internally mixed with sea salt aerosols, while the computed marine SOA originated from the DMS (~78%), dialkyl amine salts (~21%), and marine hydrocarbon oxidation (~0.1%). Using regional-scale climate model REMOTE with current emission estimates, Anttila et al. investigated SOA formation over the North East Atlantic during a period of high biological activity. Results of this study show that marine isoprene oxidation makes a negligible contribution to marine organic aerosol budget and cannot explain the observed water soluble organic carbon. Simulations of marine new particle formation and growth by Monahan et al. using the M7 modal aerosol dynamics model indicate that the open ocean new particle production through sulfuric acid ($H_2SO_4$)—iodine dioxide (OIO) driven nucleation is feasible under coastal and open ocean marine environments. However, only few particles were suggested to reach detectable sizes for OIO and $H_2SO_4$ alone. Results of Monahan et al. study show that presence of low amounts of organic vapor can have significant impact on marine aerosol number concentrations.

## Acknowledgment

We, the guest editors of this special issue of Advances in Meteorology (AMET), are grateful to all of the authors, reviewers, and AMET stuff. We hope that the papers in this issue will stimulate further development and confidence building for improved characterization of this extremely complex topic.

*Nicholas Meskhidze*
*Charles R. McClain*
*Markus D. Petters*
*Elisabetta Vignati*
*Olaf Stetzer*
*Chris Osburn*
*David J. Kieber*

Hindawi Publishing Corporation
Advances in Meteorology
Volume 2010, Article ID 310682, 10 pages
doi:10.1155/2010/310682

*Research Article*

# Primary and Secondary Organic Marine Aerosol and Oceanic Biological Activity: Recent Results and New Perspectives for Future Studies

**Matteo Rinaldi,[1] Stefano Decesari,[1] Emanuela Finessi,[1] Lara Giulianelli,[1] Claudio Carbone,[1] Sandro Fuzzi,[1] Colin D. O'Dowd,[2] Darius Ceburnis,[2] and Maria Cristina Facchini[1]**

[1] *Institute of Atmospheric Sciences and Climate, National Research Council, Via P. Gobetti 101, 40129 Bologna, Italy*
[2] *School of Physics and Centre for Climate and Air Pollution Studies, Environmental Change Institute, National University of Ireland, University Road, Galway, Ireland*

Correspondence should be addressed to Matteo Rinaldi, m.rinaldi@isac.cnr.it

Received 15 February 2010; Accepted 6 April 2010

Academic Editor: Markus D. Petters



One of the most important natural aerosol systems at the global level is marine aerosol that comprises both organic and inorganic components of primary and secondary origin. The present paper reviews some new results on primary and secondary organic marine aerosol, achieved during the EU project MAP (Marine Aerosol Production), comparing them with those reported in the recent literature. Marine aerosol samples collected at the coastal site of Mace Head, Ireland, show a chemical composition trend that is influenced by the oceanic biological activity cycle, in agreement with other observations. Laboratory experiments show that sea-spray aerosol from biologically active sea water can be highly enriched in organics, and the authors highlight the need for further studies on the atmospheric fate of such primary organics. With regard to the secondary fraction of organic aerosol, the average chemical composition and molecular tracer (methanesulfonic-acid, amines) distribution could be successfully characterized by adopting a multitechnique analytical approach.

## 1. Introduction

The literature contains a great deal of evidence that large sectors of the marine atmosphere are influenced by continental outflows (natural or anthropogenic) and by ship exhaust emissions [1, 2]. However, the ocean is an important source of fine particles, and in background marine regions aerosol populations are dominated by natural marine particles [3, 4]. Given the ocean's extension, marine aerosol constitutes one of the most important natural aerosol systems at the global level. It contributes significantly to the Earth's radiative budget, biogeochemical cycling, with impacts on ecosystems and also on regional air quality [5]. The knowledge of particle chemical composition, as a function of size, is necessary for understanding and predicting the marine aerosol properties relevant to climate, for example, their ability to act as cloud condensation nuclei (CCN) and to influence the cloud droplet number concentration (CDNC) over background ocean regions.

In recent years, particular interest has focused on the marine aerosol organic fraction, its biogenic origin and the possible sources and mechanisms responsible for the high concentrations of organics observed in the submicron size fraction [6–8]. Figure 1 summarizes schematically the main potential formation pathways of organic aerosol in the marine boundary layer (MBL). Marine aerosol can derive both from primary or secondary processes. Primary aerosol production derives from the interaction of wind with the ocean surface and results in the mechanical production of sea spray aerosol. Traditionally, sea spray has been assumed to be composed of sea salt and water, with water reaching the equilibrium with the vapor phase after ejection. Nevertheless, the hypothesis that sea spray may become enriched in organic matter (OM) when the sea surface is characterized by high concentrations of biogenic OM, dates back to the 1960s [9]. The result of the said process is an internally mixed primary marine aerosol composed of sea

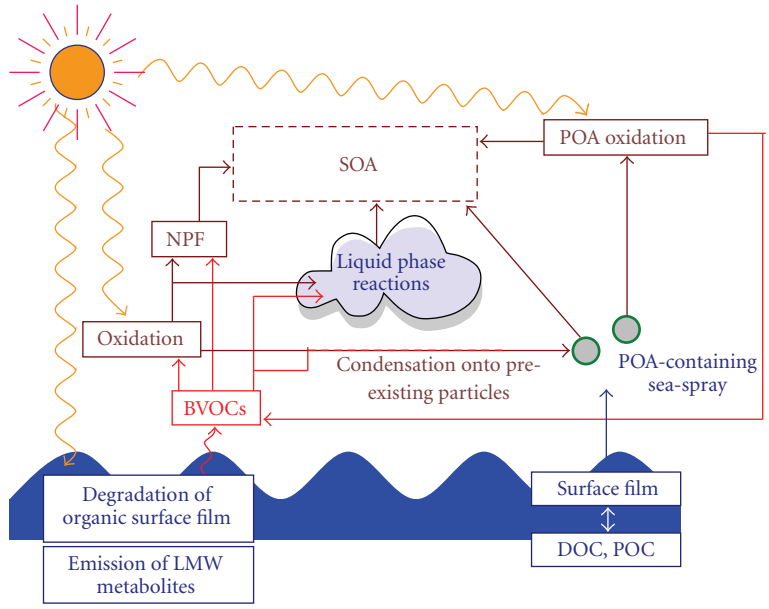


Figure 1: Diagram summarizing primary and secondary organic aerosol main formation routes in the marine boundary layer. DOC, POC and POA stand for Dissolved Organic Carbon, Particulate Organic Carbon and Primary Organic Aerosol, respectively

salt and organics, in which the organic fraction can be a major component [10].

Secondary organic aerosol (SOA) can form in the MBL through a number of different processes. Biogenic volatile organic compounds (BVOCs), emitted by the sea surface, or their oxidation products, can be involved in new particle formation (NPF) events via nucleation of stable clusters of 0.5–1 nm in size (such clusters can grow to larger sizes via condensation/coagulation processes). BVOCs and related oxidation products can also condense on preexisting particles and droplets, contributing to the particulate mass. SOA can also derive from the chemical transformation of primary or secondary components present in the condensed phase. Such transformations may take place at the particle surface [11, 12] or in the aqueous phase [13, 14], and may also involve a further step through the gas phase, in which semivolatile aerosol components can be oxidized to form new condensable products. The best known SOA component in marine aerosol is methanesulfonic acid (MSA), resulting from the atmospheric oxidation of dimethylsulphide (DMS) [15, 16]. Very recently, other formation processes, involving different precursors, such as biogenic isoprene [7], have been postulated. In spite of this, the observed high concentrations of oxidized OM in marine aerosol largely remain unexplained, suggesting that other formation processes and alternative SOA components should be considered.

To date, the most complete size segregated chemical characterisation of unperturbed marine aerosols is that provided by O'Dowd et al. [6] and Cavalli et al. [17], based on measurements performed at Mace Head (Ireland). They show that marine aerosol chemical composition is influenced by the oceanic yearly biological cycle and that, during periods of high biological oceanic activity (HBA), the organic fraction (mainly water insoluble) can contribute significantly to the submicrometer aerosol mass. Their results are consistent with the evidence that cloud condensation nuclei (CCN) concentration in remote marine regions follows a seasonal trend, with maxima in spring-summer [18] and with the more recent findings of Sorooshian et al. [19], who observed increased average CCN activity during periods of higher chlorophyll-*a* levels, probably as a result of aerosol size distribution and composition changes over the North Pacific Ocean.

During the EU Project MAP (Marine Aerosol Production; http://macehead.nuigalway.ie/map/) coastal and open ocean aerosol measurements, together with field-lab experiments, were carried out to achieve a better understanding of marine organic aerosol sources, chemical properties and effects on the climate system and on atmospheric chemistry. In the present paper, some of the main MAP results are discussed, and compared with parallel results recently published in the literature. In particular, the observed aerosol chemical composition seasonal trend and a WSOC chemical composition representative of the HBA period, never published before, are presented.

## 2. Experimental Approach

In the MAP framework, marine aerosol samples were collected at Mace Head Atmospheric Research Station. Located on the west coast of Ireland, the station is unique in Europe, offering westerly exposure to the North Atlantic Ocean and the opportunity to study atmospheric composition under Northern Hemispheric background conditions. The site location, at 53 degrees 20 minutes N, 9 degrees 54 minutes W, is in the path of the mid-latitude cyclones which frequently traverse the North Atlantic. The main Atlantic shipping routes are over 150 km away, while the transatlantic

air corridors are over 80 km away. The site characteristics are ideal for carrying out marine background aerosol and trace gas measurements. The sampling took place throughout 2006, while, during an intensive observation period, coinciding with peak oceanic biological activity (June-July 2006), measurements were also performed onboard the oceanographic vessel Celtic Explorer sailing off the Irish coast.

Details on the adopted clean sector aerosol sampling strategy and instrumentation can be found in previously published papers [20, 21]. Laboratory experiments for the production of artificial sea spray aerosol from highly biologically active ([chlorophyll-$a$] = $1.4 \pm 0.8\,\mathrm{mg\,m^{-3}}$), freshly collected, sea water were performed onboard the Celtic Explorer. Full details on the experiment, including the sea water chemical characterization, and the sample analysis are described in [22].

A complete suite of chemical characterization techniques were applied to both ambient and laboratory aerosol samples: ion chromatography (IC), for the determination of inorganic water soluble ions, amines and organic acids, and solid/liquid phase elemental analyses, for the determination of water soluble organic carbon (WSOC), water soluble organic nitrogen (WSON) and water insoluble organic carbon (WIOC). Full details on sample handling and analysis can be found in [20, 21].

The organic chemical characterization was achieved through proton nuclear magnetic resonance ($^1$HNMR) spectroscopy [21–23] and by the anion-exchange high performance liquid chromatography (HPLC-TOC) technique described by Mancinelli et al. [24]. Using HPLC-TOC, it is possible to speciate WSOC into four macroclasses: neutral-basic compounds (NB), mono-acids (MA), di-acids (DA) and poly-acids (PA, representative of humic-like substances), and to quantify each fraction in terms of organic carbon content.

Here, the acronym WSOM (water soluble organic matter) is used to indicate the estimated mass of WSOC, obtained multiplying WSOC by a conversion factor of 1.8, derived from the functional group composition of WSOC [21]. Similarly, WIOM (water insoluble organic matter) was obtained by multiplying WIOC by a conversion factor of 1.4, according to the functional group composition observed by $^1$H NMR in sea spray organic aerosols [22].

## 3. Marine Aerosol Chemical Composition during the 1-Year Sampling Campaign at Mace Head

Figure 2 shows the chemical composition of the submicron aerosol samples collected during 2006 at Mace Head. Table 1 reports the percentage contribution of each of the main submicron aerosol components, in the HBA and LBA (low biological activity) periods. Marine aerosol mainly comprised a mixture of sea salt of primary origin, $\mathrm{nssSO_4^{-2}}$, $\mathrm{NH_4^+}$, $\mathrm{NO_3^-}$, clearly secondary components, and soluble (WSOM) and insoluble (WIOM) organic compounds.

Table 1: Median, minimum and maximum (in brackets) relative contribution of the main marine aerosol components to the analyzed total mass, expressed as percentages. Median values are reported only when greater than zero. "$n$" indicates the number of samples.

| [%] | HBA ($n = 5$) | LBA ($n = 7$) |
|---|---|---|
| $\mathrm{nssSO_4^{-2}}$ | 50 (38–57) | 22 (5–27) |
| $\mathrm{NH_4^+}$ | 7 (6–9) | 1 (0–3) |
| $\mathrm{NO_3^-}$ | (0–1) | 1 (1–2) |
| WSOM | 23 (11–33) | 6 (0–11) |
| sea salt | 20 (6–25) | 65 (59–77) |
| WIOM | 7 (2–10) | 6 (2–17) |

Parallel laboratory experiments during the same project [22] showed that nascent submicron marine organics from bubble bursting mainly comprise (94%) WIOM. Moreover, the pattern of WIOM and sea-salt content in the different size intervals observed in the laboratory experiments was similar to that measured in atmospheric marine aerosol samples collected during periods of HBA, thus pointing to a WIOM/sea-salt fingerprint associated with submicron primary marine aerosol production in biologically rich waters. The indirect consequence of this observation is that WSOM observed in HBA will derive mainly from secondary processes. A secondary formation route for WSOM is also supported by the findings of a recent experiment performed at Mace Head [25], in which downward fluxes, characteristic of chemical species forming through secondary processes, were measured for submicron aerosol $\mathrm{nssSO_4^{-2}}$ and WSOM.

The seasonal trend of the main component concentrations in submicron size range exhibits maxima in spring and summer (HBA) and minima during winter (LBA), with the exception of sea salt (Figure 2), in good agreement with Mace Head aerosol climatology for the 2002–2004 period [26], thus suggesting a dependence of submicron aerosol chemical composition on the seasonal cycle of the North Atlantic biological activity. Similar results showing maximum concentration in spring-summer in conjunction with phytoplankton activity in surface sea water, have been reported by several investigators for MSA [27, 28] and $\mathrm{nssSO_4^{-2}}$ [29]. The maxima observed in atmospheric concentrations for $\mathrm{nssSO_4^{-2}}$, MSA and $\mathrm{NH_4^+}$ can be attributed to the increase in the emission of gaseous precursors, mainly DMS [16, 30] and $\mathrm{NH_3}$ [31], produced by the marine biota during the HBA period, and to the concurrent enhanced photochemical activity of the atmosphere [32]. In analogy, the WSOC spring-summer peak can be attributed to the increased emission of volatile organic compounds (VOCs) by the marine biota and to the concurrently enhanced photo-oxidative capacity of the atmosphere, generating low vapor pressure oxidation products which can condense on preexisting particles. Another potential path for WSOC production could be through the aging process of the insoluble primary fraction, obviously more efficient during period of high photochemical activity.

Submicron aerosol chemical composition is different during HBA with respect to the LBA period. During HBA the

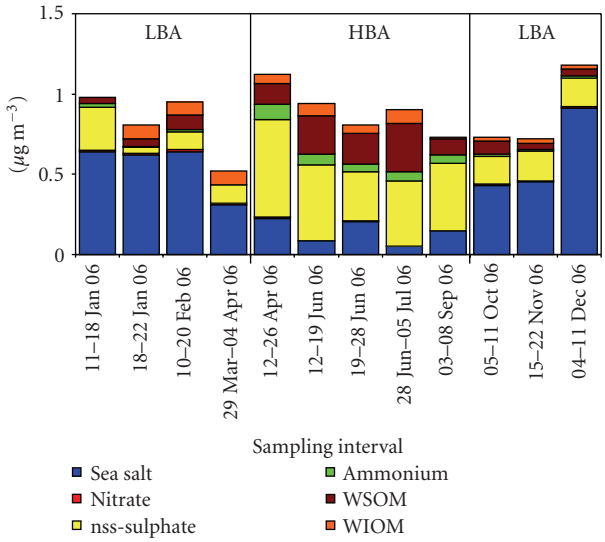


FIGURE 2: Seasonal evolution of submicron marine aerosol chemical composition observed through the twelve samples collected at Mace Head during MAP. The horizontal axis reports the nominal sampling time for each sample, that is, the time during which the filter/substrate has been exposed (the actual sampling time depended on the occurrence of the clean sector conditions during the exposition time). Samples are grouped in HBA and LBA period to evidence the differences between the two periods.

greater part of the mass was accounted for by nss$SO_4^{-2}$ and WSOM: nss$SO_4^{-2}$ median contribution to the total analyzed mass was 50% (ranging from 38 to 57%), that of WSOM 23% (11%–33%). Conversely, in the LBA period sea salt accounts for the greater part of the analyzed submicron mass, with a median contribution of 65% (59%–77%), while the contributions of nss$SO_4^{-2}$ and WSOM are reduced to 22% (5%–27%) and 6% (0%–11%), respectively. Water insoluble organics contributed almost equally to the analyzed total submicron mass during the HBA and LBA periods.

Submicron organics were clearly dominated by WSOM during the HBA period, while the contribution of soluble and insoluble organic compounds was comparable during the LBA period. This picture of marine aerosol is different from the one reported by O'Dowd et al. [6], who observed at Mace Head a submicron aerosol chemical composition dominated by water insoluble organic species during the HBA period. Such discrepancy could be due to a different location of highly biologically productive waters with respect to the Irish coast during MAP [21], or to different meteorological conditions encountered in the sampling periods: most of the samples discussed in the present work were collected in summer, when the photochemical activity is at its maximum, while most of the 2002 samples reported in O'Dowd et al. [6] were collected during spring and autumn, when sea spray production is higher. The main difference between the two datasets, indeed, regards WIOM absolute concentration during the HBA period (~0.6 $\mu$g m$^{-3}$ in 2002 and less than 0.1 $\mu$g m$^{-3}$ during MAP, averagely), while WSOM one is comparable (~0.2 $\mu$g m$^{-3}$), suggesting a lower influence of the primary source in MAP samples.

Sciare et al. [33] also reported marked seasonal trends for marine aerosol collected at Amsterdam Island (Southern Indian Ocean). WIOC, MSA and nMSA-WSOC (WSOC not deriving from MSA) showed concentration enhancement during the austral summer. Moreover, it was found that marine aerosol organics were mainly accounted for by WIOC, in agreement with the previous observation in the North Atlantic [6]. The investigators also pointed out the likely biogenic origin of marine aerosol organics, evidencing its main source in a very productive oceanic area located around 40°S. It must be concluded that submicron marine aerosol chemical composition can be extremely variable over the year and, probably, from year to year, depending on the predominance of the primary source with respect to secondary ones, ocean dynamic conditions, influence of different oceanic source regions and atmospheric photochemical activity. These studies demonstrate the importance of biogenic organic aerosols over the ocean, at high latitudes (<40°S and >40°N), during periods of high biological productivity.

In the following paragraphs, the most recent findings on primary and secondary biogenic organics in submicron marine aerosol are discussed.

## 4. Primary Organic Aerosol and Its Evolution in the Marine Boundary Layer

Several attempts to quantify and characterize sea spray organics have recently been carried out. Keene et al. [34] reported high enrichment factors for water soluble organics, in nascent lab-produced sea spray particles, with respect to sea water. WSOC was highly enriched in all aerosol size fractions and the greatest enrichments were associated with the smallest size fraction (about 80% of aerosol mass was organic at 0.13 $\mu$m). The authors concluded that bursting bubbles at the ocean surface produce significant numbers of sub$\mu$m, hygroscopic, organic-dominated aerosols, thereby supporting the hypothesis that this pathway is a potentially important global source of climate relevant particles.

Facchini et al. [22] similarly reported a high contribution of organic matter in nascent submicron sea spray particles, up to 77 ± 5% in the 0.125–0.25 $\mu$m size range (Table 2), although their analysis discriminated between water soluble and insoluble organic carbon, finding a dominant contribution of WIOM (up to 94 ± 4% of OC in the 0.125–0.25 $\mu$m size range). Moreover, Facchini et al. [22] highlighted that sea spray organics tend to aggregate and form colloids or suspended particles, making the definition of water solubility a complex issue. Whether the difference in the results of the two experiments is attributable only to the different organic carbon measurement approach, or also to differences in the chemical properties of the sea water used for generating aerosol particles by bubble bursting (oligotrophic Sargasso Sea versus North Atlantic Ocean during algal bloom) is still an issue of debate.

Furthermore, Modini et al. [35] presented the results of a similar experiment in which the organic volume contribution in lab-produced sea spray particles, indirectly determined by volatility/hygroscopicity tandem measurements (HV-TDMA), was estimated to be ($8 \pm 6\%$) in the 71–77 nm size range, corresponding to a mass contribution of only 4%. Such results may be conditioned by the interpretation of HV-TDMA measurements to calculate the organic fraction, or by the use of coastal waters (potentially high in terrestrial runoff) for spray generation. However, they could also be evidence of a high system variability, stressing the necessity for further investigation.

Several papers have reported the presence of carbohydrate-like material in marine particles, attributing this to primary sea spray processes.

Bigg and Leck [36] observed the presence of complex structures behaving as lipopolysaccharides in submicron marine aerosol. Facchini et al. [22] evidenced the presence of hydroxyl groups, both in water soluble and insoluble sea spray OM, using $^1$HNMR analyses. These hydroxyl signals were always associated in the NMR spectra to important signals due to aliphatic chains with terminal methyls, typical of lipids. Moreover, the $^1$HNMR spectra of oceanic water closely resembled that of nascent aerosol, and were in agreement with several observations in the literature reporting the presence in oceanic waters of phytoplankton exudates with a composition dominated by lipopolysaccharides [37, 38].

Very recently Russell et al. [39] observed an ocean-derived component, in marine aerosol, dominated by carbohydrate-like material, based on multi-technique measurements of submicron marine aerosol over the North Atlantic and Arctic Oceans and on Positive Matrix Factorization data elaboration. According to these authors, the primary marine signal in submicron marine aerosol is made on average for 88% of hydroxyl groups. Although the low signal-to-noise ratio of the spectra made difficult a precise quantification of the carbohydrate-like material, $^1$HNMR analyses exclude a contribution as high as the one observed by Russell et al. [39] for these components in the North Atlantic during periods of HBA.

Such new, often contrasting results on primary organics in marine aerosol reflect the limits of current knowledge on this topic. Furthermore, the fate of primary organics in the atmosphere is even more uncertain, and few data are available on sea spray organic oxidation routes, rates and products. Zhou et al. [40] evidenced that OM in marine aerosols plays a dual role, being an important precursor/source and a dominant sink for the OH radical, leading to the degradation of OM, and the likely production of a series of low-molecular weight (LMW) organic compounds. Therefore, primary and secondary organic components must be considered as closely correlated in marine aerosol, as the oxidation products of biogenic primary organics in marine aerosol particles can lead to the production of both oxidized aerosol components (belonging to the broad category of SOA) and of volatile LMW products, which can partition into the gas phase and influence the multiphase photochemical evolution of the marine troposphere (including SOA formation). Supporting evidence of this gliding boundary between primary and secondary organic aerosol components were also provided by Jimenez et al. [41], who showed, in a recent chamber experiment, how aerosolized squalane, a proxy for the refractory fraction of primary marine organic aerosol, was subjected to photochemical ageing, showing mass spectral features progressively transforming into those of oxidized organic aerosols, which are ubiquitous in the atmosphere.

## 5. Advances in Marine SOA Chemical Characterization

New results on marine WSOC chemical composition have been obtained over past years, allowing the identification of typical marine SOA components, other than MSA and DMS oxidation products.

The presence of amines and aminoacids over the oceans has been sporadically reported since the 1980s in rain samples over the ocean [42–44]. Gibb et al. [45] reported the presence of monomethylammonium ($MMA^+$), dimethylammonium ($DMA^+$) and trimethylammonium ($TMA^+$) salts in aerosol particles collected in unpolluted conditions over the Arabian Sea. The authors attributed the presence of aerosol phase alkyl ammonium salts to secondary production, due to the condensation of gaseous alkyl amines emitted by the sea, in analogy with $NH_4^+$. More recently, this hypothesis has been strengthened by evidence that alkyl amines participate in SOA formation in many different environments through reaction with acids [46–48].

Facchini et al. [20] highlighted the importance of alkyl-ammonium salts as submicron marine aerosol components, and reported dimethyl and diethyl-ammonium salts ($DMA^+$ and $DEA^+$) concentrations ranging, together between <0.4 and 56 ng m$^{-3}$ over the North Atlantic Ocean during the HBA period, turning out to be the most abundant organic species, second only to MSA, in submicron marine particles. Alkyl-ammonium salts represented on average 11% of the marine SOA and a dominant fraction (35% on average) of aerosol water soluble organic nitrogen (WSON).

The above cited paper presents considerable evidence that $DMA^+$ and $DEA^+$ are secondary aerosol components, originating from biogenic precursors emitted by the ocean. Their size distributions exhibited maxima in the accumulation mode, as is also the case of other well known secondary components ($nssSO_4^{-2}$, $NH_4^+$, MSA), supporting the hypothesis that a gas-to-particle conversion process is responsible for the accumulation of alkyl-ammonium salts in the fine aerosol fraction. The most likely hypothesis is that gaseous dimethylamine and diethylamine react with sulphuric acid or acidic sulphates, accumulating within aerosol particles in close analogy with ammonia. Regarding the precursor origin, a main anthropogenic source of gaseous alkyl-amines over the ocean can be excluded, because the aerosol $DMA^+$ and $DEA^+$ concentrations measured at Mace Head, were always higher in clean marine samples (roughly double) than in polluted air masses, in analogy with MSA. Like other reduced biogenic gases (DMS, $CH_4$) and in analogy with $NH_3$, DMA and DEA could be the end products

Table 2: Summary of the sea spray OM contribution measured in the most recent sea spray production laboratory experiments.

| Sea water sampling site | Max OM mass contribution [%] | Particle diameter [nm] | Notes | Reference |
|---|---|---|---|---|
| Sargasso Sea (oligotrophic) | ~80 | 130 | Only WSOC measured. No filtration | Keene et al. [34] |
| North Atlantic Ocean (algal bloom) | 77 ± 5 | 125–250 | WSOC and WIOC measured. Filtration. | Facchini et al. [22] |
| Moreton Bay (Australia) | 4 | 71–77 | Coastal water | Modini et al. [35] |

of microbial turnover of marine labile OM [45, 49, 50]. Furthermore, alkyl-ammonium ions in submicron aerosol particles showed the typical seasonal variation of biogenic components, with high concentrations measured in the HBA period, and much lower concentrations in the LBA period (Table 3).

Table 3 summarizes the marine aerosol alkylammonium ion concentration data so far available: two very recent papers confirm the findings of Facchini et al. [20]. Müller et al. [51] reported monomethylammonium ($MA^+$), $DMA^+$ and $DEA^+$ at non-negligible concentrations in submicrometer particles at Cape Verde, during algal blooms in 2007, attributing them to secondary formation processes. Moreover, high levels of amines were observed in coincidence with high near surface Chlorophyll-*a* concentrations. Finally, Sorooshian et al. [19] also observed $DEA^+$ in submicron particles over the North Pacific Ocean, with concentrations rather well correlated to the chlorophyll-*a* sea surface concentration.

Besides alkylammonium salts and MSA, carboxylic and di-carboxylic acids have been identified in marine aerosol [52, 53 and references therein], found to account for less than 10% of total particulate organic carbon in remote marine environments. The above mentioned papers attribute a secondary origin to detected di-carboxylic acids, citing oxalic acid as the most abundant one. However, oxidized organics, such as $C_5$–$C_{10}$ carboxylic or di-carboxylic acids, can also be produced by the oxidative degradation of primary particles generated by sea spray and rich in fatty acids [52].

Recent instrumental advances have allowed a deeper insight into organic marine aerosol chemical composition. Using liquid chromatography/negative ion electrospray ionization mass spectrometry, Claeys et al. [53] investigated marine organic aerosol chemical composition at Amsterdam Island (Southern Indian Ocean), reporting a WSOC contribution of 32 ± 12% to submicron OC. About 25% of WSOC was characterized and attributed to MSA (17%–21%), oxalate (5 ± 2%), malonate (1.8 ± 0.9%) and organosulphates (0.8 ± 1.5%). The organosulphates characterized in Claeys et al. [53] can be considered tracers for an SOA formation process that is specific to the marine environment, that is, oxidation of marine biomass. More specifically, the organosulfates correspond to sulfate esters of $C_9$–$C_{13}$ hydroxyl carboxylic acids, which are attributed to oxidation of unsaturated fatty acid residues present in algal cell membranes.

Notwithstanding recent improvements, current knowledge on the chemical composition of marine SOA remains limited, and further research is required to address the many unresolved issues. During MAP a multi-technique approach was deployed to characterize marine WSOC. Coupling HPLC-TOC and IC, it was possible to achieve an almost-complete chemical characterization of submicron marine WSOC, on a selected subset of samples (5, from both Mace Head and Celtic Explorer sampling) representative of the HBA period (Figure 3). Marine aerosol WSOC can be divided into three chemical macroclasses based on acid-base properties: neutral-basic compounds (NB), accounting for 32 (±8) % of WSOC, mono-diacids (MDA), contributing 42 (±9) %, and polyacids (PA), accounting for 4 (±3) %. Averagely 22 (±11) % of WSOC escaped this classification, probably as a result of strong and irreversible binding with the HPLC column: this fraction is labeled "uncharacterized" in the Figure. From the HPLC-TOC macroclasses average contribution, the average contribution of each compound, identified by IC, has been subtracted, obtaining the classification of Figure 3. Only 30% of WSOC was characterized at the molecular level by IC, with MSA (11 ± 5%) and oxalic acid (3 ± 2%) being the only two MDA components identified. This leaves more than a half of the dominant class of compounds still uncharacterized, although it is likely that other LMW dicarboxylic acids, like malonic and succinic acid, not identified by IC, can account together for another 1%-2%. As for the NB compounds, 6 ± 7 and 10 ± 12% of the WSOC can be ascribed to $DMA^+$ and $DEA^+$, leaving about 15% of WSOC as uncharacterized NB compounds. In WSOC extracted from marine aerosol collected during MAP, HPLC analysis showed the occurrence of fulvic-like material (polyacids macroclass), in lower concentrations than suggested by previous studies, that is, 22% [17]. The finding indicates that primary emissions of fulvic substances from seawater did not make a major contribution to marine water-soluble aerosols during MAP. This picture of submicron marine aerosol WSOC is coherent with the hypothesis of its mainly secondary origin, even though the uncharacterized fraction escaping classification in NB, MDA and PA may be due to the contribution of primarily emitted, aggregate forming, organic matter, similar to that characterized in laboratory experiments on nascent sea spray aerosol by Facchini et al. [22].

Information on the chemical composition of the uncharacterized fractions of NB, MDA and PA has been derived

Table 3: Alkylammonium ions aerosol concentration range (in brackets) and median value (when available) reported in the literature for the marine environment. All concentrations are in ng $m^{-3}$. All data refer to submicron particles except for Müller et al. [51], whose size cut was 0.14–0.42 $\mu$m, and Gorzelska and Galloway [44], who did not report any particle size information.

| Location | $MA^+$ [ng $m^{-3}$] | $DMA^+$ [ng $m^{-3}$] | $TMA^+$ [ng $m^{-3}$] | $EA^+$ [ng $m^{-3}$] | $DEA^+$ [ng $m^{-3}$] | Reference |
|---|---|---|---|---|---|---|
| North Atlantic Jun–Sep 1988 | (<dl–3.9) | | | (<dl–~1.4) | | Gorzelska & Galloway [44] |
| Arabian Sea Aug-Oct 1994 | <dl–6.1 | 1.6–4.4 | 0.018–0.78 | | | Gibb et al. [45] |
| Arabian sea Nov-Dec 1994 | 2.6–4.5 | 3.7–17.5 | 0.12–0.9 | | | Gibb et al. [45] |
| Mace Head Oct–Mar 2006 | | 1 (<1–8) | | | (<1–12) | Facchini et al. [20] |
| Mace Head Apr–Sep 2006 | | 10 (2–24) | | | 16 (4–32) | Facchini et al. [20] |
| North Atlantic Jun 2006 | | 9 (4–13) | | | 12 (7–24) | Facchini et al. [20] |
| Cape Verde May 2007 | 0.02 (0.01–0.03) | 0.21(0.13–0.36) | | | 0.06 (0.005–0.11) | Müller et al. [51] |
| Cape Verde Jun 2007 | 0.03 (0.01–0.12) | 0.21(0.05–0.39) | | | 0.07 (0.06–0.14) | Müller et al. [51] |
| Cape Verde Dec 2007 | 0.15 (0.002–0.52) | 0.54 (0.1–1.4) | | | 0.29 (0.09–0.76) | Müller et al. [51] |
| North Pacific Jul-Aug 2007 | | | | | 14–35 | Sorooshian et al. [19] |

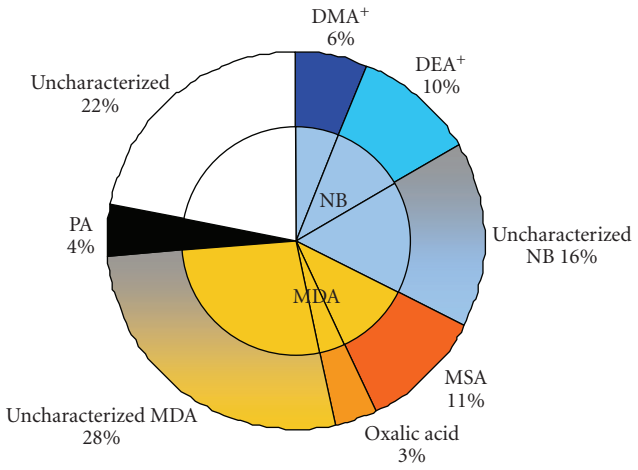


Figure 3: WSOC chemical composition representative of spring-summer conditions over the Atlantic Ocean, obtained by combining HPLC-TOC and IC (see text for more details). Percentages indicate the contribution of each compound or chemical macroclass in terms of carbon.

by NMR functional group analysis (Decesari et al., in preparation), showing aliphatic moieties substituted with oxygenated groups, like carbonyls/carboxyls and, in analogy with the findings of Russell et al. [39], hydroxyl groups.

## 6. Conclusions

Studies performed during the past years strongly suggest that biogenic organic compounds play an important role in submicron marine aerosol chemical composition over biologically productive, high latitude, marine regions, in both hemispheres. Moreover, it has been demonstrated that marine organic aerosol chemical composition is the complex result of different primary and secondary sources.

Most recent results on sea spray composition suggest that in conditions of intense oceanic biological productivity, submicron primary marine aerosol can contain a considerable fraction of OM. Further studies are necessary to obtain deeper insight into the space/time variability of the ocean primary organics production potential worldwide. Important advances can be obtained by coupling modeling with new satellite chlorophyll, dissolved and particulate organic carbon measurement instruments, as attempted for the first time by O'Dowd et al. [54] and Vignati et al. [4]. In fact, although much information has been gathered on the DMS oxidation cycle, and several predictive tools are available to model secondary products, like MSA and nss-sulfate over the oceans, only raw empiric instruments are available to predict primary organic aerosol emissions as a function of oceanic biological productivity.

To date, little is known about sea spray organic chemical composition, lifetime and fate in the marine boundary layer. Further investigation is required to address this issue, that can also help to fill the gap between observed and modeled SOA in the MBL.

As for secondary organics in the MBL, although several classes of compounds have been identified in different marine environments as typical marine SOA components (MSA, alkylammonium salts, dicarboxylic acids), most marine aerosol WSOC remains uncharacterized at the molecular level. Closer investigation of marine aerosol

WSOC chemical composition is needed to achieve a better knowledge on SOA formation routes in the MBL. Deeper insight into marine aerosol organics chemical composition is expected from the new high time resolution aerosol measurement instrumentats, namely AMS, only seldom applied to the clean MBL so far [55–57].

Furthermore, an important fraction of marine SOA, WSON, is still mostly uncharacterized. A fraction of the unaccounted organic nitrogen, especially during the warm season, can reasonably be attributed to products of the oxidative degradation of $DMA^+$, $DEA^+$ and other minor alkylammonium ions. However, alternative sources of unaccounted water soluble organic nitrogen, for example, the oxidation of insoluble primary organic material emitted by sea spray, cannot be ruled out at present. Further studies are necessary to clarify this point.

More detailed size-resolved information on marine organic aerosols in the remote MBL are needed to define the contribution of organics to marine CCN. The atmospheric fate of primary and secondary marine organic aerosols also needs to be further evaluated, as it may significantly influence the ability of marine aerosols to act as CCN in unperturbed ocean regions.

## Acknowledgements

A financial support from EU FP6 project MAP (GOCE-018332) and EPA Ireland is gratefully acknowledged.

## References

[1] G. Chen, L. G. Huey, M. Trainer, et al., "An investigation of the chemistry of ship emission plumes during ITCT 2002," *Journal of Geophysical Research D*, vol. 110, no. 10, Article ID D10S90, 15 pages, 2005.

[2] J. Huang, P. Minnis, B. Chen, et al., "Long-range transport and vertical structure of Asian dust from CALIPSO and surface measurements during PACDEX," *Journal of Geophysical Research D*, vol. 113, no. 23, Article ID D23212, 2008.

[3] D. V. Spracklen, S. R. Arnold, J. Sciare, K. S. Carslaw, and C. Pio, "Globally significant oceanic source of organic carbon aerosol," *Geophysical Research Letters*, vol. 35, no. 12, Article ID L12811, 2008.

[4] E. Vignati, M. C. Facchini, M. Rinaldi, et al., "Global scale emission and distribution of sea-spray aerosol: sea-salt and organic enrichment," *Atmospheric Environment*, vol. 44, no. 5, pp. 670–677, 2010.

[5] C. D. O'Dowd and G. de Leeuw, "Marine aerosol production: a review of the current knowledge," *Philosophical Transactions of the Royal Society A*, vol. 365, no. 1856, pp. 1753–1774, 2007.

[6] C. D. O'Dowd, M. C. Facchini, F. Cavalli, et al., "Biogenically driven organic contribution to marine aerosol," *Nature*, vol. 431, no. 7009, pp. 676–680, 2004.

[7] N. Meskhidze and A. Nenes, "Phytoplankton and cloudiness in the southern ocean," *Science*, vol. 314, no. 5804, pp. 1419–1423, 2006.

[8] E. K. Bigg, "Sources, nature and influence on climate of marine airborne particles," *Environmental Chemistry*, vol. 4, no. 3, pp. 155–161, 2007.

[9] D. C. Blanchard, "Sea-to-air transport of surface active material," *Science*, vol. 146, no. 3642, pp. 396–397, 1964.

[10] C. Oppo, S. Bellandi, N. Degli Innocenti, et al., "Surfactant components of marine organic matter as agents for biogeochemical fractionation and pollutant transport via marine aerosols," *Marine Chemistry*, vol. 63, no. 3-4, pp. 235–253, 1999.

[11] T. L. Eliason, J. B. Gilman, and V. Vaida, "Oxidation of organic films relevant to atmospheric aerosols," *Atmospheric Environment*, vol. 38, no. 9, pp. 1367–1378, 2004.

[12] S. F. Maria, L. M. Russell, M. K. Gilles, and S. C. B. Myneni, "Organic aerosol growth mechanisms and their climate-forcing implications," *Science*, vol. 306, no. 5703, pp. 1921–1924, 2004.

[13] B. Ervens, C. George, J. E. Williams, et al., "CAPRAM 2.4 (MODAC mechanism): an extended and condensed tropospheric aqueous phase mechanism and its application," *Journal of Geophysical Research D*, vol. 108, no. 14, pp. 1–21, article 4426, 2003.

[14] P. Warneck, "In-cloud chemistry opens pathway to the formation of oxalic acid in the marine atmosphere," *Atmospheric Environment*, vol. 37, no. 17, pp. 2423–2427, 2003.

[15] G. E. Shaw, "Bio-controlled thermostasis involving the sulfur cycle," *Climatic Change*, vol. 5, no. 3, pp. 297–303, 1983.

[16] R. J. Charlson, J. E. Lovelock, M. O. Andreae, and S. G. Warren, "Oceanic phytoplankton, atmospheric sulphur, cloud albedo and climate," *Nature*, vol. 326, no. 6114, pp. 655–661, 1987.

[17] F. Cavalli, M. C. Facchini, S. Decesari, et al., "Advances in characterization of size-resolved organic matter in marine aerosol over the North Atlantic," *Journal of Geophysical Research D*, vol. 109, no. 24, pp. 1–14, 2004.

[18] S. S. Yum and J. G. Hudson, "Wintertime/summertime contrasts of cloud condensation nuclei and cloud microphysics over the Southern Ocean," *Journal of Geophysical Research D*, vol. 109, no. 6, Article ID D06204, 14 pages, 2004.

[19] A. Sorooshian, L. T. Padrò, A. Nenes, et al., "On the link between ocean biota emissions, aerosol, and maritime clouds: airborne, ground, and satellite measurements off the coast of California," *Global Biogeochemical Cycles*, vol. 23, Article ID GB4007, 15 pages, 2009.

[20] M. C. Facchini, S. Decesari, M. Rinaldi, et al., "Important source of marine secondary organic aerosol from biogenic amines," *Environmental Science and Technology*, vol. 42, no. 24, pp. 9116–9121, 2008.

[21] M. Rinaldi, M. C. Facchini, S. Decesari, et al., "On the representativeness of coastal aerosol studies to open ocean studies: Mace Head-a case study," *Atmospheric Chemistry and Physics*, vol. 9, no. 24, pp. 9635–9646, 2009.

[22] M. C. Facchini, M. Rinaldi, S. Decesari, et al., "Primary submicron marine aerosol dominated by insoluble organic colloids and aggregates," *Geophysical Research Letters*, vol. 35, no. 17, Article ID L17814, 2008.

[23] S. Decesari, M. C. Facchini, S. Fuzzi, and E. Tagliavini, "Characterization of water-soluble organic compounds in atmospheric aerosol: a new approach," *Journal of Geophysical Research D*, vol. 105, no. D1, pp. 1481–1489, 2000.

[24] V. Mancinelli, M. Rinaldi, E. Finessi, et al., "An anion-exchange high-performance liquid chromatography method coupled to total organic carbon determination for the analysis of water-soluble organic aerosols," *Journal of Chromatography A*, vol. 1149, no. 2, pp. 385–389, 2007.

[25] D. Ceburnis, C. D. O'Dowd, G. S. Jennings, et al., "Marine aerosol chemistry gradients: elucidating primary and secondary processes and fluxes," *Geophysical Research Letters*, vol. 35, no. 7, Article ID L07804, 2008.

[26] Y. J. Yoon, D. Ceburnis, F. Cavalli, et al., "Seasonal characteristics of the physicochemical properties of North Atlantic marine atmospheric aerosols," *Journal of Geophysical Research D*, vol. 112, no. 4, Article ID D04206, 2007.

[27] H. Mukai, Y. Yokouchi, and M. Suzuki, "Seasonal variation of methanesulfonic acid in the atmosphere over the Oki Islands in the Sea of Japan," *Atmospheric Environment*, vol. 29, no. 14, pp. 1637–1648, 1995.

[28] S.-M. Li, L. A. Barrie, and D. Toom, "Seasonal variations of methanesulfonate, non-sea-salt sulfate, and sulfur dioxide at three sites in Canada," *Journal of Geophysical Research D*, vol. 101, no. 2, pp. 4165–4173, 1996.

[29] D. L. Savoie, R. Arimoto, W. C. Keene, J. M. Prospera, R. A. Duce, and J. N. Galloway, "Marine biogenic and anthropogenic contributions to non-sea-salt sulfate in the marine boundary layer over the North Atlantic Ocean," *Journal of Geophysical Research D*, vol. 107, no. 18, pp. 1–21, article 4356, 2002.

[30] T. W. Andreae, M. O. Andreae, and G. Schebeske, "Biogenic sulfur emissions and aerosols over the tropical South Atlantic 1. Dimethylsulfide in seawater and in the atmospheric boundary layer," *Journal of Geophysical Research*, vol. 99, no. D11, pp. 1–22, article 819, 1994.

[31] W. A. H. Asman, R. M. Harrison, and C. J. Ottley, "Estimation of the net air-sea flux of ammonia over the southern bight of the North Sea," *Atmospheric Environment*, vol. 28, no. 22, pp. 3647–3654, 1994.

[32] I. Barnes, J. Hjorth, and N. Mihalapoulos, "Dimethyl sulfide and dimethyl sulfoxide and their oxidation in the atmosphere," *Chemical Reviews*, vol. 106, no. 3, pp. 940–975, 2006.

[33] J. Sciare, O. Favez, R. Sarda-Estève, K. Oikonomou, H. Cachier, and V. Kazan, "Long-term observations of carbonaceous aerosols in the Austral Ocean atmosphere: evidence of a biogenic marine organic source," *Journal of Geophysical Research D*, vol. 114, no. 15, Article ID D15302, 2009.

[34] W. C. Keene, H. Maring, J. R. Maben, et al., "Chemical and physical characteristics of nascent aerosols produced by bursting bubbles at a model air-sea interface," *Journal of Geophysical Research D*, vol. 112, no. 21, Article ID D21202, 2007.

[35] R. L. Modini, B. Harris, and Z. D. Ristovski, "The organic fraction of bubble-generated, accumulation mode Sea Spray Aerosol (SSA)," *Atmospheric Chemistry and Physics Discussions*, vol. 9, no. 5, pp. 21399–21424, 2009.

[36] E. K. Bigg and C. Leck, "The composition of fragments of bubbles bursting at the ocean surface," *Journal of Geophysical Research D*, vol. 113, no. 11, Article ID D11209, 2008.

[37] N. Kovac, O. Bajt, J. Faganeli, B. Sket, and B. Orel, "Study of macroaggregate composition using FT-IR and $^1$H-NMR spectroscopy," *Marine Chemistry*, vol. 78, no. 4, pp. 205–215, 2002.

[38] J. Zhou, K. Mopper, and U. Passow, "The role of surface-active carbohydrates in the formation of transparent exopolymer particles by bubble adsorption of seawater," *Limnology and Oceanography*, vol. 43, no. 8, pp. 1860–1871, 1998.

[39] L. M. Russell, L. N. Hawkins, A. A. Frossard, P. K. Quinn, and T. S. Bates, "Carbohydrate-like composition of submicron atmospheric particles and their production from ocean bubble bursting," *Proceedings of the National Academy of Sciences of the United States of America*, vol. 107, no. 15, pp. 6652–6657, 2010.

[40] X. Zhou, A. J. Davis, D. J. Kieber, et al., "Photochemical production of hydroxyl radical and hydroperoxides in water extracts of nascent marine aerosols produced by bursting bubbles from Sargasso seawater," *Geophysical Research Letters*, vol. 35, no. 20, Article ID L20803, 2008.

[41] J. L. Jimenez, M. R. Canagaratna, N. M. Donahue, et al., "Evolution of organic aerosols in the atmosphere," *Science*, vol. 326, no. 5959, pp. 1525–1529, 2009.

[42] K. Mopper and R. G. Zika, "Free amino acids in marine rains: evidence for oxidation and potential role in nitrogen cycling," *Nature*, vol. 325, no. 6101, pp. 246–249, 1987.

[43] P. J. Milne and R. G. Zika, "Amino acid nitrogen in atmospheric aerosols: occurrence, sources and photochemical modification," *Journal of Atmospheric Chemistry*, vol. 16, no. 4, pp. 361–398, 1993.

[44] K. Gorzelska and J. N. Galloway, "Amine nitrogen in the atmospheric environment over the North Atlantic Ocean," *Global Biogeochemical Cycles*, vol. 4, no. 3, pp. 309–333, 1990.

[45] S. W. Gibb, R. F. C. Mantoura, and P. S. Liss, "Ocean-atmosphere exchange and atmospheric speciation of ammonia and methylamines in the region of the NW Arabian Sea," *Global Biogeochemical Cycles*, vol. 13, no. 1, pp. 161–178, 1999.

[46] S. M. Murphy, A. Sorooshian, J. H. Kroll, et al., "Secondary aerosol formation from atmospheric reactions of aliphatic amines," *Atmospheric Chemistry and Physics*, vol. 7, no. 9, pp. 2313–2337, 2007.

[47] S. Angeling, D. T. Suess, and K. A. Prather, "Formation of aerosol particles from reactions of secondary and tertiary alkylamines: characterization by aerosol time-of-flight mass spectrometry," *Environmental Science and Technology*, vol. 35, no. 15, pp. 3130–3138, 2001.

[48] P. V. Tan, G. J. Evans, J. Tsai, et al., "On-line analysis of urban particulate matter focusing on elevated wintertime aerosol concentrations," *Environmental Science and Technology*, vol. 36, no. 16, pp. 3512–3518, 2002.

[49] D. A. Hansell and C. A. Carlson, *Biogeochemistry of Marine Dissolved Organic Matter*, Academic Press, New York, NY, USA, 2002.

[50] M. Johnson, R. Sanders, V. Avgoustidi, et al., "Ammonium accumulation during a silicate-limited diatom bloom indicates the potential for ammonia emission events," *Marine Chemistry*, vol. 106, no. 1-2, pp. 63–75, 2007.

[51] C. Müller, Y. Iinuma, J. Karstensen, et al., "Seasonal variation of aliphatic amines in marine sub-micrometer particles at the Cape Verde Islands," *Atmospheric Chemistry and Physics*, vol. 9, no. 24, pp. 9587–9597, 2009.

[52] K. Kawamura and F. Sakaguchi, "Molecular distributions of water soluble dicarboxylic acids in marine aerosols over the Pacific Ocean including tropics," *Journal of Geophysical Research*, vol. 104, no. D3, pp. 3501–3509, 1999.

[53] M. Claeys, W. Wang, R. Vermeylen, et al., "Chemical characterisation of marine aerosol at Amsterdam Island during the austral summer of 2006-2007," *Journal of Aerosol Science*, vol. 41, no. 1, pp. 13–22, 2010.

[54] C. D. O'Dowd, B. Langmann, S. Varghese, C. Scannell, D. Ceburnis, and M. C. Facchini, "A combined organic-inorganic sea-spray source function," *Geophysical Research Letters*, vol. 35, no. 1, Article ID L01801, 2008.

[55] H. Coe, J. D. Allan, M. R. Alfarra, et al., "Chemical and physical characteristics of aerosol particles at a remote coastal location, Mace Head, Ireland, during NAMBLEX," *Atmospheric Chemistry and Physics*, vol. 6, no. 11, pp. 3289–3301, 2006.

[56] S. R. Zorn, F. Drewnick, M. Schott, T. Hoffmann, and S. Borrmann, "Characterization of the South Atlantic marine boundary layer aerosol using an aerodyne aerosol mass

spectrometer," *Atmospheric Chemistry and Physics*, vol. 8, no. 16, pp. 4711–4728, 2008.

[57] J. D. Allan, D. O. Topping, N. Good, et al., "Composition and properties of atmospheric particles in the eastern Atlantic and impacts on gas phase uptake rates," *Atmospheric Chemistry and Physics*, vol. 9, no. 23, pp. 9299–9314, 2009.

Hindawi Publishing Corporation
Advances in Meteorology
Volume 2010, Article ID 612132, 14 pages
doi:10.1155/2010/612132

*Research Article*

# Polysaccharides, Proteins, and Phytoplankton Fragments: Four Chemically Distinct Types of Marine Primary Organic Aerosol Classified by Single Particle Spectromicroscopy

**Lelia N. Hawkins and Lynn M. Russell**

*Scripps Institution of Oceanography, University of California, San Diego, La Jolla, CA 92117, USA*

Correspondence should be addressed to Lynn M. Russell, lmrussell@ucsd.edu

Received 5 April 2010; Accepted 14 June 2010

Academic Editor: Markus D. Petters



Carbon-containing aerosol particles collected in the Arctic and southeastern Pacific marine boundary layers show distinct chemical signatures of proteins, calcareous phytoplankton, and two types of polysaccharides in Near-Edge Absorption X-ray Fine Structure (NEXAFS) spectromicroscopy. Arctic samples contained mostly supermicron sea salt cuboids with a polysaccharide-like organic coating. Southeastern Pacific samples contained both continental and marine aerosol types; of the 28 analyzed marine particles, 19 were characterized by sharp alkane and inorganic carbonate peaks in NEXAFS spectra and are identified as fragments of calcareous phytoplankton. Submicron spherical particles with spectral similarities to carbohydrate-like marine sediments were also observed in Pacific samples. In both regions, supermicron amide and alkane-containing particles resembling marine proteinaceous material were observed. These four chemical types provide a framework that incorporates several independent reports of previous marine aerosol observations, showing the diversity of the composition and morphology of ocean-derived primary particles.

## 1. Introduction

The transfer of organic components from the ocean surface to marine aerosol through bubble bursting was shown over 40 years ago [1–3]. These components, referred to as "marine primary organic aerosol" or marine POA [4], have been observed to contribute to organic mass in remote and coastal marine locations [3, 5–8]. In some cases, primary components have been observed to compose greater than 70% of measured submicron OC [6, 7]. The production of submicron particles from bubble bursting remains a key aspect of the global radiation budget because large particle sources are limited to continental and coastal regions [9]; yet the remote marine atmosphere covers more than half of the earth's surface. In remote regions, marine-derived particles have been estimated to account for up to 90% of cloud condensation nuclei (CCN) [10]. Decreases projected for Arctic sea ice extent in response to climate warming may contribute an additional 40–200 ng $m^{-3}$ of aerosol organic carbon (OC) by 2100 from a combination of increased surface ocean productivity and increased spatial extent of wave action [11]. This change in OC is significant considering that background concentrations of less than 1 $\mu$g $m^{-3}$ are common in the remote MBL [8, 10, 12–15].

In ocean surface waters, rising bubbles scavenge organic material that is transferred to the atmosphere as the bubble bursts [1, 16, 17]. Much of this scavenged organic material has been classified as "exopolymers," which are mostly composed of polysaccharides [18]. The potential for breaking waves to contribute organic mass to aerosol particles increases with the high concentration of surface active organic compounds and microorganisms enriched in the surface microlayer (SML), relative to the underlying water [19–21]. Observed enrichment factors (EFs) are several orders of magnitude for dissolved and particulate organic carbon (OC) and for specific components like bacteria and viruses. The production of sea spray from bubble bursting results in further enrichment of OC [8, 21, 22]. EFs for organic components in marine aerosol particles have been reported from 5 (viruses and bacteria) to over 100

(organic carbon) from the SML [8, 21]. Since the surface ocean is the primary source of marine POA, the types and relative contributions of organic compounds are expected to be similar. Chemical characterization of the SML and surface water has revealed that carbohydrates constitute 80% of TOC [23], although lipid and protein components have also been observed [21, 24]. Investigations of the composition of airborne marine organic particles have shown multiple lines of evidence for carbohydrates [5, 7, 8, 22, 25–27], amino acids [22, 28], and marine microorganisms [21, 25], confirming that many of the organic components found in the SML and surface ocean are transferred to the marine atmosphere. It is crucial for understanding the role of sea spray aerosol in marine aerosol-cloud interactions that we not only quantify the organic fraction but also characterize its composition, since the hygroscopicity of organic components varies so widely. One important question that remains is how these marine organic components are mixed in airborne particles, since the CCN activity of organic particles can be significantly altered by small amounts of soluble material [29].

To better characterize marine POA in the remote marine boundary layer, aerosol particles were collected during research cruises in the Arctic and southeastern Pacific oceans in local springtime. Single particle X-ray spectromicroscopy was used to separate individual particles into four distinct types of marine POA using organic functional groups, particle morphology, and elemental composition. The findings of this analysis are compared in the context of previous marine POA observations using a variety of analytical techniques.

## 2. Methods

*2.1. Sample Collection.* Ambient aerosol particles for Scanning Transmission X-ray Microscopy with Near-Edge X-ray Absorption Fine Structure (STXM-NEXAFS) analysis were collected in 2008 as part of the International Chemistry Experiment in the Arctic LOwer Troposphere (ICEALOT) and VAMOS Ocean Cloud Atmosphere Land Study Regional Experiment (VOCALS-REx) research cruises, using nearly identical sample collection techniques. The ICEALOT cruise through the North Atlantic and Arctic Oceans was conducted in March and April 2008 on the UNOLS R/V *Knorr* to investigate the composition and sources of atmospheric aerosol and gas phase species to the northern polar region. Detailed descriptions of the ICEALOT cruise track, sampled air mass histories, and related aerosol measurements are described in [8] and the associated supplementary material. All ICEALOT single particles presented here were collected north of 63°N; most particles were collected within the Arctic Circle (north of 66.56°N). In October and November 2008, the NOAA R/V *Ronald Brown* traveled in the southeastern Pacific Ocean in the region along 20°S as part of VOCALS-REx, a multiplatform campaign designed to investigate ocean-atmosphere interface processes and to probe aerosol-cloud interactions in the stratocumulus-topped MBL [30]. Details of the VOCALS-REx cruise track, sampled air mass histories, and aerosol chemistry are described in [15]. VOCALS-REx single particle samples were collected along the 20°S portion of the cruise track, including both coastal and remote marine locations. For simplicity, all ICEALOT particles will be referred to as "Arctic" and all VOCALS-REx particles will be referred to as "Pacific."

Particles were collected through a shared, isokinetic sampling inlet 18 m above sea level [31] and impacted onto silicon nitride windows ($Si_3N_4$, Silson, Ltd., Northampton, England) at 1 LPM (providing a 2.5 $\mu$m 50% efficiency size cut) using a rotating impactor (Streaker, PIXE International Corp., Tallahassee, FL). This impactor was located in a humidity-controlled enclosure; the relative humidity was below 30% during ICEALOT and was controlled at 55% during VOCALS-REx. Windows were sealed and stored frozen until analysis.

*2.2. Analysis*

*2.2.1. STXM-NEXAFS.* Particles were analyzed on Beamline 5.3.2 at the Advanced Light Source in Lawrence Berkeley National Laboratory (Berkeley, CA) at atmospheric temperature and under dry He (1 atm). Details of STXM-NEXAFS analysis of atmospheric aerosol particles are described in [32, 33], and a brief description is provided here. Image scans from 278 to 320 eV (with up to 0.2 eV resolution) of individual particles provide X-ray absorption spectra of the carbon K-edge, with characteristic peaks from various energy transitions of the bound carbon atoms. Organic and inorganic carbon-containing functional groups are identified by their specific absorption energy between 280 and 320 eV (Table 1). Potassium L-edge transitions also occur in this region. Only particles with measurable difference in absorbance between 280 and 292 eV (the carbon edge) are selected for image scans. Energy calibrations were performed within 48 hours of particle analysis using $CO_2$ as the reference material. All necessary adjustments were less than 0.05 eV. Absorption spectra from each pixel within the two-dimensional particle image are averaged and normalized following the procedure described in [33]. Spectra normalization entailed subtracting background absorbance (278–283 eV) followed by normalizing to total carbon content (301–305 eV). This normalization provides more uniform spectra for qualitative comparison. Image alignments were performed in Matlab (Mathworks Inc.) using a normalized cross-correlation algorithm implemented in the Matlab image-processing toolbox [33]. An automated algorithm for peak fitting [33] provides relative absorption of aromatic/alkene R(C=C)R′, ketone R(C=O)R′, alkyl $R(C–H)_nR'$, carboxylic carbonyl R(C=O)OH, alcohol R–COH, and carbonate $CO_3^{2-}$ carbon. Spherical-equivalent geometric diameter is used to approximate particle size and is equal to the diameter of a sphere having the same area as the sum of individual pixels with signal above the background level.

Individual particle spectra were clustered using a guided Ward clustering algorithm based on a training set of spectra from the 14 particle classes described in [32]. Following clustering, visual inspection of the resulting classes identified 4 spectra types whose class assignments did not accurately

Table 1: X-ray spectra carbon K-edge, near-edge, and postedge features.

| Component | Transition | Energy (eV) |
|---|---|---|
| Aromatic/alkene, R(C=C)R′ | C 1s-$\pi^*_{C=C}$ | 284.4–286.4[a] |
| Ketone, R(C=O)R′ | C 1s-$\pi^*_{C=O}$ | 286.2–290.9[a] |
| Alkyl, R(C–H)$_n$R′ | C 1s-$\sigma^*_{C-H}$ | 287.4–288.5[a] |
| Amide carbonyl, R–NH(C=O)R′ | C 1s-$\pi^*_{C=O}$ | 288.3 ± 0.2[b] |
| Carboxylic carbonyl, R(C=O)OH | C 1s-$\pi^*_{C=O}$ | 288.2–288.9 ± 0.3[a] |
| Alcohol, R–COH | C 1s-3p/$\sigma^*_{C-OH}$ | 289.5 ± 0.3[b] |
| Inorganic carbonate, $CO_3^{2-}$ | C 1s-$\pi^*_{C=O}$ | 290.4[a] |
| Alkyl, R(C–H)$_n$R′ | C 1s-$\sigma^*_{C-C}$ | 290.8–293[a] |
| Potassium, K | $L_{2,3}$ edges | 297.4 ± 0.2 and 299 ± 0.2[c] |

[a][34], [b][35], [c][36].

represent their spectral features. These spectra had not been observed in previous STXM-NEXAFS studies of atmospheric particles and therefore were not represented in the 14-class training set. The interpretation of these spectra is described in detail in Section 3.

*2.2.2. SEM-EDX.* Following STXM-NEXAFS analysis, a subset of analyzed carbon-containing single particles (11 particles) were investigated for elemental composition using Scanning Electron Microscopy with Energy Dispersive X-rays (SEM-EDX) at the Scripps Institution of Oceanography Analytical Facility (La Jolla, CA) using a model FEI Quanta 600 microscope at 10 keV. Samples were uncoated and were analyzed under moderate vacuum. All samples showed Si and N absorption due to the sample substrate. Identified elements include C, O, Ca, S, Na, Mg, and Cl.

## 3. Results and Discussion

Figure 1 shows the distribution of analyzed carbonaceous particles in Pacific and Arctic samples categorized by particle-average spectra. Nonmarine particle types include soil dust, combustion, and secondary particles. These particle types have been observed in previous measurements in urban locations (e.g., Mexico City) and areas affected by urban outflow (e.g., offshore China, the Caribbean, and the Pacific Northwest) [32]. Soil dust particles are characterized by carbonate, potassium, and carboxylic acid-containing organic components (Type "f" in [32]) and are attributed to air masses passing near Santiago and other urban areas along the arid Chilean coast before reaching the ship [15].

Combustion particles show strong aromatic/alkene absorbance at 285 eV and broad alkyl carbon absorption at 292 eV (similar to Type "d" in [32]). With one exception, these particles were submicron, and four out of eight particles were below 300 nm spherical equivalent diameter.

Table 2: Summary of observed marine particle types in southeast Pacific and Arctic samples.

| Type | No. of Marine Particles | |
|---|---|---|
| | Pacific | Arctic |
| Polysaccharide | | |
| with carboxylic acid (PsI) | 0 | 43 |
| without carboxylic acid (PsII) | 7 | 0 |
| Protein | 2 | 4 |
| Phytoplankton | 19 | 0 |
| Total | 28 | 47 |

Secondary type particles (type "a" in [32]) are characterized by broad carbon absorption beyond 300 eV and by carboxylic carbonyl absorption at 288.7 eV. In previous studies in marine locations, these particles have been the most commonly observed type [32]. In Pacific samples, however, much of the carboxylic acid-containing organic mass is associated with soil dust particles, consistent with measurements reported in [37] of internal mixtures of oxalic and malonic acids with mineral dust.

All organic particles not included in the soil dust, combustion, or secondary particle types were identified as marine origin and fell into four types: carboxylic acid-containing polysaccharides (Arctic), low-solubility polysaccharides (Pacific), calcareous phytoplankton fragments (Pacific), and proteinaceous material (Arctic and Pacific) (Table 2). Marine particles were observed in both Pacific and Arctic samples; however, most of the particles collected in the Arctic region were supermicron. The features and interpretation of the NEXAFS spectra and STXM morphology of particles in each marine type are discussed in detail in the following sections. In addition, three Pacific particles were identified with carbonate and potassium absorption but without any signatures of organic carbon. Their spectra are very similar to type "E" particles found in ocean sediments in [38], which were identified as marine calcium carbonate. These particles are labeled "$CaCO_3$" in Figure 1 but are not included below since they lack organic components.

*3.1. Carboxylic Acid-Containing Polysaccharides on Sea Salt.* Figure 2(a) shows single particle spectra (and category average) for the most commonly observed marine particle type. Spectra in this category have strong carboxylic carbonyl peaks and weak alcohol, carbonate, and potassium peaks. These particles were seen in Arctic samples and compose 43 of the 48 analyzed Arctic particles. Two particles collected at a coastal site in California, which is frequently influenced by marine air masses, also share these features [39]. This particle type is distinct from Type "a" particles in [32] in the stronger contribution of the carboxylic carbonyl peak and the broad alkyl absorption near 293 eV. Filter measurements of submicron particles from the Arctic show a large contribution from alcohol (C–OH) groups to OM attributed to marine carbohydrate-like compounds [8], consistent with previous chemical characterization of the surface microlayer as 80% carbohydrate [23] and with exopolymer

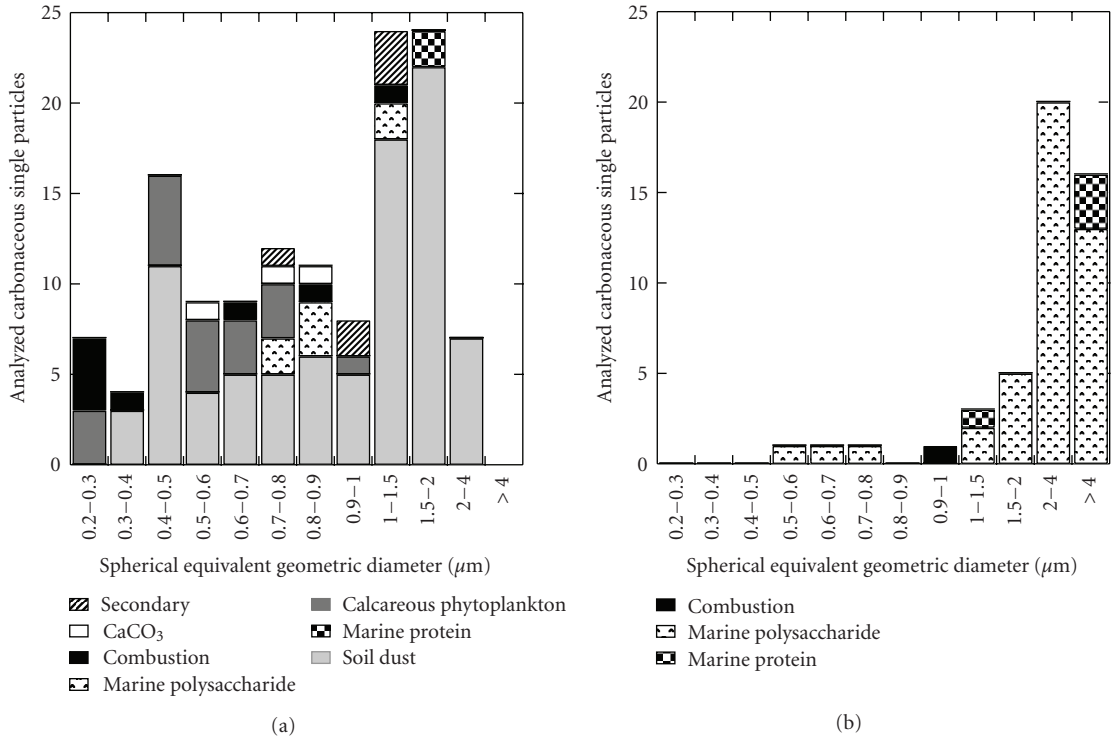


Figure 1: Distribution of the number of analyzed particles from (a) southeastern Pacific and (b) Arctic marine boundary layers. Particles labeled as "marine polysaccharide" in Arctic samples correspond to Figure 2(a) (PsI) while those in southeastern Pacific samples correspond to Figure 2(b) (PsII). Particle frequency for the collected samples is partly a result of sampling bias and does not represent the observed particle size distribution.

secretions (EPSs) repeatedly identified in submicron marine aerosol [7, 25–27]. Just under 90% of the observed Arctic supermicron particles do not show a significant peak at 289.5 eV (C–OH transition), which is different from most of the reported carbohydrate reference spectra [35]. A fraction of these observed spectra do have a shoulder located near 289.5 eV; yet all spectra are dominated by a large peak near 288.7 eV (carboxylic carbonyl). Relative NEXAFS absorption of carboxylic carbonyl and alcohol groups in acid-group-containing reference polysaccharides shows a similar trend; for example, muramic acid and alginic acid show stronger carboxylic carbonyl ($\pi^*$ transition) peaks than alcohol ($\sigma^*$ transition) peaks [35] despite the fact that the molar ratio of carboxylic acid to alcohol groups is 0.33 in muramic acid and 0.5 in alginic acid. These compounds are found in bacterial (muramic) and brown algae (alginic) cell walls as structural polysaccharides. Glucuronic acid is another carboxylic acid containing component of polysaccharides that shows strong carboxylic carbonyl absorption (288.65 eV) [35].

Alginic acid is a relevant example for marine POA since the brown algae family includes giant kelp and seaweed found in cold, northern hemisphere oceans [40]. Figure 3 shows the similarities between the average spectrum of particles in this category and an alginic acid reference spectrum [41]. Both spectra show a strong, narrow peak at 288.7 eV and a weaker, broad absorption at 293 eV, without any other organic carbon peaks. Carbonate and potassium absorbances in the average carboxylic acid-type spectrum can be attributed to the sea salt associated with these particles. Many of the particles in this type were characterized by inorganic cuboid structures with an uneven, organic coating (Figure 4(a)), which also were absent in the previously observed secondary particles. EDX spectra of four particles from this class are shown in Figure 5 of Russell et al. [8]; observed peaks include Na and Cl for all four particles. This small amount of organic relative to crystallized sea salt is consistent with the lower organic enrichment expected for supermicron particles rather than submicron particles. This morphology suggests that the organic components on these particles are more soluble than previously reported polysaccharides, which are generally colloidal spherules not associated with sea salt [25–27]. The association with seawater components is also consistent with the assignment of these particles as carboxylic acid-containing polysaccharides like alginic acid, since it has a strong tendency to take up water. These particles are referred to as "Type I polysaccharides" or PsI.

*3.2. Low-Solubility Polysaccharides.* Figure 2(b) shows single particle spectra (and category average) for particles with visible alcohol C–OH absorption (289.5 eV) accompanied by aromatic, ketonic, and carboxylic carbonyl carbon peaks found only in Pacific samples. Here the carboxylic carbonyl absorption is approximately equal to the alcohol carbon absorption. Reference polysaccharides with equivalent peak heights at or near 288.7 (carboxylic carbonyl) and

Table 3: Observed types of marine primary organic aerosol and the suggested biological relevance of specific particle types.

| Location | Method(s) | Particle Size | Dominant Component(s) or Spectral Feature | Biological Relevance |
|---|---|---|---|---|
| | | Polysaccharides | | |
| Arctic[a] | TEM, | <100 nm | Colloidal spherules | EPS gels |
| Various[b] | TEM | <1 $\mu$m | Colloidal spherules | EPS gels |
| | X-ray backscatter, and solubility | | | |
| Mediterranean Sea and Long Island Sound[c] | Alcian blue dye | 1–50 $\mu$m | Semi-transparent colloids | Polysaccharides |
| W. Pacific[d] | TEM, | <50 nm | Colloidal spherules | EPS gels |
| | SEM with X-ray backscatter, and solubility | | | |
| North Atlantic[e,*] | HNMR (WSOC and WIOC) | 60–1000 nm | Hydroxylate aliphatics | Lipopolysaccharides |
| | | | Lipid-like aliphatics | |
| Arctic[f] | FTIR spectroscopy | <1 $\mu$m | Organic hydroxyl groups | Polysaccharides |
| | | | Alkane groups | |
| SE Pacific[g] | FTIR spectroscopy | <1 $\mu$m | Organic hydroxyl groups | Polysaccharides |
| SE Pacific[h] | STXM-NEXAFS | <1 $\mu$m | Organic hydroxyl groups | Polysaccharides |
| Arctic[h] | STXM-NEXAFS | >1 $\mu$m | Carboxylic acid groups | Polysaccharides |
| | | Protein and amino acid compounds | | |
| Arctic[i] | TEM and Extraction | >50 nm | Hydrophobic organic aggregates | Amino acids |
| Mediterranean Sea and | HPLC and | not provided | Asp, Glu, Ser, Ala | Amino acids |
| Long Island Sound[c] | Coomassie Blue dye | 1–50 $\mu$m | Semi-transparent colloids | Proteins |
| Arctic[h] | STXM-NEXAFS | >1 $\mu$m | Alkane and amide groups | Protein |
| SE Pacific[h] | STXM-NEXAFS | >1 $\mu$m | Alkane and amide groups | Protein |
| | | Micro-organisms and their fragments | | |
| Arctic[i] | TEM and Extraction | 400 nm | | Bacteria and diatoms |
| Arctic[a] | TEM, | 200–5000 nm | | Micro-organisms and fragments |
| | X-ray backscatter, and solubility | | | |
| W. Pacific[d] | TEM, | >400 nm | $CaCO_3$ | Coral-related |
| | SEM with X-ray backscatter, and solubility | 3.7 to 7.5 $\mu$m | | Bacteria |
| SE Pacific[h] | STXM-NEXAFS | <1 $\mu$m | $CaCO_3$ and alkane groups | Calcareous phytoplankton fragments |
| | | None listed | | |
| Tasmania[j] | PALMS | >160 nm | Organic mass fragments | |
| Arctic[k] | TEM | >100 nm | Organic liquid | Proteins |
| Ireland[l] | IC, | <1.5 $\mu$m | WIOC (not characterized) | |
| | EGA, | | WSOC (aliphatic groups | |
| | HNMR, | | near heteroatoms, HULIS, | |
| | and TOC | | and partially oxidized species | |

*HNMR characterized aerosol was generated in a laboratory setting from collected seawater.
[a][25], [b][26], [c][22], [d][27], [e][7], [f][8], [g][15], [h]This work, [i][28], [j][14], [k][42], [l][6].

289.5 eV (alcohol) include chitin and L-rhamnose [35]. Chitin does not contain any carboxylic carbonyl groups but does contain amide carbonyl groups (monomers are N-acetylglucosamine) which may be responsible for the peak at 288.4 eV. Glucosamine is also present in a 1 : 1 ratio with muramic acid monomers in peptidoglycan, which has been shown to be a major constituent of marine dissolved organic matter (DOM) [43]. Therefore, the observed peak in the average alcohol-type spectrum near 288.7 eV could be attributed either to carbonyl in amide groups or to a mixture with carboxylic carbonyl-containing polysaccharides. It is more probable that these particles contain a mixture of structural polysaccharides than isolated compounds, resulting in less pronounced spectral features than the reference spectra. In fact, the most similar spectrum to the category average comes from a sediment sample of marine particulate organic matter (POM, [38]) (Figure 3). [38] used factor analysis to separate different biological compounds in marine POM, and one factor with significant C–OH absorption was identified as carbohydrate material. The carbohydrate-containing marine POM shares the aromatic and ketonic carbon absorbances with the spectra of these particles, while reference (pure) structural polysaccharide spectra in [35] do not. Particles of this type are referred to as "Type II polysaccharides" or PsII.

Filter-based FTIR spectroscopic measurements of Pacific submicron particles show a significant contribution from marine OM (from factor analysis) that is most prominent in sampled air masses with low $PM_1$ particle mass ($<1\,\mu g\,m^{-3}$) and with low radon concentration ($<200\,mBq\,m^{-3}$), indicating little continental influence [15]. Complementary ion chromatography (IC) measurements show low concentrations of submicron $Na^+$ ($<0.1\,\mu g\,m^{-3}$) or $Cl^-$ ($<0.07\,\mu g\,m^{-3}$), which is consistent with the relatively calm seas encountered during the cruise. PsII particles are spherical, with no cuboidal inorganic core (Figure 4(b)), similar to the spherical colloidal structures observed in TEM by [25–27]. The lack of cuboids is consistent with the lower fraction of Na/OM expected in submicron particles [44].

*3.3. Calcareous Phytoplankton Fragments.* Figure 2(c) shows single particle spectra (and category average) for particles with three strong, narrow peaks at 288.1, 290.4, and 292 eV associated with alkyl $R(C–H)_nR'$ ($\pi^*$), inorganic carbonate $CO_3^{2-}$ ($\pi^*$), and alkyl $R(C–H)_nR'$ ($\sigma^*$) transitions, respectively. These particles were strictly submicron and found in Pacific samples. A particle with this same characteristic signal was also found in a sample collected at a California coastal site [39]. Compared with all other particle-average spectra, these spectra have much stronger signal-to-noise and have little particle-to-particle variability. These particles also have very little pre-edge absorbance indicating that they are entirely composed of the absorbing (carbonaceous) material, consistent with their strong signal. The narrow alkyl peaks indicate little variation in the neighbors of the absorbing alkyl carbon atoms (e.g., straight-chain alkane compounds) as does the absence of other organic carbon peaks.

The carbonate peak at 290.4 eV is also strong and narrow, indicating that other than the long-chain hydrocarbon compounds, the particle is mostly some form of carbonate. The reference spectrum for $CaCO_3$ is shown in Figure 3. $CaCO_3$ shares the sharp peak at 290.4 eV and the multiple, broad peaks to the right of 295 eV with the average spectrum. To determine the type of carbonate-based mineral, 6 of the 19 particles in this category were analyzed with SEM-EDX; all particles showed strong C, O, and Ca signals while S, Na, Mg, and Cl were absent or weak (Figure 5(c)). These particles show a variety of nonspherical shapes. Some particles appear elliptical with sharp points (Figure 4(c)) and others are amorphous. Based on their appearance, the particles resemble small, dust-like fragments. However, their chemical composition is not consistent with aged or processed dust transported to the remote MBL. In addition, long-chain hydrocarbons are not typical of secondary organic aerosol [45]; the absence of S in EDX spectra also makes it unlikely that atmospheric processing is responsible for the majority of organic mass in these particles.

Previous observations of excess $Ca^{2+}$, relative to sea salt ratios, in marine aerosol have been attributed to fragments of calcium carbonate-producing phytoplankton (coccolithophores) emitted to the atmosphere during bubble bursting [46]. Other possible sources of elevated calcium include EPS, which have been shown to incorporate calcium in gel formation [47]. These single-celled phytoplankton produce delicate, calcium carbonate scales (coccoliths) that continually slough off the organisms during their growth and that are released during predation [48]. These scales are oval-shaped and are typically 500–3000 nm in length, resulting in fragments that are consistent with the observed size range of these alkane/carbonate particles. Coccolithophores (especially Emiliania huxleyi) are abundant in both high- and low-latitude oceans and are responsible for about half of the total oceanic carbonate production [49]. Their blooms are so large and persistent that they can been seen from space in satellite images of ocean color as patches of light green against the dark blue ocean. A recent study measuring whole coccolithophores, detached scales, and calcite fragments in surface waters in the same region as the VOCALS-REx cruise has documented their abundance in the Peru-Chile Upwelling (PCU) and the South Pacific Gyre (SPG) [49]. The measured seawater carbonate particle surface area distribution in their work showed a large peak between 2 and 3 $\mu$m (corresponding to whole coccoliths with diameters between 1.6 and 2 $\mu$m) and a smaller peak at 250 nm (corresponding to coccolith fragments with diameters around 560 nm). This smaller mode is consistent with the size range of observed particles in this category.

In addition to producing a large fraction of oceanic carbonate, coccolithophores are known to produce extremely stable, lipid-like compounds called alkenones ($nC_{37}$–$C_{39}$), which contain one ketone group and two or three degrees of unsaturation [50]. Although the exact function of these compounds is unknown, an investigation of alkenones in various organelles and membranes of Emiliania huxleyi has shown that they are predominantly located in the coccolith-producing compartment (CPC) of the cell and are most likely

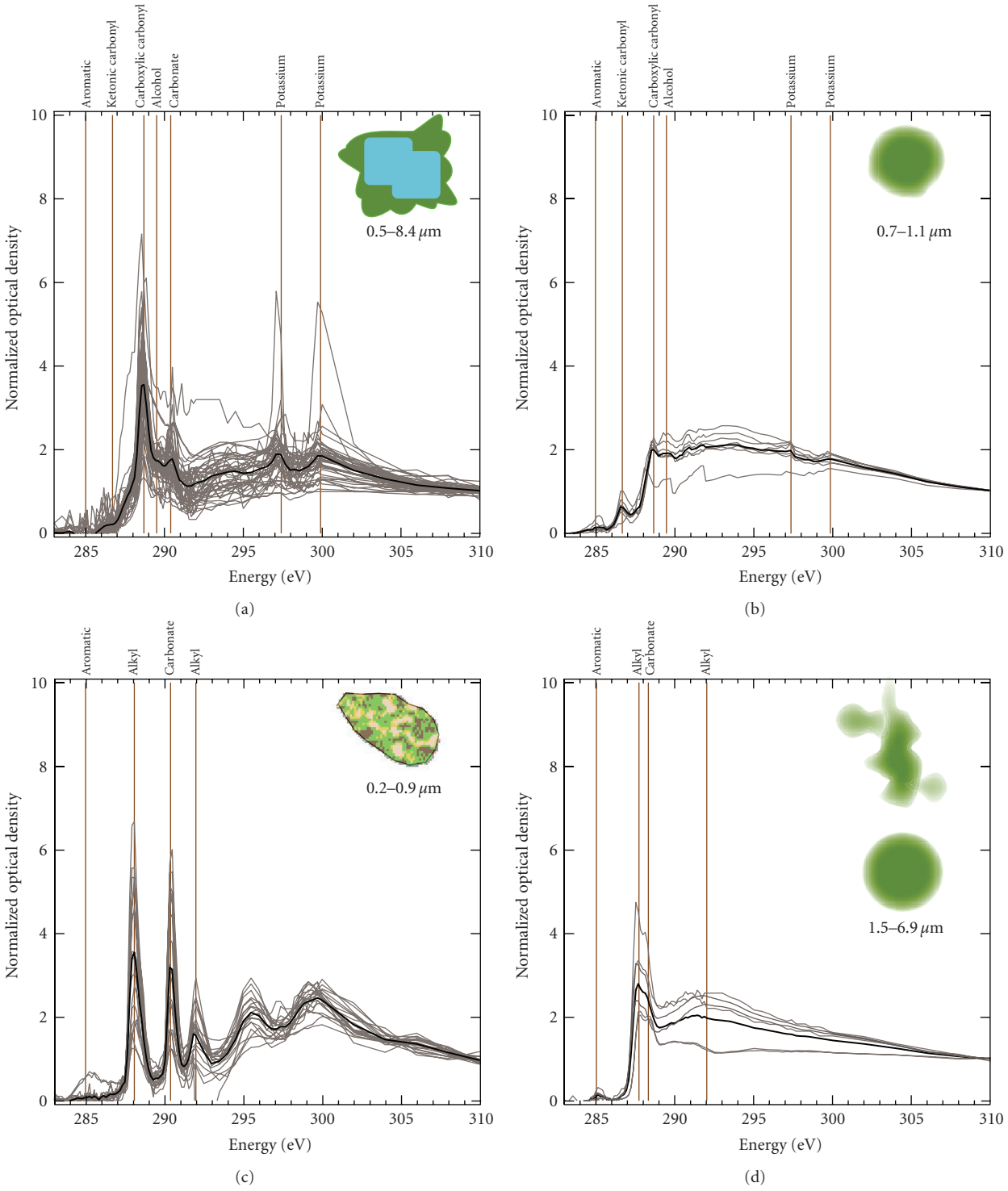


Figure 2: Individual (grey) and average (black) NEXAFS spectra of the four marine particle types including (a) PsI, (b) PsII, (c) calcareous phytoplankton fragments, and (d) proteinaceous particles. Illustrations in each panel represent commonly observed morphologies associated with each spectra type. The observed size range for each type is shown below the illustrations.

membrane-unbound lipids associated with the function of the CPC [51]. The coproduction of these long-chain alkanes with calcite coccoliths is consistent with the strong, sharp alkyl peaks present in our alkane/carbonate particle spectra and with the absence of other groups, such as carboxylic acids. Coproduction would also result in a similar ratio of the two species (alkane and carbonate) over the particle, rather than separate carbonate and alkane-dominated regions. Figure 5(b) shows the pixel-by-pixel normalized alkane absorption compared with normalized carbonate

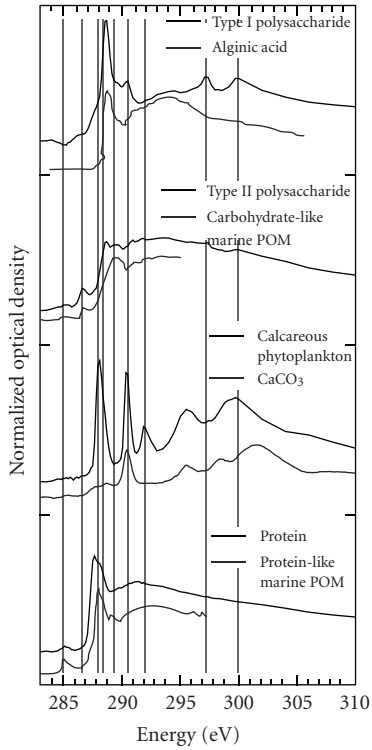


Figure 3: Normalized average spectra for each of the four marine particle types and (below) corresponding reference spectra with similar features. Spectra were reproduced from [41] (alginic acid), [38] (carbohydrate and protein-like marine POM), and http://xray1.physics.sunysb.edu/~micros/xas/xas.html, unpublished ($CaCO_3$). Vertical grey lines mark relevant transitions (from left to right): 285 eV (R(C = C)R′), 286.7 eV (R(C=O)R′), 288.1 eV ($R(C–H)_nR'$), 288.3 eV (R–NH(C=O)R′), 289.5 eV (R–COH), 290.4 eV ($CO_3^{2-}$), 292 eV ($R(C–H)_nR'$), 297.4 eV (K), and 299 eV (K).

absorption for each of the 19 alkane/carbonate-type particles. Correlations between these two groups are strong (12 of the 19 particles have $r > 0.75$). These strong correlations demonstrate the uniformity of the two groups over individual particles, though the relative amounts of alkane and carbonate groups (i.e., the fitted slopes) vary among particles. Given these observations, the alkane/carbonate particles will be referred to as "Calcareous phytoplankton fragments" in the remaining sections.

*3.4. Proteinaceous Particles.* Figure 2(d) shows single particle spectra (and category average) for particles with aromatic/alkene, alkyl, and amide carbon absorptions at 285, 287.7, and 288.2 eV, respectively. The aromatic/alkene peak at 285 eV has a shoulder at 285.4 eV in all 6 particles indicating the presence of multiple unsaturated carbon environments. These spectra, like the calcareous phytoplankton spectra, have low noise and are quite similar to one another in terms of peak locations, shapes, and relative peak heights. Unlike the other categories, particles with this signature are found in both Arctic and Pacific samples but with slightly different morphologies. The two Pacific particles are spherical and all four of the Arctic particles are loose agglomerations of carbonaceous material (Figure 4(d)). The most unique feature of these spectra is the shoulder at 288.2 eV, corresponding to carbonyl carbon in an amide group [34, 35]. Amide groups have also been identified from the CNH $\sigma^*$ transition at 289.5 eV [34, 52]. Amide groups (known as peptide bonds when found in proteins) are formed from dehydration reactions of the carboxylic acid group of one amino acid monomer and the amine group of another. Therefore, reference spectra for amino acids that have strong carboxyl carbonyl absorption [35] are not representative of bound amino acid monomers in proteins. The broad alkyl absorption near 292 eV indicates that a variety of alkyl carbon environments exist in these particles, contrasting the sharp peak at 292 eV in the calcareous phytoplankton fragments. In addition, the presence of two alkyl carbon peaks and the absence of the carboxylic carbonyl peak indicate that these proteinaceous compounds may be related to lipoproteins that are found in the membranes of chloroplasts. Lipoproteins contain both lipid and protein components and could be responsible for the significant alkyl absorption seen here. Aromatic and alkene groups are found in proteins as well. Phenylalanine, tyrosine, histidine, and tryptophan are all amino acids with aromatic or alkene side groups.

The fourth pair of spectra in Figure 3 show the spectral similarities between the average amide-type particle spectrum and the protein-like component of marine POM identified in [38]. The two spectra share the small shoulder at 285.4 eV and the amide and broad alkyl absorption regions. However, the amide-type average spectrum has more $\pi^*$ alkyl absorption (287.7 eV) (which is associated with long-chain hydrocarbons such as lipids) than the protein-like marine POM. The lipid component may give these particles more surface active properties and may result in preferential concentration in the surface microlayer. If this is the case, lipid-containing proteinaceous material would be preferentially transferred to the atmosphere during bubble bursting over nonlipid proteinaceous compounds. The particle images in this type, both spherical and agglomerative, show little evidence of sea salt, which is consistent with hydrophobic organic material. In collocated filter measurements of both Pacific and Arctic MBL air masses, primary amines composed 8% of marine OM (from factor analysis). In fact, primary amine groups have been identified in marine OM factors from all ambient measurements where marine factors were identified [8]. That the Pacific and Arctic proteinaceous POA spectra are indistinguishable reflects the apparent chemical similarity of the protein components in marine POA.

*3.5. Reconciling Marine POA Observations.* Over 10 years of measurements of marine POA are summarized in Table 3; although the collection encompasses particle properties determined from diverse techniques from TEM-EDX to HNMR, most observations can be assigned to one of three main types: (1) polysaccharides, (2) proteins and amino acids, or (3) microorganisms and their fragments. Figure 6 illustrates the three main types and their surface

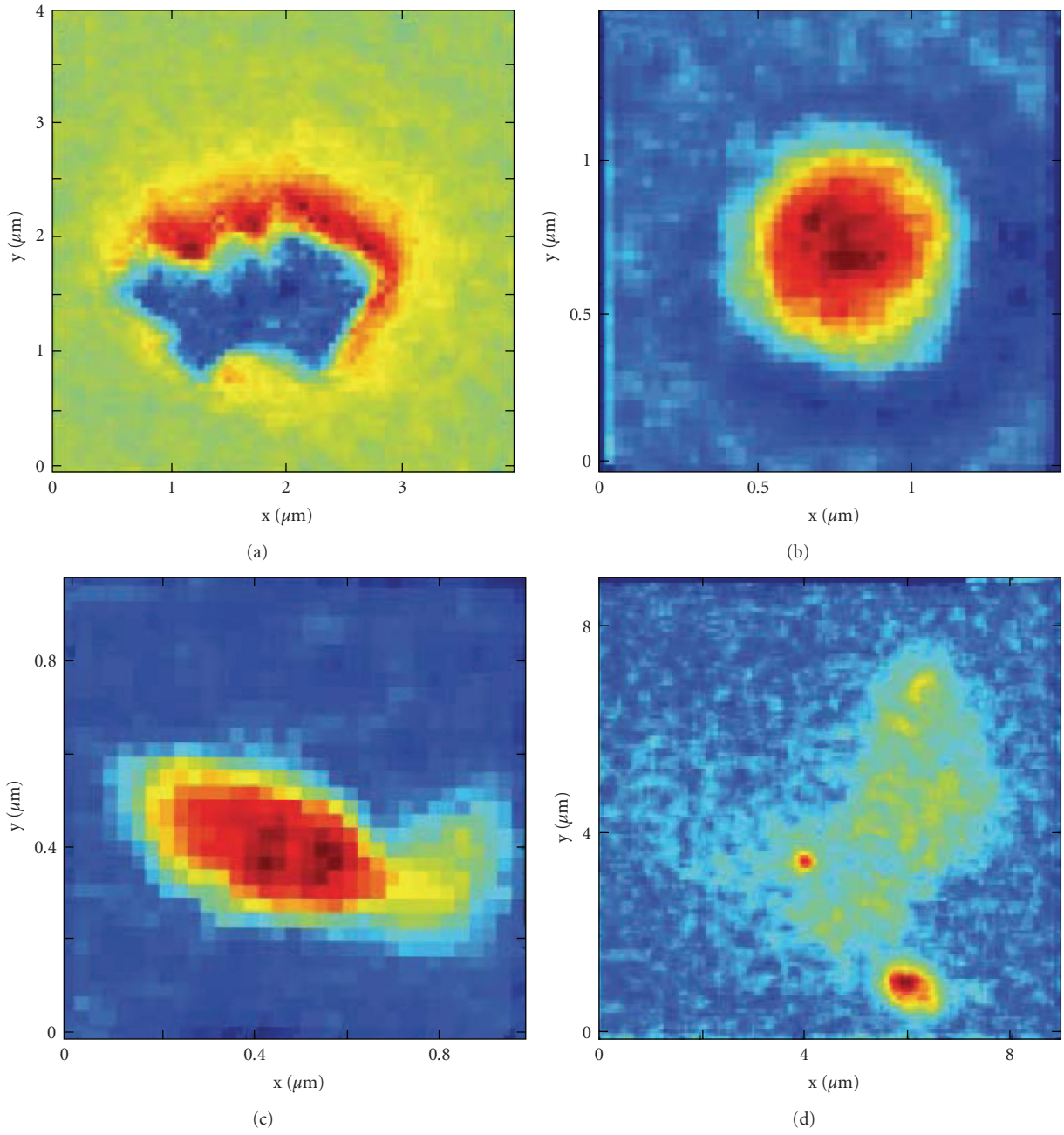


FIGURE 4: Relative carbon images of representative particles for (a) PsI, (b) PsII, (c) calcareous phytoplankton, and (d) proteinaceous particle types. For each image, the red-blue color scale is relative to individual particle carbon absorption, where red denotes the maximum carbon absorption and blue denotes the minimum.

ocean counterparts using the four types of marine POA particles observed in this study. The chemical characterization of single marine POA particles suggests that biogenic organic components and microorganisms observed in this and previous studies are present as an external mixture including—but not limited to—polysaccharides, proteins, and microorganisms.

Using TEM images of colloidal spherules, X-ray backscatter of elemental components, and tests for solubility, Leck and Bigg [25, 26] deduced that the hydrated, heat-resistant, hydrophobic organic substance present in submicron marine aerosol was related to exopolymer secretions (EPSs), which are high molecular weight, hydrated polysaccharides. This finding was consistent with numerous reports of large concentrations of EPS in surface ocean water [18, 47]. The colloidal structure of the hydrophobic particles is also consistent with the observation of gel formation from the marine EPS [47, 53]. Although the attributes of their measurements of particle shape, size, and solubility were consistent with EPS characteristics, little chemical evidence was available

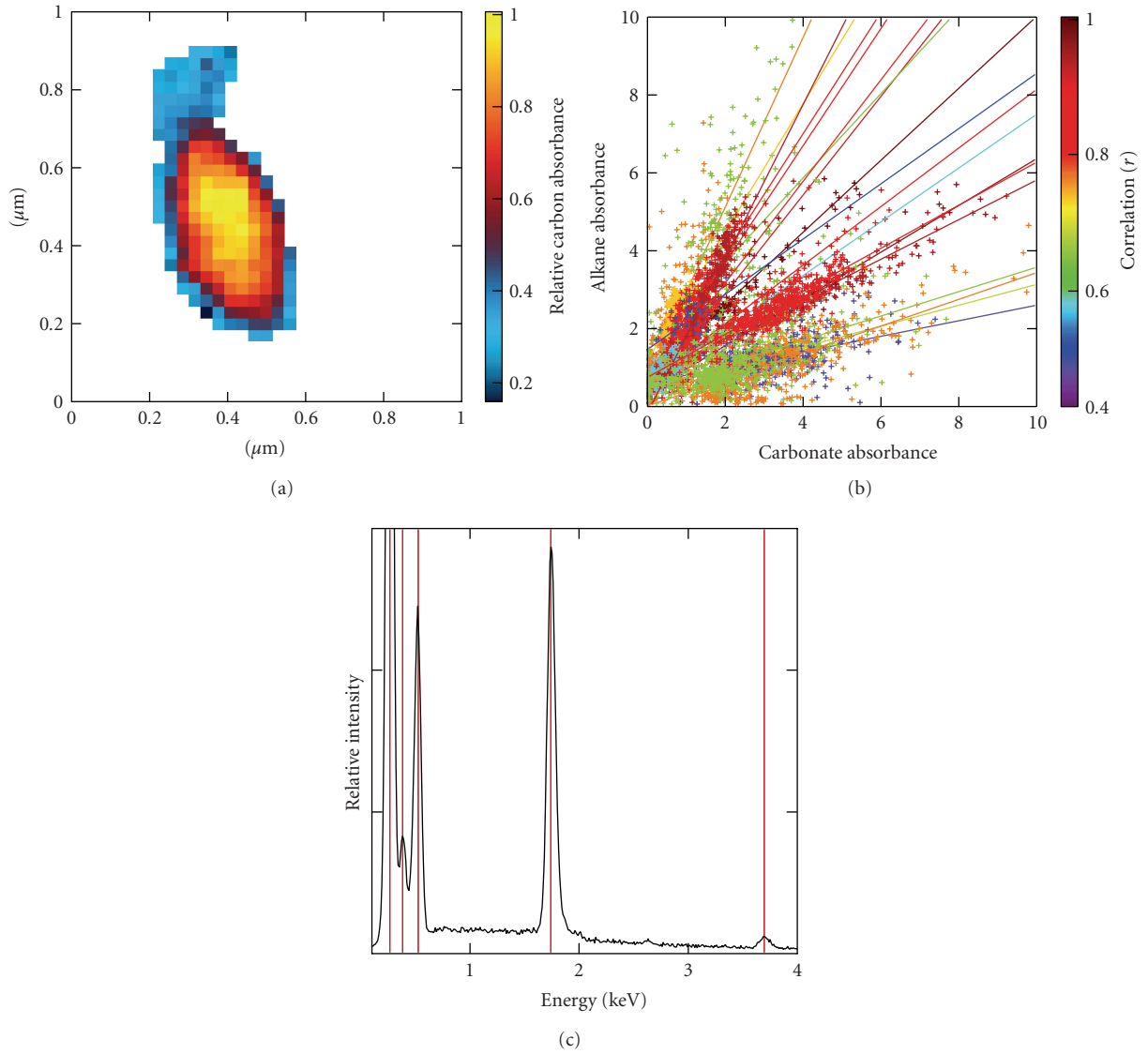


Figure 5: (a) Relative carbon absorbance per pixel from integrated NEXAFS particle-average spectrum for a calcareous phytoplankton fragments. (b) Alkane absorbance compared with carbonate absorbance for pixel-by-pixel fit of NEXAFS spectra of all calcareous phytoplankton type particles. Markers are colored by the correlation coefficient for each least-squares linear regression (one color per particle). (c) EDX spectrum of the same particle at 10 keV accelerating voltage. Vertical red lines mark the C, N, O, Si, and Ca absorbances from left to right. N and Si absorbances are from the sample substrate.

to confirm their composition as polysaccharides. Near the same time, ambient marine particles from the Mediterranean and Atlantic were shown to contain polysaccharide-rich gels using Alcian blue dye, a stain sensitive to all types of polysaccharides [22]. EI-MS measurements of marine aerosol in the western Pacific also showed substantial contributions from carbohydrates (i.e., levoglucosan and glucose) partially attributed to organics from the ocean surface [5]. A subsequent HNMR study of laboratory-generated aerosol (using North Atlantic seawater) corroborated the presence of polysaccharide-like organic components in marine POA by reporting aliphatic and hydroxylated functional groups in addition to lipid-like signatures [7]. The authors proposed lipopolysaccharides as a possible explanation for the observed groups. Evidence that polysaccharides accounted for 44–61% of marine submicron OM was provided in Russell et al. [8] using FTIR spectroscopy. Their work used the chemical similarity of alcohol C–OH groups in ambient marine submicron aerosol with reference FTIR spectra of 11 different polysaccharides (e.g., pectin, glucose, and xylose). That study was the first to report large quantities of specific signatures of polysaccharides associated with sea salt in submicron ambient marine aerosol, consistent with both the physical attributes reported in [25, 27] and the chemical signatures of simulated marine aerosol in [7]. Using single particle spectromicroscopy, we have observed that polysaccharide-containing particles make up a majority of the measured carbonaceous single particles in two marine

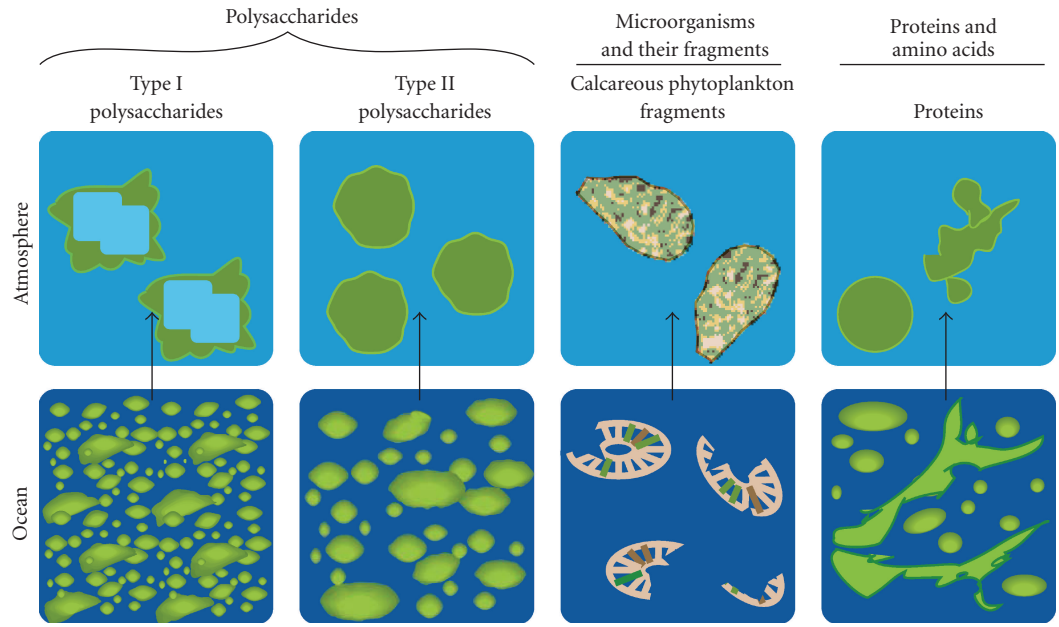


Figure 6: Illustration of the four observed marine particle types in the ocean and atmosphere.

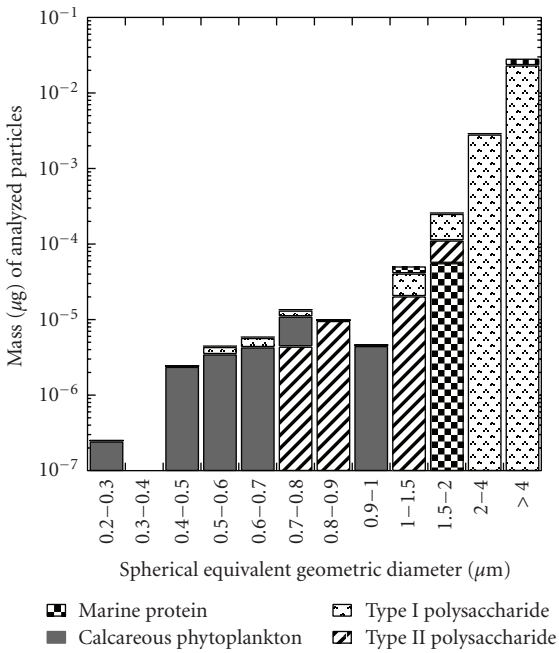


Figure 7: Estimated mass of marine particle types from both Arctic and Pacific samples.

regions. From these single particle measurements we have also estimated the mass distribution of Arctic and Pacific marine particles, using the spherical equivalent diameter approximated for each particle and an average density of $1\,\mu g\,m^{-3}$ (for simplicity). Figure 7 shows the combined, approximate mass distribution of Arctic and Pacific marine POA. Together, Type I and II polysaccharides compose 57% of measured submicron particle mass (and 83% of total particle mass), consistent with the observations of [8]. We also show that multiple types of polysaccharides, including water-insoluble compounds resembling chitin, exist in airborne marine particles.

Prior to the discovery of polysaccharides in marine aerosol, TEM analysis of Arctic submicron aerosol particles indicated that the spherical, hydrophobic organic particles could be related to amino acids (i.e., L-methionine) based on the surface active nature of the aerosol particles and on measurements of surface active proteins being scavenged by bubbles in seawater [28]. However, the same properties attributed to proteins in Leck and Bigg [28] could also be attributed to EPS [25–27]. More recently, Kuznetsova et al. [22] used Coomassie blue dye to confirm that some of the colloidal gel-like material surrounding bacteria and virus in Mediterranean and Atlantic marine aerosol samples was indeed proteinaceous. Here we report observations of amide-containing hydrophobic marine aerosol particles from two distant ocean environments that match the characteristic spectral signatures of proteinaceous marine POM, indicating that protein-like organic compounds also contribute to marine POA in many parts of the marine atmosphere.

Marine microorganisms clearly play a large role in marine aerosol formation and composition. In addition to secreting nonvolatile organic components (e.g., polysaccharides, lipids, and proteins) and emitting gas phase precursors to marine aerosol (e.g., dimethyl sulfide, DMS), they can themselves be lofted to the atmosphere where they can serve as surfaces for heterogeneous reactions and as cloud condensation nuclei [1, 21, 25, 28]. Most observations of airborne microorganisms have reported bacteria or diatom fragments,

mostly because these particles have distinct shapes easily discernible from other particles in TEM images. Submicron fragments, especially if mixed with gel-like organic material concentrated in the surface microlayer, are extremely difficult to identify based solely on morphology. SEM coupled with EDX can confirm the presence of C, O, and nutrient-affiliated elements like N and P but cannot provide the chemical specificity needed to identify the components of intact cell walls, chloroplasts, or other organelles. For this, X-ray spectromicroscopy is well-suited [38, 41]. Using STXM-NEXAFS we have identified submicron fragments of calcareous phytoplankton (coccolithophores) previously suggested to contribute significant quantities of nss-Ca in MBL aerosol [46]. The unique signature of $CaCO_3$ coupled with straight-chain alkane groups in the average spectra was combined with subparticle resolution spectra—confirming the uniform distribution of the two components—to support the classification of these particles as biological.

## 4. Conclusion

Ambient sub- and supermicron marine aerosol particles were collected in Pacific and Arctic marine boundary layers and subsequently analyzed using single particle STXM-NEXAFS, revealing four distinct types of marine POA. Although two-thirds of marine particles were characterized as polysaccharides, important differences exist even among those seemingly similar biogenic compounds, including the association with sea salt and the inferred differences in hygroscopicity. We also report evidence of proteinaceous compounds and the first observation of calcifying phytoplankton in marine POA.

In previous chemical characterizations of marine aerosol, most observations of marine POA show either hydrophobic, polysaccharide-like material or morphologically distinct microorganisms (i.e., bacteria and diatoms). The particles presented here, while consistent with those observations, provide a more detailed, chemically specific picture of marine aerosol that resolves some of the uncertainties associated with previous observations. These observations also confirm that multiple, distinct types of marine particles are emitted to the atmosphere as external mixtures.

## Acknowledgments

This work was supported by NSF Grant ATM-0744636. The authors thank George Flynn for providing the calcium carbonate reference spectrum. The authors would like to acknowledge Satoshi Takahama and Shang Liu for contributing to the analysis of single particles by STXM-NEXAFS and David Kilcoyne at Beamline 5.3.2 for technical assistance with beamline operation. They would also like to thank Derek Coffman, James Johnson, Drew Hamilton, and Catherine Hoyle for their assistance in sample collection and analysis as well as the captain and crew of the NOAA R/V *Ronald Brown* and the UNOLS R/V *Knorr* for their support in the field.

## References

[1] D. C. Blanchard, "Sea-to-air transport of surface active material," *Science*, vol. 146, no. 3642, pp. 396–397, 1964.

[2] E. J. Hoffman and R. A. Duce, "Factors influencing the organic carbon content of marine aerosols: a laboratory study," *Journal of Geophysical Research*, vol. 81, no. 21, pp. 3667–3670, 1976.

[3] R. B. Gagosian, O. C. Zafiriou, E. T. Peltzer, and J. B. Alford, "Lipids in aerosols from the tropical North Pacific: temporal variability," *Journal of Geophysical Research*, vol. 87, no. 13, pp. 11113–11144, 1982.

[4] M. Kanakidou, J. H. Seinfeld, S. N. Pandis et al., "Organic aerosol and global climate modelling: a review," *Atmospheric Chemistry and Physics*, vol. 5, no. 4, pp. 1053–1123, 2005.

[5] K. K. Crahan, D. A. Hegg, D. S. Covert et al., "Speciation of organic aerosols in the tropical mid-Pacific and their relationship to light scattering," *Journal of the Atmospheric Sciences*, vol. 61, no. 21, pp. 2544–2558, 2004.

[6] F. Cavalli, M. C. Facchini, S. Decesari et al., "Advances in characterization of size-resolved organic matter in marine aerosol over the North Atlantic," *Journal of Geophysical Research D*, vol. 109, no. 24, pp. 1–14, 2004.

[7] M. C. Facchini, M. Rinaldi, S. Decesari et al., "Primary submicron marine aerosol dominated by insoluble organic colloids and aggregates," *Geophysical Research Letters*, vol. 35, no. 17, p. 5, 2008.

[8] L. M. Russell, L. N. Hawkins, A. A. Frossard, P. K. Quinn, and T. S. Bates, "Carbohydrate-like composition of submicron atmospheric particles and their production from ocean bubble bursting," *Proceedings of the National Academy of Sciences of the United States of America*, vol. 107, no. 15, pp. 6652–6657, 2010.

[9] C. H. Twohy, M. D. Petters, J. R. Snider et al., "Evaluation of the aerosol indirect effect in marine stratocumulus clouds: droplet number, size, liquid water path, and radiative impact," *Journal of Geophysical Research D*, vol. 110, no. 8, pp. 1–16, 2005.

[10] A. D. Clarke, S. R. Owens, and J. Zhou, "An ultrafine sea-salt flux from breaking waves: Implications for cloud condensation nuclei in the remote marine atmosphere," *Journal of Geophysical Research D*, vol. 111, no. 6, pp. 1–2, 2006.

[11] A. Ito and M. Kawamiya, "Potential impact of ocean ecosystem changes due to global warming on marine organic carbon aerosols," *Global Biogeochemical Cycles*, vol. 24, p. 10, 2010.

[12] D. M. Murphy, J. R. Anderson, P. K. Qulnn et al., "Influence of sea-salt on aerosol radiative properties in the Southern Ocean marine boundary layer," *Nature*, vol. 392, no. 6671, pp. 62–65, 1998.

[13] P. K. Quinn, D. J. Coffman, V. N. Kapustin, T. S. Bates, and D. S. Covert, "Aerosol optical properties in the marine boundary layer during the First Aerosol Characterization Experiment (ACE 1) and the underlying chemical and physical aerosol properties," *Journal of Geophysical Research D*, vol. 103, no. 13, pp. 16547–16563, 1998.

[14] A. M. Middlebrook, D. M. Murphy, and D. S. Thomson, "Observations of organic material in individual marine particles at Cape Grim during the First Aerosol Characterization Experiment (ACE 1)," *Journal of Geophysical Research D*, vol. 103, no. 13, pp. 16475–16483, 1998.

[15] L. N. Hawkins, L. M. Russell, D. S. Covert, P. K. Quinn, and T. S. Bates, "Carboxylic acids, sulfates, and organosulfates in processed continental organic aerosol over the southeast Pacific Ocean during VOCALS-REx 2008," *Journal of Geophysical Research*, vol. 115, p. 16, 2010.

[16] D. C. Blanchard, "Bubble scavenging and the water-to-air transfer of organic material in the sea," *Advances in Chemistry Series*, vol. 145, pp. 360–387, 1975.

[17] R. Tseng, J. T. Viechnicki, R. A. Skop, and J. W. Brown, "Sea-to-air transfer of surface-active organic compounds by bursting bubbles," *Journal of Geophysical Research*, vol. 97, no. 4, pp. 5201–5206, 1992.

[18] A. W. Decho, "Microbial exopolymer secretions in ocean environments—their role (s) in food webs and marine processes," *Oceanography and Marine Biology*, vol. 28, pp. 73–153, 1990.

[19] S. M. Henrichs and P. M. Williams, "Dissolved and particulate amino acids and carbohydrates in the sea surface microlayer," *Marine Chemistry*, vol. 17, no. 2, pp. 141–163, 1985.

[20] M. Kuznetsova and C. Lee, "Dissolved free and combined amino acids in nearshore seawater, sea surface microlayers and foams: influence of extracellular hydrolysis," *Aquatic Sciences*, vol. 64, no. 3, pp. 252–268, 2002.

[21] J. Y. Aller, M. R. Kuznetsova, C. J. Jahns, and P. F. Kemp, "The sea surface microlayer as a source of viral and bacterial enrichment in marine aerosols," *Journal of Aerosol Science*, vol. 36, no. 5-6, pp. 801–812, 2005.

[22] M. Kuznetsova, C. Lee, and J. Aller, "Characterization of the proteinaceous matter in marine aerosols," *Marine Chemistry*, vol. 96, no. 3-4, pp. 359–377, 2005.

[23] L. I. Aluwihare, D. J. Repeta, and R. F. Chen, "A major biopolymeric component to dissolved organic carbon in surface sea water," *Nature*, vol. 387, no. 6629, pp. 166–169, 1997.

[24] K. Larsson, G. Odham, and A. Södergren, "On lipid surface films on the sea. I. A simple method for sampling and studies of composition," *Marine Chemistry*, vol. 2, no. 1, pp. 49–57, 1974.

[25] C. Leck and E. K. Bigg, "Biogenic particles in the surface microlayer and overlaying atmosphere in the central Arctic Ocean during summer," *Tellus B*, vol. 57, no. 4, pp. 305–316, 2005.

[26] C. Leck and E. K. Bigg, "Source and evolution of the marine aerosol—a new perspective," *Geophysical Research Letters*, vol. 32, no. 19, pp. 1–4, 2005.

[27] C. Leck and E. K. Bigg, "Comparison of sources and nature of the tropical aerosol with the summer high Arctic aerosol," *Tellus. Series B*, vol. 60, no. 1, pp. 118–126, 2008.

[28] C. Leek and E. Keith Bigg, "Aerosol production over remote marine areas—a new route," *Geophysical Research Letters*, vol. 26, no. 23, pp. 3577–3580, 1999.

[29] G. C. Roberts, P. Artaxo, J. Zhou, E. Swietlicki, and M. O. Andreae, "Sensitivity of CCN spectra on chemical and physical properties of aerosol: a case study from the Amazon Basin," *Journal of Geophysical Research D*, vol. 107, no. 20, pp. 1–37, 2002.

[30] R. Wood, C. Bretherton, B. Huebert, C. R. Mechoso, and R. Weller, "VOCALS SouthEast Pacific Regional Experiment (REx)," *Scientific program overview*, 2006, http://www.usclivar.org/science_status/VOCALS_SPO_Revised_Complete.pdf.

[31] T. S. Bates, P. K. Quinn, and D. Coffman, "Boundary layer aerosol chemistry during TexAQS/GoMACCS 2006: insights into aerosol sources and transformation processes," *Journal of Geophysical Research*, vol. 113, p. 18, 2008.

[32] S. Takahama, S. Gilardoni, L. M. Russell, and A. L. D. Kilcoyne, "Classification of multiple types of organic carbon composition in atmospheric particles by scanning transmission X-ray microscopy analysis," *Atmospheric Environment*, vol. 41, no. 40, pp. 9435–9451, 2007.

[33] S. Takahama, S. Liu, and L. M. Russell, "Coatings and clusters of carboxylic acids in carbon-containing atmospheric particles from spectromicroscopy and their implications for cloud-nucleating and optical properties," *Journal of Geophysical Research*, vol. 115, 2010.

[34] S. C. B. Myneni, "Soft X-ray spectroscopy and spectromicroscopy studies of organic molecules in the environment," *Reviews in Mineralogy and Geochemistry*, vol. 49, no. 1, pp. 485–579, 2002.

[35] D. Solomon, J. Lehmann, J. Kinyangi et al., "Carbon (1s) NEXAFS spectroscopy of biogeochemically relevant reference organic compounds," *Soil Science Society of America Journal*, vol. 73, no. 6, pp. 1817–1830, 2009.

[36] T. H. Yoon, K. Benzerara, S. Ahn, R. G. Luthy, T. Tyliszczak, and G. E. Brown Jr., "Nanometer-scale chemical heterogeneities of black carbon materials and their impacts on PCB sorption properties: soft X-ray spectromicroscopy study," *Environmental Science and Technology*, vol. 40, no. 19, pp. 5923–5929, 2006.

[37] R. C. Sullivan and K. A. Prather, "Investigations of the diurnal cycle and mixing state of oxalic acid in individual particles in Asian aerosol outflow," *Environmental Science and Technology*, vol. 41, no. 23, pp. 8062–8069, 2007.

[38] J. A. Brandes, C. Lee, S. Wakeham et al., "Examining marine particulate organic matter at sub-micron scales using scanning transmission X-ray microscopy and carbon X-ray absorption near edge structure spectroscopy," *Marine Chemistry*, vol. 92, no. 1–4, pp. 107–121, 2004.

[39] S. Liu, D. A. Day, and L. M. Russell, "Afternoon increase of oxygenated organic functional groups at a coastal site in Southern California," in preparation.

[40] C. van den Hoek, "Phytogeographic distribution groups of benthic marine algae in the North Atlantic Ocean. A review of experimental evidence from life history studies," *Helgoland Marine Research*, vol. 35, no. 2, pp. 153–214, 1982.

[41] J. R. Lawrence, G. D. W. Swerhone, G. G. Leppard et al., "Scanning transmission X-ray, laser scanning, and transmission electron microscopy mapping of the exopolymeric matrix of microbial biofilms," *Applied and Environmental Microbiology*, vol. 69, no. 9, pp. 5543–5554, 2003.

[42] E. K. Bigg and C. Leck, "Properties of the aerosol over the central Arctic Ocean," *Journal of Geophysical Research D*, vol. 106, no. 23, pp. 32101–32109, 2001.

[43] R. Benner and K. Kaiser, "Abundance of amino sugars and peptidoglycan in marine particulate and dissolved organic matter," *Limnology and Oceanography*, vol. 48, no. 1, pp. 118–128, 2003.

[44] C. Oppo, S. Bellandi, N. Degli Innocenti et al., "Surfactant components of marine organic matter as agents for biogeochemical fractionation and pollutant transport via marine aerosols," *Marine Chemistry*, vol. 63, no. 3-4, pp. 235–253, 1999.

[45] Q. Zhang, J. L. Jimenez, M. R. Canagaratna et al., "Ubiquity and dominance of oxygenated species in organic aerosols in anthropogenically-influenced Northern Hemisphere midlatitudes," *Geophysical Research Letters*, vol. 34, no. 13, p. 6, 2007.

[46] H. Sievering, J. Cainey, M. Harvey, J. McGregor, S. Nichol, and P. Quinn, "Aerosol non-sea-salt sulfate in the remote marine boundary layer under clear-sky and normal cloudiness conditions: ocean-derived biogenic alkalinity enhances sea-salt sulfate production by ozone oxidation," *Journal of Geophysical Research D*, vol. 109, no. 19, pp. 1–12, 2004.

[47] P. Verdugo, A. L. Alldredge, F. Azam, D. L. Kirchman, U. Passow, and P. H. Santschi, "The oceanic gel phase: a bridge in

the DOM-POM continuum," *Marine Chemistry*, vol. 92, no. 1–4, pp. 67–85, 2004.

[48] R. H. M. Godoi, K. Aerts, J. Harlay et al., "Organic surface coating on Coccolithophores—*Emiliania huxleyi*: its determination and implication in the marine carbon cycle," *Microchemical Journal*, vol. 91, no. 2, pp. 266–271, 2009.

[49] L. Beaufort, M. Couapel, N. Buchet, H. Claustre, and C. Goyet, "Calcite production by coccolithophores in the south east Pacific Ocean," *Biogeosciences*, vol. 5, no. 4, pp. 1101–1117, 2008.

[50] R. W. Jordan and A. Kleijne, "A classification system for living coccolithophores," in *Coccolithophores*, pp. 83–105, Cambridge University Press, Cambridge, UK, 1994.

[51] K. Sawada and Y. Shiraiwa, "Alkenone and alkenoic acid compositions of the membrane fractions of Emiliania huxleyi," *Phytochemistry*, vol. 65, no. 9, pp. 1299–1307, 2004.

[52] L. M. Russell, S. F. Maria, and S. C. B. Myneni, "Mapping organic coatings on atmospheric particles," *Geophysical Research Letters*, vol. 29, no. 16, p. 4, 2002.

[53] W.-C. Chin, M. V. Orellana, and P. Verdugo, "Spontaneous assembly of marine dissolved organic matter into polymer gels," *Nature*, vol. 391, no. 6667, pp. 568–572, 1998.

Hindawi Publishing Corporation
Advances in Meteorology
Volume 2010, Article ID 365131, 11 pages
doi:10.1155/2010/365131

*Research Article*

# The Influence of Algal Exudate on the Hygroscopicity of Sea Spray Particles

**H. Wex,[1] E. Fuentes,[2] G. Tsagkogeorgas,[1] J. Voigtländer,[1] T. Clauss,[1] A. Kiselev,[1] D. H. Green,[3] H. Coe,[2] G. McFiggans,[2] and F. Stratmann[1]**

[1] *Leibniz-Institute for Tropospheric Research, Permoser Strabe 15, 04318 Leipzig, Germany*
[2] *Centre for Atmospheric Sciences, University of Manchester, Manchester, M13 9PL, UK*
[3] *The Scottish Association for Marine Science, PA37 1QA Oban, UK*

Correspondence should be addressed to H. Wex, wex@tropos.de

Received 7 February 2010; Accepted 7 June 2010

Academic Editor: Chris Osburn



We examined the effect of organic matter released by four different algal species on the hygroscopic growth and droplet activation behaviour of laboratory-generated marine aerosol particles. Hygroscopic growth factors and dry diameters for activation were reduced by less than 10%, compared to that of sodium chloride or of artificial seawater that was devoid of marine surfactants. Concentration-dependent nonideal behaviour was observed for the artificial seawater. But within measurement uncertainty, the measured hygroscopic growth and droplet activation behaviour for the samples that contained organic matter were consistent with a hygroscopicity parameter that was constant between the sub- and supersaturated measurement points. Also, the hygroscopic growth measured for hydrated particles after 3 and after 10 seconds was similar, which implies that in this time range no kinetic effects were detected.

## 1. Introduction

Approximately 71% of the Earth's surface is covered by oceans, which provide a constant source of marine aerosol particles. Atmospheric marine aerosols consist of particulate matter with both, primary and secondary origin. Marine primary particles are produced on the ocean surface by bubble-bursting and tearing from breaking waves, that is, by processes depending on the wind speed. Secondary particulate matter originates from gas-to-particle conversion processes, such as nucleation and condensation [1], and, in the marine case, comprises substances as non-sea-salt sulphate and organic species.

Regarding the Earth's radiation budget, marine particles affect both the aerosol direct and indirect effects. Pilinis et al. [2] stated that the single most important parameter in determining direct aerosol forcing is the relative humidity (RH), and the most important process is the increase of the aerosol mass as a result of water uptake. Compared to continental aerosol, marine aerosol particles generally are more hygroscopic (see e.g., [3], where the particle hygroscopicity parameter $\kappa$ [4] of the more hygroscopic particle fraction was determined to be around 0.3 for continental and 0.45 for marine aerosol, and with a $\kappa$ of 0.95 for an additional (small) sea-salt mode for the marine case). This makes marine aerosol particles particularly susceptible to changes in relative humidity. Likewise, they easily can be activated to cloud droplets at atmospheric relevant supersaturations. The largest sea-salt particles may behave as giant Cloud Condensation Nuclei (CCN), [5] and their role in the initiation of precipitation in warm shallow clouds is still under discussion (e.g. [6–8]).

Model results obtained by Textor et al. [9] showed that worldwide all-model-average emissions are dominated by the mass of sea-salt, followed by dust, non-sea-salt sulphate, particulate organic matter, and finally black carbon. Marine stratus and stratocumulus clouds contribute about 30% to 40% to the Earth's albedo [10, 11]. Therefore, overall, marine aerosol particles can be assumed to play an important role for the Earth's atmosphere on a global scale.

The chemical compounds present in an aerosol particle influence its hygroscopic growth and its activation to a

cloud droplet. The influence of organic material contained in marine particles on their hygroscopic growth and activation behaviour continues to be the subject of intensive investigation. Organic material in these particles can originate from different sources. For marine aerosol, one source is the metabolic activity of oceanic phytoplankton which produces a complex mixture of dissolved and particulate species, including organic compounds such as carboxylic acids, lipids, amino acids, and carbohydrates [12]. These components can become incorporated into particles during the bubble-bursting process. A further source for organic material in marine aerosol is of secondary nature; volatile gases (e.g., isoprene produced by phytoplankton, but also gases emitted by the terrestrial biosphere or such of anthropogenic origin) can be precursors for substances condensing onto the existing particles [13, 14].

Different studies have examined marine aerosol with respect to its content of organic matter. Randles et al. [15] assumed this content to constitute up to 50% of the dry submicron marine aerosol mass. Cavalli et al. [16] found water-soluble and water-insoluble organic carbon (WSOC and WINSOC, resp.) in samples of marine aerosol collected during a phytoplankton bloom period in the North Atlantic. WINSOC was found to be the dominant submicron and the second dominant supermicron aerosol species (only exceeded by sea-salt), followed by WSOC as the next abundant species in both cases. The WSOC comprised about 20% to 30% of the total carbon and consisted of aliphatic and partially oxidized species and humic-like substances. The organic fraction found by Cavalli et al. [16] was reported to feature appreciable surface-active properties, where the bulk surface tension reduction could be expressed in terms of the concentration of dissolved organic carbon using the Szyszkowsky-Langmuir expression. Results from Cavalli et al. [16] agree with those described in [17], where North Atlantic marine aerosol arriving at the west coast of Ireland (Mace Head) was analyzed. O'Dowd et al. [17] observed that organic matter in the aerosol occurred in correlation with biological activity in the ocean. They also observed an increase in the organic fraction with decreasing size. Among the analyzed WSOC from the particles, they found partly oxidized species which, they assume, could potentially cause large decreases in surface tension.

Mochida et al. [18] examined marine aerosol from the North Pacific and found that concentrations of lower molecular weight (C14 to C19) saturated fatty acids correlated with sea-salt concentration and occurred in correspondence to algal bloom periods. They concluded that the fatty acids were released from the ocean surface to the atmosphere, and they also stated that fatty acids are among the substances that are potentially filmforming and that could, therefore, influence the behaviour of the particles upon hydration.

Tervahattu et al. [19, 20] analyzed atmospheric particles of marine origin using aerosol mass spectrometry and electron microscopy and found fatty acids present in the particles. The possible influence of the fatty acids on the particles was discussed, and two opposing effects were mentioned. One of the discussed effects was the formation of a hydrophobic organic film that could act as a barrier to hygroscopic growth, a possibility that already earlier has been discussed in connection to sea-spray generated aerosols by Ellison et al. [21]. The second effect was a lowering of the particle surface tension, which in turn would facilitate the activation to a cloud droplet, as discussed in [22]. Such a surface tension reduction has been found in seawater samples that were enriched in organic matter through desalting by Moore et al. [23]. The carbon concentration at which a reduction of the surface tension of 1% (compared to that of water) was found was in the range from 300 to 800 mg/L, which is above that naturally observed in seawater.

Sellegri et al. [24] examined the influence of a synthetic surfactant (SDS) on the particle generation from artificial seawater in the laboratory, using bubble-bursting processes to produce the particles. They observed from their measurements that both temperature and the surfactant concentration in the seawater influence the produced aerosol and its size distribution. They compared the obtained particle number size distributions to those typically measured for North Atlantic marine aerosol. This comparison is generally limited due to the possible addition of organic particulate matter from the gas phase to the marine particles. But Sellegri et al. [24] still suggest that marine submicron primary aerosol modes may mainly result from bubble bursting processes on a first approximation.

A modeling study by Randles et al. [15] showed that the direct aerosol effect is affected by the large amount of organic matter that can be contained in marine aerosol particles, in that this direct effect is noticeably diminished when the organic fraction is taken into account, compared to assuming the particles to consist of pure NaCl. This is largely due to the hygroscopicity of the organic matter being lower than that of NaCl. Additionally, as described above, chemical compounds that were said to potentially influence the surface tension of aerosol particles have been identified in marine samples. It is known that a significant suppression of surface tension has a large effect particularly on particle activation (e.g., [25]). Furthermore, solutions of NaCl and seawater samples are known to show a concentration-dependent nonideal behaviour, that is, the degree of nonideality changes with the concentration of the solute in the particle/droplet [26, 27]. It is pertinent to ask whether hygroscopic growth and activation of multicomponent aerosol particles representative of those in the marine atmosphere may be described by a simple approximation to the Köhler equation or whether nonideality variation or the presence of surface active components invalidate such an approach.

To further elucidate this question, the present study examines the behaviour of seawater enriched by algal exudate. The algae species that were cultured to obtain algal exudates were *Chaetoceros* sp. (*Chaet*), *Emiliana huxleyi* (*E. huxleyi*), *Phaeocystis* (*Phaeo*), and *Thalassiosira rotula* (*T. rotula*). *Chaet* and *T. rotula* both belong to the group of diatoms which is one of the most common types of phytoplankton. *E. huxleyi* occurs in great abundance in the Earth's oceans, from the tropics to subarctic waters [28]. The *Phaeocystis* specie, too, is widely distributed throughout the world's oceans and is even found in sea ice. It can form floating colonies with hundreds of cells embedded in a

polysaccharide gel matrix that can multiply massively during blooms [29]. These algae species are all major contributors to primary production of organic matter in the ocean, having an important role in marine food chains and in the global carbon cycle.

A bubble-bursting generator described in Fuentes et al. [30] was used in our study to generate particles from samples of artificial seawater and from samples containing additional organic material, that is, algal exudate from cultures of the above mentioned algae species. Size selected particles were used to measure hygroscopic growth and activation of the particles. The different data sets were used to derive particle hygroscopicities for a wide range of water activities, where we used the hygroscopicity parameter $\rho_{\text{ion}}$ as defined in [31].

## 2. Theory

The main goal of this study was to examine the hygroscopic behaviour of particles that consisted of salts contained in seawater and additional organic matter originating from algae. Hygroscopic diameter growth factors and critical dry diameters for activation were interpreted in terms of particle hygroscopicity. For that, the Köhler theory, which connects particle size and hygroscopicity to hygroscopic growth and activation, was used. The theory connects water vapor saturation at the surface of the droplet, $S_d$, to the Kelvin term accounting for the curvature of the droplet, $K$, and the water activity or Raoult term accounting for dissolved matter in the solution, $a_w$

$$S_d = Ka_w = \exp\left(\frac{4M_w\sigma_s}{RT\rho_w d_d}\right) * \exp\left(-\frac{\phi\nu\rho_s V_s}{M_s n_w}\right), \quad (1)$$

with the molecular weight of water $M_w$, the surface tension of the solution $\sigma_s$, the ideal gas constant $R$, the temperature $T$, the density of water $\rho_w$, and the diameter of the hydrated particle/droplet $d_d$, the osmotic coefficient $\phi$ (accounting for nonideality of the solution), the number of ions per solute molecule $\nu$, the solute density $\rho_s$, the volume of the solute (i.e., of the dry particle), $V_s$, the solute molecular weight $M_s$, and the number of water molecules in the droplet $n_w$.

The solute parameters of the Raoult term can be combined into a single hygroscopicity parameter, $\rho_{\text{ion}}$ [31]:

$$\rho_{\text{ion}} = \frac{\phi\nu\rho_s}{M_s}. \quad (2)$$

This approach is useful when the solute properties are unknown, as often is the case for organic compounds or for mixtures. If the properties of all the components in a mixture are known, then $\rho_{\text{ion}}$ can be obtained by applying a volume mixing rule. This will be used later in this study for an artificial seawater sample. Values of $\rho_{\text{ion}}$ are generally comparable to $\kappa$ as defined in [4]. As explained in [32], at $a_w > 0.95$, $\rho_{\text{ion}}M_w/\rho_w = \kappa$ to better than 3%.

The osmotic coefficient included in $\rho_{\text{ion}}$ is often assumed constant for dilute solutions such as at the high RH values considered in this study, that is, a possible change in nonideal solution behaviour with the concentration of the solute in the particle/droplet solution is omitted. This results in a constant value for $\rho_{\text{ion}}$. However, it is well known that, for example, NaCl or ammonium sulphate show a concentration-dependent nonideal behaviour (e.g., [26]). When the nonideality of a solution in dependence of the solute concentration (i.e., the component activity coefficient) is known, a concentration-dependent description of $\rho_{\text{ion}}$ is possible. Or, vice versa, measurements can be made at different concentrations (e.g., by measuring hygroscopic growth at different relative humidities (RHs)), and if $\rho_{\text{ion}}$ derived from these measurements shows a concentration dependence, this could indicate a concentration-dependent nonideal behaviour.

We will make use of this in evaluating the influence of algal exudates on the hygroscopic behaviour of seawater in this work. In the analysis, $\rho_{\text{ion}}$ as derived from measured hygroscopic growth and activation (through use of (1) and (2)) will be employed.

## 3. Sample Preparation

Data from six different samples will be shown in this study. One sample was artificial seawater devoid of organics, one algae medium (natural seawater with nutrients), and four samples were seawater proxies containing mixes of exudates produced by four different algae species, namely *Chaetoceros* sp. (*Chaet*), *Emiliana huxleyi* (*E. huxleyi*), *Phaeocystis* (*Phaeo*), and *Thalassiosira rotula* (*T. rotula*).

The artificial seawater was prepared from analytical grade salts and deionised water following the method described by Kester et al. [33]. The ionic mass ratios of $Na^+$, $Cl^-$, $Mg^{2+}$, $HCO_3{}^-$, and $SO_4{}^{2-}$ were comparable to those in seawater. The salt mixture contained, by mass, 73.6% NaCl, 14.5% $MgCl_2$, 11.5% $Na_2SO_4$, and 0.4% $NaHCO_3$. Seawater samples of 3.5% salinity were prepared by adjusting the solution density at the laboratory temperature using a hydrometer. This corresponds to concentrations of the salts in the artificial seawater of 22.9 g/L NaCl, 4.6 g/L $MgCl_2$, 3.6 g/L $Na_2SO_4$, and 0.01 g/L $NaHCO_3$.

Algal growth medium was prepared based on natural seawater from the North Atlantic (Tiree passage, Scotland, UK) that had been filtered with GF/C (Whatman), amended with F/2 nutrients and either selenite or silicate [34], and sterilized by autoclaving (121°C for 15 min).

For the preparation of the different seawater proxies enriched with biogenic organics, the filtered natural seawater amended with algal medium was used for growing four different phytoplankton cultures in the laboratory. The algae cultures were grown in glass Erlenmeyer flasks. Monitoring of algal growth was done by measuring in vivo chlorophyll-a fluorescence every 2 days using a Turner Trilogy fluorometer. Following algae growth, the cell biomass was removed by filtration. Details of the culturing and subsequent filtering procedures can be found in [30].

Artificial seawater devoid of organics and natural seawater enriched with the produced biogenic matter were combined to prepare seawater proxies at 512 $\mu$M DOC (Dissolved Organic Carbon), where DOC analysis was done using a Shimadzu TOC-V CPH/CPN. The samples were prepared

such that one of the algal exudates comprised 50% of the total organic concentration, while the rest of the organic content was equally divided between the other three algal exudates on study (i.e., 16.7% of total DOC for each algal exudate). The samples were named after the algae species which was the most abundant (e.g., the organic fraction in *E. huxleyi* Mix consisted to 50% of *E. huxleyi* exudate and to 16.7% of each of the other three algal exudates). The organic concentration selected (about 0.01 g/L) is within the range of concentration expected for organics in naturally enriched seawater in areas of high biological activity [35, 36]. This value for the organic concentration was derived from the adjusted value of 512 $\mu$M DOC by considering the phytoplankton average elemental composition following Fraga [37], which then yields a molar mass of 2.38 kDa and a molecule to C mass ratio of 1.87.

The samples (each about 6 L in total) were kept frozen until shortly (some hours) before measurements took place, when they were left to thaw at laboratory temperature.

## 4. Experimental Setup

A bubble-bursting aerosol generation method, using the recirculation of liquid samples by means of a peristaltic pump, was used to produce a marine aerosol proxy (see Figure 1). Experiments were performed using a PTFE tank (internal dimensions: 20.5 cm height, 19.5 cm width, and 27.5 cm length) filled with 3.5–6 L of sample. The sample was recirculated and impinged on the sample surface in the tank. With this technique, air entrained in the sample by water impingement was dispersed in a rising plume of bubbles that burst at the sample surface. In order to generate a statistically significant number of particles for the aerosol experiments, the recirculating flow was divided in eight separate jets by using a flow distributor. The bubble plume penetration distance was about 5–7 cm. Whilst bubble paths and lifetimes in the small-scale tank employed in this study were shorter than those expected in oceanic conditions [30], theoretical analysis of the kinetics of adsorption of marine organics on rising bubbles indicated that the time required for adsorption equilibrium is rapid compared to the characteristic bubble lifetimes in small-scale systems [30]. Hence, the experimental configuration employed should be valid for conducting studies on the effects of biogenic organics on the sea spray aerosol.

A chemically resistant Teflon composite tube (Masterflex I/P 70) was employed for water recirculation in order to avoid contamination of the samples and adhesion of surfactants on the tubing wall. The water flow (4 Lpm) was controlled by setting the peristaltic pump rotating speed to 35–40 rpm and monitored using a rotameter.

Thorough cleaning procedures were applied in order to minimize the presence of contaminants in the system. The tank walls and bubbling apparatus were rubbed with chloroform and isopropanol, rinsed and washed with deionised water. Deionised water was recirculated for 30–60 min in order to rinse the pump tubing prior the experiments.

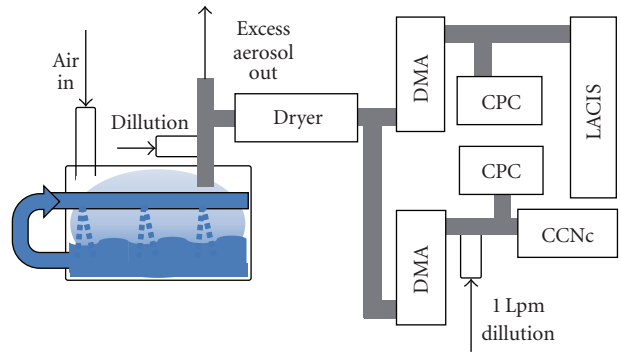


Figure 1: Sketch of the experimental setup.

For the aerosol experiments, the PTFE tank was sealed and swept with a continuous particle-free air flow of 3–3.5 Lpm. The humidity of the aerosol flow extracted from the outlet of the tank was reduced by dilution with dry, particle-free air (see Figure 1). The excess flow was vented through a T-connector, and the flow needed to feed the different instruments was led through a diffusion dryer, reducing the humidity to a value below 10% RH. After that, the dry aerosol flow was divided into two flows and distributed to the instruments.

In each of the two lines, dry particle sizes were selected by use of a neutralizer (Kr 85) and a Differential Mobility Analyzer (DMA) (Type Vienna Medium, aerosol to sheath flow rate of 1 to 10 Lpm). Downstream of each of the two DMAs, the particle number concentration of the quasi monodisperse aerosol were determined with a CPC (TSI-3010 Condensation Particle Counter, TSI Inc., St. Paul Minnesota, USA).

In one line, the CPC measured with an aerosol flow of 0.9 Lpm, while the remaining 0.1 Lpm was used for hygroscopic growth measurements with LACIS (Leipzig Aerosol Cloud Interaction Simulator, [38]). The number concentration measured with this CPC was only used to monitor the stability of the particle generation system. The size selected by the respective DMA, that is, the dry particle mobility diameter used for LACIS measurements was 200 nm. For the measurements, the LACIS flow tube had a total length of 7 m, and hygroscopically grown particles were detected at a tube length of 1 m and 7 m, using two optical particle spectrometers (OPSs, [39]) simultaneously. Prior to the measurement campaign, the OPSs were calibrated with PSL-particles with diameters of 300, 400, 500, 700, 800, and 1600 nm. The RH obtained in the LACIS flow tube was constantly controlled after each of the measurements by measuring the hygroscopic growth of size-selected ammonium sulphate particles. The RH needed to grow the particles to the measured sizes was inferred from Köhler theory. From these measurements, an uncertainty range for RHs adjusted in LACIS was obtained. LACIS measured hygroscopic growth for RHs between 90% and 99%. More details about LACIS calibrations and typical uncertainty ranges can be found in [32, 38].

In the second aerosol line, the aerosol coming from the DMA was diluted with 1 Lpm dry particle-free air. From the resulting 2 Lpm, 1 Lpm was fed into the CPC and a CCNc (Cloud Condensation Nuclei counter, [40], Droplet Measurement Technologies, two column version), each. The size at the DMA was scanned to obtain a number size distribution in the range from 25 to 500 nm, measuring at 40 different dry diameters with a logarithmic equidistant spacing. The DMA selected one size for 50 s before selecting the next one. The CCNc kept a constant supersaturation during the scan of the whole size distribution. To obtain the activated fraction from CPC and CCNc data, the data measured during the first 30 s after the change of the size at the DMA were discarded and the following 10 s of data were used. The CCNc was adjusted to supersaturations $s$ between 0.1% and 0.4% ($s = S_d - 1$). The calibration curve of the CCNc was determined prior to the measurements for $s$ ranging from 0.1% to 0.7%. For this, the activation of size-segregated ammonium sulphate particles was measured, and the respective $s$ was inferred via Köhler theory, giving the relation between $s$ and the instrument settings, that is, the calibration curve. This curve was kept constant during the experiments, and tests of this calibration were done before, during and after the experiment period by repeatedly measuring again the activation of size-segregated ammonium sulphate particles. These repeated measurements were used to derive an uncertainty range for $s$ of the CCNc. Typical uncertainty ranges that were found for the CCNc were already given in [32].

In this study, also data obtained from measurements of the hygroscopic particle growth conducted with a Humidity Tandem Differential Mobility Analyzer (H-TDMA, University of Manchester) and the same marine aerosol generator will be used [41]. For a description of the H-TDMA instrument see Fuentes et al. [30].

## 5. Shape Factor

It has long been known that dry NaCl particles are not spherical [42]. A nonspherical shape has also been observed for particles generated from seawater samples that contained NaCl as the main component [27]. When particles are not spherical, a shape correction has to be accounted for to obtain a volume equivalent diameter of the particles (which is one of the parameters in the Köhler theory) from the mobility diameter selected by the DMA. The shape of particles does, however, also depend on the particle generation and on the subsequent drying process (see e.g., [30, 43]).

Therefore, to obtain the shape factor valid for the particles generated in this study, we particularly examined particles produced from artificial seawater and from the *Chaet* Mix sample. Particles of different dry sizes were selected by the DMA and their sizes were measured in LACIS, which was operated at dry conditions (<5% RH) for these measurements. For the evaluation of the OPS signals, a refractive index of 1.55 was used. This value was obtained using a volume mixing rule and the particle composition as given in Section 3. (This value for the refractive index was still valid if an enhancement of the organic fraction due to the particle generation [41] was accounted for.) A comparison of diameters measured by the OPS with those selected by the DMA can be seen in Figure 2. When no shape factor is used, the diameters selected by the DMA are larger than those obtained from the LACIS measurement for both examined samples. The best agreement between the data and the 1-to-1 line (also shown in Figure 2) was obtained, when assuming a shape factor of 1.06. This value of 1.06 was used to calculate the volume equivalent diameters from the mass equivalent diameters for all particles generated in this study.

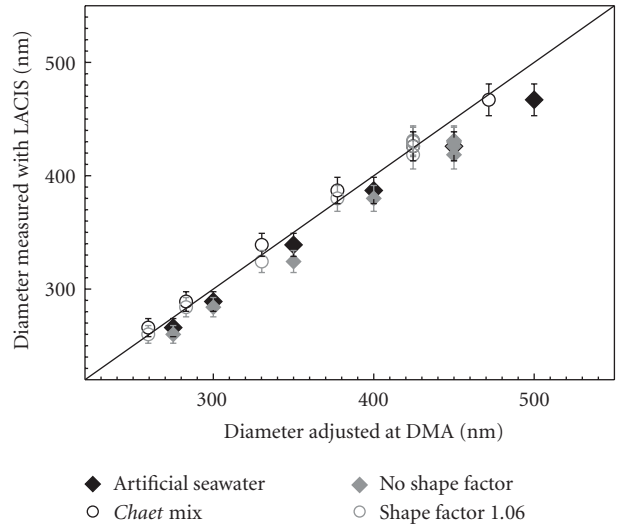


Figure 2: Comparison of dry particle diameters as selected by the DMA with the respective values measured with LACIS. The black line is the 1-to-1 line.

## 6. Results and Discussion

In Figure 3 we show measured hygroscopic growth factors and critical diameters for activation of the different samples. It is difficult to distinguish between the data obtained for the different samples, but Figure 3 serves to show that all the samples had a comparably similar behaviour with respect to hygroscopic growth and activation. For comparison, the theoretical values for sodium chloride and ammonium sulphate were added as well. The ammonium sulphate curves are indicated by the light grey lines. The sodium chloride curves are displayed as dark grey lines surrounded by grey shaded areas, where the shaded areas indicate the range of measurement uncertainties in water vapor saturation (for LACIS: in RH (i.e., $a_w$) and for the CCNc in $s$). These ranges correspond to uncertainties of $2\sigma$ (i.e., the 95% confidence range) and were obtained from repeated measurements with particles from a well-known substance (ammonium sulphate), as described in Section 4.

Measured values shown for artificial seawater in Figure 3 stand out slightly from the others, as particles generated from this sample showed the largest hygroscopic growth,

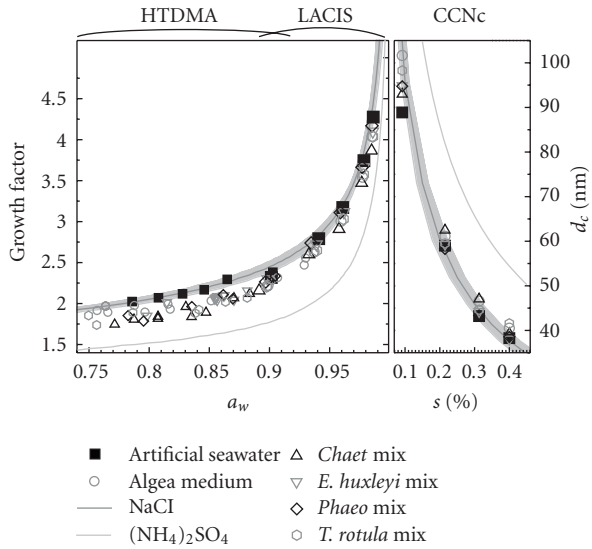


Figure 3: Left panel: Measured hygroscopic growth factors from the H-TDMA (smaller symbols) and LACIS (larger symbols). Right panel: Measured $d_c$ from the CCNc. Additional curves in both panels show the theoretical curves for sodium chloride and ammonium sulphate.

consistent with showing the lowest critical diameters for activation, $d_c$. These values are close to those for sodium chloride for both hygroscopic growth and activation. The theoretical data for ammonium sulphate particles clearly separate from all others, with their hygroscopic growth being smaller and their activation occurring at larger values for $d_c$ than for particles of any of the examined samples.

Measurements with the H-TDMA and LACIS were conducted at different dry particle diameters (240 nm or 200 nm selected by the DMA, that is, volume equivalent diameters, $d_p$, of 226 nm or 188 nm when including the shape factor correction for H-TDMA and LACIS, respectively), so we show hygroscopic growth factors ($= d_d/d_p$) as a function of water activity $a_w$ (i.e., of $S_d/K = (\mathrm{RH}/100)/K$). The ranges of $a_w$ in which data from the H-TDMA and LACIS are shown are indicated at the top of Figure 3. The further examination of the data, which will be shown next, gives a clearer picture of the overlap between data from the two different instruments. The critical dry diameters for activation, $d_c$, as shown in the right panel of Figure 3, were derived from CCNc measurements and were also shape factor corrected with the above derived value of 1.06. While in general the data measured for hygroscopic growth and activation of the artificial seawater sample were close to those of pure NaCl (within measurement uncertainty), $d_c$ measured at $s = 0.1\%$ was lower than that of NaCl, that is, it seemed to be easier to activate and differed from that of NaCl by more than the measurement uncertainty. As NaCl is the most hygroscopic compound in the artificial seawater, this result might indicate a problem with the CCNc at $s = 0.1\%$. During the calibration of the CCNc with size-selected ammonium sulphate particles, a deviation of the linear relationship between the temperature gradient in the CCNc column and the supersaturation was observed at $s = 0.1\%$. The supersaturation at this lowest value likely was larger than adjusted, but could not be determined with a high accuracy. Therefore, although the values for $\rho_{\mathrm{ion}}$ were calculated from these data points, they were not considered in the further data evaluation.

For the calculation of $\rho_{\mathrm{ion}}$ from the measurements, a value for the surface tension $\sigma_s$ was needed. In [41] it is described in detail how, based on measurements, surface tension isotherms were determined for the algal exudates that were also used to prepare the samples in our study. From this, $\sigma_s$ of droplet solutions at the point of activation can be calculated. Droplets activating at smaller particles (and larger supersaturations) have more concentrated solutions at the point of activation, hence, smaller particles show a larger decrease in $\sigma_s$, if surface active compounds are present. The smallest particles for which activation was measured in our study had diameters of about 40 nm, for which a surface tension reduction at the point of activation for the different algal exudate mixtures was found in the range from 0.5 to 3%, where the largest reduction was observed for *Chaet* Mix [41]. For particles with sizes >100 nm, this reduction was <1%. Also, particle hygroscopic growth for RHs < 95% is insensitive to $\sigma_s$ [25]. Therefore, in the present study, we used the surface tension of water for the determination of $\rho_{\mathrm{ion}}$ in our study. As surface tension depends on temperature, for data measured with the CCNc care was taken to account for the temperature in the instrument.

Figure 4 shows $\rho_{\mathrm{ion}}$ derived from the measurements through the use of (1) and (2) (for details on these calculations see e.g., [32]). Data is shown separately for the different samples. As mentioned above (Section 2), values of $\rho_{\mathrm{ion}}$ are generally comparable to $\kappa$, and for example, $\rho_{\mathrm{ion}} = 70 * 10^3$ mol/m$^3$ corresponds to a $\kappa$ value of 1.26.

The overlap regions for data being derived from H-TDMA and LACIS for the different samples can be seen clearly for the different samples in Figure 4. The data from the two different instruments are in agreement within measurement uncertainty. Also, no large deviations were found between $\rho_{\mathrm{ion}}$ determined with LACIS at high RHs and those derived from CCNc measurements. As particle activation is sensitive to $\sigma_s$ [25], if the assumed value for $\sigma_s$ deviated much from the actual ones, this would show in differences of the $\rho_{\mathrm{ion}}$ values obtained from LACIS and the CCNc data. A clear example for this can be found, for example, in [25], a study examining laboratory-generated SOA (Secondary Organic Aerosol). Such differences, however, were not observed in the study presented here.

In Figure 4, again theoretical curves were added. The dotted black line in the two upper panels shows the theoretical curve for sodium chloride. The red curve depicted in all panels is the theoretical curve for ammonium sulphate. The blue curve shows the theoretical values that would be expected based on the composition of artificial seawater, together with assuming a nonideal behaviour as that of NaCl. To obtain the curve, $\rho_{\mathrm{ion}}$ for fully dissolved artificial seawater was derived from the mass fractions of the different components contained in the sample (see Section 3), together with using a volume mixing rule

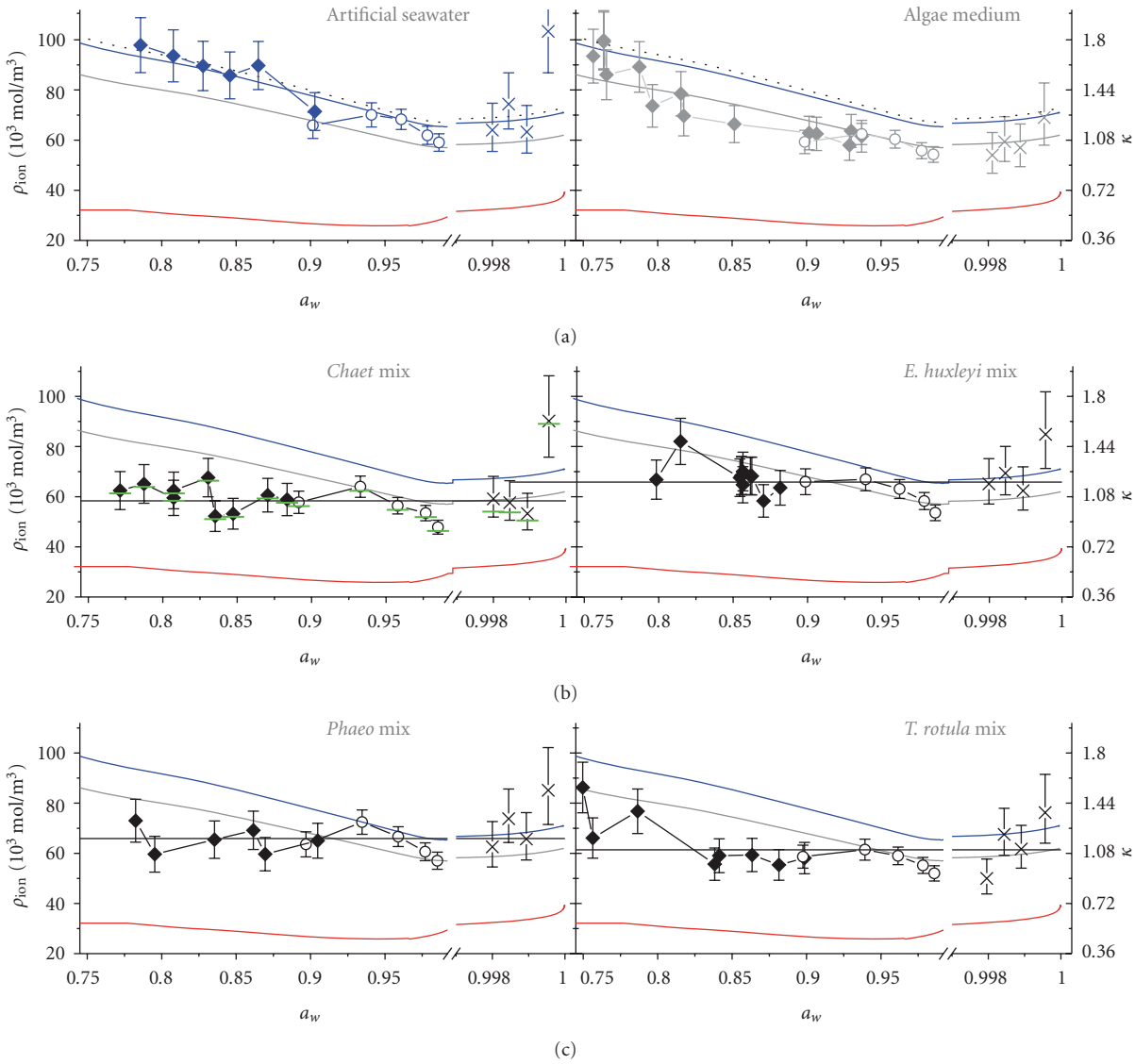


FIGURE 4: $\rho_{ion}$ derived from measured hygroscopic growth and activation; filled and open symbols were derived from H-TDMA and LACIS measurements, respectively, crosses from CCNc measurements (respective $\kappa$ values are indicated at the right axis). Additional curves are thought as guide for the eye. More details about them are given in the text.

and the properties ($\rho_s$, $M_s$, $\nu$) of the respective components. This yielded a value of 72.3 $*$ $10^3$ mol/m$^3$ (as compared to 74.1 $*$ $10^3$ mol/m$^3$ for fully dissolved NaCl). This value for the fully dissolved solution was then overlain with the same nonideal behaviour that is described for pure NaCl (see [26]), the main component of the artificial seawater. When comparing this blue curve with the $\rho_{ion}$ values derived from the measurements for the artificial seawater (blue symbols in the upper panel on the left side of Figure 4), we obtained an $R^2$-value of 0.77. Therefore, we conclude that the artificial seawater sample shows a nonideal behaviour similar to that of NaCl.

The grey line shown in all the panels of Figure 4 was obtained from the blue line (i.e., the artificial seawater curve) through lowering it by a constant factor. This factor was obtained by minimizing the least square value between the lowered (grey) curve and the $\rho_{ion}$ values obtained from the algae medium measurements (upper panel on the right side). The minimum least square was obtained for a curve that came from multiplying the curve for the artificial seawater with a factor of 0.872. This corresponds to a $\rho_{ion}$ for the highly diluted algae medium sample of 63.0 $*10^3$ mol/m$^3$. This lowering of $\rho_{ion}$ by 12.8% compared to that of artificial seawater can be attributed to the additives that were added to the seawater to produce the algae medium. The $R^2$-value between the lowered (grey) curve and the measured values is 0.78. This degree of agreement between the grey curve and $\rho_{ion}$ for the algae medium shows that a nonideal behaviour close to that of NaCl was also observed for this sample.

For the examined algal exudate samples, the blue and grey lines described above are also shown for comparison in

the different panels of Figure 4. However, for all of these samples, additional horizontal straight black lines are given in the panels. These lines indicate the average $\rho_{\text{ion}}$ from the data shown in the respective panel. The values are 58.3, 65.9, 65.8, and $61.3 * 10^3$ mol/m$^3$ for *Chaet* Mix, *E. huxleyi* Mix, *Phaeo* Mix, and *T. rotula* Mix, respectively. For highly diluted solutions, these average $\rho_{\text{ion}}$ values for the algal exudate samples agree with that of the algae medium within measurement uncertainty. The components with lower hygroscopicities contained in the algae medium (i.e., the nutrients) were different to those in the algal exudate samples. The algal exudate samples will not contain substantial nutrient levels, as these were consumed by the algae during growth. Therefore, it is merely coincidental that $\rho_{\text{ion}}$ values from the algae medium are similar to those of the algal exudate samples. But this will be used later in our study to compare the concentration-dependent $\rho_{\text{ion}}$ found for the algae medium to the $\rho_{\text{ion}}$ values obtained for the algal exudate samples.

For *Chaet* Mix, green bars in Figure 4 indicate $\rho_{\text{ion}}$ determined using the concentration-dependent surface tension of Fuentes et al. [41], as opposed to the surface tension of water. This leads to a lowering of the average $\rho_{\text{ion}}$ of about 3% (to $56.5 * 10^3$ mol/m$^3$). As *Chaet* Mix showed the largest surface tension reduction, the respective effect for the other algal exudate samples would be even smaller. The trend of $\rho_{\text{ion}}$ with respect to the changing solution concentration is not affected.

Our measurements can be compared to those done by Sellegri et al. [44], where hygroscopic growth at 84% RH was measured for particles with a dry diameter of 85 nm. Particles were produced by bubble bursting from artificial seawater (a mixture of purely inorganic salts) and natural seawater (containing organic matter). $\rho_{\text{ion}}$ values that can be derived from their measurements are $72.2 * 10^3$ mol/m$^3$ for the artificial seawater (as compared to $86.1 * 10^3$ mol/m$^3$ at 84% RH in our study) and $61.1 * 10^3$ mol/m$^3$ for the natural seawater. While this value for the natural seawater is within those obtained for our algal exudate samples, the hygroscopicity obtained for the artificial seawater in our study exceeds that given by Sellegri et al. [44] by almost 20%. This difference, however, could originate in different concentrations of the salts in the artificial seawater, which is difficult to test as the concentrations used by Sellegri et al. [44] are not given in their publication. Sellegri et al. [44] also measured hygroscopic growth for ambient marine particles at the western coast of Ireland (Mace Head) and found growth factors that were still lower than those of laboratory-generated particles from natural seawater, corresponding to $\rho_{\text{ion}}$ of $52.2 * 10^3$ mol/m$^3$.

Recently, Wex et al. [3] derived average particle hygroscopicities from collections of H-TDMA data. The data had been measured around the globe during more than a decade and were collected in overview papers by Kandler and Schütz [45] and Swietlicki et al. [46]. Wex et al. [3] give hygroscopicities in terms of the parameter $\kappa$, with $\kappa$ for the more hygroscopic particle fraction being around 0.3 for continental and 0.45 for marine aerosol, and with $\kappa$ being 0.95 in an additional (small) sea-salt mode for the marine case. These values correspond to $\rho_{\text{ion}}$ of 16.7, 25.0, and $52.8 * 10^3$ mol/m$^3$, respectively. The hygroscopicity derived from ambient data in Sellegri et al. [44] agrees well with that obtained for the average sea-salt mode in [3]. However, these values are still about 20% smaller than those measured for laboratory-generated particles from natural seawater or from the algal exudate samples examined in this study. This might be a hint towards difficulties in imitating marine aerosol in the laboratory, which possibly can be due to the addition of particulate organic matter from the gas phase in the marine atmosphere.

We now get back to the analysis of the data shown in Figure 4. The ability of the grey curve to represent the $\rho_{\text{ion}}$ values obtained for the algal exudate samples was evaluated. For all four samples, $R^2 < 0.5$ was obtained (with $R^2$ as low as 0.03 for *Phaeo* Mix). The variances between the $\rho_{\text{ion}}$ values and the grey curve were larger than those between the $\rho_{\text{ion}}$ values and the average $\rho_{\text{ion}}$ by a factor of 6.8, 1.4, 3.6, and 1.6 for *Chaet* Mix, *E. huxleyi* Mix, *Phaeo* Mix, and *T. rotula* Mix, respectively. From both, the $R^2$-values and the variances, it follows that using a constant, average $\rho_{\text{ion}}$ (i.e., independent of the solution concentration) describes the data better than using the grey curve. The addition of the algal exudates seems to cause the nonideal behaviour of the solutions to become independent of the solution concentration.

We also examined a possible influence of kinetic effects on the measured hygroscopic growth. Data were obtained from the two LACIS-OPCs that were positioned after the first meter of the flow tube and at its end after 7 meters. These positions correspond to residence times of the particles in the hydrated state of about 3 and 10 seconds. Figure 5 shows the measured hygroscopic growth factors. The grey area indicates the uncertainty in $a_w$ for the measurements done in the upper part of the flow tube ($2\sigma$, i.e., 95% confidence range), the error bars indicate the same for the measurements done at the end of the flow tube. No noticeable difference between the measured values after 3 and after 10 seconds can be seen. Therefore, in the data presented here, we do not see an influence of kinetics on the hygroscopic growth behaviour of the examined samples for the examined time scale of 3 to 10 seconds.

Summarizing we can say that rather than complicating, the addition of algal exudates to sea-salt particles seems to simplify the description of their hygroscopic behaviour. Hygroscopic growth and activation could be described by using values for $\sigma_s$ and $\rho_{\text{ion}}$ that were independent of the solution concentration over the wide range of concentrations examined in this study. This is consistent with no substantial effect of surface tension and a constant nonideality with respect to solute concentration. This, however, is contrary to well-established behaviour of NaCl [26] and sea-salt solutions (e.g., [27], and artificial seawater examined in our study). It is possible that this simplification in the hygroscopic behaviour could be caused by cancellation of effects that are/could be concentration dependent, such as nonideality, shape factor, stepwise deliquescence, or surface tension (where it has to be repeated that hygroscopic growth for RHs < 95% has been shown to be insensitive to surface tension, [25]). Overall, the limited data set that was examined in this study does not allow to examine the underlying effects in more detail.

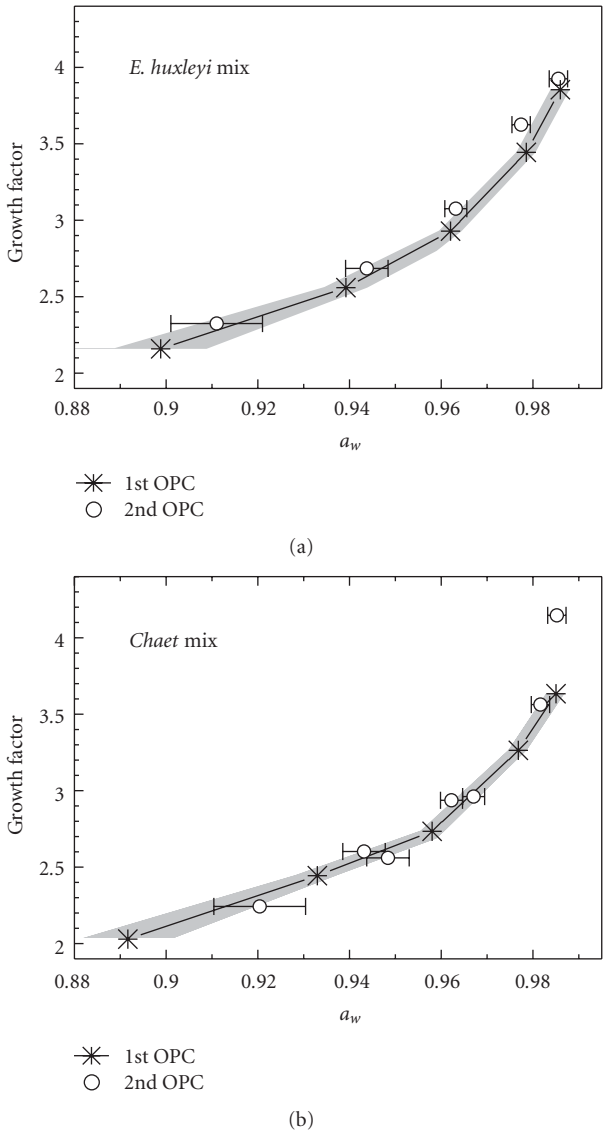


Figure 5: Comparison of hygroscopic growth measured with LACIS at two different positions of the LACIS flow tube, that is, after different residence times of 3 and 10 seconds.

The independence of $\sigma_s$ and $\rho_{\text{ion}}$ from the solution concentration enables the description of the particle hygroscopicity with a single parameter, be it $\rho_{\text{ion}}$ or $\kappa$. The average $\rho_{\text{ion}}$ shown in in Figure 4 corresponds to $\kappa$ of 1.05, 1.19, 1.19, and 1.10. When the hygroscopic growth factors of, for example, a 100 nm particle at 90% RH is calculated from these average $\rho_{\text{ion}}$ values, it is found to range from 2.15 to 2.24. These growth factors are slightly larger than those given by McFiggans et al. [47] for atmospheric marine particles, which range from 2.06 to 2.14 for the above mentioned particle size and RH. This discrepancy, however, can be attributed to additional particulate matter that can be acquired by marine particles, for example, from the gas phase. Among the possible candidates are non-sea-salt sulphates from Dimethylsulfide (DMS, [48]) or additional SOA mass from biogenic sources [13], but also secondary aerosol mass originating from sources as the terrestrial biosphere or from anthropogenic origin that are transported over the ocean [14]. Therefore, as, due to its vast size, a complete marine environment can not be imitated, our focus here was on a subsystem, that is, on the influence of algal exudates on hygroscopic growth and activation, for which it was found that a simple description is possible.

## 7. Summary and Conclusion

In the present study, an examination of the influence of algal exudate, that is, of biogenic organics, in seawater samples on hygroscopic growth and droplet activation behaviour of particles produced from the samples was introduced. The algal exudates were obtained from culturing four different phytoplankton species and subsequent removal of the cell biomass by filtration. Algal exudate was produced from either *Chaetoceros* sp., *Emiliana huxleyi*, *Phaeocystis*, and *Thalassiosira rotula*, which are all major contributors to primary production of organic matter in the ocean. Mixtures of these exudates were added to seawater, yielding seawater proxies with concentrations of dissolved organic carbon on the order of those expected in regions of high biological activity. These, thus, prepared samples were examined, together with a sample of artificial seawater (that contained no organics) and with algae medium, which was the initial natural seawater sample with added nutrients employed for growing the algal cultures. The hygroscopic growth of samples containing algal exudate was measured twice, once after 3 and once after 10 seconds of residence time at humidified conditions. No change in the measured hygroscopic growth was detected, that is, no kinetic effects could be observed in this time range.

Hygroscopic growth and particle activation of the algal exudate samples and of the algae medium were found to be reduced by less than 10%, compared to artificial seawater, and they were clearly above that of ammonium sulphate. For the determination of the hygroscopicity parameter of the samples, the surface tension of water was used. Concentration-dependent nonideal behaviour was observed for the artificial seawater and for the algae medium sample, following that described for NaCl [26]. This concentration dependence was not observed for the samples containing algal exudate. Therefore, it is possible to use a single parameter description of the hygroscopicity of the particles generated from the algal exudate samples, independent of the concentration of inorganic and organic solutes in the particle or droplet solution, with parameters as, for example, $\rho_{\text{ion}}$ [31] or $\kappa$ [4].

Overall, the examined algal exudates in the samples did not complicate the description of the hygroscopic behaviour of particles generated from these samples but rather made it more simple. It should be stressed, however, that marine particles can contain additional matter acquired from the gas phase, where marine sources can add inorganic matter (e.g., non-sea-salt sulphates from Dimethylsulfide, [48]) and organic matter [13], and to which also anthropogenic sources and the terrestrial biosphere can contribute.

## Acknowledgments

This work was performed as part of EUROCHAMP-II and also supported by the UK Natural Environment Research Council (Grant numbers NE/D005175/1 and NE/G000247/1). G. Tsagkogeorgas was funded by a Marie Curie Initial Training Network [CLOUD-ITN, No 215072]. The authors thank Ottmar Möhler from the KIT in Karlsruhe, Germany, for providing the CCNc.

## References

[1] C. D. O'Dowd and G. de Leeuw, "Marine aerosol production: a review of the current knowledge," *Philosophical Transactions of the Royal Society A*, vol. 365, no. 1856, pp. 1753–1774, 2007.

[2] C. Pilinis, S. N. Pandis, and J. H. Seinfeld, "Sensitivity of direct climate forcing by atmospheric aerosols to aerosol size and composition," *Journal of Geophysical Research*, vol. 100, no. 9, pp. 18–754, 1995.

[3] H. Wex, G. McFiggans, S. Henning, and F. Stratmann, "Influence of the external mixing state of atmospheric aerosol on derived CCN number concentrations," *Geophysical Research Letters*, vol. 37, no. 10, Article ID L10805, 2010.

[4] M. D. Petters and S. M. Kreidenweis, "A single parameter representation of hygroscopic growth and cloud condensation nucleus activity," *Atmospheric Chemistry and Physics*, vol. 7, no. 8, pp. 1961–1971, 2007.

[5] A. H. Woodcock, C. F. Kientzler, A. B. Arons, and D. C. Blanchard, "Giant condensation nuclei from bursting bubbles," *Nature*, vol. 172, no. 4390, pp. 1144–1145, 1953.

[6] G. Feingold, W. R. Cotton, S. M. Kreidenweis, and J. T. Davis, "The impact of giant cloud condensation nuclei on drizzle formation in stratocumulus: implications for cloud radiative properties," *Journal of the Atmospheric Sciences*, vol. 56, no. 24, pp. 4100–4117, 1999.

[7] A. M. Blyth, S. G. Lasher-Trapp, W. A. Cooper, C. A. Knight, and J. Latham, "The role of giant and ultragiant nuclei in the formation of early radar echoes in warm cumulus clouds," *Journal of the Atmospheric Sciences*, vol. 60, no. 21, pp. 2557–2572, 2003.

[8] H. E. Gerber, G. M. Frick, J. B. Jensen, and J. G. Hudson, "Entrainment, mixing, and microphysics in trade-wind-cumulus," *Journal of the Meteorological Society of Japan*, vol. 86A, pp. 87–106, 2008.

[9] C. Textor, M. Schulz, S. Guibert et al., "Analysis and quantification of the diversities of aerosol life cycles within AeroCom," *Atmospheric Chemistry and Physics*, vol. 6, no. 7, pp. 1777–1813, 2006.

[10] D. A. Randell, J. A. Coakley Jr., C. W. Fairall, R. A. Kropfli, and D. H. Lenschow, "Outlook for research on subtropical marine stratiform clouds," *Bulletin of the American Meteorological Society*, vol. 65, no. 12, pp. 1290–1301, 1984.

[11] B. A. Albrecht, "Aerosols, cloud microphysics, and fractional cloudiness," *Science*, vol. 245, no. 4923, pp. 1227–1230, 1989.

[12] L. I. Aluwihare and D. J. Repeta, "A comparison of the chemical characteristics of oceanic DOM and extracellular DOM produced by marine algae," *Marine Ecology Progress Series*, vol. 186, pp. 105–117, 1999.

[13] N. Meskhidze and A. Nenes, "Phytoplankton and cloudiness in the southern ocean," *Science*, vol. 314, no. 5804, pp. 1419–1423, 2006.

[14] E. G. Stephanou, "Analysis of anthropogenic and biogenic lipids in the aerosol of a coastal area in East Mediterranean Sea," *Fresenius' Journal of Analytical Chemistry*, vol. 339, no. 10, pp. 780–784, 1991.

[15] C. A. Randles, L. M. Russell, and V. Ramaswamy, "Hygroscopic and optical properties of organic sea salt aerosol and consequences for climate forcing," *Geophysical Research Letters*, vol. 31, no. 16, Article ID L16108, 2004.

[16] F. Cavalli, M. C. Facchini, S. Decesari et al., "Advances in characterization of size-resolved organic matter in marine aerosol over the North Atlantic," *Journal of Geophysical Research D*, vol. 109, no. 24, Article ID D24215, 2004.

[17] C. D. O'Dowd, M. C. Facchini, F. Cavalli et al., "Biogenically driven organic contribution to marine aerosol," *Nature*, vol. 431, no. 7009, pp. 676–680, 2004.

[18] M. Mochida, Y. Kitamori, K. Kawamura, Y. Nojiri, and K. Suzuki, "Fatty acids in the marine atmosphere: factors governing their concentrations and evaluation of organic films on sea-salt particles," *Journal of Geophysical Research D*, vol. 107, no. 17, article 4325, 2002.

[19] H. Tervahattu, K. Hartonen, V.-M. Kerminen et al., "New evidence of an organic layer on marine aerosols," *Journal of Geophysical Research D*, vol. 107, no. 7, article 4053, 2002.

[20] H. Tervahattu, J. Juhanoja, and K. Kupiainen, "Identification of an organic coating on marine aerosol particles by TOF-SIMS," *Journal of Geophysical Research D*, vol. 107, no. 16, article 4319, 2002.

[21] G. B. Ellison, A. F. Tuck, and V. Vaida, "Atmospheric processing of organic aerosols," *Journal of Geophysical Research D*, vol. 104, no. 9, pp. 11633–11641, 1999.

[22] M. C. Facchini, M. Mircea, S. Fuzzi, and R. J. Charlson, "Cloud albedo enhancement by surface-active organic solutes in growing droplets," *Nature*, vol. 401, no. 6750, pp. 257–259, 1999.

[23] R. H. Moore, E. D. Ingall, A. Sorooshian, and A. Nenes, "Molar mass, surface tension, and droplet growth kinetics of marine organics from measurements of CCN activity," *Geophysical Research Letters*, vol. 35, no. 7, Article ID L07801, 2008.

[24] K. Sellegri, C. D. O'Dowd, Y. J. Yoon, S. G. Jennings, and G. de Leeuw, "Surfactants and submicron sea spray generation," *Journal of Geophysical Research D*, vol. 111, no. 22, Article ID D22215, 2006.

[25] H. Wex, F. Stratmann, D. Topping, and G. McFiggans, "The Kelvin versus the raoult term in the köhler equation," *Journal of the Atmospheric Sciences*, vol. 65, no. 12, pp. 4004–4016, 2008.

[26] H. R. Pruppacher and J. D. Klett, *Microphysics of Clouds and Precipitation*, Kluwer Academic Publishers, Dordrecht, The Netherlands, 1997.

[27] D. Niedermeier, H. Wex, J. Voigtländer et al., "LACIS-measurements and parameterization of sea-salt particle hygroscopic growth and activation," *Atmospheric Chemistry and Physics*, vol. 8, no. 3, pp. 579–590, 2008.

[28] C. W. Brown and J. A. Yoder, "Coccolithophorid blooms in the global ocean," *Journal of Geophysical Research*, vol. 99, no. 4, pp. 7467–7482, 1994.

[29] V. Schoemann, S. Becquevort, J. Stefels, V. Rousseau, and C. Lancelot, "Phaeocystis blooms in the global ocean and their controlling mechanisms: a review," *Journal of Sea Research*, vol. 53, no. 1-2, pp. 43–66, 2005.

[30] E. Fuentes, H. Coe, D. Green, G. De Leeuw, and G. McFiggans, "Laboratory-generated primary marine aerosol via bubble-bursting and atomization," *Atmospheric Measurement Techniques*, vol. 3, pp. 1–22, 2010.

[31] H. Wex, T. Hennig, I. Salma et al., "Hygroscopic growth and measured and modeled critical super-saturations of an

atmospheric HULIS sample," *Geophysical Research Letters*, vol. 34, no. 2, Article ID L02818, 2007.

[32] H. Wex, M. D. Petters, C. M. Carrico et al., "Towards closing the gap between hygroscopic growth and activation for secondary organic aerosol—part 1: evidence from measurements," *Atmospheric Chemistry and Physics*, vol. 9, no. 12, pp. 3987–3997, 2009.

[33] D. Kester, I. Duedall, D. Conners, and R. Pytkowicz, "Preparation of artificial seawater," *Limnology and Oceanography*, vol. 12, pp. 176–179, 1976.

[34] R. Guillard, "Culture of phytoplankton for feeding marine invertebrates," in *Culture of Marine Invertebrate Animals*, pp. 26–60, Plenum Press, New York, NY, USA, 1975.

[35] V. Ittekkot, "Variations of dissolved organic matter during a plankton bloom: qualitative aspects, based on sugar and amino acid analyses," *Marine Chemistry*, vol. 11, no. 2, pp. 143–158, 1982.

[36] M. W. Lomas, P. M. Glibert, D. A. Clougherty et al., "Elevated organic nutrient ratios associated with brown tide algal blooms of Aureococcus anophagefferens (Pelagophyceae)," *Journal of Plankton Research*, vol. 23, no. 12, pp. 1339–1344, 2001.

[37] F. Fraga, "Phytoplanktonic biomass synthesis: application to deviations from Redfield stoichiometry," *Scientia Marina*, vol. 65, no. 2, pp. 153–169, 2001.

[38] H. Wex, A. Kiselev, F. Stratmann, J. Zoboki, and F. Brechtel, "Measured and modeled equilibrium sizes of NaCl and $(NH_4)_2SO_4$ particles at relative humidities up to 99.1%," *Journal of Geophysical Research D*, vol. 110, no. 21, Article ID D21212, 2005.

[39] A. Kiselev, H. Wex, F. Stratmann, A. Nadeev, and D. Karpushenko, "White-light optical particle spectrometer for in situ measurements of condensational growth of aerosol particles," *Applied Optics*, vol. 44, no. 22, pp. 4693–4701, 2005.

[40] G. C. Roberts and A. Nenes, "A continuous-flow streamwise thermal-gradient CCN chamber for atmospheric measurements," *Aerosol Science and Technology*, vol. 39, no. 3, pp. 206–221, 2005.

[41] E. Fuentes, H. Coe, D. Green, and G. McFiggans, "On the impacts of phytoplankton-derived organic matter on the properties of primary marine aerosol," in preparation.

[42] W. P. Kelly and P. H. McMurry, "Measurement of particle density by inertial classification of differential mobility analyzer-generated monodisperse aerosols," *Aerosol Science and Technology*, vol. 17, no. 3, pp. 199–212, 1992.

[43] D. Rose, S. S. Gunthe, E. Mikhailov et al., "Calibration and measurement uncertainties of a continuous-flow cloud condensation nuclei counter (DMT-CCNC): CCN activation of ammonium sulfate and sodium chloride aerosol particles in theory and experiment," *Atmospheric Chemistry and Physics*, vol. 8, no. 5, pp. 1153–1179, 2008.

[44] K. Sellegri, P. Villani, D. Picard, R. Dupuy, C. O'Dowd, and P. Laj, "Role of the volatile fraction of submicron marine aerosol on its hygroscopic properties," *Atmospheric Research*, vol. 90, no. 2–4, pp. 272–277, 2008.

[45] K. Kandler and L. Schütz, "Climatology of the average water-soluble volume fraction of atmospheric aerosol," *Atmospheric Research*, vol. 83, no. 1, pp. 77–92, 2007.

[46] E. Swietlicki, H.-C. Hansson, K. Hämeri et al., "Hygroscopic properties of submicrometer atmospheric aerosol particles measured with H-TDMA instruments in various environments: a review," *Tellus Series B*, vol. 60, no. 3, pp. 432–469, 2008.

[47] G. McFiggans, P. Artaxo, U. Baltensperger et al., "The effect of physical and chemical aerosol properties on warm cloud droplet activation," *Atmospheric Chemistry and Physics*, vol. 6, no. 9, pp. 2593–2649, 2006.

[48] P. K. Quinn, D. S. Covert, T. S. Bates, V. N. Kapustin, D. C. Ramsey-Bell, and L. M. McInnes, "Dimethylsulfide/cloud condensation nuclei/climate system: relevant size-resolved measurements of the chemical and physical properties of atmospheric aerosol particles," *Journal of Geophysical Research*, vol. 98, no. 6, pp. 411–427, 1993.

Hindawi Publishing Corporation
Advances in Meteorology
Volume 2010, Article ID 754941, 7 pages
doi:10.1155/2010/754941

*Research Article*

# Eddy Correlation Measurements of Ozone Fluxes over Coastal Waters West of Ireland

**Philip McVeigh, Colin O'Dowd, and Harald Berresheim**

*School of Physics, Centre for Climate and Air Pollution Studies, National University of Ireland, Galway, Ireland*

Correspondence should be addressed to Harald Berresheim, harald.berresheim@nuigalway.ie

Received 15 February 2010; Revised 12 May 2010; Accepted 15 June 2010

Academic Editor: Nicholas Meskhidze



Measurements of ozone fluxes using the eddy-correlation (EC) technique were carried out for the first time at the Mace Head atmospheric research station, on the west coast of Ireland between August-October 2009. Vertical exchange of ozone was measured from a tower platform at 22 m above mean sea level to study fluxes over coastal waters excluding the tidal region. The results were averaged over 30 min and exhibited predominantly downward but also upward transport of ozone in the boundary layer. Data quality was found to be high based on inspection of cospectra and micrometeorological measurements. During the study period, a major physical influence on $O_3$ fluxes was found to be wind speed. Measured fluxes were of the same magnitude as reported in previous open ocean studies ranging from approximately +0.2 to $-0.5\,\mu g\ m^{-2}\ s^{-1}$ ($-0.017\,\mu g\ m^{-2}\ s^{-1}$ on average, corresponding to a deposition velocity of 0.25 mm $s^{-1}$ or a surface resistance of 4.13 s $mm^{-1}$). These results are considered to represent ozone fluxes over shallow coastal waters west of Ireland for conditions during summer and fall not affected by phytoplankton blooms.

## 1. Introduction

Tropospheric ozone has potential negative impacts on human health and vegetation, and also acts as an important greenhouse gas. Background ozone levels at Mace Head Research Station in western Ireland, currently at an annual average of 35 ppbv, have shown a steady increase over the past two decades at an overall rate of 0.31 ppbv/year between 1987 and 2007 [1]. During the same period the relative contribution to these increasing ozone levels from air advected over the North Atlantic has also significantly grown. Deposition of ozone to surface ocean waters via physical uptake (solubility, turbulent mixing) and chemical reactions in the surface layer [2–4] likely constitute a significant, albeit highly variable "buffer" curtailing the rate of ozone increase in this region.

It has been proposed that ozone can be rapidly degraded by chemical reactions with biogenically produced compounds such as iodide in surface seawater [5–7] leading to the release of iodine compounds followed by rapid particle nucleation [8]. Recent measurements over the northern coast of France by Whitehead et al. [9] appear to confirm the link between ozone deposition fluxes to exposed tidal flats and the reactions of ozone with volatilized iodine compounds producing new particles and contributing to particle growth and formation of cloud condensation nuclei. This study was primarily aimed at understanding particle production involving ozone deposition over tidal regions whereas very little is known to date about the potential importance of this process over open ocean waters.

The spatial extent of tidal regions is insignificant compared to the open ocean water scale. It has been shown that despite its moderate water solubility the physical removal of ozone by air-sea exchange can be substantial at high wind speeds, increasing by a factor of up to five as wind speed increases from 0 to 20 m $s^{-1}$ [6]. Nevertheless, ozone deposition velocities over ocean waters are relatively low compared to exposed tidal or continental regions (typically <0.1 cm $s^{-1}$) and are therefore difficult to measure. Due to these challenging conditions, very few corresponding field measurements have been conducted up to now [9–12].

Future model simulations and predictions of ozone removal rates in North Atlantic marine air are in progress to establish a baseline for the seasonal ozone influx to western

Europe and, specifically, to Ireland (see [13] this issue). The biochemical removal rate of ozone may also exhibit a seasonal signal in conjunction with phytoplankton blooms occurring mainly during spring and summer. Therefore, model improvement requires complementary direct measurements of ozone deposition fluxes to surface seawater over at least one full seasonal cycle. In the present paper we report first data for ozone fluxes measured by eddy correlation at the Mace Head Atmospheric Research station during the period August–October 2009. The primary goal of this study was to provide a data base for large-scale model simulations by measuring ozone fluxes over continental shelf waters excluding tidal regions.

## 2. Experimental

The Mace Head observatory is located on the west coast of Ireland (53°20′N, 9°54′W). The local meteorology, research facilities, and measurement programme have previously been described in detail by Jennings et al. [14] and O'Connor et al. [15]. Mace Head is located on a peninsula with the oceanic footprint from the North Atlantic corresponding to the local 220°–320° wind sector. On a yearly average, westerly winds from this sector prevail (55%), the average wind speed is 7 m $s^{-1}$, and water depths within the flux footprint vary between 10–33 m.

In August 2009, a Rapid Ozone Flux Instrument (ROFI; [16]) based on the technique developed by Gusten et al. [17], was installed on top of the 22 m tower at Mace Head. The shoreline in front of the 22 m tower is inhomogeneous, rocky, and slanted with a tidal region that extends from 80 m to 180 m away from the base of the tower. The tower is supported by guy wires to reduce vibrations, and has been constructed in order to minimize shadowing on sensors or obstruction to airflow from the marine sector.

Previous footprint and micrometeorological analyses by Norton et al. [18] and Kunz and de Leeuw [19] under marine air mass conditions had shown that flux measurements from the top of the tower (22 m) maximize the oceanic footprint. This has also been confirmed by further micrometeorological studies at Mace Head which established relationships between wind speed and $CO_2$ flux [20] and between wind speed and primary marine aerosol fluxes [21, 22].

In addition to the ROFI instrument, the eddy flux system used in the present study included a three-dimensional ultrasonic anemometer (Sonic R3; Gill) measuring the three orthogonal wind velocity components $u$, $v$, $w$ at 10 Hz, a UV photometric ozone analyser (model 49i; Thermo Scientific) measuring ambient $O_3$ mixing ratios at 22 m height with a 1 min resolution, and an open path, nondispersive $H_2O/CO_2$ infrared gas analyser (LI-7500; Licor). The latter instrument was used to obtain water vapour data for the Webb correction (see next section), and the $CO_2$ data were used to identify and remove rainfall periods from the $O_3$ flux records.

The ROFI recorded ozone fluctuations at 10 Hz by measuring the chemiluminescence generated from the reaction of $O_3$ with a coumarin-based dye coated on a disc installed perpendicular to the sample air stream across from a photomultiplier tube. The temperature of the disc was maintained at 30°C, and the sample flow rate was kept at 100 litres per minute according to the users manual. The intake tubing length and diameter were 5 m and 0.019 m, respectively. The raw voltage signals from the ROFI were calibrated in ppbv units based on the 1 min resolution measurements of the UV photometric analyzer. The effective coating on one disc lasted on average for about 3–5 days after which a new disc was prepared and installed.

The system components were located on the marine sector side of the tower. The anemometer head, the Licor head, and the ROFI intake tubing were all colocated on the end of a 3 m boom extending towards the marine sector, with minimal separation between the ROFI intake and the sonic head (0.1 m in the vertical, 0 m in the horizontal plane). The boom was supported by an extended arm to reduce vibrations in the vertical and horizontal planes, and the anemometer head was leveled with the horizon to decrease errors in subsequent coordinate rotations.

## 3. Theory

Eddy covariance (EC) is a direct micrometeorological technique for measuring turbulent fluxes in the atmospheric boundary layer. The peak of the spectrum of eddy size depends on the measurement height, the surface roughness height, and wind speed, since eddies increase in size with height and decreased surface roughness. A scalar flux can be measured provided the instrumentation is sufficiently fast-response (10–20 Hz) to capture the dominant range of eddy sizes contributing to the flux.

In general, it is assumed that EC measurements made at one point are representative of the area upwind and that the footprint is large enough for the entire fetch to fall within it. It is also assumed that most net vertical transfer is carried out by eddies, and that there are no low-frequency trends in the data (*stationarity requirement*). Application of a 5 min running mean (high-pass filter) ensured that the stationarity requirement was met, and data were subsequently checked to verify that the running mean was correctly applied. Such detrending may cause a slight underestimation of flux but can be compensated for through spectral analysis [23]. However, such corrections were not applied since corresponding changes in absolute flux magnitudes amount to less than 18% having no effect on flux direction [20].

The height-independent bulk transfer process for heat or trace gases is treated as the sum of the turbulent transfer of the scalar variable from a height $z$ (m) above the surface in question, to the zero plane displacement height, $d$ (m) as well as the transfer across a diffusive sublayer that extends a few millimetres above the surface. Both of these pathways can be represented by resistances, assuming that no storage or chemical conversion occurs within the measurement height on the scale of turbulent transport [24].

The aerodynamic atmospheric resistance ($r_a$) is used to represent the first pathway, and is calculated assuming gradient transport theory. This resistance depends on turbulent intensity, which in turn depends on atmospheric stability. An additional resistance representing the near-surface laminar

sublayer ($r_b$), across which transport is governed by molecular diffusion to the surface, represents the second pathway, and can vary spatially and temporally, providing the main resistance to deposition. The total resistance $r_t$ is defined as

$$r_t = r_a + r_b + \cdots = -\frac{X_{O_3}}{F_{O_3}} = -\frac{1}{v_d}, \quad (1)$$

where $v_d$ represents the deposition velocity, and $X_{O_3}$ and $F_{O_3}$ represent the ozone concentration and ozone flux at the measurement height, respectively. The aerodynamic and molecular sublayer transport define the maximum possible deposition velocity. Additional resistance terms due to other processes may be inferred from the difference between total flux measurements and the computed resistance terms.

## 4. Data Reduction

As already described in Section 2, rainfall contaminated data periods were removed as well as periods with wind directions outside of the marine sampling sector. To ensure that data quality from the ROFI was satisfactory, a procedure was implemented to identify and discard erroneous or low-quality data points. The first few hours of a disc sampling period sometimes contained spurious values, and so all data up to 2 hours immediately after renewing a disc were removed. Ozone mixing ratios obtained from the UV photometric instrument were plotted against ROFI output voltages for each sample disc at a 1 min resolution as well as the ratios between both data sets. Outliers and periods of questionable data were removed, especially towards the end of a disc sampling period, when sensitivity was reduced to about 1-2 V output signal. A more detailed description of this procedure can be found in Muller et al. [25]. In order to maximize correlation, corresponding data sets were phase-shifted to compensate for any time delays in the data logging process. The time delay for the ROFI instrument was calculated to be 0.85 sec based on intake tube dimensions and flow rate (see Section 2).

Ultrasonic anemometer temperature data were used to calculate the virtual air temperature, which was then corrected for water vapour fluctuations to obtain the true air temperature. Performing a running mean on data sets acted like a recursive high-pass filter, whereby lower frequency trends were attenuated by using a running mean time constant of 5 min. Coordinate rotations were applied in order to minimize errors caused by vertical advection or human error in sonic leveling. Two-dimensional coordinate rotations were used, and basically pointed $\overline{u}$ in the direction of mean incident air flow by minimizing $\overline{v}$ and $\overline{w}$ to zero.

Covariances were calculated and then block-averaged over 30 min periods to yield momentum flux ($\tau$), friction velocity ($u^*$), drag coefficient ($C_D$), roughness length ($z_0$), sensible heat flux ($H$), latent heat flux ($LE$), and Monin-Obukhov length ($L$). The latter was used to define a dimensionless scaling parameter, z/L, to define the thermal stability state of the boundary layer.

Three different methods were applied to obtain ozone fluxes: the Ratio Method (RM), the Ratio Offset Method (ROM), and the Disc calibration method (DCM). For the RM method, raw covariances of the vertical wind component with the raw $O_3$ signal (voltages from the ROFI), were divided by the mean voltage to provide the deposition velocity, which was then multiplied by the absolute ozone concentration. This method assumes that the voltages are proportional to the absolute concentrations including a zero offset. The ROM method is based on the RM method, with a modification that accounts for the offset (mean output at zero ozone concentration) in the analyser. The offset was obtained by calculating the intercept of ozone concentrations plotted against voltages by using 1 min averages for each hour of data. The DCM method applies a calibration factor to the raw flux for each disc period, which was obtained by calculating the slope of the relationship between the output voltage and $O_3$ concentration. This calibration factor was then multiplied by the raw flux to obtain absolute ozone fluxes. A detailed comparison of these three methods can be found in Muller et al. [25].

In a further step, the Webb correction [26] was applied to the fluxes of $H_2O$ and $O_3$. A small but significant vertical velocity known as the Webb velocity may arise from the fact that turbulent motion can also consist of ascending or descending air parcels due to density differences and must be taken into account when evaluating EC flux measurements.

The water vapour flux was corrected for density variations due to temperature fluctuations which was then used along with the temperature flux to calculate the Webb velocity:

$$\overline{w} = \mu \frac{\overline{w'q'}}{\rho_d} + (1 + \mu\sigma) \frac{\overline{w'T'}}{\overline{T}}. \quad (2)$$

Here, $\mu$ is the ratio of the molecular masses of air to water (1.6077), $\sigma$ is the ratio of moist and dry air densities, and $\rho_d$ is the density of dry air. The resulting Webb velocity was then applied to the raw $O_3$ flux:

$$F_{X,O_3} = \overline{w'X'_{O_3}} + \overline{w}\overline{X_{O_3}}. \quad (3)$$

The filtering of data was divided into two main categories, and only data meeting certain criteria were retained.

(1) Filtering for an *oceanic footprint.*

   (a) *Wind direction* ($220° \leq \text{WD} \leq 320°$). Data with a wind direction outside this range were removed to obtain an oceanic fetch.

   (b) *Stability* ($-2 \leq \text{z/L} \leq 2$). Data with a stability scaling parameter outside this range were removed to ensure that extreme stability cases were excluded. This was also the range investigated by Kaimal et al. [27], making cospectral comparisons more relevant.

   (c) *Source Region* (≥90% of cumulative normalized contribution to flux, CNF, at ≥700 m distance from tower). Data points that had more than 10% of their CNF within 700 m distance of the tower were removed to exclude any remaining influences from exposed land surfaces.

(2) Filtering for *data quality.*

(a) *Wind speed variability* ($\sigma_{U_{22}} \leq (U_{22}/7.5)$). Data points with a high 22 m level wind speed variability (or standard deviation, $\sigma_{U_{22}}$) were removed assuming $U_{22}/7.5$ as a suitable cutoff level.

(b) *Correlation between raw* $O_3$ *signal voltages and* $O_3$ *concentrations.* If the correlation coefficient between these two variables was <0.5 for any 30 minute period, the data was deemed unsatisfactory. Correlation coefficients were computed using the same data used for computing the offsets and calibration factors for the ROM and DCM methods.

## 5. Results and Discussion

Figure 1 shows the results of the filtered data set consisting of 69 half-hour periods. The three methods used to determine ozone fluxes (RM, ROM and DCM) produced nearly identical results. Therefore, only fluxes obtained using the ROM method are presented. $O_3$ fluxes ranged from +0.2 to $-0.5\,\mu g\,m^{-2}\,s^{-1}$ ($-0.017\,\mu g\,m^{-2}\,s^{-1}$ on average, corresponding to a deposition velocity of $0.25\,mm\,s^{-1}$ or a surface resistance of $4.13\,s\,mm^{-1}$). The large variability and range of fluxes observed here are comparable to values reported previously for other coastal areas [9, 11, 12] as well as recent shipboard measurements over open ocean regions [10]. Daytime and nighttime periods are also indicated in Figure 1. Corresponding average fluxes were $-0.038\,\mu g\,m^{-2}\,s^{-1}$ and $-0.021\,\mu g\,m^{-2}\,s^{-1}$, respectively, which suggest a diurnal cycle similar to what has been reported by Gallagher et al. [11]. However, the difference between both values was not statistically significant.

Data loss resulted mostly from data filtering due to out-of-sector wind conditions, rainfall, and poor disc quality. Four distinct periods can be identified from Figure 1. $O_3$ fluxes during the third period (early October, yearday 276–278) were conspicuously low and virtually zero. The data were deemed to be sound since no evidence was found for malfunction of the instruments during the corresponding period. Therefore, cospectra of all $O_3$ fluxes with values between $|0.01|$ and $|0.02|\,\mu g\ m^{-2}\,s^{-1}$ were averaged and are shown as a single line ($wX$) in Figure 2, approximating to the temperature cospectra ($wT$). Since smaller high-frequency eddies transport scalars more effectively than lower frequency eddies, they are of most interest here. The theoretical ideal slope described by Kaimal et al. [27] displaying a $-4/3$ power law is shown for comparison. It agrees well with both the $wX$ and $wT$ cospectra at higher frequencies. This shows that the data were of good quality and suggests that noise was negligible in this frequency range.

Back trajectories of air masses were evaluated for each measurement period. Figure 3 shows an example for September 6 (yearday 250) which, overall, was typical for the periods shown in Figure 1. Therefore, the variations found in the data were likely not caused by major changes in air mass composition. As outlined in Section 2, any influence by tidal movements on the recorded fluxes was expected to be negligible (see also Figure 5). Footprint contributions were calculated and averaged for 30 min periods based on the model by Schuepp et al. [28]. The model applies to neutral stability conditions which were predominant during all study periods and typically prevail at Mace Head during westerly flow due to moderate to high wind speeds producing a well-mixed boundary layer [22]. A cumulative normalised contribution to the flux measurements curve (CNF) was estimated as a function of distance from the measurement point. This curve was differentiated to obtain the relative contribution to the measured flux as a function of distance and was calculated for an average of all half-hour high wind speed (≥8 m/s) and low wind speed (<8 m/s) data normalised to a height of 10 m ($U_{10}$ wind speed) for an oceanic fetch. These two curves are shown in Figure 4, with distance given on a logarithmic scale on the $x$-axis. The peak contribution, or most likely source region for both wind speed regimes was close to 1 km, verifying that the footprint was large enough for the majority of the fetch of interest to fall within it and thereby matching one of the key EC theory assumptions. The higher wind speed curve gives greater accuracy and confidence in locating the source region due to its narrower width and higher peak. The two black vertical lines represent upper and lower tidal limits (80 m and 180 m, resp.). The peak contribution for both high and low wind speeds was thus from significantly beyond the lower tidal limit, suggesting the impact of the tidal zone to be minimal and the measurement height of 22 m to be adequate.

Figure 5 shows a scatter plot of $O_3$ fluxes versus the corresponding $O_3$ mixing ratios. The latter varied between about 25 ppbv and 45 ppbv during the entire measurement period, that is, over a relatively small range. This may partially explain why a consistent relationship between both data sets was not evident. However, a moderately strong relationship between wind speed and $O_3$ fluxes was found as shown in

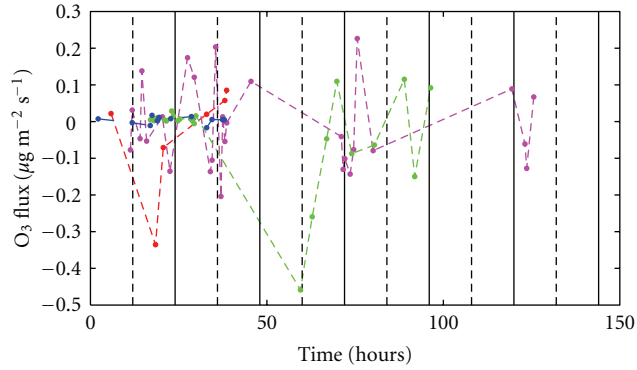


Figure 1: Time series of 30 min averaged $O_3$ fluxes (dots) during August–October 2009 showing the four main measurement periods; red: 28-29 August (Yearday 240-241), magenta: 4–9 September (Yearday 247–252), blue: 3-4 October (Yearday 276–278), and green: 22–26 October (Yearday 295-299). Time in hours from 00:00 on the first day of each period is shown on the $x$-axis, with 12:00 and 00:00 marked sequentially with a dotted and solid vertical line, respectively.

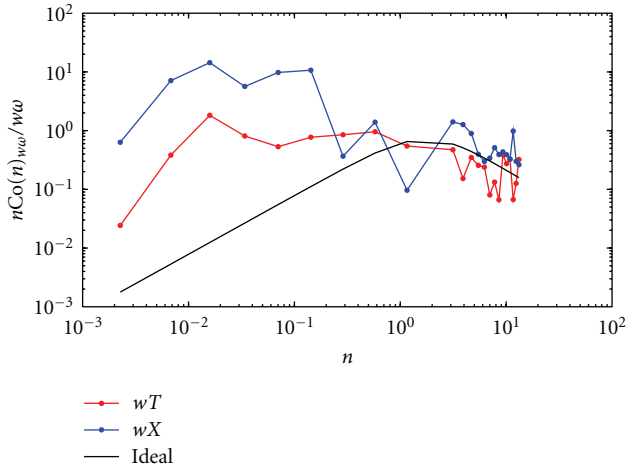


FIGURE 2: Averaged smoothed and normalized temperature cospectra ($wT$, in red) and $O_3$ cospectra ($wX$, in blue) for all $O_3$ flux values between |0.01| and |0.02| $\mu g\,m^{-2}\,s^{-1}$. The symbols $T$, $X$, $w$, $n$, and $\omega$ represent temperature, $O_3$ signal, vertical wind speed component, and frequency, respectively. The theoretical (ideal) slope according to Kaimal et al. [27] displaying a −4/3 power law is also shown.

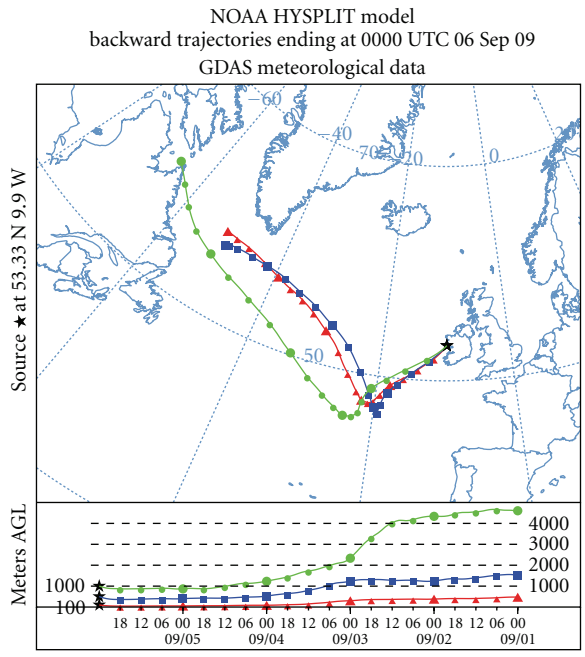


FIGURE 3: NOAA HYSPLIT back trajectories for Mace Head shown for period (2). These clean air sector trajectories were typical for all four periods shown in Figure 1. The red line shows 100 m, the blue line 500 m, and the green line 1000 m trajectory altitudes.

Figure 6. A power-law regression was applied and resulted in a best fit curve shown by the solid black line of the form $F_{O_3} = 7.75 \times 10^{-4}(U_{10})^{1.56}$. Ozone deposition fluxes tended to increase with higher wind speeds, which were coincident with the largest negative fluxes shown in Figure 1. Previously, McVeigh [20] reported a qualitatively similar relationship between wind speed and $CO_2$ fluxes measured at Mace Head.

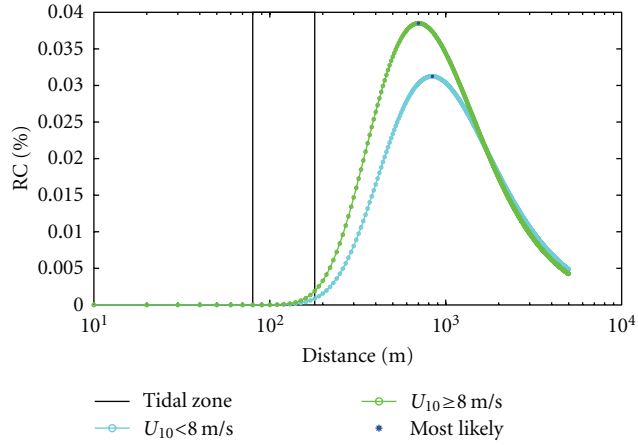


FIGURE 4: Relative flux contribution for EC measurements at 22 m height on the Mace Head tower. Footprint distance from the measurement location is shown on the $x$-axis. The tidal zone is represented by the two vertical black lines.

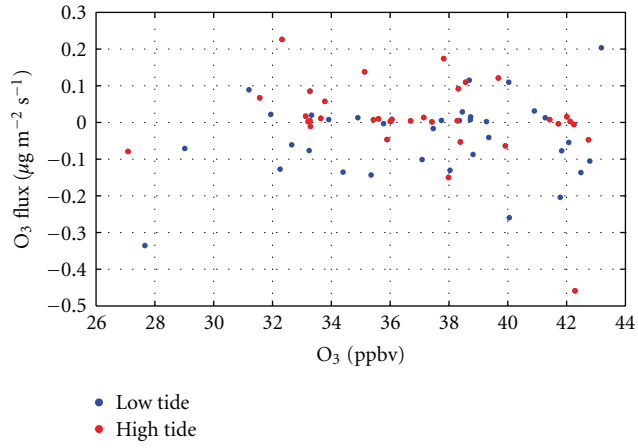


FIGURE 5: Scatter plot of $O_3$ fluxes versus $O_3$ mixing ratios showing a relatively low correlation between both data sets ($r^2 = 0.038$). High-tide and low-tide fluxes are also shown by different coloured symbols.

However, to a certain extent the scatter in the ozone flux data may also be due to chemical reactions in the atmospheric boundary and the sea surface layer. On the other hand, based on Aqua satellite observations by the MODIS (Moderate Resolution Imaging Spectroradiometer) instrument (http://oceancolor.gsfc.nasa.gov/products/chlo.html) we found no evidence for major phytoplankton blooms occurring in the footprint area during any of the observation periods. This may rule out the presence of high concentrations of reactive hydrocarbons affecting ozone deposition. With respect to the very low fluxes measured during the third period (also in the beginning of the fourth period) the red symbols in Figure 6 highlight the corresponding data showing that their magnitudes were independent of wind speed, and therefore other reasons must exist for their relatively small values.

$O_3$ fluxes were found to be both negative and positive in their direction of transport, which was not expected because

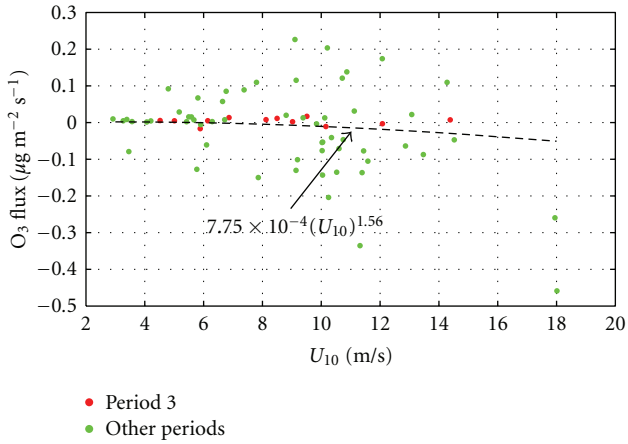


FIGURE 6: Relationship between 10 m wind speed and $O_3$ fluxes measured at 22 m. The black line represents the power-law relation between the 10 m wind speed and $O_3$ fluxes which was calculated as $F_{O_3} = 7.75 \times 10^{-4}(U_{10})^{1.56}$ ($r^2 = 0.344$). The red data points represent data from period (3) in Figure 1.

there are no processes at the sea surface that are known to produce $O_3$. A possible explanation for the positive fluxes may be signal noise since more flux values were measured below $-0.1\,\mu g\,m^{-2}\,s^{-1}$ than above $0.1\,\mu g\,m^{-2}\,s^{-1}$. However, given that the $O_3$ cospectra in Figure 2, which represent all fluxes between $|0.01|$ and $|0.02|\,\mu g\,m^{-2}\,s^{-1}$ exhibited a good shape and were similar to the temperature cospectra, noise was unlikely to be a major problem in this range.

## 6. Conclusions

First measurements of ozone fluxes during late summer and fall season have been conducted over shallow coastal waters west of Ireland based on the eddy flux covariance method. The results were comparable with previous studies at other coastal locations and over open ocean areas. We consider our results as baseline $O_3$ fluxes in the absence of major phytoplankton blooms which did not occur during the measurement periods in the footprint region as verified from satellite observations by the Aqua/MODIS instrument. The measurement height of 22 m was appropriate for excluding any significant influence by tidal movements on the measured fluxes. A diurnal signal was suggested by the average results but could not be statistically distinguished.

The main physical influence on $O_3$ fluxes was wind speed. Chemical reactions in the air and sea surface may have significantly influenced deposition rates, being the most plausible reason for the large degree of scatter observed. Although not highly significant, the power-law fit in Figure 6 points in a negative (downward) direction, consistent with the mean $O_3$ flux value measured in this study. Negative fluxes were expected according to theory, but the present results suggest that at the relatively small exchange rates encountered over open waters (compared to continental and exposed tidal environments) transport can occur in both directions, most likely due to its turbulent nature (see also [10]).

The current measurements are planned to be continued over a longer time period in order to investigate the seasonality of the fluxes, as well as any biological influences in more detail. Larger deposition rates are expected over regions with emissions from phytoplankton blooms due to increased chemical removal of ozone by reactions with hydrocarbons such as isoprene. Shipborne investigations during the occurrence of such blooms would be important to further establish the potential importance of the oceanic biosphere in curtailing atmospheric ozone levels with implications for particle nucleation, and to provide more data for corresponding global model simulations.

## Acknowledgments

The authors would like to thank Mhairi Coyle for building the ROFI instrument, for training and many helpful comments. They would also like to thank Dilip Chate for help in setting up the measurements, as well as EPA Ireland for providing financial support under Grant 2007-CCRP-5.3.

## References

[1] R. G. Derwent, P. G. Simmonds, A. J. Manning, and T. G. Spain, "Trends over a 20-year period from 1987 to 2007 in surface ozone at the atmospheric research station, Mace Head, Ireland," *Atmospheric Environment*, vol. 41, no. 39, pp. 9091–9098, 2007.

[2] L. Ganzeveld, D. Helmig, C. W. Fairall, J. Hare, and A. Pozzer, "Atmosphere-ocean ozone exchange: a global modeling study of biogeochemical, atmospheric, and waterside turbulence dependencies," *Global Biogeochemical Cycles*, vol. 23, no. 4, 16 pages, 2009.

[3] D. I. Reeser, A. Jammoul, D. Clifford et al., "Photoenhanced reaction of ozone with chlorophyll at the seawater surface," *Journal of Physical Chemistry C*, vol. 113, no. 6, pp. 2071–2077, 2009.

[4] D. Clifford, D. J. Donaldson, M. Brigante, B. D'Anna, and C. George, "Reactive uptake of ozone by chlorophyll at aqueous surfaces," *Environmental Science and Technology*, vol. 42, no. 4, pp. 1138–1143, 2008.

[5] M. Martino, G. P. Mills, J. Woeltjen, and P. S. Liss, "A new source of volatile organoiodine compounds in surface seawater," *Geophysical Research Letters*, vol. 36, no. 1, Article ID L01609, 2009.

[6] W. Chang, B. G. Heikes, and M. Lee, "Ozone deposition to the sea surface: chemical enhancement and wind speed dependence," *Atmospheric Environment*, vol. 38, no. 7, pp. 1053–1059, 2004.

[7] G. McFiggans, H. Coe, R. Burgess et al., "Direct evidence for coastal iodine particles from Laminaria macroalgae—linkage to emissions of molecular iodine," *Atmospheric Chemistry and Physics*, vol. 4, no. 3, pp. 701–713, 2004.

[8] C. D. O'Dowd, J. L. Jimenez, R. Bahreini et al., "Marine aerosol formation from biogenic iodine emissions," *Nature*, vol. 417, no. 6889, pp. 632–636, 2002.

[9] J. D. Whitehead, G. B. Mcfiggans, M. W. Gallagher, and M. J. Flynn, "Direct linkage between tidally driven coastal ozone deposition fluxes, particle emission fluxes, and subsequent CCN formation," *Geophysical Research Letters*, vol. 36, no. 4, 5 pages, 2009.

[10] L. Bariteau, D. Helmig, C. W. Fairall, J. E. Hare, J. Hueber, and E. K. Lang, "Determination of oceanic ozone deposition by ship-borne eddy covariance flux measurements," *Atmospheric Measurement Techniques*, vol. 2, no. 4, pp. 1933–1972, 2009.

[11] M. W. Gallagher, K. M. Beswick, and H. Coe, "Ozone deposition to coastal waters," *Quarterly Journal of the Royal Meteorological Society*, vol. 127, no. 572, pp. 539–558, 2001.

[12] M. W. Gallagher, K. M. Beswick, G. McFiggans, H. Coe, and T. W. Choularton, "Ozone dry deposition velocities for coastal waters," *Water, Soil, and Air Pollution: Focus*, vol. 1, no. 5-6, pp. 233–242, 2001.

[13] L. Coleman, S. Varghese, O. P. Tripathi, S. G. Jennings, and C. D. O'Dowd, "Investigating the chemical impact of iodide on ozone deposition to the ocean in the North Atlantic using regional climate model REMOTE," *Advances in Meteorology*.

[14] S. G. Jennings, C. Kleefeld, C. D. O'Dowd et al., "Mace Head Atmospheric Research Station—characterization of aerosol radiative parameters," *Boreal Environment Research*, vol. 8, no. 4, pp. 303–314, 2003.

[15] T. C. O'Connor, S. G. Jennings, and C. D. O'Dowd, "Highlights of fifty years of atmospheric aerosol research at Mace Head," *Atmospheric Research*, vol. 90, no. 2–4, pp. 338–355, 2008.

[16] M. Coyle, *The gaseous exchange of ozone at terrestrial surfaces: non-stomatal deposition to grassland*, Ph.D. thesis, University of Edinburgh, 2005.

[17] H. Gusten, G. Heinrich, R. W. H. Schmidt, and U. Schurath, "A novel ozone sensor for direct eddy flux measurements," *Journal of Atmospheric Chemistry*, vol. 14, no. 1–4, pp. 73–84, 1992.

[18] E. G. Norton, G. Vaughan, J. Methven et al., "Boundary layer structure and decoupling from synoptic scale flow during NAMBLEX," *Atmospheric Chemistry and Physics*, vol. 6, no. 2, pp. 433–445, 2006.

[19] G. J. Kunz and G. De Leeuw, "Micrometeorological characterisation of the Mace Head field station during PARFORCE," in *New Particle Formation and Fate in the Coastal Environment (PARFORCE)*, C. O'Dowd and K. Hämeri, Eds., vol. 48 of *Rep. Ser. Aerosol Sci.*, pp. 5–62, Finn. Assoc. Aerosol Res., Helsinki, Finland, 2000.

[20] P. McVeigh, *Micrometeorological and CO2 fluxes in the coastal environment*, Ph.D. thesis, School of Physics, National University of Ireland Galway, 2009.

[21] D. Ceburnis, C. D. O'Dowd, G. S. Jennings et al., "Marine aerosol chemistry gradients: elucidating primary and secondary processes and fluxes," *Geophysical Research Letters*, vol. 35, no. 7, Article ID L07804, 2008.

[22] M. Geever, C. D. O'Dowd, S. van Ekeren et al., "Submicron sea spray fluxes," *Geophysical Research Letters*, vol. 32, no. 15, Article ID L15810, 2005.

[23] G. Buzorius, U. Rannik, J. M. Mäkelä, T. Vesala, and M. Kulmala, "Vertical aerosol particle fluxes measured by eddy covariance technique using condensational particle counter," *Journal of Aerosol Science*, vol. 29, no. 1-2, pp. 157–171, 1998.

[24] J. H. Duyzer, G. Deinum, and J. Baak, "The interpretation of measurements of surface exchange of nitrogen oxides, corrections for chemical reactions," *Philosophical Transactions of the Royal Society A*, vol. 351, pp. 231–248, 1995.

[25] J. B. A. Muller, C. J. Percival, M. W. Gallagher, D. Fowler, M. Coyle, and E. Nemitz, "Sources of uncertainty in eddy covariance ozone flux measurements made by dry chemiluminescence fast response analysers," *Atmospheric Measurement Techniques*, vol. 3, no. 1, pp. 163–176, 2010.

[26] E. K. Webb, G. I. Pearman, and R. Leuning, "Correction of flux measurements for density effects due to heat and water vapour transfer," *Quarterly Journal Royal Meteorological Society*, vol. 106, no. 447, pp. 85–100, 1980.

[27] J. C. Kaimal, Y. Izumi, J. C. Wyngaard, and R. Cote, "Spectral characteristics of surface-layer turbulence," *Quarterly Journal of the Royal Meteorological Society*, vol. 98, no. 417, pp. 563–589, 1972.

[28] P. H. Schuepp, M. Y. Leclerc, J. I. MacPherson, and R. L. Desjardins, "Footprint prediction of scalar fluxes from analytical solutions of the diffusion equation," *Boundary-Layer Meteorology*, vol. 50, no. 1–4, pp. 355–373, 1990.

Hindawi Publishing Corporation
Advances in Meteorology
Volume 2010, Article ID 243701, 16 pages
doi:10.1155/2010/243701

*Research Article*

# Regional-Scale Ozone Deposition to North-East Atlantic Waters

**L. Coleman, S. Varghese, O. P. Tripathi, S. G. Jennings, and C. D. O'Dowd**

*School of Physics and Centre for Climate and Air Pollution Studies,
National University of Ireland, Galway, Ireland*

Correspondence should be addressed to L. Coleman, colin.odowd@nuigalway.ie

Received 15 February 2010; Revised 28 May 2010; Accepted 16 July 2010

Academic Editor: Elisabetta Vignati



A regional climate model is used to evaluate dry deposition of ozone over the North East Atlantic. Results are presented for a deposition scheme accounting for turbulent and chemical enhancement of oceanic ozone deposition and a second non-chemical, parameterised gaseous dry deposition scheme. The first deposition scheme was constrained to account for sea-surface ozone-iodide reactions and the sensitivity of modelled ozone concentrations to oceanic iodide concentration was investigated. Simulations were also performed using nominal reaction rate derived from *in-situ* ozone deposition measurements and using a preliminary representation of organic chemistry. Results show insensitivity of ambient ozone concentrations modelled by the chemical-enhanced scheme to oceanic iodide concentrations, and iodide reactions alone cannot account for observed deposition velocities. Consequently, we suggest a missing chemical sink due to reactions of ozone with organic matter at the air-sea interface. Ozone loss rates are estimated to be in the range of 0.5–6 ppb per day. A potentially significant ozone-driven flux of iodine to the atmosphere is estimated to be in the range of 2.5–500 M molec $cm^{-2}$ $s^{-1}$, leading to a mixing-layer enhancement of organo-iodine concentrations of 0.1–22.0 ppt, with an average increase in the N.E. Atlantic of around 4 ppt per day.

## 1. Introduction

Ozone plays a key role in atmospheric chemistry, absorbing harmful UV rays in the stratosphere whilst simultaneously acting as a greenhouse gas (radiative forcing of tropospheric ozone is around 25% that of $CO_2$ [1]), and acting as a harmful pollutant in the troposphere [2–4]. Influencing the oxidising capacity of the atmosphere as a powerful oxidising agent, it is the dominant precursor to the ubiquitous hydroxyl radical which acts as an atmospheric cleansing agent by determining the lifetime of important atmospheric trace gases. It is vital, therefore, that tropospheric ozone concentrations are realistically simulated in modelling both air pollution and chemistry-climate interactions.

600–1000 $Tg\,O_3$ $year^{-1}$ is removed from the troposphere via dry deposition [5]. The deposition of ozone to water surfaces is small compared to deposition to land [6]: typically, the rate of dry deposition of ozone to the continent is nearly six times faster than the dry deposition rate of ozone to the ocean [7]. However, considering 70% of the globe has ocean coverage, the loss of marine boundary layer ozone via oceanic dry deposition still represents a significant sink for the global ozone budget. Obtaining an accurate prediction of ozone flux to the sea is imperative not only in predicting ambient ozone concentrations, but also because of the biogeochemical consequences of ozone reactions in the sea surface.

For example, recent work [8, 9] has shown that ozonation of iodide in the sea surface can result in the formation of reactive organoiodine products that result in iodocarbon emissions from the sea surface. These iodocarbons photodissociate rapidly form iodine atoms which are known to catalytically destroy ozone [10], resulting in further reduction of marine boundary layer ozone levels. Also, ozonation of iodine atoms results in formation of iodine oxide (IO) radicals which have the potential to lead to new marine aerosol formation [11]. This newly discovered mechanism could have significant biogeochemical consequences, in terms of the feedback mechanism in halogen-mediated ozone destruction, the halogen source in coastal areas which

could account for the hitherto unexplained elevated levels of IO observed at Cape Verde [12], and the subsequent formation of new particles which could influence the solar radiation budget.

There is still major uncertainty regarding the amount of ozone lost to the ocean by dry deposition [13]. The dry deposition of ozone to the ocean involves a number of complex processes: physical, chemical, and biological. Transport of ozone through the atmosphere depends on surface roughness, wind speed, and atmospheric turbulence; transport across the quasilaminar boundary layer is limited by the diffusivity of the gas in air, while the ocean-surface uptake of ozone depends on the water-side turbulence conditions, ozone solubility, and availability of reacting chemicals in the surface layer [14, 15]. Up to now, these processes have been poorly understood and have not generally been considered in deposition schemes commonly applied in atmospheric chemistry models. The difficulty in the definition, and therefore the parameterisation of these processes is exacerbated by the scarcity of *in situ* measurements of ozone dry deposition velocities. Wesely and Hicks [16] found deposition velocities of ozone to the sea surface to vary between 0.01 and 0.05 cm $s^{-1}$. However, the eddy correlation studies of Gallagher et al. [17] carried out in the North Sea indicate deposition velocities as high as 0.1 cm $s^{-1}$.

The rate of gaseous dry deposition to a surface is parameterised by deposition velocity, $V_d$ (cm $s^{-1}$). $V_d$ is used to calculate the downward flux of ozone to the ocean, $F_{O3} = V_d C$ where $C$ denotes surface level gas concentration. $V_d$ is computed (in analogy with electrical transport) as the reciprocal of the sum of the resistances encountered by the gas on its journey to the surface sink. Using the standard resistance model to compute deposition velocity, resistances to gaseous deposition are atmospheric resistance, quasilaminar resistance and surface resistance [14].

The gaseous dry deposition scheme of Wesely [18] is widely applied in air quality, atmospheric chemistry, and chemistry climate models to represent gaseous dry depositional sinks. In its evaluation of deposition velocity, this scheme calculates explicitly only aerodynamic resistance and resistance to transfer across the quasilaminar surface layer. Surface resistance is calculated as a series of smaller resistances which are generally provided by look-up tables, with values differing according to land use type, species in question and season. In this system, derivation of surface resistance to deposition at water surfaces is neglected and surface resistance is set to a constant value of 2000 $m^{-1}$ s. The same surface resistance is applied to all water surfaces, irrespective of water body classification, climate, or meteorological conditions, thereby grossly simplifying the complex mechanisms involved in surface transfer. Surface resistance is the most significant parameter in the case of ozone deposition to the ocean [19] and in reality, surface resistance is greatly diminished by turbulence in the ocean surface and by the presence of ocean-depleting chemicals in the ocean surface—namely iodide [20, 21], and organic matter [22], for example, chlorophyll [23] and DMS [5, 20]. Due to the highly reactive nature of ozone, these ocean surface reactions can have a very significant enhancing effect on oceanic ozone deposition and the chemical reactions between ozone and organic matter and chlorophyll have yet to be parameterised and constrained in dry deposition models.

Due to it's parameterisation of surface resistance, the dry deposition scheme of Wesely [18] underestimates deposition rate of ozone to the ocean at both high- and low-wind speeds compared to observations [20].

The advanced Fairall et al. [13] scheme described in Section 2.1 is an explicit parameterisation of ozone deposition to the ocean, allowing for enhanced ozone deposition due to ocean surface turbulence and ocean surface layer reactions.

The Fairall et al. scheme has recently been incorporated into a global model, with analysis, discussion on role of controlling parameters, and validation the parameterisation conducted by Ganzeveld et al. [5]. In this study, the parameterisation is scaled to include reactions of ozone with iodide, dimethyl sulfide (DMS), alkenes, and organic chemistry. The study finds the role of biogeochemistry to dominate in computation of deposition velocities in the tropical and subtropical regions whereas the turbulent forcing of ozone deposition dominated over biogeochemical factors in the mid to high latitudinal regions. Simulation results indicate a small sensitivity of marine boundary layer ozone concentrations to varying biogeochemical and turbulent conditions, despite the wide range of deposition rates simulated using the Fairall et al. [13] scheme which is scaled to include organic reactions. This occurs partly due to interaction of different factors affecting deposition velocity. For example, in tropical regions, the reducing effect of high water temperature values on ozone solubility in water counteracted higher chemical ozone transfer due to elevated iodide concentrations. As a result, applying enhanced iodide concentrations in coastal regions did not explain discrepancies between observed and simulated $V_{dO3}$. Furthermore, the lack of sensitivity of simulated boundary layer ozone concentration to dry deposition velocity illustrates the role of compensating effects in climate models due to atmospheric transport and chemistry which maintain ozone concentrations within the marine boundary layer, despite the temporal and spatial variability in oceanic ozone uptake. The global model study also found the use of the advanced Fairall et al. [13] scheme in the model only slightly reduced (~6%) the total dry deposition flux of ozone to the ocean compared to simulations ran using the Wesely [18] scheme with constant surface-resistance. This shows that the Wesely [18] scheme is appropriate for modelling ozone deposition on a global scale for an annual period, but it is thought that due to the North East. Atlantic region being both organically active and prone to turbulent conditions, use of the chemically enhanced Fairall et al. [13] scheme on ozone concentrations in this area may be more significant due to regional-scale, short-term effects than indicated by findings of the global model study of Ganzeveld et al. [5]. Also, as the effect of temperature on molecular diffusivity is accounted for in this study, it is thought that the limiting effect of ozone water solubility on computed deposition velocities will be less pronounced than found in the global model study (see Section 2.2.3). Furthermore, in contrast

with the global model simulations, in this study the effect of salinity on ozone solubility, diffusivity, and ozone-iodide reaction rates are included. Our analysis shows that effect of salinity on ozone-iodide reactions can enhance reaction rates by as much as 23% (Section 2.3.1). Including the effect of salinity on key parameters accounts for further variations between results the global model study and results of regional model simulations presented here.

For this study, the Fairall et al. [13] parameterisation has been adapted to account for enhanced deposition due to iodide-ozone reactions in the ocean-surface layer. Furthermore, a mechanistic scaling to account for marine organic chemistry using oceanic chlorophyll concentrations as a proxy for organic activity has been included in the scheme. The parameterisation is then incorporated into the regional climate model with tracer extensions (REMOTE) [24, 25] and the sensitivity of simulated ozone flux and ambient ozone concentrations to varying oceanic iodide concentrations and inclusion of organic chemistry is investigated.

## 2. Methods

*2.1. Details of the Fairall et al. [13] Parameterisation of Oceanic Ozone Deposition.* The ozone deposition parameterisation of Fairall et al. [13] calculates oceanic ozone dry deposition velocity by integration of the turbulent-molecular transport equation in the ocean, while accounting for increased deposition of ozone to the ocean due to sea surface turbulence and due to surface-level chemical reactions. The sea-surface turbulence is a function of wind speed, water density, and the buoyancy flux of water [26].

Chemical reactions are integrated into the scheme by way of reactivity time-scale term, $A_{oz}$ ($s^{-1}$) which characterises the time scale of a chemical reaction for ozone in the sea water. It is calculated as the product of the sea-surface concentration of the ozone reactant ($C_i$) and a second order rate constant ($k_i$) for the reaction in question

$$A_{\text{ozone}} = \sum C_i k_i. \quad (1)$$

Instead of using the three-resistance approach of Wesely [18], this parameterisation combines atmospheric and quasilaminar resistance into one resistance term which is calculated using the tropical ocean global atmosphere coupled ocean-atmosphere response experiment (TOGA-COARE) gas transfer model [27, 28]. The bulk of the parameterisation serves the computation of the turbulence-dependent surface resistance with an added chemical enhancement term. The scheme has been modified to allow for variation of iodide reaction rates with temperature [29], variation of ozone diffusivity in water due to temperature [30] and salinity [31], and variation of ozone solubility with temperature [32].

### 2.2. Sensitivity Analysis

*2.2.1. Turbulent/Nonturbulent Scheme.* The Fairall et al. [13] scheme computes surface resistance by first solving the conservation equation for the case of negligible turbulence. From this solution, the turbulent solution is calculated by considering a turbulent eddy diffusivity term obtained using surface-layer similarity scaling [27]. From the scheme, deposition velocities are effectively calculated for two cases: negligible turbulence and nonnegligible turbulence. Figure 1 depicts deposition velocities obtained from the turbulent and nonturbulent schemes as a function of reactivity for various wind speeds, displaying how the turbulent and nonturbulent schemes converge for very high water-side reactivity values. This convergence occurs due to destruction of ozone in the surface layer occurring so rapidly that ocean turbulence has no enhancing effect on deposition velocity. The magnitude of the effect of ocean surface turbulence on deposition velocity depends on the reactivity term. For high-wind speeds (conditions of significant ocean surface turbulence), the deposition velocity is less dependent on reactivity than in the nonturbulent case (lower wind speeds). This illustrates the dominance of turbulent forcing over the reactive sink at high-wind speed.

*2.2.2. Sensitivity of Deposition Velocity to Reactivity Term.* The deposition velocities predicted by the Fairall et al. [13] scheme following a simulation in REMOTE were plotted against their corresponding wind speeds for various reactivity values, in order to look at the sensitivity of deposition velocity to the reactivity time scale factor ($A_{oz}$), as shown in Figure 2. Deposition velocities computed by the Wesely [18] scheme were also plotted in Figure 2, for comparative purposes. A significant increase in deposition velocity from the Fairall et al. [13] scheme is observed in Figure 2 for wind speeds over $4\,m\,s^{-1}$ for reactivities exceeding $1000\,s^{-1}$. At lower reactivities, the Wesely [18] scheme predicts higher deposition velocities, especially at low-wind speeds.

The reactivity value needed in the Fairall et al. [13] parameterisation to match deposition velocities computed by the Wesely [18] scheme depends on the wind speed value. For low-wind speeds (under $4\,m\,s^{-1}$), reactivity of $1000\,s^{-1}$ yields similar deposition velocities to those predicted by Wesely [18]. For high-wind speeds (over $10\,m\,s^{-1}$), water-side reactivity of $100\,s^{-1}$ would yield deposition velocities in the same range as those predicted by Wesely [18]. Therefore, for deposition velocities exceeding those predicted by the nonchemical, nonturbulent Wesely [18] scheme, reactivity in the ocean should exceed $1000\,s^{-1}$. At low reactivities, the Fairall et al. [13] parameterisation predicts a linear relationship between deposition velocity and wind speed, due to the dominance of the turbulent driven deposition over the chemical sink, as discussed in the previous section.

In their sensitivity analysis of the parameterisation, Fairall et al. [13] found that using the chemically enhanced turbulent deposition scheme, typical observed ozone deposition velocities of $0.05\,cm\,s^{-1}$ would require a reactivity rate of $1000\,s^{-1}$. This can be observed from Figure 2. Gallagher et al. [17] observed ozone deposition velocities to the ocean as high as $0.1\,cm\,s^{-1}$ in the North Sea. Deposition velocities of this magnitude would require a reactivity rate of the order of $10^4\,s^{-1}$ using the Fairall et al. [13] scheme at low to moderate wind speeds.

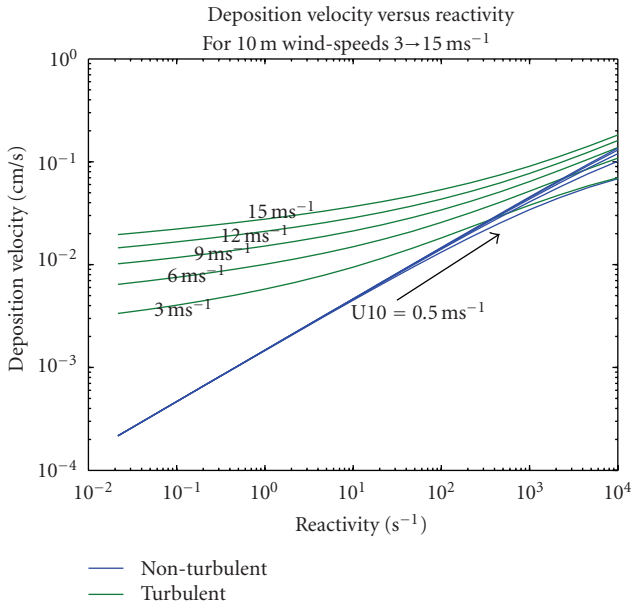


Figure 1: Comparison of deposition velocity as a function of reactivity for the nonturbulent and the turbulent Fairall et al. [13] scheme for differing 10 m wind-speeds (U10). Nonturbulent deposition velocity is obtained by solution of the basic ozone conservation equation, whereas the turbulent deposition velocity is obtained by solution of the conservation equation including a turbulent eddy diffusivity term that is obtained from surface-layer similarity scaling [27]. Note how both schemes converge for high reactivity values. This occurs because in incidences of very high oceanic reactivity, ozone is destroyed so rapidly in the ocean surface layer that ocean turbulence has no enhancing effect on deposition velocity.

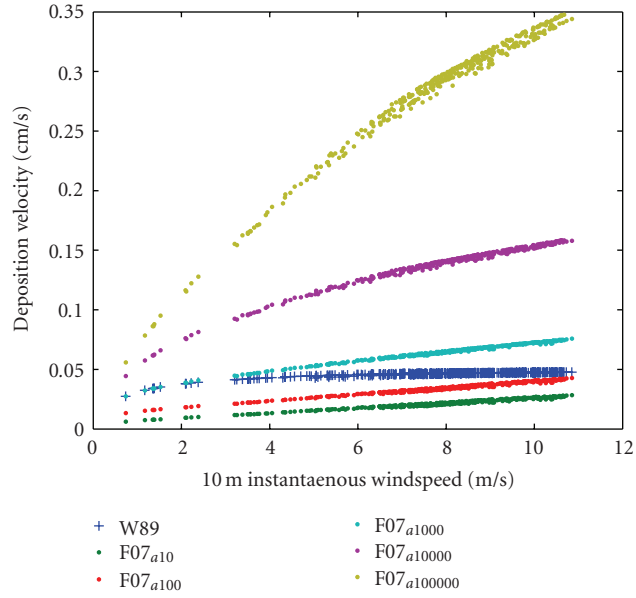


Figure 2: Deposition velocities computed from the Fairall et al. [13] (F07) and Wesely [18] (W89) schemes running within REMOTE. In the figure legend above, the subscript following the F07 label refers to the reactivity time-scale factor in operation for that scheme.

*2.2.3. Sensitivity of Deposition Velocity to Sea-Surface Temperature (SST).* As mentioned in Section 2.1, the Fairall et al. [13] parameterisation has been constrained to allow for variation of ozone diffusivity in water due to temperature [30] and salinity [33] and variation of ozone solubility with temperature [34]. Using box model simulations, the effect of SST on the deposition velocity was investigated for typical North Eastern Atlantic conditions (wind speed of 8 m s$^{-1}$ and oceanic reactivity of 500 s$^{-1}$). See Figure 3.

Results from box-model simulations confirm that inclusion of temperature dependence of molecular diffusivity renders the simulated deposition velocities less sensitive to SST variations. From Figure 3, the slope of the relationship between ozone deposition velocity and SST is 50% steeper when the effect of SST on molecular diffusivity of ozone is not considered; in this case, the computed deposition velocities are likely to be oversensitive to SST. As discussed in the introduction to this paper, the effect of including variability of ozone diffusivity with SST is thought to compensate for the limiting effect of low-ozone solubility on simulated ozone deposition velocities, compared to the results of the global model study of Ganzeveld et al. [5].

*2.3. Chemical Scaling of the Reactivity Term.* Accounting for chemical reactions in the Fairall et al. [13] parameterisation requires scaling of the chemical reactivity term $A_{oz}$, as defined in (1). In their exploration of impact of chemical reactions on ozone deposition, Chang et al. [20] identified iodide as the most likely chemical compound residing in the sea surface to drive ozone deposition compared to other substances (DMS, alkenes). DMS was recognised as having potential to enhance ozone deposition, but only at extreme oceanic concentrations. At mean oceanic concentrations of DMS, deposition velocity due to molecular gas transfer and chemical reactions of ozone with DMS was an order of magnitude lower than the deposition velocity due to molecular diffusion and chemical reactions of ozone and iodide and deposition velocity due to molecular gas transfer. Reactions of ozone and alkenes were a further two orders of magnitude lower again. For this reason, reactions of ozone with DMS and alkenes were not considered in this study, their chemically enhancing effects on ozone deposition being overshadowed by iodide reactions. Chang et al. [20] did not investigate the effect of chlorophyll on ozone deposition which Clifford et al. [23] found to have a significant enhancement effect of the same order of magnitude as for iodide reactions. In this study, analysis of chemical enhancement to ozone deposition is limited to iodide and chlorophyll reactions.

*2.3.1. Iodide Reactions.* To scale $A_{oz}$, the kinetics between ozone and it's various reactants needed to be determined. The enhancing effect of iodide reactions on ozone deposition has been long documented [20, 21]. From the kinetics

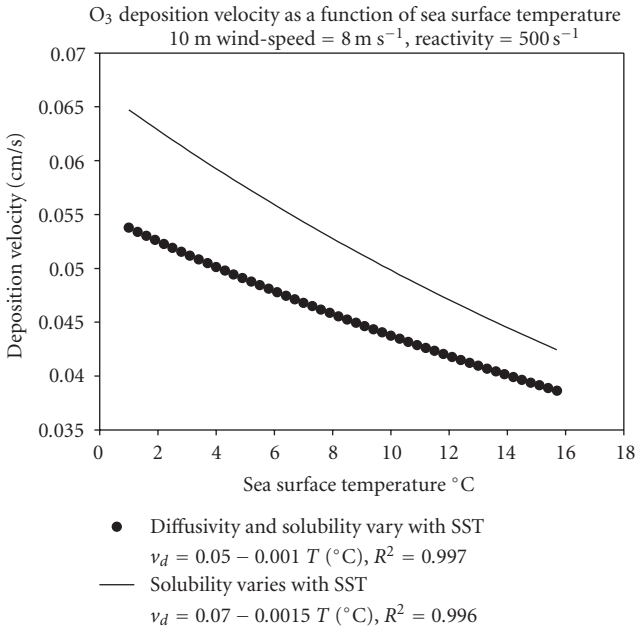


Figure 3: Box-model-derived relationship between deposition velocity and sea-surface temperature, using a typical Atlantic wind speed of 8 m s$^{-1}$ and reactivity of 500 s$^{-1}$. The solid line depicts a relationship between deposition velocity and SST when only temperature dependence of ozone solubility in seawater is considered based on the theory of Kosak-Channing and Helz [34]. The filled circles represent a relationship between deposition velocity and SST when temperature dependence of both ozone solubility and molecular diffusivity in seawater is considered. Variation of ozone diffusivity in seawater is based on the theory of Johnson and Davis [30] and Jahne et al. [31]. Linear correlations between ozone deposition velocity and SST are given in the legend.

of the ozone-iodide reaction derived by Magi et al. [29], relationships between ozone-iodide rate constant and water salinity were derived for different water temperatures. From this, a relationship between the second order reaction rate $k_{\text{salt}}$ and saline water temperature $T$ was deduced for water of ionic strength of seawater (0.7 M) resulting in the linear relationship of (2), where $k_{\text{salt}}$ refers to the reaction rate of ozone in salt water of ionic strength 0.7 M and $T$ refers to water temperature in degrees Kelvin

$$k_{\text{salt}}(10^9\ \text{s}^{-1}) = -40.85 + 0.15\,T\,(\text{K}). \quad (2)$$

From the work of Magi et al. [29], the effect of salinity enhances ozone-iodide reaction rates by as much as 23% compared to those for pure water, and so it was considered important to account for the salinity of seawater in parameterising ozone-iodide reactions.

Oceanic iodide concentrations in the North Atlantic vary between 0 and 150 nM [35]. For this study, constant iodide concentrations were varied between 50 nM and 200 nM to evaluate the sensitivity of simulated ozone levels and resulting ozone fluxes to the effect of changing iodide concentrations, in contrast to the global modelling study of Ganzeveld et al. [5] who infer oceanic concentrations using an anticorrelation between nitrate and iodide developed by Campos et al. [36]. Furthermore, the global model study did not include the effect of salinity of seawater on ozone-iodide reaction kinetics, as is done in this study.

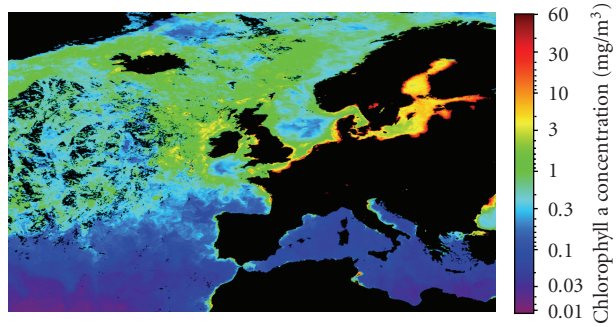


Figure 4: Monthly averaged chlorophyll-a concentration (mg m$^{-3}$), as detected by MODIS for June, 2003. Taken from the NASA OceanColor website (http://oceancolor.gsfc.nasa.gov/.)

*2.3.2. Organic Enhancement of Ozone Deposition.* It has been long postulated that organic reactions in the sea surface layer can have a significant enhancing effect on ozone deposition [22]. Clifford et al. [23] suggest that the reaction between ozone and chlorophyll can increase ozone deposition velocity by up to a factor of 3 for wind speeds up to 20 m s$^{-1}$ compared to deposition velocities computed solely on ozone-iodide reactions. Considering the ubiquity of chlorophyll in the ocean, the organic enhancement of ozone deposition could have a significant effect on ozone concentrations in the marine boundary layer. This organic enhancement of ozone deposition was mechanistically incorporated into the Fairall et al. [13] deposition scheme using satellite chlorophyll data from MODIS (moderate resolution imaging spectroradiometer) [37]. The upper and lower limits of oceanic chlorophyll concentrations were set to 3 mg m$^{-3}$ and 0 mg m$^{-3}$, respectively, and oceanic iodide concentration was set to a typical value of 100 nM. Figure 4 shows monthly averaged chlorophyll concentrations for June 2003, as detected by MODIS. Although chlorophyll values as high as 30 mg m$^{-3}$ in coastal regions are visible in Figure 4, the upper limit of chlorophyll concentration was set to 3 mg m$^{-3}$ because open ocean chlorophyll concentrations in the North East Atlantic do not exceed this value. Also, when the resolution of the model is taken into consideration, chlorophyll values averaged over a single grid cell never exceed 3 mg m$^{-3}$, even in coastal areas. Therefore, 3 mg m$^{-3}$ is a sensible upper limit for open ocean chlorophyll concentrations for this study.

Ozone deposition velocity was computed as before using the Magi et al. [29] iodide chemistry and increased according to a linear chlorophyll-dependent enhancement factor: deposition velocity increased by a factor of 3 at the upper limit of chlorophyll concentration values. Deposition velocity was left unchanged at the lower limit of chlorophyll concentration where deposition velocity was based only on iodide chemistry.

The technique employed in this study differs from that of Ganzeveld et al. [5] who applied linear dependence of reactivity term $A_{oz}$ on chlorophyll concentrations whereas in this study, the deposition velocity increases linearly with chlorophyll and the organic reactions are not represented in $A_{oz}$. This organically enhanced version of the Fairall et al. [13] deposition scheme is herein referred to as the mechanistic ozone deposition scheme.

This scaling is a crude approach to the quantification of organic reactions in the computation of ozone deposition velocity and should be interpreted as a first-order representation of organic chemistry within the Fairall et al. [13] scheme, oceanic chlorophyll concentration being used as a proxy for biological activity. Further work is needed to parameterise the role of organic reactions in ozone deposition.

*2.4. Ozone-Deposition Driven Upward Iodine Flux.* The major source of iodine to the atmosphere is most likely due to emission of organoiodine compounds from the ocean [38]. Martino et al. [8] have recently shown that a proportion of organic iodide found in the marine atmosphere can be formed from volatile organoiodine compounds (VOIs) which are produced via ozone-iodide reactions in the sea surface, thereby uncovering a potentially significant iodine source to the marine atmosphere which is kick started by the deposition of ozone to the sea surface. The VOI species identified by Martino et al. [8] resulting from ozone deposition are $CH_2I_2$, $CH_2ICl$, and $CHI_3$. Based on the findings of Martino et al. [8] and the work of Garland et al. [21], the extreme upper limit of iodine vapours released to the atmosphere can be estimated from the ozone flux of ozone to the ocean, assuming all of the new VOIs are emitted from the ocean surface, without any being transported to the ocean mixed layer or being destroyed by photolysis at the sea-air interface. This newly defined halogen source in the marine boundary layer could have significant biogeochemical consequences, in terms of both marine boundary layer (MBL) ozone depletion and new particle formation.

## 3. Simulation Results and Discussion

Monthly REMOTE simulations were carried out for the month of June, 2003. The model domain spans Northern Europe and is depicted in Figure 11. Resolution of the model is set to 0.5 deg, giving an average grid cell size of 50 km $\times$ 50 km. Meteorological and chemical initial and boundary conditions are taken from ECMWF (European Centre for Medium-Range Weather Forecasts) and used to initialise all grid points at the start of each simulation. Lateral boundaries are enforced at six hourly intervals and emission scenarios were supplied from the EMEP site. In 2003, monthly average chlorophyll concentrations in the North East. Atlantic were at an annual peak in the month of June [37].

*3.1. Ozone Concentration Fields.* Figure 5 shows surface level mean monthly ozone concentrations simulated using different deposition schemes within REMOTE. There is little or no difference between simulated surface level ozone concentrations using the nonchemical Wesely [18] scheme and the Fairall et al. [13] scheme for 50 nM or 200 nM iodide concentrations, consistent with findings of the global model study of Ganzeveld et al. [5]. One can conclude from this that ozone concentrations predicted using the Fairall et al. [13] scheme within REMOTE are insensitive to iodide reactions at realistic Atlantic iodide concentrations—even at an upper limit of oceanic iodide concentration of 200 nM. Therefore, although variation in iodide concentration and reaction rate causes variation in ozone deposition velocity, these deposition velocities are not sufficiently significant to overcome other compensating effects in the climate model and substantially decrease simulated ozone concentrations. However, a notable decrease in ozone concentrations is observed around the North East Atlantic when the mechanistic ozone deposition scheme of Fairall et al. [13] is employed. Simulated ozone depletion in this region is due to the relatively high chlorophyll concentrations. In regions of low oceanic chlorophyll concentration (e.g., the Mediterranean), the mechanistic ozone deposition scheme models similar ozone concentrations as computed using the Wesely [18] scheme.

Figure 6 depicts ozone concentrations in the North East. Atlantic region as predicted by REMOTE using three permutations of the Fairall et al. [13] scheme and using the nonchemical Wesely [18] scheme. The Fairall et al. [13] scheme including 100 nM iodide chemistry predicts ozone concentrations similar to those simulated using the Wesely [18] scheme. The impact of chlorophyll on simulated ozone levels in this region can be seen by comparing the mean monthly ozone levels simulated using the Fairall et al. [13] scheme scaled to include iodide chemistry alone (100 nM I scheme), and the mechanistic version scaled to include both iodide chemistry and organic reactions. Ozone levels simulated by the mechanistic dry deposition scheme are as much as 15 ppb lower than ozone levels simulated by both the Wesely [18] scheme and the 100 nM I scheme. The Fairall et al. [13] 100 nM I scheme and the mechanistic scheme differ only by organic enhancement of deposition velocity and so the lower ozone concentrations simulated by the mechanistic schemes are due to inclusion of organic chemistry alone.

Figure 7 compares ozone concentrations measured at the Mace Head atmospheric research station measurement site off the west coast of Ireland to modelled ground-level ozone concentrations in this region. Ozone levels were measured at Mace Head using a continuous ozone analyser by UV photometry. See Tripathi et al. [39] for full description of this data and measurements. All simulated ozone concentrations agree quite well with observations, but the Mace Head ozone concentrations simulated by the mechanistic scheme correlate better with the observed ozone concentrations than other schemes. The root mean square (RMS) deviation between *in situ* ozone measurements at Mace Head and modelled ozone concentration for this region was 7.7 ppb when using the mechanistic scheme whereas the next closest correlations were obtained using the Fairall et al. [13]

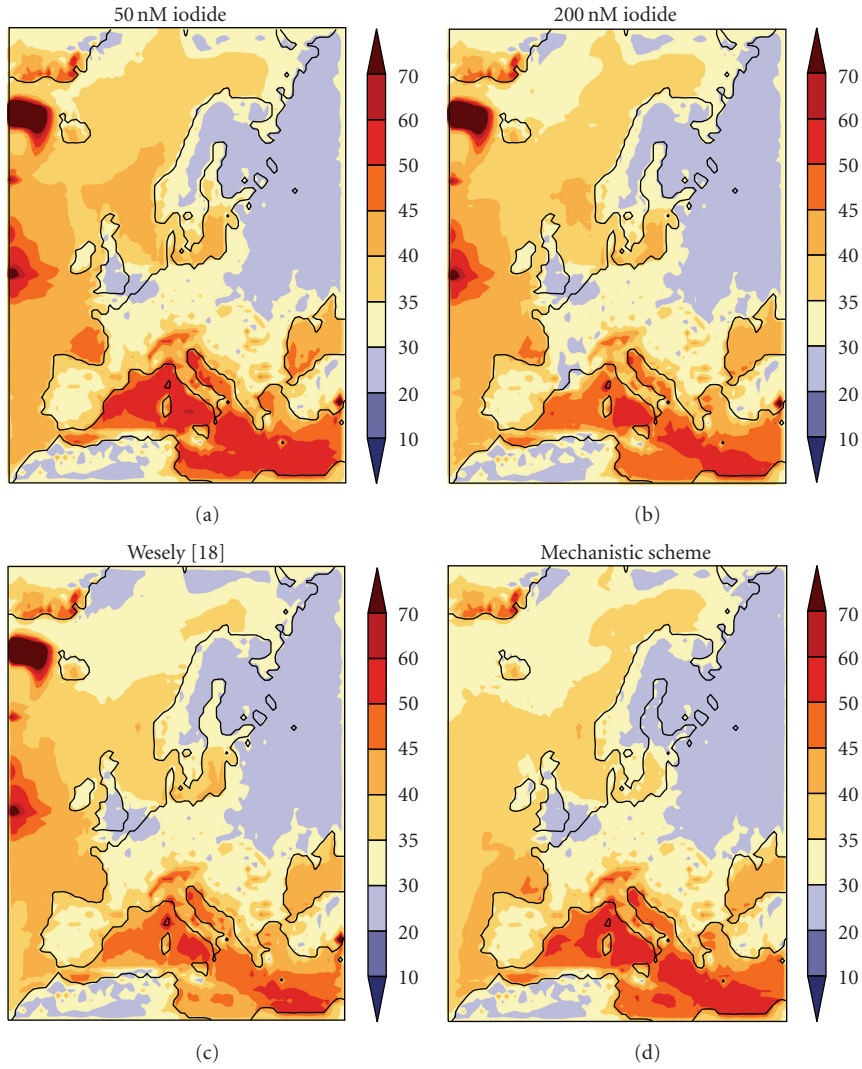


Figure 5: Monthly average $O_3$ concentrations in ppb as predicted by REMOTE for June 2003 for various dry deposition schemes. 50 nM I plot and 200 nM I plot show simulated ozone concentrations (ppb) using the iodide-only chemical Fairall et al. [13] parameterisation with oceanic iodide concentrations set to 50 nM and 200 nM, respectively. The Wesely [18] plot shows the ozone concentrations simulated by the nonchemical scheme and the Mechanistic Scheme plot depicts the $O_3$ concentrations simulated using the Fairall et al. [13] scheme with inclusion of a first-approach chlorophyll-based organic chemistry.

scheme with reactivity set to 1000 $s^{-1}$, and the Wesely [18] scheme which gave RMS deviations of 9.1 ppb and 11.6 ppb, respectively. This shows that on average, deviations between simulated ozone concentrations and *in situ* measurements are less for results obtained using the mechanistic ozone dry deposition scheme than those generated using other dry deposition schemes. However, firm conclusions on accuracy of dry deposition parameterisation cannot be drawn here, as simulated ozone-mixing ratio is dependent on other model processes including atmospheric chemistry, transport, and boundary conditions. In addition, the *in situ* measurements represent a point measurement of ozone-mixing ratio, whereas the model output represents average ozone mixing ratio over a grid cell which spans 50 km × 50 km. In this analysis, attempts have been made to account for this by comparing modelled ozone concentrations with *in situ* ozone measurements averaged over 1.75 hours, the time taken for an air mass to traverse the length of one grid cell (50 km), assuming an average easterly wind speed of 8 m $s^{-1}$. However, localised effects influencing ozone concentrations at Mace Head will not be represented in model simulations due to the effect of averaging over the grid cell area and so simulated ozone concentrations will not have the same variation as ozone measurements at Mace Head. This would explain large variations between simulated and measured ozone concentrations for example, measurements between Julian Day 166 and 171 are much lower than all model results.

From Figure 7, it can be seen that the 100 nM I Fairall et al. [13] scheme and the Wesely [18] scheme predict higher ozone concentrations than observations or other model set ups during periods of low-wind speeds (e.g., between days 165 and 171). The reactivity of the 100 nM I scheme

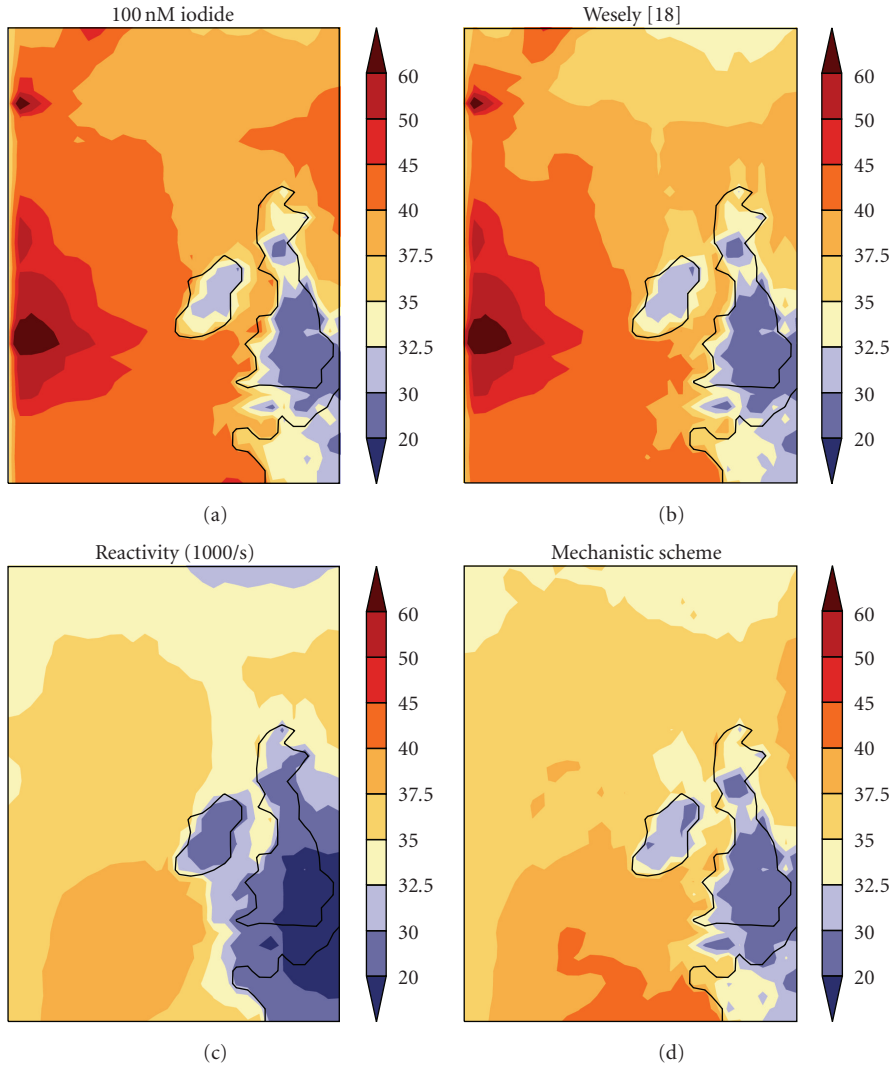


FIGURE 6: Monthly average $O_3$ concentrations in ppb in the North East Atlantic region as predicted by REMOTE for June 2003 for various dry deposition schemes. 100 nM I plot depicts simulated ozone concentrations (ppb) using the iodide-only chemical parameterisation of Fairall et al. [13] with oceanic iodide concentrations set to 100 nM. The Wesely [18] plot shows the ozone concentrations simulated by the nonchemical scheme. Reactivity 1000/s plot shows ozone concentrations simulated using the Fairall et al. [13] scheme with reactivity term set to constant 1000 $s^{-1}$ and mechanistic scheme plot depicts the ozone concentrations simulated using the Fairall et al. [13] scheme with inclusion of first-approach chlorophyll-based organic chemistry.

is not large enough to account for ozone water surface transfer at low-wind speed and the Wesely [18] scheme does not account for chemical ozone transfer at all. Therefore, using either of these schemes, REMOTE over predicts ozone concentrations at periods of low-wind speed.

Simulations using the Fairall et al. [13] scheme with constant reactivity set to 1000 $s^{-1}$ predict very similar ozone concentrations around Mace Head to the simulations using the mechanistic scheme (reactivity due to 100 nM Iodide and organic enhancement). Therefore, around the western Irish coast, it can be deduced that effect of organic chemistry causes oceanic reactivity of the order of 1000 $s^{-1}$. Figure 8 shows monthly average values of deposition velocities computed for the various deposition schemes. In the mechanistic scheme, organic reactions are parameterised by increasing deposition velocity according to oceanic chlorophyll concentration, and so organic reactions are not represented in the reactivity term, $A_{oz}$ of the Fairall et al. [13] parameterisation. However, by comparing average deposition velocities depicted in Figure 8 with relationship between reactivity and deposition velocity shown in Figures 1 and 2, it can be deduced that the deposition velocities obtained around the Irish coast using the mechanistic scheme (0.6–0.1 cm $s^{-1}$) would require reactivity values exceeding 1000 $s^{-1}$, assuming moderate windspeeds. Variation of $V_d$ in the Wesely [18] scheme and the *Reactivity 1000* $s^{-1}$ scheme occurs due to turbulent effects alone.

*3.2. Ozone-Loss Rate.* The loss rate of ozone from the mixing volume to the ocean due to dry deposition was calculated in

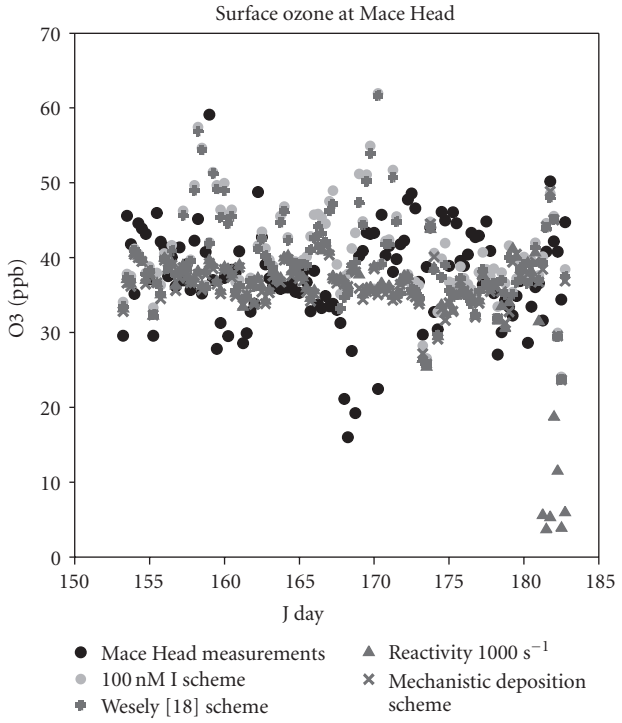


Figure 7: Ozone concentrations (ppb) simulated by REMOTE and measured ozone concentrations (ppb) at Mace Head for June 2003.

order to assess the impact of varying ozone deposition on the rate of atmospheric ozone loss to the ocean as a result of dry deposition and the consequential effect on ambient ozone concentration. The loss rate is given by

$$\text{Loss Rate} = \frac{F_{O3}}{L}, \tag{3}$$

where $F_{O3}$ is the dry deposition flux of ozone to the ocean (the product of deposition velocity and ambient ozone concentration) and $L$ is the boundary layer height. Deposition velocities and ozone concentrations were extracted from REMOTE and boundary layer height taken as a constant 800 m. Figure 9 shows ozone-loss rates computed for the various dry deposition schemes.

A higher deposition velocity does not necessarily denote a higher ozone-loss rate, as the loss rate is proportional to both ozone concentration and deposition velocity.

The loss rate of ozone to the ocean varies with oceanic iodide concentration as seen from the first two plots of Figure 9, using the iodide-only constrained scheme of Fairall et al. [13]. This occurs due to the different deposition velocities generated from the dry deposition schemes based on reactivity. However, it can be seen that the variation of the iodide concentration has no significant effect on ground level ozone concentration and so the variation in ozone-loss rate due to differences in iodide concentration is too subtle to have a bearing on ambient ozone concentrations, indicating the dominance of other processes over the dry deposition sink in regulation of ambient boundary layer ozone concentrations within REMOTE for lower dry depositional loss rates.

The Wesely [18] scheme predicts a greater ozone-loss rate than the mechanistic ozone deposition scheme. This occurs due to the depletion of ambient ozone concentrations because of enhanced dry deposition in the presence of marine biological activity.

*3.3. Upward Iodine Flux.* 20% of ozone deposited to the sea surface reacts with iodide [21]. 1% of iodide oxidised by ozone reacts with organic matter to form the VOIs ($CH_2I_2$, $CH_2ICl$, or $CHI_3$) that are released from the sea surface [8]. The upper limit of potential iodine flux to the marine atmosphere as a result of ozone deposition is predicted using these relationships. Resulting VOI fluxes are shown in Figure 10. The upward VOI flux is derived directly from the downward ozone flux, and so the same factors influence both the downward ozone flux and the upward iodine flux. The upward VOI flux also varies with oceanic iodide concentration. It is stressed that this potential VOI flux to the atmosphere represents an extreme upper limit, and is to be interpreted as such.

The upward VOI flux predicted using the Wesely [18] scheme exceeds that predicted by the Fairall et al. [13] scheme constrained by iodide reactions. The mechanistic ozone dry deposition scheme predicts VOI flux exceeding that predicted using Wesely [18] in some regions ( north east of Britain) while the flux is less than that predicted using Wesely [18] in other areas (off the southern Irish coast).

This ozone deposition-driven flux of iodine from the ocean is likely to have significant biogeochemical consequences. Marine aerosols and cloud condensation nuclei (CCN) can be formed from iodine vapours in coastal environments [11, 40]. The addition of new aerosols to the coastal atmosphere could have a significant impact on the global solar radiation budget due to their role in scattering of incoming solar radiation, and therefore accurate prediction of the VOI flux is imperative in predicting future climatic scenarios. To fully assess the atmospheric implications of this extra iodine source in the MBL, the upward organoiodine flux and resulting chemical reactions and particle formation would have to be included in the chemical scheme of REMOTE.

*3.4. Area-Averaged Study of Simulation Results.* A quantitative comparison of simulation results using the various dry deposition schemes was performed by taking an area average of various parameters over a boxed region in the North Atlantic, off the Irish coast—a region of relatively high biological activity. The region is displayed in Figure 11. In this area, average, maximum, and minimum deposition velocities from the various schemes were compared, as were the average simulated ozone concentrations, average ozone-loss rates, average upward VOI flux and derived average increase in the daily rate of the VOI-mixing ratio. Results are tabulated in Table 1.

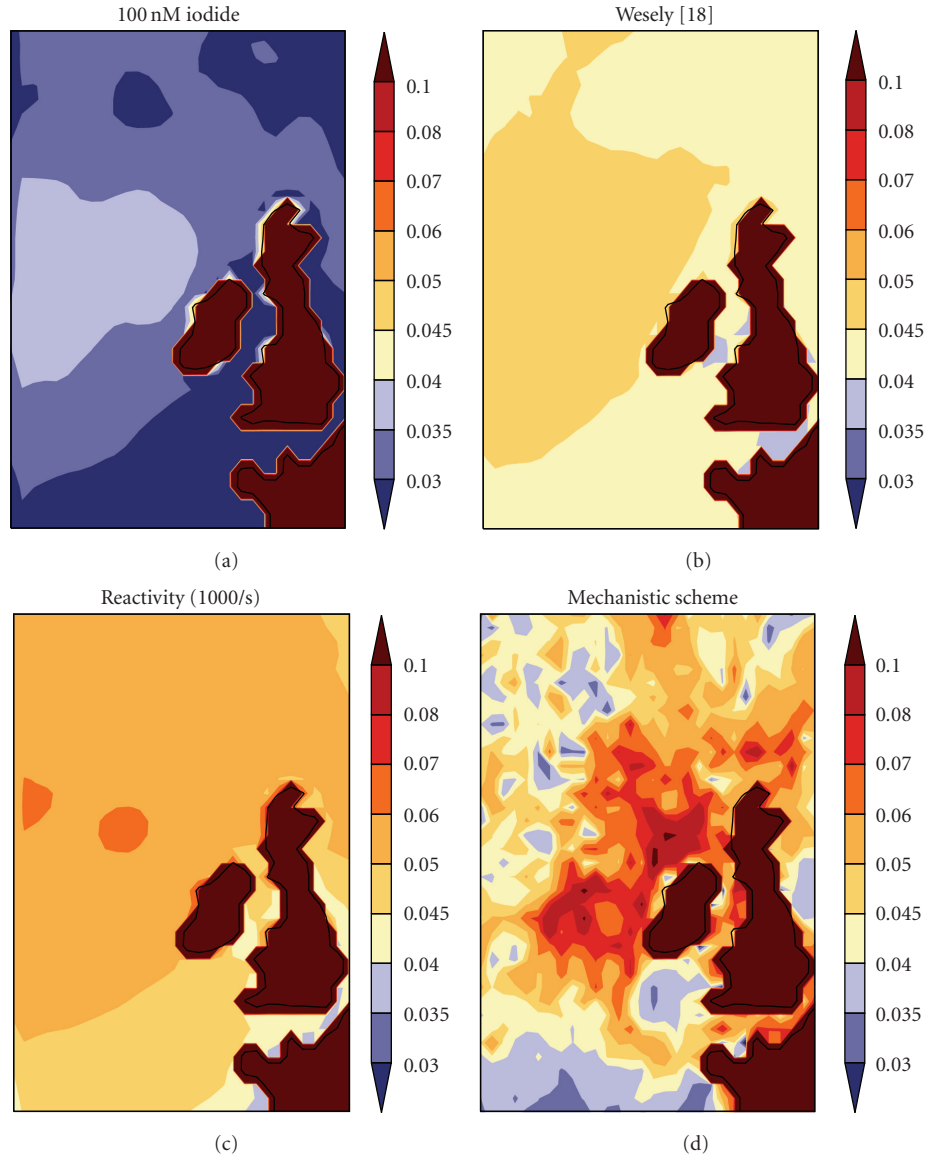


Figure 8: Monthly mean deposition velocity in the North East Atlantic region as predicted by REMOTE for June 2003 for various dry deposition schemes. 100 nM I plot depicts deposition velocity using the Fairall et al. [13] parameterisation with oceanic iodide concentrations set to 100 nM. The Wesely [18] plot shows deposition velocity simulated by the nonchemical scheme. Reactivity 1000/s plot shows deposition velcity simulated using the Fairall et al. [13] scheme with reactivity term set to constant 1000 $s^{-1}$ and mechanistic scheme plot depicts the deposition velocity simulated using the Fairall et al. [13] scheme with inclusion of first-approach chlorophyll-based organic chemistry.

*3.4.1. Deposition Velocity.* Deposition velocities simulated using the Fairall et al. [13] parameterisation vary with oceanic iodide concentration, but as we have seen earlier, these variations are too subtle to have a significant effect on ambient ozone concentrations. The mechanistic scheme computes deposition velocities in this region exceeding those computed using the [18] scheme by 18%. Neither the Wesely [18] scheme nor the Fairall et al. [13] scheme constrained to iodide chemistry can account for deposition velocities as high as the observations of Gallagher et al. [17]. Surface resistance is set to a constant 2000 $m^{-1}$ s in the Wesely [18] scheme, and so maximum deposition velocity computed by this scheme deviates very little from the average deposition velocity; using this nonchemical scheme, deposition velocities cannot match the upper limit of observations under any conditions.

Additional chemical reactions must be included in the dry deposition scheme in order to realise deposition velocities as high as observations. Only the mechanistic ozone deposition scheme predicts deposition velocities higher than observations of Gallagher et al. [17]. Therefore, only by integration of organic chemistry into the dry deposition scheme can deposition velocities as high as observations be realised.

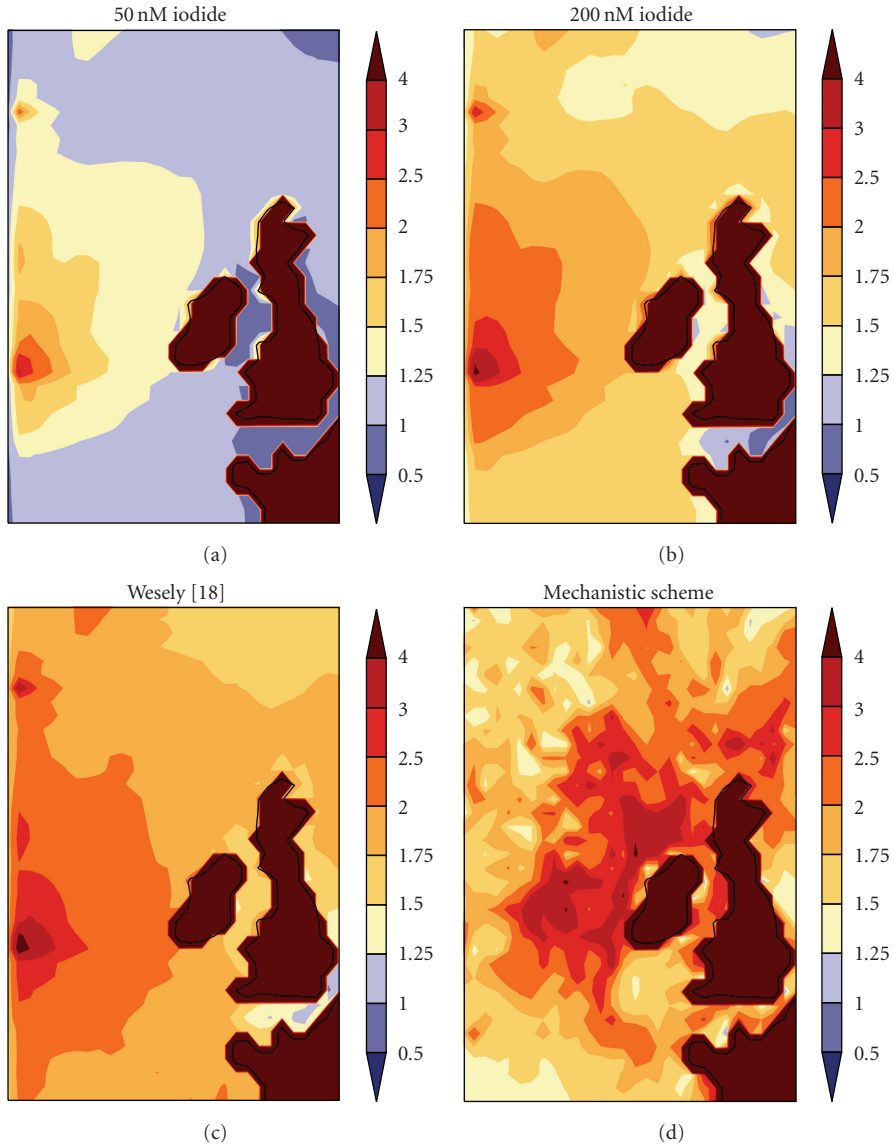


Figure 9: Monthly mean $O_3$ loss rates (ppb per day) as predicted by REMOTE June 2003 for various dry deposition schemes. Simulated loss rates using the Fairall et al. [13] parameterisation with oceanic iodide concentrations set to 50 nM and 200 nM, respectively, are shown. The Wesely [18] plot shows the ozone-loss rates simulated by the nonchemical Wesely [18] scheme and the mechanistic scheme shows the $O_3$ loss rate simulated using the Fairall et al. [13] scheme with inclusion of first-approach chlorophyll-based organic chemistry.

*3.4.2. Ozone Concentration.* Simulated average ozone concentrations in this area are relatively insensitive to oceanic iodide concentration. Inclusion of first-order organic chemistry parameterisation based on Clifford et al. [23] into the dry deposition parameterisation causes a decrease in simulated ozone concentration in the area of 20.5% or 9.5 ppb compared to concentrations simulated using the Wesely [18] scheme. This increase in ozone deposition occurs due to the enhancement of ozone deposition velocity due to inclusion of organic reactions in the mechanistic ozone deposition scheme, as discussed above. The Wesely [18] scheme predicts an average ozone concentration in this area 1.6% lower than that predicted using the Fairall et al. [13] parameterisation constrained by an oceanic iodide concentration of 100 nM.

*3.4.3. Ozone-Loss Rate.* Average ozone-loss rate computed by Wesely [18] exceeds that computed by the mechanistic ozone deposition scheme by nearly 6% in this region. The lower loss rate is due to the lower ambient ozone concentrations in the boundary layer due to organic enhancement of ozone deposition computed by the mechanistic ozone deposition scheme. The less reactive scheme constrained only by iodide reactions also computes ozone-loss rate less than that of the Wesely [18] scheme due to the higher deposition velocity

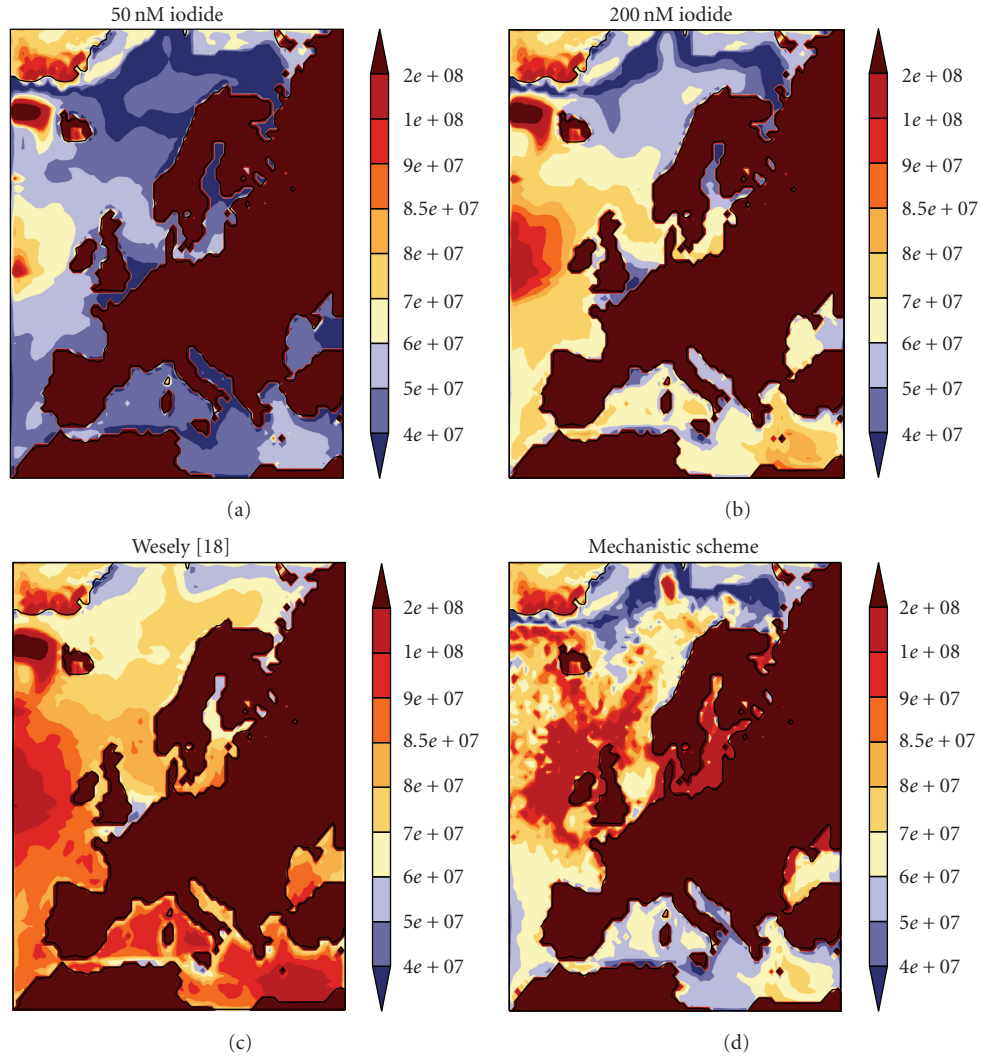


FIGURE 10: Monthly average upward iodine flux in molecules per $cm^{-2}\,s^{-1}$, as predicted by REMOTE for June 2003 shown for the European region. Simulated flux using the Fairall et al. [13] parameterisation with oceanic iodide concentrations set to 50 nM and 200 nM, respectively, are shown. The Wesely [18] plot shows the flux simulated by the nonchemical Wesely [18] scheme and the mechanistic scheme shows the flux simulated using the Fairall et al. [13] parameterisation using a first-approach organic chemistry scaling.

computed by the Wesely [18] scheme. The relatively small changes in loss rates are shown not to have a large effect on ambient ozone concentrations in REMOTE, but accurate estimation of ozone dry deposition flux is necessary to evaluate ozone-deposition driven upward VOI flux.

*3.4.4. Potential Upward VOI Flux.* This flux is estimated linearly from the downward ozone flux. The simulated potential VOI flux emitted from the ocean in this area is of the order of $10^8$ molecules $cm^{-2}\,s^{-1}$. Martino et al. [8] compute a typical downward depositional iodine flux of $3 \times 10^7$ atoms $cm^{-2}\,s^{-1}$. The potential upward VOI flux exceeds the depositional iodine flux, thus constituting a significant additional source of atmospheric iodine in marine environments, especially in regions of high biological activity when organic enhancement of ozone deposition is factored into the dry deposition parameterisation.

*3.4.5. Increase of VOI-Mixing Ratio.* Recent measurements of iodocarbon fluxes taken in the North East. Atlantic [41] have found open ocean sea-air fluxes of the ozone-deposition derived VOIs ($CH_3I$, $CH_2I_2$, and $CH_2ICl$) as high as $9.6 \times 10^7$ molecules $cm^{-2}$ $day^{-1}$, which would lead to a mixing ratio increase of 4.24 ppt per day. The average flux value observed in this region would lead to a VOI increase of 1.2 ppt per day. In the more biologically active shelf and coastal regions, measured VOI sea-air fluxes have been measured that would result in mixing ratio increases as high as 9.3 ppt per day and 18.1 ppt per day, respectively. The measurements were taken in the biologically active regions off the west coast of Ireland where organic enhancement of ozone deposition is likely to occur.

The average simulated increase of potential VOI-mixing ratio in this area is of the order of 4 ppt per day and the range of ozone-driven iodocarbon flux in this region

Table 1: Results from area average analysis carried out over a boxed region in the North Atlantic.

| Scheme | Average deposition velocity (cm/s) | Maximum deposition velocity (cm/s) | Minimum deposition velocity (cm/s) | Average [O3] in ppb | Average O3 loss rate (ppb per day) | Average upward VOI flux (molecules $cm^{-2}\,s^{-1}$) | Average mixing ratio VOI increase (ppt per day) |
|---|---|---|---|---|---|---|---|
| Reactivity of 50 nM Iodide | 0.0305 | 0.0509 | 0.00123 | 47.8647 | 1.57031 | 7.11*E* + 07 | 3.14*E* + 00 |
| Reactivity of 100 nM Iodide | 0.0355 | 0.0575 | 0.00127 | 47.5876 | 1.82221 | 8.26*E* + 07 | 3.64*E* + 00 |
| Reactivity of 150 nM Iodide | 0.0392 | 0.0623 | 0.00129 | 47.3911 | 2.0009 | 9.07*E* + 07 | 4.00*E* + 00 |
| Reactivity of 200 nM Iodide | 0.0421 | 0.0661 | 0.0013 | 47.2334 | 2.1445 | 9.72*E* + 07 | 4.29*E* + 00 |
| Reactivity 1000 $s^{-1}$ | 0.0573 | 0.0848 | 0.00134 | 36.6113 | 2.26644 | 1.03*E* + 08 | 4.53*E* + 00 |
| Wesely [18] scheme | 0.0463 | 0.0488 | 0.0019 | 46.8433 | 2.34064 | 1.06*E* + 08 | 4.68*E* + 00 |
| Mechanistic scheme (Reactivity of 100 nM Iodide and Organic reactions) | 0.0547 | 0.161 | 0.00173 | 37.2185 | 2.20302 | 9.98*E* + 07 | 4.40*E* + 00 |
| Percentage difference between Wesely [18] and Mechanistic Scheme | −18.171 | −230.38 | 8.86149 | 20.5468 | 5.87979 | 5.87979 | 5.87979 |
| Percentage difference between Wesely [18] and 100 nM $I^-$ scheme | 23.1573 | −17.915 | 33.0857 | −1.5888 | 22.1493 | 22.1493 | 22.1493 |

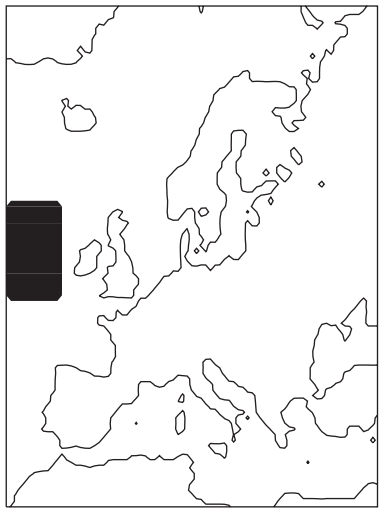

Figure 11: Location of boxed region in the North Atlantic off the west coast of Ireland in which the area-averaged analysis was performed.

is 2.5–500 M molec $cm^{-2}\,s^{-1}$ which would correspond to a mixing-layer enhancement of VOI concentrations of 0.1–22.0 ppt per day. This enhancement to the mixing ratio was calculated using ideal gas theory and assuming a boundary layer height of 800 m and should be interpreted as the extreme upper limit of potential VOI flux occurring as a result of ozone deposition—in reality, a proportion of this flux would be mixed downwards and a further proportion will be photolysed at the sea surface [8]. Taking this into consideration, simulated VOI-mixing ratio enhancement is well within range of the recently observed iodocarbon fluxes [41], especially considering large iodocarbon fluxes observed in shelf and coastal regions. Considering the molar mixing ratio of total organic iodine ranges between 3–4 pptv in the boundary layer [42–44], even a small mixing ratio enhancement of these proportions would enhance atmospheric iodine concentrations considerably.

The extra iodine compounds released to the atmosphere could further add to ozone depletion in the marine boundary layer, thus forming a catalytic cycle of ozone destruction. Read et al. [45] investigated halogen-mediated ozone destruction over the tropical Atlantic Ocean and found that based on typical organic iodine molar mixing ratios of 3–4 ppt in the MBL [44], resulting IO concentrations of 1 ppt would cause ozone loss of 1.24 ppb per day due to atmospheric reactions with IO. Crudely assuming a linear relationship between organic iodine concentrations and resulting ozone loss, additional influx of 22 ppt organic iodine per day into the mixing layer due to the ozone-deposition driven VOI flux would result in a further ozone loss of 7.8 ppb per day. Even though this case represents the upper limit VOI flux to MBL, it is evident that the halogen-mediated ozone destruction cycle is likely to have significant consequences for ozone concentrations in the marine boundary layer, depleting ozone mixing ratios to the order of a ppb per day. To further investigate this feedback mechanism, REMOTE would need to be adapted to include halogen chemistry and the upward VOI flux. This is scheduled for further work.

## 4. Conclusions

Consistent with results of global model study conducted by Ganzeveld et al. [5], our results show that ozone

concentrations predicted by the Fairall et al. [13] parameterisation within REMOTE are insensitive to realistic variations of oceanic iodide concentrations. Furthermore, the ozone concentrations predicted by this turbulent and chemically enhanced deposition scheme do not exceed those predicted by the highly parameterised Wesely [18] scheme when the parameterisation is constrained by iodide chemistry alone for typical oceanic iodide concentrations. In order for the new scheme to simulate deposition rates as high as field observations, oceanic reactivity must be in the order of $1000\ s^{-1}$. The source of this extra reactivity is most likely due to ozone reacting with organic matter and chlorophyll in the sea surface [22, 23].

Deposition velocities as high as the observations of Gallagher et al. [17] were realised in regions of high biological activity using the mechanistic ozone deposition scheme, in which a crude first-approach scaling of organic ozone reactions was applied to the Fairall et al. [13] parameterisation. Use of this mechanistic ozone deposition scheme including organic reactions yielded boundary layer ozone concentrations much lower than those predicted using the highly parameterised, constant surface-resistance deposition scheme of Wesely [18]. This result is in contrast with findings of Ganzeveld et al. [5] who found the use of mechanistic approach to evaluation of surface resistance in fact reduced total dry deposition flux of ozone to the ocean compared to simulations ran using the Wesely [18] scheme with constant surface-resistance, even though the global model study incorporated additional chemical reactions of ozone with DMS, $C_2H_4$, and $C_3H_6$, which were deemed negligible in this study. However, variations between the global model results and results from this are most likely due to variation between the temporal and spatial resolution of the two model studies: the focus of this study is limited to a biologically active region for a time of year in which biological activity is at a maximum and so it would be expected that biochemical effects would be significant in resulting simulations. In contrast, the Ganzeveld et al. [5] study was performed on a global scale for a yearly period and simulated annual mean mixing ratios were analysed which would not reflect short-term seasonal effects. As stated in the introduction, the Wesely [18] scheme serves well in simulating ozone deposition for large-scale simulations, but the mechanistic Fairall et al. [13] parameterisation serves best for simulating ozone deposition velocity to the ocean for particular regional or seasonal effects, as in the case of high biological activity due to a phytoplankton bloom. In addition, Ganzeveld et al. [5] used variable inferred oceanic iodide concentration fields as opposed to constant oceanic iodide fields utilised in this study. Also, the global model study did not allow for the enhancing effect of high sea surface temperature (SST) on diffusivity of ozone in water and so ozone transfer in regions of high SST was limited by solubility and the enhancing effect of seawater salinity on ozone-iodide reaction kinetics was not considered in the global model study.

Based on the findings of this study, it is postulated that high ozone fluxes can be theoretically explained only by consideration of reactions of ozone with ocean dwelling organic matter.

Simulated ozone concentrations agree closely with *in situ* measurements at Mace Head. On average the mechanistic ozone deposition scheme displayed least deviation from measurements. This indicates a closer correlation between actual ozone concentrations and simulated ozone concentrations using the mechanistic scheme (RMS deviation of 7.7 ppb) than using the iodide-only scheme or the nonchemical Wesely [18] scheme (RMS deviation of 11.6 ppb).

Ozone dry deposition flux depends on both ozone concentration and deposition. Variations in ozone flux do not necessarily have a significant effect on ambient ozone concentration due to dominance of other model processes over the dry deposition processes at low deposition velocities.

To the best of authors' knowledge, this is the first study to use the advanced mechanistic ozone deposition scheme of Fairall et al. [13] to quantitatively evaluate the newly discovered ozone deposition-driven upward flux of iodine from the ocean outlined by Martino et al. [8], which is likely to have significant biogeochemical consequences. Ambient ozone concentrations are insensitive to oceanic iodide concentrations, but ozone dry deposition flux (and resulting upward iodine flux) varies with oceanic iodide concentration and so iodide reactions must be explicit within dry deposition models to adequately simulate biogeochemical consequences of dry depositional ozone flux.

## Acknowledgments

The authors gratefully acknowledge the Environmental Protection Agency (EPA) for its support (EPA Project 2006-AQ-MS-50: Ozone levels, changes and trends over Ireland—an Integrated Analysis). Chris Fairall of NOAA is also gratefully acknowledged for making available the parameterisation used in this study. The authors would also like to thank anonymous reviewers for their comments and reviews that served to significantly improve the quality of the paper.

## References

[1] IPCC, 2001.

[2] IPCC, "Climate Change 2007: the Physical Science Basis. Contribution of Working Group I to the Fourth Assessment Report of the Intergovernmental Panel on Climate Change," 2007.

[3] K. A. Hunter and P. S. Liss, "Organic sea surface films," in *Marine Organic Chemistry: Evolution, Composition, Interactions and Chemistry of Organic Matter in Seawater*, Elsevier, Amsterdam, The Netherlands, 1981.

[4] US-EPA, "Ozone: good up high, bad nearby," edited by U.S. Environmental Protection Agency, 2003, http://www.epa.gov/oar/oaqps/gooduphigh/.

[5] L. Ganzeveld, D. Helmig, C. W. Fairall, J. Hare, and A. Pozzer, "Atmosphere-ocean exchange: a global modeling study of biogeochemical, atmospheric, and waterside turbulence dependencies," *Global Biogeochemical Cycles*, vol. 23, Article ID GB4021, 16 pages, 2009.

[6] L. Ganzeveld and J. Lelieveld, "Dry deposition parameterization in a chemistry general circulation model and its influence on the distribution of reactive trace gases," *Journal of Geophysical Research*, vol. 100, no. D10, pp. 20999–21012, 1995.

[7] D. A. Hauglustaine, C. Granier, G. P. Brasseur, and G. Megie, "The importance of atmospheric chemistry in the calculation of radiative forcing on the climate system," *Journal of Geophysical Research*, vol. 99, no. 1, pp. 1173–1186, 1994.

[8] M. Martino, G. P. Mills, J. Woeltjen, and P. S. Liss, "A new source of volatile organoiodine compounds in surface seawater," *Geophysical Research Letters*, vol. 36, no. 1, Article ID L01609, 5 pages, 2009.

[9] D. I. Reeser, C. George, and D. J. Donaldson, "Photooxidation of halides by chlorophyll at the air-salt water interface," *Journal of Physical Chemistry A*, vol. 113, no. 30, pp. 8591–8595, 2009.

[10] D. Davis, J. Crawford, S. Liu et al., "Potential impact of iodine on tropospheric levels of ozone and other critical oxidants," *Journal of Geophysical Research D*, vol. 101, no. 1, pp. 2135–2147, 1996.

[11] C. D. O'Dowd, J. L. Jimenez, R. Bahreini et al., "Marine aerosol formation from biogenic iodine emissions," *Nature*, vol. 417, no. 6889, pp. 632–636, 2002.

[12] A. S. Mahajan, J. M. C. Plane, H. Oetjen, et al., "Measurement and modelling of reactive halogen species over the tropical Atlantic Ocean," *Atmospheric Chemistry and Physics Discussions*, vol. 9, no. 6, pp. 24281–24316, 2009.

[13] C. W. Fairall, D. Helmig, L. Ganzeveld, and J. Hare, "Water-side turbulence enhancement of ozone deposition to the ocean," *Atmospheric Chemistry and Physics*, vol. 7, no. 2, pp. 443–451, 2007.

[14] J. H. Seinfeld and S. N. Pandis, *Atmospheric Chemistry and Physics*, John Wiley & Sons, New York, NY, USA, 1997.

[15] M. Z. Jacobson, *Fundamentals of Atmospheric Modeling*, Cambridge University Press, Cambridge, Mass, USA, 2005.

[16] M. L. Wesely and B. B. Hicks, "A review of the current status of knowledge on dry deposition," *Atmospheric Environment*, vol. 34, no. 12–14, pp. 2261–2282, 2000.

[17] M. W. Gallagher, K. M. Beswick, G. McFiggans, H. Coe, and T. W. Choularton, "Ozone dry deposition velocities for coastal waters," *Water, Air and Soil Pollution: Focus*, vol. 1, no. 5-6, pp. 233–242, 2001.

[18] M. L. Wesely, "Parameterization of surface resistances to gaseous dry deposition in regional-scale numerical models," *Atmospheric Environment*, vol. 23, no. 6, pp. 1293–1304, 1989.

[19] D. H. Lenschow, R. Pearson Jr., and B. B. Stankov, "Measurements of ozone vertical flux to ocean and forest," *Journal of Geophysical Research*, vol. 87, no. 11, pp. 8833–8837, 1982.

[20] W. Chang, B. G. Heikes, and M. Lee, "Ozone deposition to the sea surface: chemical enhancement and wind speed dependence," *Atmospheric Environment*, vol. 38, no. 7, pp. 1053–1059, 2004.

[21] J. A. Garland, A. W. Etzerman, and S. A. Penkett, "The Mechanism for dry deposition of ozone to seawater surfaces," *Journal of Geophysical Research*, vol. 85, no. C12, pp. 7488–7492, 1980.

[22] S. Schwartz, "Factors governing dry deposition of gases to surface water," in *Precipitation Scavenging and Atmosphere-Surface Exchange*, pp. 789–801, Hemisphere Publishing Corporation, Washington, DC, USA, 1992.

[23] D. Clifford, D. J. Donaldson, M. Brigante, B. D'Anna, and C. George, "Reactive uptake of ozone by chlorophyll at aqueous surfaces," *Environmental Science and Technology*, vol. 42, no. 4, pp. 1138–1143, 2008.

[24] B. Langmann, "Numerical modelling of regional scale transport and photochemistry directly together with meteorological processes," *Atmospheric Environment*, vol. 34, no. 21, pp. 3585–3598, 2000.

[25] B. Langmann, "REMOTE-Regional Model with Tracer Extension," 2005.

[26] C. W. Fairall, E. F. Bradley, J. S. Godfrey, G. A. Wick, J. B. Edson, and G. S. Young, "Cool-skin and warm-layer effects on sea surface temperature," *Journal of Geophysical Research C*, vol. 101, no. 1, pp. 1295–1308, 1996.

[27] C. W. Fairall, J. E. Hare, J. B. Edson, and W. McGillis, "Parameterization and micrometeorological measurement of air-sea gas transfer," *Boundary-Layer Meteorology*, vol. 96, no. 1-2, pp. 63–105, 2000.

[28] J. E. Hare, C. W. Fairall, W. R. McGillis, J. B. Edson, B. Ward, and R. Wanninkhof, "Evaluation of the National Oceanic and Atmospheric Administration/ Coupled-Ocean Atmospheric Response Experiment (NOAA/COARE) air-sea gas transfer parameterization using GasEx data," *Journal of Geophysical Research C*, vol. 109, no. 8, Article ID C08S11, 11 pages, 2004.

[29] L. Magi, F. Schweitzer, C. Pallares, S. Cherif, P. Mirabel, and C. George, "Investigation of the uptake rate of ozone and methyl hydroperoxide by water surfaces," *Journal of Physical Chemistry A*, vol. 101, no. 27, pp. 4943–4949, 1997.

[30] P. N. Johnson and R. A. Davis, "Diffusivity of ozone in water," *Journal of Chemical and Engineering Data*, vol. 41, no. 6, pp. 1485–1487, 1996.

[31] B. Jahne, G. Heinz, and W. Deitrich, "Measurement of the diffusion coefficients of sparingly soluble gases in water," *Journal of Geophysical Research*, vol. 92, no. C10, pp. 10767–10776, 1987.

[32] L. F. Kosak-Channing and G. R. Helz, "Solubility of ozone in aqueous solutions of 0–0.6 M ionic strength at 5–30°C," *Environmental Science and Technology*, vol. 17, no. 3, pp. 145–149, 1983.

[33] B. Jahne, T. Wais, and M. Barabas, "A new optical bubble measuring device: a simple model for bubble contribution to gas exchange," in *Gas Transfer at Water Surfaces*, pp. 237–246, D. Reidel, Norwell, Mass, USA, 1984.

[34] L. F. Kosak-Channing and G. R. Helz, "Solubility of ozone in aqueous solutions of 0–0.6 M ionic strength at 5–30°C," *Environmental Science and Technology*, vol. 17, no. 3, pp. 145–149, 1983.

[35] V. W. Truesdale, A. J. Bale, and E. M. S. Woodward, "The meridional distribution of dissolved iodine in near-surface waters of the Atlantic Ocean," *Progress in Oceanography*, vol. 45, no. 3-4, pp. 387–400, 2000.

[36] M. L. A. M. Campos, R. Sanders, and T. Jickells, "The dissolved iodate and iodide distribution in the South Atlantic from the Weddell Sea to Brazil," *Marine Chemistry*, vol. 65, no. 3-4, pp. 167–175, 1999.

[37] MODIS, "Oceancolor Web," http://oceancolor.gsfc.nasa.gov/.

[38] G. McFiggans, J. M.C. Plane, B. J. Allan, L. J. Carpenter, H. Coe, and C. O'Dowd, "A modeling study of iodine chemistry in the marine boundary layer," *Journal of Geophysical Research D*, vol. 105, no. D11, pp. 14371–14385, 2000.

[39] O. P. Tripathi, S. G. Jennings, C. D. O'Dowd, et al., "Statistical Analysis of Eight Surface Ozone Measurement Series for various sites in Ireland," *Journal of Geophysical Reseach*. In press.

[40] G. McFiggans, H. Coe, R. Burgess et al., "Direct evidence for coastal iodine particles from Laminaria macroalgae—linkage to emissions of molecular iodine," *Atmospheric Chemistry and Physics*, vol. 4, no. 3, pp. 701–713, 2004.

[41] C. E. Jones, K. E. Hornsby, R. Sommariva, et al., "Quantifying the contribution of marine organic gases to atmospheric iodine," Geophys. Res. Lett, in press.
[42] K. A. Rahn, R. D. Borys, and R. A. Duce, "Tropospheric halogen gases: inorganic and organic components," *Science*, vol. 192, no. 4239, pp. 549–550, 1976.
[43] S. Yoshida and Y. Muramatsu, "Determination of organic, inorganic and particulate iodine in the coastal atmosphere of Japan," *Journal of Radioanalytical and Nuclear Chemistry*, vol. 196, no. 2, pp. 295–302, 1995.
[44] R. Vogt, R. Sander, R. Von Glasow, and P. J. Crutzen, "Iodine chemistry and its role in halogen activation and ozone loss in the marine boundary layer: a model study," *Journal of Atmospheric Chemistry*, vol. 32, no. 3, pp. 375–395, 1999.
[45] K. A. Read, A. S. Mahajan, L. J. Carpenter et al., "Extensive halogen-mediated ozone destruction over the tropical Atlantic Ocean," *Nature*, vol. 453, no. 7199, pp. 1232–1235, 2008.

Hindawi Publishing Corporation
Advances in Meteorology
Volume 2010, Article ID 408696, 24 pages
doi:10.1155/2010/408696

*Review Article*

# Production and Emissions of Marine Isoprene and Monoterpenes: A Review

**Stephanie L. Shaw,[1] Brett Gantt,[2] and Nicholas Meskhidze[2]**

[1] *Electric Power Research Institute, Palo Alto, CA 94304, USA*
[2] *North Carolina State University, Raleigh, NC 27695, USA*

Correspondence should be addressed to Stephanie L. Shaw, slshaw@alum.mit.edu

Received 14 March 2010; Revised 17 June 2010; Accepted 5 August 2010

Academic Editor: Olaf Stetzer



Terrestrial and marine photosynthetic organisms emit trace gases, including isoprene and monoterpenes. The resulting emissions can impact the atmosphere through oxidative chemistry and formation of secondary organic aerosol. Large uncertainty exists as to the magnitude of the marine sources of these compounds, their controlling factors, and contribution to marine aerosol. In recent years, the number of relevant studies has increased substantially, necessitating the review of this topic. Isoprene emissions vary with plankton species, chlorophyll concentration, light, and other factors. Remote marine boundary layer isoprene mixing ratios can reach >300 pptv, and extrapolated global ocean fluxes range from <1 to >10 Tg C year$^{-1}$. Modeling studies using surface chlorophyll concentration as an isoprene emissions proxy suggest variable atmospheric impacts. More information is needed, including emission fluxes of isoprene and monoterpenes from various biogeographical areas, the effects of species and nutrient limitation on emissions, and the aerosol yields via condensation and nucleation, in order to better quantify the atmospheric impacts of marine isoprene and monoterpenes.

## 1. Introduction

It is has been well established that photosynthetic organisms can emit trace gases, collectively known as biogenic volatile organic compounds (BVOCs), that play a role in the formation of ozone ($O_3$) and help extend the lifetime of important atmospheric gases such as methane and carbon monoxide. Isoprene ($C_5H_8$) is the atmosphere's most ubiquitous BVOC with annual global emissions estimated at 500–750 Tg of carbon [1]. While terrestrial vegetation has the highest isoprene emission rates, it has been shown that productive areas of remote ocean, coastal upwelling regions, and wetlands [2–4] can all emit isoprene at rates that can potentially influence the oxidation capacity of the atmosphere in remote marine and coastal regions [5–9]. In addition to its photochemical role, isoprene has been shown to be an important precursor to secondary organic aerosol (SOA) formation [10, 11]. Recent studies revealed that SOA can strongly impact the radiation balance of the atmosphere, modify cloud microphysics, and participate in chemical transformations. Marine SOA of biogenic origin could be especially important for understanding the cloud-mediated effects of aerosols on climate, because cloud properties respond to aerosols in a nonlinear way and are most sensitive to the addition of particles when the background concentration is low [12]. While the role of ocean ecology in shaping the microphysical properties of low-level marine clouds and planetary albedo is highly uncertain, it has been found that organic aerosol emitted over biologically active oceanic regions can potentially influence number concentration and chemical composition of accumulation mode marine aerosols [13–18]. The incomplete characterization of these impacts in remote marine regions is seen as a major obstacle for improved understanding of radiative balance, contributing up to 80% uncertainty in simulated values of aerosol indirect effect [19].

While it is clear that heterotrophic bacteria, marine phytoplankton, and seaweeds can all emit isoprene [2, 20–22], current debate centers on (1) the magnitude and spatial distribution of global marine fluxes of isoprene,

(2) sensitivities of marine isoprene emissions to environmental parameters (e.g., incoming solar radiation, temperature, and nutrient abundance), (3) dependence of marine isoprene emissions on phytoplankton speciation, (4) contribution of marine isoprene-derived SOA to submicron marine aerosol mass, (5) relative amounts of marine isoprene-derived SOA to SOA formed from other marine BVOCs, (6) the role of marine isoprene-derived organic vapors on potential enhancement of nucleation events and growth of ultrafine particles in coastal and remote ocean environments, and (7) the nature of marine monoterpene emissions, which were only very recently discovered in both laboratory and field work. Finally, due to its ubiquitous production by photosynthetic vegetation, marine isoprene can also be used as a tracer of ocean biological processes when continental influence is eliminated.

In order to better quantify the roles of marine isoprene and monoterpenes in atmospheric chemistry and climate, the spatial distribution of the production and emission mechanisms need to be better constrained. This paper will review the state of the science of marine isoprene and monoterpene research through 2009 (~70 publications including articles in press and recent conference results) and give recommendations for improvement of present marine emission parameterizations. Three general types of studies are described: laboratory measurements on monocultures or simple mixtures of phytoplankton and other organisms, field measurements (including transects and mesocosm studies), and global estimates by modeling approaches. Each of these has their own benefits and drawbacks. For example, laboratory studies can better elucidate processes/mechanisms, and more closely approximate cause-and-effect experiments. Field studies can directly measure emission fluxes, integrate various simultaneously-acting source and sink mechanisms on chemical concentration, and are not subject to bottle effects. As all three types of studies provide information on production or emission rates of isoprene and monoterpenes, all are included and distinguished when relevant. When necessary some production rates or fluxes were converted between various units or estimated based on information provided in the publications.

## 2. Marine Isoprene Seawater Concentrations

The first report of marine isoprene, and observed correlations between seawater isoprene and chlorophyll concentration, was in the field measurements of Bonsang et al. [2]. In depth profiles from various Pacific Ocean and Mediterranean Sea sites, it was observed that the isoprene concentration maxima were broadly consistent with chlorophyll concentration maxima (based on chlorophyll fluorescence). Other field studies [24–26] also found subsurface isoprene concentration maxima at depth broadly coinciding with chlorophyll in the Florida Straits, eastern Atlantic Ocean, and Northeast Pacific sites. It should be noted that throughout the paper we will refer to both chlorophyll and chlorophyll-a as "chlorophyll" when authors do not make clear distinction of specific pigment composition. When specified, "chlorophyll-a" or "Chl-a" will be used.

Surface seawater measurements conducted in the North Sea and the Southern Ocean showed positive correlations of isoprene and chlorophyll that were independent of the presence of individual phytoplankton species [3]. These authors observed a seasonal isoprene concentration cycle of two orders of magnitude, with isoprene consistently supersaturated in seawater relative to its ambient concentrations. These commonly observed positive correlations of isoprene and chlorophyll imply a direct biogenic source of isoprene from phytoplankton. Published observations of isoprene concentrations in seawater are listed in Table 1 and depicted in Figure 1.

Field enclosures and mesoscale enrichment experiments in surface ocean waters populated by phytoplankton have clearly shown rapid isoprene production responses after changes in ambient conditions. For example, Wingenter et al. [23] observed 3-to 7-fold increases in isoprene concentrations in air equilibrated with seawater inside an iron-fertilized patch during the Southern Ocean Iron Experiment (SOFEX) experiment. These concentrations were positively correlated with biological productivity (which coincided with a shift in plankton species present), suggesting that phytoplankton community growth and speciation shifts are also important controls on isoprene emissions. Based on these results, the authors hypothesized that the glacial era iron fertilization may have impacted the atmosphere through release of isoprene and other biogenic trace gases. A separate iron fertilization experiment in the North Pacific [24] exhibited 6-fold higher isoprene production rates inside the fertilized patch as compared to outside of the patch. A mesocosm study in a Norwegian fjord [39] showed that air concentrations of isoprene peaked from 12–4 pm, the portion of day with highest typical light and temperate intensity, and were at minimum levels at night. Interestingly, some isoprene emission occurred in overcast skies and at night, which the authors hypothesize was likely due to ventilation of built up mixed layer concentrations produced during daylight hours.

## 3. Marine Isoprene Production Rates

*3.1. Laboratory Studies of Environmental and Physiological Controls.* In addition to ambient measurements, isoprene production has also been detected from more than 27 phytoplankton species grown in the laboratory by a number of researchers under varying conditions. The results summarized in Table 2 (and Figure 2) exhibit a large variation in production rates ranging over several orders of magnitude.

Shaw et al. [21] tested the effects of a variety of physiological parameters and microorganism interactions on isoprene production rates by phytoplankton monocultures. They showed that isoprene production by phytoplankton exhibited maxima at certain light (>150 $\mu$E/m$^2$/sec) and temperature conditions (23°C). A rapid increase in isoprene production was observed at low light levels, with a gradual increase as irradiance increased, until production rates leveled off. This pattern of isoprene production was shown to be similar to that of terrestrial vegetation (e.g., [43]). A comparison by Gantt et al. [22] of chlorophyll-normalized

Table 1: Isoprene concentrations in seawater.[a]

| Species | Location represented | Time | Study type | Concentration (pmol/L) | Reference[b] | Notes |
|---|---|---|---|---|---|---|
| Seawater | Southern Ocean | Jan-Feb 2002 | Field | 1.8 out of patch; 7.3 in patch | Wingenter et al. 2004 [23] | Southern Ocean Iron Enrichment Experiment (SOFEX) |
| | Northeast Pacific | Jul 2002 | Field | 2–6.5 out of patch; 5.5–12 in patch | Moore and Wang 2006 [24] | iron fertilization experiment |
| | Bellinghausen Sea (Southern Ocean) | Nov-Dec 1992 | Field | 1–20 | Broadgate et al. 1997 [3] | diatoms correlated with highest concentrations |
| | Mediterranean Sea | May and Oct 1990 | Field | 6.7–25 | Bonsang et al. 1992 [2] | |
| | Mace Head, Ireland | Sep-Oct 1998 | Field | 10–20.8 | Broadgate et al. 2004 [20] | at coast and 3 km offshore |
| | Florida Straits, Gulf Stream | Sep 1993 | Field | 9.8–50.8 at surface | Milne et al. 1995 [25] | to 91.2 at subsurface maxima |
| | North Sea | Jun 1993–Jul 1994 | Field | 0.7–90 | Broadgate et al. 1997 [3] | 3 miles offshore; concentrations during *Phaeocystis* bloom (mucus-forming colony) lower than expected; diatoms correlated with highest concentrations; <2 in December, >10 in June |
| Primarily diatoms; dinoflagellates | eastern Atlantic Ocean | May 1997 | Field | 5–55 | Baker et al. 2000 [26] | correlation to chlorophyll only accounts for a small portion of the variability |
| | Pacific Ocean | Apr–Jun 1987–1990 | Field | 3.6–98 | Bonsang et al. 1992 [2] | |
| | North Pacific | May 2001 | Field | <12–94; avg day 56, avg night 27 | Matsunaga et al. 2002 [27] | |

Table 1: Continued.

| Species | Location represented | Time | Study type | Concentration (pmol/L) | Reference[b] | Notes |
|---|---|---|---|---|---|---|
| | Colne Estuary, UK | Mar 2009 | Field enclosure | 0.7–900 | Acuna-Alvarez et al. 2009 [28] | high values are freshwater end of estuary, low values marine end |
| Seaweed-filled rockpools | Mace Head, Ireland | Sep-Oct 1998 | Field enclosure | 24.9–865 (333 average) | Broadgate et al. 2004 [20] | concentration range over 9.5 hr monitoring in sunny day |
| | gyre | 1998 annual | Remote sensing (SeaWIFS) | 0.2–5 | Erickson and Hernandez 2002 [29] | |
| | coastal and mid-latitude | 1998 annual | Remote sensing (SeaWIFS) | 5–80 | Erickson and Hernandez 2002 [29] | |
| | North Sea | 1998 annual | Remote sensing (SeaWIFS) | 20–80 | Erickson and Hernandez 2002 [29] | |
| Diatoms | Southern Ocean | Jan-Feb 2002 | Remote sensing (SeaWiFS) | (A) 3–130 (30 mean) in patch; (B) 1.4–34 (8.4 mean) in patch | Meskhidze and Nenes 2006, 2007 [17, 30] | (A) use Palmer and Shaw 2005 for isoprene-chlorophyll relationship; (B) SOFEX scaled to SeaWiFS chlorophyll [23, 31] |

[a] References are grouped by study type (e.g., field or remote sensing-based modeling studies), in roughly increasing order of concentration.
[b] Only first and second authors were listed to conserve space.

Table 2: Reported marine isoprene production or emission rates.[a]

| Species | Location represented | Time | Study type | Global flux (Tg C/yr) | Production and/or emission rate[b] | Reference[c] | Notes[d] |
|---|---|---|---|---|---|---|---|
| Production rates | | | | | | | |
| *Biddulphia mobiliensis, Phaeodactylum tricornutum, Thalassiosira weissflogii* (diatoms); *Heterocapsa pygmaea* (dinoflagellate); *Synechococcus sp.* (cyanobacteria); *Prymnesium parvum*[e] | | | Lab | | not detected | Milne et al. 1995 [25] | |
| *Thalassiosira rotula* | | | Lab | | | Ratte et al. 1998 [32] | isoprene observed close to levels of cell-free control; biogenic source unclear |
| *Nitzschia sp., Porosira glacialis, Ondontella mobiliensis* (diatoms); *Amphidinium sp.* (dinoflagellate)[e] | | | Lab | | Unquantified | Moore et al. 1994 [33] | all species produced isoprene |
| *Phaeodactylum tricornutum, Chaetoceros neogracilis* (diatoms), *Calcidiscus leptoporus, Emiliania huxleyi* (coccolithophores), and *Dunaliella tertiolecta* (chlorophyte)[e] | | | Lab | | all produced isoprene | Colomb et al. 2008 [34] | 2.8–28.5 pmol/L/Chl a(biomass-normalized concentration for C. neogracilis) |
| *E. huxleyi* (coccolithophore); *Skeletonema costatum, Chaetocerous neogracilis, Chaetoceros debilis* (diatoms); *Synechococcus, Trichodesmium* (cyanobacteria)[e] | S. costatum coastal; Tricho. and Synechococcus-tropic/ subtropic | | Lab | | 0.0003 to 0.0037 $\mu$moles/gchl/day | Yassaa et al. 2008 [35] | **sum of monoterpenes** |
| *Phaeodactylum tricornutum* and *Fragilariopsis kerguelensis* (diatom)[e] | F. kerguelensis-Southern Ocean | | Lab | | 0.04 to 0.07 $\mu$moles/g chl/day | Yassaa et al. 2008 [35] | **sum of monoterpenes** |

Table 2: Continued.

| Species | Location represented | Time | Study type | Global flux (Tg C/yr) | Production and/or emission rate[b] | Reference[c] | Notes[d] |
|---|---|---|---|---|---|---|---|
| *Dunaliella tertiolecta* (chlorophyceae) | | | Lab | | 0.23 $\mu$moles/g chl/day | Yassaa et al. 2008 [35] | **sum of monoterpenes;** primarily p-ocimene and limonene |
| *Prochlorococcus, Synechococcus* (cyanobacteria)[e] | oligotrophic tropics and subtropics | | Lab | | 1.5 $\mu$moles/g chl/day | Shaw et al. 2003 [21] | Alternate units: 1 to $5 \times 10^{-21}$ moles/cell/day |
| *Micromonas pusilla, Pelagomonas calceolata* (picoeukaryotes); *Emiliania huxleyi* (coccolithophore)[e] | | | Lab | | 1 to 1.6 $\mu$moles/g chl/day | Shaw et al. 2003 [21] | Alternate units: 0.2 to $3.8 \times 10^{-19}$ moles/cell/day) |
| *Skeletonema costatum* (diatom) | | | Lab | | 1.8 $\mu$moles/g chl/day | McKay et al.and 1996 [36] | estimated in Shaw 2003 |
| *Trichodesmium* (nitrogen fixer) | | | Lab | | 1.6–4.7 $\mu$moles/g chl/day | Arnold et al. 2009 [37] | |
| Haptophytes; diatoms (S. Ocean); diatoms (elsewhere)[e] | | | Lab | | 0–10 $\mu$moles/g chl/day (phytoplankton type-specific means: 2, 1.2, 2.5, resp.) | Arnold et al.2009 [37] | |
| *Prochlorococcus;* cyanobacteria; unidentified[e] | | | Lab | | 0–22 $\mu$moles/g chl/day (phytoplankton type-specific means: 9.7, 7.8, 3.1, resp.) | Arnold et al. 2009 [37] | |
| *Emiliania huxleyi* (coccolithophore); *Thalassiosira weissflogii, Thalassiosira pseudonana, Chaetoceros neogracile* (diatoms)[e] | | | Lab | | 0–67 $\mu$moles/g chl/day | Gantt et al. 2009 [22] | |
| *Dunaliella tertiolecta* | Colne estuary, UK | various 2006–2009 | Lab | | $8.3 \times 10^{-19}$ moles/cell/day | Acuna-Alvarez et al. 2009 [28] | Estimated here assuming sample vessel volumes based on [28, Figure 8] |

Table 2: Continued.

| Species | Location represented | Time | Study type | Global flux (Tg C/yr) | Production and/or emission rate[b] | Reference[c] | Notes[d] |
|---|---|---|---|---|---|---|---|
| *Phaeodactylum tricornutum* | Colne estuary, UK | various 2006–2009 | Lab | | $1.5\times10^{-18}$ moles/cell/day | Acuna-Alvarez et al. 2009 [28] | Estimated here assuming sample vessel volumes based on [28, Figure 8] |
| *Chaetoceros affinis, Skeletonema costatum* (diatoms); *Emiliania huxleyi* (coccolithophore)[e]; *Amphidinium perculatum* (dinoflagellate)[e] | | | Lab | | 1 to 7 $\times$ $10^{-18}$ moles/cell/day | Milne et al.1995 [25] | |
| *Thalassiosira pseudonana* | | | Lab | | $3.8\times10^{-18}$ moles/cell/day | Evans and Mak 2009 [38] | unpublished conference poster; 30 day incubation average |
| Sediments | Colne estuary, UK | various 2006–2009 | Lab | | 0.15 to 0.71 pmoles/cm$^2$/hr | Acuna-Alvarez et al. 2009 [28] | No net production of isoprene in water; production in sediments |
| *Laminaria digitata, Ascophylum nodosum, Pelvetia canaliculata, Fucus vesiculosus, Fucus serratus, Halidrys siliquosa, Laminaria saccharina* (brown algae) and *Chondrus crispus* (red alga)[e] | Mace Head, Ireland | Sep-Oct 1998 | Field enclosure | | 0.3 to 1.4 pmoles/g dry weight/hr | Broadgate et al. 2004 [20] | |
| *Asparagopsis armata* (red alga) and *Ulva intestinalis* (green alga) | Mace Head, Ireland | Sep-Oct 1998 | Field enclosure | | 3.5 to 5.3 pmoles/g dry weight/hr | Broadgate et al. 2004 [20] | |
| Emission Rates (fluxes) | | | | | | | |
| | North Sea | Jul 1993-Jul 1994 | Field | 0.19 | 0.1 to 4.7 $\times$ $10^7$ molecules/cm$^2$/sec; 1.7 $\times$ $10^7$ mean | Broadgate 1997 [3] | 3 miles offshore |
| | Northeast Pacific | July 2002 | Field | | 0.2 to 2 $\times$ $10^7$ molecules/cm$^2$/sec out of patch; 3.5 to 7 $\times$ $10^7$ molecules/cm$^2$/sec in patch | Moore and Wang 2006 [24] | iron fertilization experiment; alternate units: 0.7 to 1.3 $\mu$mol/(g chl)/day |

Table 2: Continued.

| Species | Location represented | Time | Study type | Global flux (Tg C/yr) | Production and/or emission rate[b] | Reference[c] | Notes[d] |
|---|---|---|---|---|---|---|---|
| | Florida Straits, Gulf Stream | Sep 1993 | Field | 0.38 | 0.7 to $7 \times 10^7$ molecules/cm$^2$/sec | Milne et al. 1995 [25] | |
| Primarily diatoms, with dinoflagellates | Eastern Atlantic Ocean | May 1997 | Field | 0.09–0.6 | 0.8 to $6.4 \times 10^7$ molecules/cm$^2$/sec ($4 \times 10^7$ mean) | Baker et al. 2000 [26] | |
| | North Pacific | May 2001 | Field | 0.23–2.4 | 2.2 to $21 \times 10^7$ molecules/cm$^2$/sec | Matsunaga et al. 2002 [27] | |
| Diatoms; *Emiliania huxleyi* and other coccolithophor[e] | Raunefjord, Southern Norway | May-Jun 2005 | Field mesocosm | 1.2 | 0 to $88 \times 10^7$ molecules/cm$^2$/sec ($11 \times 10^7$ mean) | Sinha et al. 2007 [39] | many phytoplankton types detected, species listed bloomed; macroalgae also present outside mesocosms |
| | Mediterranean Sea; Pacific Ocean | Apr–Jun (Pac.); May–Oct (Med.); combined years | Field | 1.2 | $1.1 \times 10^8$ molecules/cm$^2$/sec | Bonsang et al.1992 [2] | |
| | Mace Head, Ireland | Sep-Oct 1998 | Field enclosure | | $6.8 \times 10^8$ molecules/cm$^2$/sec (max) | Broadgate et al. 2004 [20] | estimated from concentrations |
| | Coastal Crete | Feb–Oct 2004 | Field | | $10^8$ to $6 \times 10^9$ molecules/cm$^2$/sec | Liakakou et al. 2007 [9] | |
| | East Atlantic bloom; Pacific Ocean; Sargasso Sea | | Lab | | 3.4 to $5.6 \times 10^7$; 3.6 to $4.1 \times 10^7$; 1 to $6 \times 10^7$ molecules/cm$^2$/sec | Shaw et al. 2003 [21] | estimated flux |
| | global | 1998 annual | Remote sensing: SeaWiFS | 0.085 | | Erickson and Hernandez 2002 [29] | used Broadgate 1997 relationship to chlorophyll; low because included ocean gyre regions |

Table 2: Continued.

| Species | Location represented | Time | Study type | Global flux (Tg C/yr) | Production and/or emission rate[b] | Reference[c] | Notes[d] |
|---|---|---|---|---|---|---|---|
| | global | 2001 annual | Remote sensing: SeaWiFS | 0.31–1.09 (0.92 mean) | $5 \times 10^5$ to $6 \times 10^8$ molecules/cm$^2$/sec | Gantt et al. 2009 [22] | highest rates in mid-latitude spring and summer; coastal and runoff areas |
| | gyres | 1998 annual | Remote sensing: SeaWiFS | | 0.1 to $2 \times 10^7$ molecules/cm$^2$/sec | Erickson and Hernandez 2002 [29] | used Broadgate 1997 relationship to chlorophyll |
| | coastal and high chlorophyll areas | 1998 annual | Remote sensing: SeaWiFS | | 2 to $30 \times 10^7$ molecules/cm$^2$/sec | Erickson and Hernandez 2002 [29] | used Broadgate 1997 relationship to chlorophyll |
| Diatoms | Southern Ocean | Jan-Feb 2002 | Remote sensing: SeaWiFS | | (A) 0.2 to $8.6 \times 10^8$ molecules/cm$^2$/sec ($1.8 \times 10^8$average); (B) 0.1–$2.2 \times 10^8$ molecules/cm$^2$/sec ($0.6 \times 10^8$ average) | Meskhidze and Nenes 2006, 2007 [17, 30] | (A) use Palmer & Shaw 2005 for isoprene concentrations; (B) use Wingenter 2004 and 2007 [23, 31] scaled to SeaWiFS chlorophyll |
| Diatoms | coastal U.S. | Jul 2001 | Remote sensing: SeaWiFS | | $< 1 \times 10^8$ to $> 4 \times 10^9$ molecules/cm$^2$/sec | Gantt et al. 2010 [40] | New York, Los Angeles, New Orleans |
| | global | | Remote sensing: MODIS | 0.12 | $10^7$ to $10^9$ molecules/cm$^2$/sec | Palmer and Shaw 2005 [41] | |
| | global | 2000 annual | Remote sensing: SeaWIFS and PHYSAT model | 0.27 (0.18 5th %ile, 0.45 95th %ile) | $1.3 \times 10^5$ to $1.6 \times 10^9$ molecules/cm$^2$/sec ($2.7 \times 10^7$ mean) | Arnold et al. 2009 [37] | bottom-up; global ensemble results |

Table 2: Continued.

| Species | Location represented | Time | Study type | Global flux (Tg C/yr) | Production and/or emission rate[b] | Reference[c] | Notes[d] |
|---|---|---|---|---|---|---|---|
| | global | 2000 annual | Remote sensing: SeaWIFS and PHYSAT model | 0.27 to 1.68 | | Arnold et al. 2009 [37] | Bottom-up and top-down estimates |
| | global | 2006 annual | Remote sensing: MODIS and SeaWIFS | 0.32 bottom-up; 11.6 top-down | | Luo and Yu 2010 [42] | **isoprene**; top-down adjusted upwards in comment to reviewers |
| | global | 2006 annual | Remote sensing: MODIS and SeaWIFS | 0.013 bottom-up; 29.5 top-down | | Luo and Yu 2010 [42] | **α-pinene**; top-down adjusted upwards in comment to reviewers |

[a]Entries are first grouped by production rate or ocean-atmosphere emission rate (i.e., flux). Within these groups, study types are then listed together (e.g., laboratory versus field studies), in increasing order of production or emission rate.
[b]When sufficient information was provided, the units of production rate were converted to preferentially $\mu$mol/g chl/day, or alternatively to moles/cell/day. Similarly, ocean-atmosphere emission rates (i.e., fluxes) were converted to molecules/cm$^2$/sec. If insufficient information was provided, the reported units were used.
[c]Only first and second author listed to conserve space.
[d]Chemical referred to is isoprene, unless otherwise noted. If multiple chemicals are reported for a single reference, all are specified and reported separately.
[e]If multiple species or phytoplankton functional types were tested in a study, results were reported as a range (sometimes also with a mean). If the results for a subset of the organisms tested were substantially different from those for other organisms, the results were reported as separate rows.

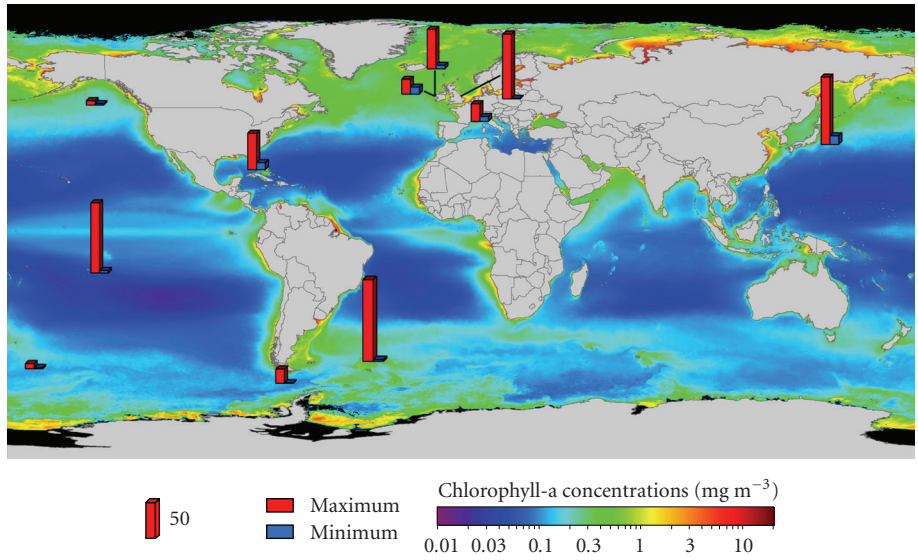


Figure 1: Marine Isoprene Seawater Concentrations. Concentrations in pmol/L. All values reported in the corresponding table are included, except for global modeling studies for which individual locations were not reported. Only "out of bloom" values reported for fertilization experiments. Representative lat./long. coordinates chosen when necessary. Figure background shows SeaWiFS retrieved surface [Chl-$\alpha$]. Figure 1 only: Two high points removed [20, 28] to bring all other points in range.

isoprene production rates for diatoms and coccolithophores and photosynthetically active radiation (PAR) showed consistency with these results, despite a limited number of light levels tested. In contrast, production rates dropped at higher temperatures. While these exact conditions may be linked to species-specific growth requirements and cannot be easily generalized to all species, the measurements of Shaw et al. [21] clearly show the importance of sunlight and water temperature on isoprene production rates by phytoplankton.

The impact of addition of both grazers and viruses on isoprene production rates by phytoplankton was also tested in separate experiments by Shaw et al. [21]. The presence of these other microorganisms was found to affect isoprene production only through the impacts of these organisms on phytoplankton cell counts. For example, the grazers ate the phytoplankton cells, and thus there were less phytoplankton available to produce isoprene, and thus less isoprene. However, the grazers themselves did not produce or consume isoprene. Shaw et al. [21] also showed that the presence of several selected species of heterotrophic bacteria did not impact production rates; that is, there was no evidence of isoprene production or consumption by these bacterial species.

Additional results by these authors showed that chlorophyll-normalized production rates were constant across the species tested. This fact, combined with low absolute production rates and percentages of fixed carbon loss to isoprene (approximately $10^{-4}$% for phytoplankton as compared to 0.5%–2% for higher plants; Shaw et al. [21]) suggested that isoprene may be emitted as a waste product. As the species tested by Shaw et al. [21] represent oligotrophic oceanic regions with low community growth rates, reported marine isoprene production rates might be expected to be lower than those for phytoplankton species representative of more nutrient-replete areas. More recently Arnold et al. [37] confirmed the previously observed linear relationship of isoprene with chlorophyll, although the slopes varied with species.

Laboratory isoprene emission rates of Colomb et al. [34] and Moore et al. [33] were not included in Table 2, as the detectable isoprene production could not be easily converted to units comparable to other studies.

*3.2. Field Studies on Environmental and Physical Controls.* As discussed above, a number of relationships have been observed between ambient concentrations of seawater isoprene and (1) chlorophyll concentration, (2) phytoplankton species, and (3) diel cycles (likely reflecting light and/or temperature variations) [2, 3, 23–27, 39]. Despite the inability to explicitly test cause-and-effect of these parameters in the field, and the use of concentration rather than production rate, the results of these studies are broadly similar to the corresponding relationships to production rates observed in laboratory studies.

*3.3. Effects of Phytoplankton Species and/or Functional Type.* Isoprene production is dependent on the phytoplankton species or functional type, as well as changes in ambient conditions. Therefore, it is informative to review the specific effects that phytoplankton speciation may have on marine isoprene emissions. Table 2 lists 10 species (or genera with unspecified species) whose isoprene production rates have been measured across the various studies reviewed. Due to the paucity of studies on isoprene production by phytoplankton, results from both laboratory and field studies are included in this analysis when relevant. For five

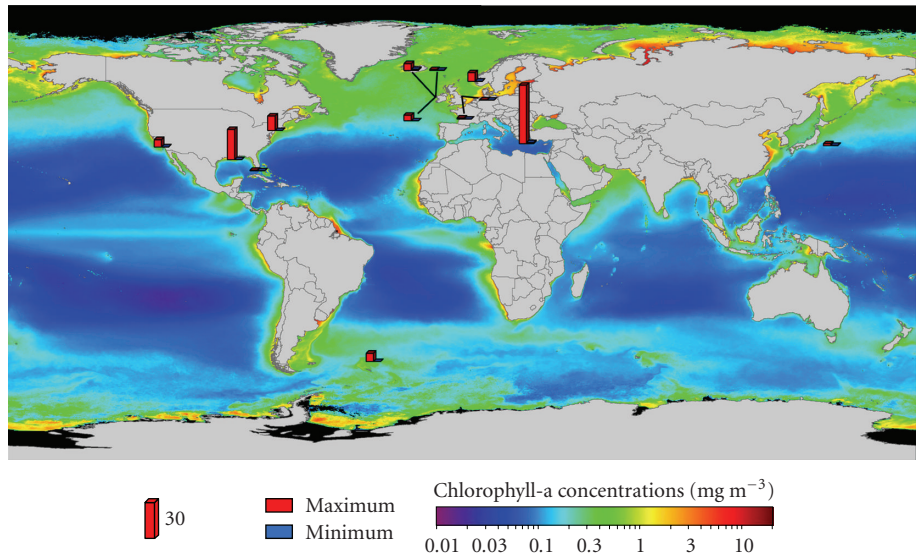


Figure 2: Marine Isoprene Flux Measurements and Estimates. Fluxes reported as $\times 10^8$ molecules/cm$^2$/sec. Otherwise as for Figure 1.

species/genera (*Skeletonema costatum*, *Chaetoceros neogracilis*, *Thalassiosira pseudonana*, *Dunaliella tertiolecta*, and *Amphidinium sp.*), isoprene production is always detected but the rates cannot be directly compared due to the lack of quantifiable or consistent units. In the case of *Phaeodactylum tricornutum*, *Synechococcus sp.*, and *Thalassiosira weissflogii*, there are conflicting reports of detected production. This is likely due to a characteristic culturing choice or detection limit issue as in all cases the "not detected" value was from the same report [25]. The two species whose reported isoprene production rates have comparable units (*Prochlorococcus*, *Emiliania huxleyi*) have rates within a factor of 10 of each other.

In order to simplify the characterization of marine isoprene production, individual species have been grouped by phytoplankton functional type (PFT) as follows: chlorophytes, coccolithophores, haptophytes, cyanobacteria, nitrogen fixers, diatoms, dinoflagellates, picoeukaryotes, and unclassified species. Within several functional types, and specifically diatoms, the range of isoprene production rates was quite variable, ranging from zero to $4\times10^{-18}$ moles/cell/day (or 67 $\mu$mol/(g chl)/day for a second diatom species), two of the highest production rates reported for any species. The coccolithophore and cyanobacteria production rates were within 2 orders of magnitude. Haptophyte and picoeukaryote production rates were similar within each group with the variation less than 1 order of magnitude, although only 2 studies for each PFT exist. The isoprene production rates for diatoms have been most extensively measured in previous studies based on the number of individual species tested. Due to the relative lack of available measurements, but high values for some production rates, we suggest the need for additional sampling of the chlorophyte, haptophyte, and dinoflagellate functional types.

*3.4. Isoprene Production by Other Marine Organisms.* In addition to the work just discussed on microalgae, isoprene measurements related to the presence of other marine organisms have been made. Broadgate et al. [20] measured isoprene concentrations in enclosed coastal rockpools which were filled with various macroalgal (e.g., seaweed) species. Isoprene in seawater increased 6-fold from dark to light periods, and up to 62-fold over the course of a sunny day. Increasing temperature also increased seawater isoprene concentration up to 10-fold. These observations, in combination with increased fluxes during periods of ebbing tide, led the authors to hypothesize that seaweeds are similar to higher plants in that isoprene may contribute to their thermotolerance. Isoprene has also been detected in other studies of coastal waters inhabited by macroalgae [44].

Isoprene production by bacteria was also recently observed in estuary sediments at levels of 0.15 to 0.71 pmoles/cm$^2$/hr [28]. However, the focus of the Acuna-Alvarez et al. [28] study was on isoprene consumption, which will be described in the next section.

Aquatic plants of a higher order than phytoplankton, such as the sedges, mosses (e.g., *Sphagnum sp.*), grasses, and shrubs grown in the boreal and subarctic wetlands of Finland and Sweden, have also been shown to produce isoprene [4, 45–48]. In both their physiology and isoprene production rates, these plants are more similar to terrestrial plants than algae. However, they share some traits with isoprene production by phytoplankton as well. Along with other marine and terrestrial biogenic isoprene producers, isoprene production in aquatic plants generally increases with light and temperature [46]. Nutrient availability also plays a role in isoprene production by these species; increasing nitrogen or phosphorus reduced isoprene emissions in both *Phragmites australis* and sedges [4, 48].

*3.5. Summary of Isoprene Production Rates.* In summary, isoprene production rates by phytoplankton and macroalgae have been shown (in laboratory and field work) to vary with plankton species, light level, temperature, and chlorophyll. Isoprene production is related to cellular chlorophyll content. The mean species-specific rates from 4 studies normalized by Chl-a concentrations [21, 22, 36, 37] are within one and a half orders of magnitude (1 to 70 $\mu$moles/(g Chl-a)/day). Production rates normalized to cell counts ranged over 4 orders of magnitude, from $1\times10^{-21}$ to $3\times10^{-18}$ moles/cell/day (Table 2). Only some studies have reported the rates in comparable units. We suggest that future work in this area use one or both of the following two units for reporting of production rates due to their simplicity and the fact that most of the necessary parameters are typically measured in moles/(g Chl-a)/day, or moles/cell/day. The first option is preferred as there is field and laboratory evidence that suggests isoprene production is related to cellular chlorophyll content, and certainly the biological synthesis process for chlorophyll consists of linking monomer isoprene units together [49]. In addition, such production rates would be able to be scaled by remotely-sensed chlorophyll data from satellites. A cell-normalized production rate is less optimal as it does not account for cell size, chlorophyll content, or photosynthetic activity, which all may act to influence isoprene production. The larger 4 order of magnitude range of production rates for the former units, as compared to 1.5 for the latter, clearly show the resulting imprecision. However, due to the many biological, chemical and physical parameters desired in biogenic trace gas emission studies, it is unfortunately true that many authors do not collect or report all desired information, such as chlorophyll content. Although we do not suggest that this is good practice, a simple cell count is often within the reach of most investigators, especially in laboratory settings, and would certainly serve as an improvement upon no standardized normalizing factor, which is not uncommon in the literature at this time.

## 4. Marine Isoprene Losses in Seawater

Although some evidence exists to demonstrate possible isoprene losses in seawater, very little is known about the main parameters controlling this loss. While the few bacterial species tested in laboratory work [21] were not suggested to exhibit consumption of marine isoprene due to statistically identical isoprene production rates regardless of the presence of heterotrophs, indications of consumption do exist from field work in the ocean water column. Depth profiles, taken over several weeks after an in situ iron fertilization experiment [24], qualitatively suggested that if biological consumption occurred in the water column it was at rates lower than production; this was based on expected influences of various sources and sinks on net production rate. A mesocosm study in a Norwegian fjord reported a relationship between increasing cell counts of *Synechococcus sp.* and decreasing ocean-atmosphere isoprene fluxes, implying that some phytoplankton species could actively consume isoprene [39]. It should be noted that the corresponding observed relationships between the cell counts of other phytoplankton species or functional types (*Emiliania huxleyi*, nanoplankton, picoplankton, and heterotrophic bacteria) and isoprene fluxes were positively correlated, suggesting biogenic sources. Most recently Acuna-Alvarez et al. [28] investigated isoprene consumption by bacteria in temperate (Mediterranean Sea), tropical (Indonesia), and coastal waters and sediments (Colne Estuary, U.K.). Consumption rates were higher for water samples (without sediment) that were spiked with lower levels of isoprene (0.082 ppm) as compared to higher levels (0.82 ppm). The authors showed that the regions with most rapid rates of isoprene consumption coincided with highest isoprene production areas (i.e., estuarine sediments as compared to waters). The dominant consumer species present in the sediments were *Actinobacteria*, *Alphaproteobacteria*, and *Bacterdetes*.

In contrast to biological consumption, only arithmetic estimates of chemical losses based on assumptions have been made. Due to the minimum amount of data available, both biological and chemical losses are still merely estimates and highly uncertain [22, 37, 40, 41]. For example, Palmer and Shaw [41] estimated an isoprene lifetime due to bacterial consumption and chemical oxidation of ~17 and ~19 days, respectively. The bacterial consumption rate ($k$ = 0.06/day) was assumed to be similar to that previously estimated for methyl bromide, while the chemical loss rates to OH and $^1O_2$ were also estimated (using typical seawater concentrations, as well as respective loss rates of $6\times10^{10}$ and $10^6$ $M^{-1}s^{-1}$). These values resulted in the hypothesis that seawater isoprene is removed primarily by air-sea exchange.

Only one field study [24] attempted to observe physical losses in the water column. A vertical diffusive flux was calculated as a diffusion coefficient times the isoprene concentration gradient across bottom of the mixed layer. The authors determined that there was a negligible diffusive flux from the subsurface isoprene maxima into the mixed layer, equal to only 3%–5% of the ocean-atmosphere flux. Measurements in the Florida Straits [25] demonstrated the lack of a strong diurnal pattern in depth profiles of isoprene concentration, suggesting that net water column losses of biological, chemical, and/or physical types occurred on time scales longer than production (which occurs during the day).

## 5. Isoprene Mixing Ratios in Coastal and Remote Marine Atmospheres

Atmospheric mixing ratios of marine isoprene over the remote oceans, or at coastal sites for time periods determined to be unaffected by terrestrial sources, have been directly measured in a number of field campaigns to be as high as 300 pptv (Table 3 and Figure 3). These mixing ratios varied with time of day, season, and location.

Field studies performed in coastal environments will be reviewed first. In three studies by Lewis and colleagues [7, 8, 50], strong diurnal isoprene variations were detected at the Cape Grim Baseline Air Pollution Station, Tasmania and the Mace Head Atmospheric Research Station, Ireland. In all cases sharp mid-day peaks were observed when winds came from the ocean over periods of several days. These

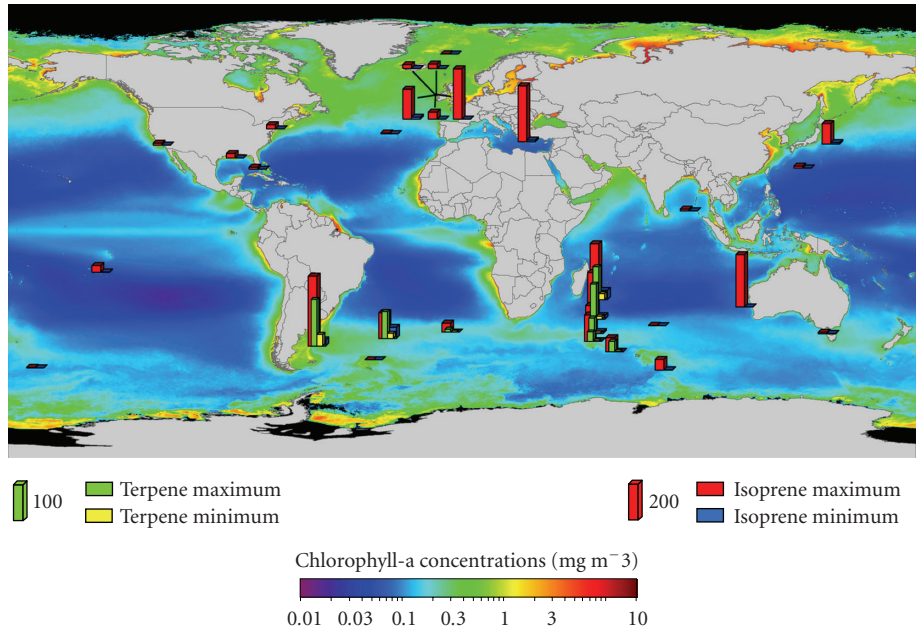


Figure 3: Marine Isoprene and Monoterpene Atmospheric Mixing Ratios. Mixing ratios in pptv. Otherwise as for Figure 1. Figure 3 only: one high point [39] removed to bring other points in range.

peaks in marine boundary layer isoprene mixing ratios occurred earlier than the mid-afternoon isoprene peaks typically observed from terrestrial plant sources. Vertical profiles of isoprene from the ocean surface to 200 m were measured at a coastal site 5 km from Mace Head, Ireland by other authors [51]. Reported mean isoprene mixing ratios decreased from 68 pptv near the surface to 14 pptv at 200 m [51]. However, as the flux footprint encompassed open ocean as well as coastal and rocky land, the influence of coastal emissions on reported vertical profiles of isoprene in this study cannot be easily determined. Based on the ratios of isoprene abundance to that of its degradation products measured at Cape Grim, Australia, a local marine source of isoprene was also suggested in the Southern Ocean by Galbally et al. [52]. Long-term measurements at Finokalia sampling station on the island of Crete showed seasonal variability of isoprene in air masses identified as "marine-derived" [9]. Highest mixing ratios (250–300 pptv) were observed from May through July. Isoprene mixing ratios in ambient air increased with light and temperature, in agreement with laboratory observations [21].

Isoprene mixing ratios have also been reported from field studies of the remote marine boundary layer. Yokouchi et al. [53] reported isoprene mixing ratios in the Southern Indian Ocean ranging from less than 10 to 280 pptv. This demonstrates the high spatial variability often observed in marine isoprene abundance. In other locations visited on this cruise, values of >100 ppt tended to be observed near tropical islands and those of <100 ppt when "open-ocean air masses" were measured. However, the Southern Indian Ocean sites' mixing ratios represented 2-day back trajectories over remote waters, which is much larger than the <1 to 4 hour estimated typical lifetime of isoprene over the ocean [3, 40, 41, 52]. Colomb et al. [54] measured mixing ratios of isoprene and monoterpenes in the Southern Indian Ocean for air masses with 5-day marine back trajectories and found that isoprene was correlated with both the sum of isoprene secondary products (methacrolein and methyl vinyl ketone) and the sum of monoterpenes. Diurnal patterns of isoprene and monoterpene mixing ratios were observed with maxima at 10:00–12:00 local time; this is similar to the results of prior work at the Cape Grim and Mace Head coastal sites [7, 8, 50]. A consistent reduction in mixing ratios was observed as the ship track moved away from biologically active ocean waters. Matsunaga et al. [27] reported marine boundary layer isoprene mixing ratios in the western Pacific in a range of 30–70 pptv. They also reported other isoprene mixing ratios as high as 110 pptv but believed them somehow influenced by terrestrial sources as they calculated very low (<5 pptv) atmospheric mixing ratios that should result from the ocean-atmosphere fluxes they measured.

Review of the published literature shows that the higher isoprene mixing ratios of higher than several hundred pptv reported by some authors often occurred when sampling was performed nearer to coastal areas, suggesting the mixing rations may not be consistent with marine sources and subsequent atmospheric transformation. This is certainly possible; terrestrial boundary layer mixing ratios of isoprene can reach from several hundred to several thousand pptv. However, in almost all cases the authors have attempted to evaluate whether or not their methods have been influenced by terrestrial emissions (such as though the use of several day back-trajectories (e.g., [53]) or avoiding coastal areas [37]), and have concluded this was likely not the case. Another example is the work of Luo and Yu [42] who show that without the inclusion of oceanic emission

Table 3: Ambient air mixing ratios of isoprene (or monoterpenes where noted).[a]

| Species | Location represented | Time | Study type | Mixing ratio (pptv) | Reference[b] | Notes |
|---|---|---|---|---|---|---|
| | Tropical Pacific, N. hemisphere | Feb-Mar 2006 | Field | <1 (mean) | Galbally et al. 2007 [52] | aircraft data from 0–2 km altitude |
| | Amsterdam Island, S. Indian Ocean | Mar 1986–May 1987 | Field | <2 | Bonsang et al. 1992 [2] | suspect canister losses, values perhaps to 10 ppt |
| | Arctic Ocean | Aug 1999 | Field | <2 | Hopkins et al. 2002 [66] | 53–81°N; continuous Arctic sunlight |
| | Southern Ocean | Jan-Feb 2002 | Field | <3 | Wingenter et al. 2004 [23] | Southern Ocean Iron Enrichment Experiment (SOFEX) |
| | Pacific Ocean | May-Jun 1987 | Field | <2–36 | Bonsang et al. 1992 [2] | |
| | Cape Grim, Tasmania | Jan-Feb 1999 | Field | 1.8–7.9 range (5.7 day mean, <1.6 night mean) | Lewis et al. 2001 [8] | marine winds |
| | Florida Straits, Gulf Stream | Sep 1993 | Field | <11 | Milne et al. 1995 [25] | also report modeled concentrations <1 ppt based on calculated fluxes |
| | Cape Grim, Tasmania | Feb-Mar 2006 | Field | 14 (mean) | Galbally et al. 2007 [52] | methyl vinyl ketone and methacrolein (isoprene degradation products) <2 ppt; short isoprene lifetime (<0.1 day) |
| Seaweed-filled rockpools | Mace Head, Ireland | Sep-Oct 1998 | Field | 0–22 (7 mean) | Broadgate et al. 2004 [20] | estimated concentration based on flux |
| | Mace Head, Ireland | July-Aug 1996 | Field | 0–25 (6.2 mean for SW winds, 3.9 mean for NW winds) | Lewis et al. 1997 [7] | NW or SW winds |
| | Mace Head, Ireland | Apr-May 1997 | Field | 0–37 (2.6 mean) | Lewis et al. 1999 [50] | polar/tropical/westerly winds |
| Diatoms and haptophytes dominant | Southern Indian Austral Ocean | Dec 2004 | Field | 0–50 | Colomb et al. 2009 [54] | **isoprene**; 40–49°S; Zones IIb, IIc, III; species suggested from satellite data & PHYSAT model |
| | Southern Ocean | Dec 1997–Mar 1998 | Field | <1–57 (13 mean) | Yokouchi et al. 1999 [53] | very variable concentrations; highest levels south of 45 °S when winds from west and south |
| | North Pacific | May 2001 | Field | 7.2–110; day mean 31, night mean 70 | Matsunaga et al. 2002 [27] | 3.2 pptv is estimated max concentration supported by measured oceanic flux |

Table 3: Continued.

| Species | Location represented | Time | Study type | Mixing ratio (pptv) | Reference[b] | Notes |
|---|---|---|---|---|---|---|
| | West Pacific, Indian Ocean, S.E. Asian Sea | Nov–Feb; 1996-1997 | Field | <10 Indian Ocean and East China Sea; >100 near islands and Australia | Yokouchi et al. 1999 [53] | highest levels were near land (to 286 pptv); however, near-Australia values had back trajectories from Southern Ocean, not land |
| *Prochlorococcus* and haptophytes dominant | Southern Indian Austral Ocean | Dec 2004 | Field | 40–150 | Colomb et al. 2009 [54] | **isoprene**; 24–39.5°S; Zones I–IIa North of Aghula Front; species suggested from satellite data & PHYSAT model |
| | Mace Head, Ireland | Jul–Sep 2002 | Field | <270 | Heard et al. 2006 [67] | When winds from ocean |
| | coastal Crete | Feb–Oct 2004 | Field | 10–300 | Liakakou et al. 2007 [9] | for marine-derived back-trajectories; values >100 from May–Aug |
| Prochlorophytes and cyanobacteria | South Atlantic | Jan–Mar 2007 | Field | 48 max (26 mean) before bloom | Yassaa et al. 2008 [35] | **isoprene;** species suggested by pigments |
| Dinoflagellates, diatoms. pelagophytes | South Atlantic | Jan–Mar 2007 | Field | 32–375 (187 mean) during bloom | Yassaa et al. 2008 [35] | **isoprene;** species suggested by pigments |
| Prochlorophytes and cyanobacteria | South Atlantic | Jan–Mar 2007 | Field | 14 max (5 mean) before bloom | Yassaa et al. 2008 [35] | ***α*-pinene** dominant monoterpene; species suggested by pigments |
| Dinoflagellates, diatoms. Pelagophytes | South Atlantic | Jan–Mar 2007 | Field | 56–225 (125 mean) during bloom | Yassaa et al. 2008 [35] | ***α*-pinene** dominant monoterpene; species suggested by pigments |
| *Prochlorococcus* and haptophytes dominant | Southern Indian Austral Ocean | Dec 2004 | Field | 20–100 | Colomb et al. 2009 [54] | **sum monoterpenes;** 24–39.5°S; Zones I–IIa North of Aghula Front; species suggested from satellite data and PHYSAT model |
| Diatoms and haptophytes dominant | Southern Indian Austral Ocean | Dec 2004 | Field | 0–40 | Colomb et al. 2009 [54] | **sum monoterpenes;** 40–49°S; Zones IIb,IIc,III; species suggested from satellite data and PHYSAT model |
| Diatoms; *Emiliania huxleyi* and other coccolithophores | Raunefjord, Southern Norway | May-Jun 2005 | Field mesocosm | <60–2400 (180 median) | Sinha et al. 2007 [39] | many phytoplankton types detected, species listed bloomed; macroalgae also present outside mesocosms |
| Diatoms | Southern Ocean | Jan-Feb 2002 | Remote sensing (SeaWiFS) | 0.03–0.68 (0.17 mean) | Meskhidze and Nenes 2006, 2007 [17, 30] | Palmer & Shaw 2005 for isoprene-chlorophyll relationship; SOFEX scaled to SeaWiFS chlorophyll (Wingenter 2004, 2007 [23, 31]) |

Table 3: Continued.

| Species | Location represented | Time | Study type | Mixing ratio (pptv) | Reference[b] | Notes |
|---|---|---|---|---|---|---|
| Diatoms | coastal U.S. | Jul 2001 | Remote sensing (SeaWiFS) | 10 (midday mean) NY and NOL; 2.5 (midday mean) LA | Gantt et al. 2010 [40] | New York, Los Angeles, New Orleans |
| | | 2006 annual | Remote sensing (MODIS & SeaWIFS) | 0–280 | Luo and Yu 2010 [42] | **Isoprene** |
| | | 2006 annual | Remote sensing (MODIS & SeaWIFS) | 0–170 | Luo and Yu 2010 [42] | **$\alpha$-pinene** |

[a]References are grouped by study type (e.g., field or remote sensing-based modeling studies), in roughly increasing order of mixing ratios.
[b]Only first and second authors were listed to conserve space.

fluxes in their model the atmospheric concentrations of $\alpha$-pinene and isoprene are essentially zero in the remote marine boundary layer, a result clearly at odds with a number of field studies (Table 3). The conclusion that terrestrial emissions are typically not being detected seems very reasonable when comparing multiday back trajectories against mixing ratios of chemicals whose lifetime is on the order of hours to a day. One case does exist for which contradictory results were found [27], suggesting that the sea-air flux was insufficient to explain the atmospheric isoprene mixing ratios. An explanation for these higher mixing ratios is still in question and should be an active research topic.

As a comparison to the field measurements and modeling results, we have also calculated the atmospheric mixing ratios based on typical seawater concentrations (Table 3) in two ways. First, we assume dynamic equilibrium between the water and atmosphere (i.e., simple Henry Law calculation). For seawater concentrations ranging from 1 to 100 pM (typical for open ocean conditions), the corresponding atmospheric mixing ratio ranged from approximately 100 ppt to 10 ppb. These could be considered maximum possible mixing ratios. However, various field observations have shown that isoprene is supersaturated in sea water by up to 3 orders of magnitude [2, 23–25], and so this simple approach is not representative and results in overestimated atmospheric mixing ratios. The second approach was to consider fluxes, which are a function of temperature, wind, boundary layer height, OH concentration, and so forth. In this case, for seawater isoprene concentrations of 1 to 100 pM the resulting atmospheric mixing ratios ranged from approximately 0.15 to 15 ppt. These numbers are in agreement with modeling studies using CMAQ [22, 40, 55].

## 6. Marine Monoterpenes

Marine terpenoids have been known to be produced by micro- and macroalgae, sponges, and corals, with particularly high rates in red and green seaweeds [56, 57]. They are synthesized from the same precursors as terrestrial terpenes, but through different mechanisms, which results in a variety of different types of complex (not mono-) terpenes. Their ring structures can be quite different from the terpenes commonly reported as being emitted from terrestrial plants, and are often acyclic and quite halogenated because of high seawater concentration of halides [56, 57]. These terpenes are generally thought to be used as a chemical defense mechanism against herbivory [56, 57].

While earlier field measurements of Sartin et al. [58] at coastal Mace Head, Ireland did not detect monoterpenes or sesquiterpenes in marine air and seaweed enclosures, observations of terrestrial-like marine monoterpenes (e.g., $\alpha$-pinene, limonene, p-ocimene, and others) were recently reported in both laboratory cultures and shipboard measurements by Yassaa et al. [35]. Air mixing ratios of the sum of monoterpenes during a field campaign in the Southern Atlantic Ocean were as high as 150–200 pptv [35], which considering the short atmospheric lifetime of monoterpenes strongly suggested an oceanic source. The reported air mixing ratios of isoprene and $\alpha$-pinene were positively correlated, (especially in the region of an active phytoplankton bloom) indicating a similar source [35].

Monoterpene production rates from phytoplankton monocultures tested in the laboratory in the same manuscript were 3-4 orders of magnitude smaller than those for isoprene [35]. The tested species can be grouped into two categories, those for which isoprene emissions were a factor of 30–40 times higher compared to monoterpene

emissions (for *Prochlorococcus* and diatom species), and those for which isoprene emissions were >3000 times higher than monoterpene emissions (for haptophytes, other cyanobacteria, and unidentified species) [42]. Higher isoprene than monoterpene emissions is also observed for terrestrial plants. In one compilation report, 80 species of higher plants (e.g., trees and shrubs) in 27 families for which both isoprene and monoterpene emissions were measured show isoprene to monoterpene emission rate ratios ranged over more than 3 orders of magnitude from 0.07–500 [59]. There was no discontinuity between low and high ratio species as there is with current minimal amount of phytoplankton data (e.g., 30–40 and >3000 ratios). Assuming the isoprene production rates from species tested by Yassaa represent similar percent of fixed carbon as previously suggested by Shaw et al. [21], monoterpenes could also be emitted through some sort of waste process (e.g., metabolic overflow or leak). Earlier field campaign reports of bacterial consumption of various terpenes do exist for Alaskan coastal seawater samples affected by spruce runoff [60], but even less is known about marine monoterpene consumption than production at this time.

## 7. Modeling of Marine Isoprene Emissions and Mixing Ratios

A variety of modeling techniques, ranging from simple photochemical box models to more complex global chemical transport models, have been used to investigate marine isoprene emissions and resulting atmospheric mixing ratios. This section will discuss the research performed using three different types of models: photochemical box models, global emission maps, and chemical transport models. Summaries of all modeled emission rates and atmospheric mixing ratios are depicted in Figures 2 and 3, respectively.

*7.1. Photochemical Box Models.* Several studies have used 0D photochemical box models [9, 25, 26] to estimate marine boundary layer mixing ratios of isoprene and subsequent implications, such as impacts on oxidant mixing ratios. Milne et al. [25] used measured sea-to-air fluxes of isoprene to calculate atmospheric mixing ratios and diurnal variations that were consistent with their measured mixing ratios. Baker et al. [26] used measured fluxes offshore of western Ireland to determine resulting concentrations at the coastal Mace Head site after the 50–200 km transit. They found that the measured marine isoprene fluxes were insufficient to explain the 0–37 pptv of isoprene observed at Mace Head, suggesting potentially large isoprene sources closer to the shore. Palmer and Shaw [41] estimated that marine isoprene emissions represented 1% of OH losses in the remote marine boundary layer. A separate study [9] determined that the presence of marine isoprene on the island of Crete reduced nitrate radical mixing ratios by up to 25%, increased daytime peroxy, organic oxy, and odd hydrogen radicals (i.e., $RO_X$) by a factor of 4, and increased nighttime hydroxyl (OH) and hydroperoxy ($HO_2$) radicals by about 25%–30%.

*7.2. Emission Maps.* The lack of widespread in situ measurements, combined with a poor understanding of the processes controlling production and loss of marine isoprene, has made it difficult to create reliable regional and global isoprene flux estimates. Fortunately, several novel modeling techniques based on remotely-sensed oceanic chlorophyll concentrations data have emerged. To estimate global marine isoprene fluxes, these models use surface chlorophyll-*a* concentration ([Chl-$\alpha$]) as a proxy for marine isoprene production.

The first modeling attempt was by Guenther et al. [61], who assumed that the water concentration of various VOC, including isoprene, was linearly related to [Chl-$\alpha$], and combined it with a standard flux formulation based on surface wind speeds. Erickson and Hernandez [29] took a similar approach, but estimated water concentrations of isoprene based on observations of the isoprene-chlorophyll relationship [3]. They found that the seasonal flux on global scale was very consistent due to hemispheric seasonal differences. Palmer and Shaw [41] combined the isoprene-chlorophyll relationship of Shaw et al. [21] with the Moderate Resolution Imaging Spectroradiometer (MODIS) retrieved [Chl-$\alpha$] data to calculate marine isoprene flux. A steady-state water column model was assumed, including chemical losses and losses to bacteria, and air-sea exchange, with the latter to be a major controlling factor of oceanic lifetime of isoprene. Highest isoprene fluxes were shown to occur in high latitudes during times of elevated biological productivity. As mentioned above, due to the use of plankton species representative of oligotrophic oceans, the global fluxes reported by Palmer and Shaw [41] could be on the low end. This is described more fully in the next section on chemical transport models.

A new approach was taken by Arnold et al. [37] who combined satellite [Chl-$\alpha$] and satellite-derived phytoplankton type maps (using the PHYSAT model [62]) to estimate marine isoprene emission maps. This is described more fully in the next section. Gantt et al. [22] followed on the work of Arnold et al. [37] by creating a physically-based parameterization incorporating variable light intensity and euphotic zone depth, new laboratory isoprene production rates, and maps based on phytoplankton functional type (PFT). The authors found very high production rates in the tropics due to high solar radiation, even when [Chl-$\alpha$] concentrations were relatively low. Two different PFT identification methods (the PHYSAT model [62] and the Nutrient Depleting Temperature model [63]) produced similar results. The emissions results suggested that <1% of submicron OC was due to isoprene on an annual global scale. However, this study modeled for the first time hourly and peak marine isoprene fluxes. The model predicted large range of daytime-maximum to nighttime-minimum emissions also emphasized the importance of correctly capturing diurnal variations

*7.3. Chemical Transport Models.* While global emission maps provided some insight into the contributions of isoprene to OC formation, the alternate use of chemical transport models (CTMs) allows for incorporation of a wider range of

controlling factors and can provide improved results. CTMs can also provide important constraints on emission fluxes (such as through top-down and bottom-up comparisons, and the fitting of models to observational data), and other atmospheric chemistry insights. The next 5 studies discussed involve combination of the remotely-sensed seawater chlorophyll data used for creating emission maps with the GEOS-Chem or CMAQ chemical transport models.

Spracklen et al. [64] found that 3-day back trajectory-weighted chlorophyll concentrations from Sea-viewing Wide Field-of-view Sensor (SeaWiFS) satellite instrument were highly correlated with atmospheric organic aerosol concentrations, suggesting an oceanic source of organic aerosol. By fitting observed organic carbon (OC) concentrations at Amsterdam Island, Mace Head, and the Azores, to global chemical transport model (GEOS-Chem) estimated OC, authors calculated an oceanic source of organic aerosol on the order of 8 Tg OC/yr. Assuming that this OC was solely created from marine-derived isoprene, the authors calculated a required flux of 250 Tg isoprene/yr. This is several orders of magnitude higher than current estimates. Similarly, applying an assumption of a 3% isoprene yield of SOA (as did Spracklen et al. [64]) to the SOA flux estimates of Roelofs [65], the required isoprene flux would be a factor of 3–5 times higher than 250 Tg isoprene/yr, suggesting additional sources of SOA precursors besides isoprene are needed to match the observed and/or estimated OC concentrations.

Arnold et al. [37] combined new satellite maps of PFT created from SeaWiFS data and the PHYSAT model [62], with new lab measurements of isoprene production rate to improve bottom-up global estimates of isoprene flux. Probability density functions of production rates were created for each PFT to account for large range of measured values and propagated through the global emission calculation. Bottom-up fluxes were insufficient to account for isoprene measurements in ambient air. The authors also used a "top down" approach by scaling the flux to minimize model bias. The two approaches had dissimilar results, likely due to a number of uncertainties including the limited amount of ambient and laboratory data, climatology, and retrievals. The results provided "top-down" fluxes in the same range as previously published values, good agreement with a selection of measured fluxes in the Atlantic, Norwegian Sea, and Southern Ocean, and a significant improvement over Palmer and Shaw [41] flux estimates in the Pacific. Flux estimates of Arnold et al. [37] from the top-down results also indicated that isoprene has an insignificant role (<1%) in forming marine organic aerosol by secondary processes.

Gantt et al. [40] performed the first full regional modeling study of marine isoprene in coastal areas, by focusing on the continental United States. Marine isoprene emissions were found to have a minor role on air quality in coastal urban areas, resulting in <1% changes in SOA and $O_3$ concentrations. It was shown that the diurnal pattern of isoprene mixing ratios and fluxes are not the same because of the photochemical loss occurring during the daytime. A more recent study by the same authors [55] included marine isoprene, monoterpenes, and primary organic aerosol emissions. They found that over the remote ocean as well as coastal regions, marine isoprene and monoterpenes contribute <10% of total marine organics aerosol concentration through SOA formation and increase ozone concentrations by 0.5%.

The most recent isoprene [37] and monoterpene [35] production rate measurements were used in a global modeling study by Luo and Yu [42]. They used both bottom-up and top-down methods of estimating global ocean emissions of $\alpha$-pinene and isoprene. Using the bottom-up method of Arnold et al. [37], which was based on surface flux measurements, resulted in emissions of 0.013 Tg C/yr of $\alpha$-pinene and 0.32 Tg C/yr of isoprene. The $\alpha$-pinene emissions are much smaller than isoprene emissions due to their lower production rates, as discussed previously in Section 6. The top-down method added solar radiation and gas transfer terms to the parameterization of emission flux used in the bottom-up estimates, and model was then fit to observed atmospheric mixing ratios in the Southern Ocean [35]. In this way, estimates of the emissions necessary to match the observations were determined to be 29.5 Tg C/yr and 11.6 Tg C/yr for $\alpha$-pinene and isoprene, respectively. These top-down estimates are by far the largest reported for isoprene, and are even larger for $\alpha$-pinene. For example, the corresponding top-down estimate of isoprene emissions from Arnold et al. [37] was 1.7 Tg C/yr. This suggests that $\alpha$-pinene emissions from the top-down method could be significant to global budgets, and that subsequent SOA formation from $\alpha$-pinene may be a significant contributor to OC in marine environments.

While both the top-down and bottom-up methods of Luo and Yu [42] are subject to high uncertainties, there is a clear discrepancy in the results, particularly for $\alpha$-pinene. The authors suggest this may be due to incomplete understanding of the phytoplankton species that produce these chemicals and resulting production rates (bottom-up method), or the emission parameterizations, model spatial resolutions, and assumed homogeneity of mixing ratios throughout entire height of boundary layer (top-down method). It is not clear which method may be more in error. Inclusion of only the bottom-up emissions estimates into the model was not able to replicate the high atmospheric mixing ratios observed [35], but use of surface mixing ratios throughout entire model boundary layer grid cells may overestimate the top-down emission fluxes. When the authors assume a vertical decay they estimate emissions as low as 10–15 Tg C/yr for $\alpha$-pinene and 4–6 Tg C/yr for isoprene. If any of these top-down estimates are correct, additional sources (e.g., additional phytoplankton species that produce these chemicals, or increased production rates) are needed to account for the ocean boundary layer mixing ratio observations [35].

Overall, the model estimates of global ocean isoprene fluxes range from $1\times10^5$ to $4\times10^9$ molecules/cm$^2$/sec, approximately in the same range as for field observations and extrapolations from laboratory studies ($1\times10^6$ to $6\times10^9$), but extending to lower values. Coastal regions were found to have greater isoprene fluxes compared to the open ocean areas [9, 28, 40], although the impact of marine isoprene on local photochemistry and air pollution is predicted to be small [40, 55].

## 8. Current Issues

This review of the literature on marine isoprene and monoterpenes demonstrates the progress made over the past 20 years since Bonsang et al. [2] first reported isoprene measurements in the oceans. A small body of knowledge now exists on the relevant organisms, major controlling factors for production and emissions, and potential impacts on atmospheric chemistry and SOA production. Despite this, knowledge gaps still exist which limit our ability to assess the global and regional effects of marine emissions.

Despite an increasing amount of recent research interest, the data available on production rates and ambient fluxes is insufficient to elucidate the mechanisms behind marine isoprene production, and to constrain the magnitude of ocean-atmosphere isoprene flux. In some cases, measured fluxes were insufficient to explain atmospheric mixing ratios present at, or somewhat downwind of, the measurement locations [26, 27]. For example, measured fluxes in the North Pacific support an ambient mixing ratio of 3.2 pptv, while the measured marine boundary layer mixing ratios were typically between 30–70 pptv [27]. These discrepancies could be due to the heterogeneity of production and loss processes. Considering the lack of understanding of these process mechanisms, it could also be attributed to inadequate parameterizations of the mechanism within the model.

Similarly, a large disconnect also exists between bottom-up and top-down emissions estimates determined from use of more complex model calculations. Predicted fluxes or mixing ratios from bottom-up methods can often not account for observed values or scaled values [26, 37, 42]. In one study this discrepancy was much larger for $\alpha$-pinene than isoprene, which may be due to the single set of $\alpha$-pinene measurements available [35]. Other reasons for these discrepancies include misclassification or omission of certain phytoplankton species in the models, including incorrect characterization of high production rates, a lack of reliable ambient data, inaccurate emission parameterizations, insufficient model spatial resolutions, assumed homogeneity of mixing ratios throughout entire height of boundary layer, a reliance on satellite [Chl-$\alpha$] retrievals which may not accurately represent the chlorophyll concentrations that can influence isoprene or monoterpene emissions (e.g., may not sense chlorophyll from the full water depth that is ventilated), different phytoplankton communities suggested by PHYSAT than actually exist in the ocean, or a combination of all these uncertainties. It has been suggested by some authors that certain studies may have been influenced by isoprene abundances in terrestrial air masses passing over the ocean. However, as discussed previously due to lack of air mass contact with land within the short chemical lifetimes of these gases, coastal influence was ruled out for most open-ocean marine isoprene mixing ratio measurements. Even if some of these bottom-up fluxes are overestimated due to terrestrial influence, this would only act to mitigate the top-down and bottom-up flux discrepancies.

Isoprene has been suggested as a possible precursor of marine SOA based on the magnitude and direction of its ocean-atmosphere flux and established SOA formation mechanisms. Several recent estimates suggest the global isoprene flux is too small to account for a majority of marine-derived organic aerosol. However, exceptions may occur when submicron OC, short time scales (e.g., peak emission hours), certain regions (e.g., tropics), or local scale impacts are considered [22, 40, 55]. Estimates from the recent modeling work of Luo and Yu [42] suggest large oceanic emission fluxes for $\alpha$-pinene (29.5 TgC/yr) and isoprene (11.6 TgC/yr), which are larger than most, but not all, estimates of global ocean submicron primary OC emissions [22, 64, 65, 68]. Combined with the inherent heterogeneity of ocean fluxes, the $\alpha$-pinene emissions may be sufficiently high (in combination with its higher reactivity and SOA yield than for isoprene), to be considered an important source of submicron marine SOA. Furthermore, organic vapors from marine sources of VOC have been implicated to aid nucleation events and growth of ultrafine particles in coastal environments [69, 70]. A month-long intensive measurement campaign conducted at a remote coastal site south of the Great Barrier Reef on the east coast of Australia revealed coastal nucleation events in clean, marine air masses on 65% of the days. The timing of the events (starting ~10:00 local time and continuing for 1–4 hrs) as well as environmental conditions for the onset of nucleation (solar intensity above 1000 $Wm^{-2}$ and RH <60%) are consistent with requirements for elevated marine VOC emissions. The measurements for volatility and hygroscopic properties of freshly nucleated particles suggested that the condensation of sulfate and/or organic vapors was most likely responsible for driving particle growth [70]. A different approach to investigating isoprene as a marine SOA precursor was taken by Claeys et al. [71]. Ambient measurements of chemical markers of isoprene-derived SOA, as determined for terrestrial environments, were taken in marine air at Amsterdam Island in the Southern Ocean. Due to the absence of sulfate esters of tetrols (isoprene-specific markers), it was concluded that the source of the water soluble component of marine organic aerosols at the site may be attributed to the oxidation of primary emissions of phytoplankton biomass rather than isoprene. However, this may not be true of other geographical areas. It was previously found that despite the abundance of high isoprene-producing diatoms at Amsterdam Island, air mixing ratios of isoprene were <2 pptv with an expected maximum of <10 pptv [2, 54]. Repetition of this work in locations where isoprene has been determined to be more abundant is needed to conclusively determine the source-attribution of marine organic aerosols.

## 9. Suggested Future Directions

Over the past decade, laboratory and field measurements, satellite remote sensing, and modeling efforts have substantially improved our understanding of the temporal and spatial distribution of marine isoprene and monoterpene emissions and their potential effects on marine aerosol number concentration and chemical composition. However, an improved understanding of the impacts of marine isoprene emissions requires additional data collection from several

directions. Several suggestions for future work are described below.

(1) Few laboratory (e.g., bottle) studies of isoprene production have been reported, and more are necessary to explain production mechanisms, confirm the dependence of emission rates on phytoplankton speciation, and determine the conditions that promote and inhibit production. Both laboratory measurements and field studies have their limitations. It is often very hard to mimic actual ambient conditions in the laboratory, and field campaigns suffer from their geographically sparse coverage and short-duration that may lead to missed events or conditions of interest due to changing natural conditions and the inherent heterogeneity of biogenic trace gas production and emission processes. Models can provide a global and highly temporal perspective, but require field and laboratory measurements for validation. Therefore, it is recommended that all these approaches be pursued simultaneously in future studies.

(2) Following on the first suggested research direction, it will also be important to pursue experiments that retain group dynamics of microorganism communities while measuring production rates from phytoplankton species, or identifying controlling factors thereupon. The few studies that have looked into such organism combinations have found evidence to suggest some interactions exist. These include predator-prey impacts in laboratory studies [21], and in situ shifts microorganism community structure that correlates with changes in ocean emission rates [23]. The analysis of production rate by phytoplankton species or functional type also clearly demonstrates a wide variety of responses by different species that can coexist. Testing of group dynamics can be done through controlled laboratory experiments, or in mesocosm studies which allow whole ecosystem testing [39].

(3) Approximately 27 phytoplankton species in 9 PFTs have already been tested for isoprene or monoterpene production capabilities. However, the resulting production rates are highly variable, ranging over several orders of magnitude. Future testing should focus on several key species or PFTs. First, due to the lack of measurements, but large values for some production rates, additional sampling of the charophyte, haptophyte, and dinoflagellate species is recommended. Second, species typical of the tropics and remote oceans should be tested, due to the importance of isoprene and monoterpene emission impacts on atmospheric chemistry and aerosol formation potential in these biogeographical regions. For ease of comparison across studies, we recommend one of the following production rate units be used for future reporting of production rates: (1) moles/g Chl-$\alpha$/day or (2) moles/cell/day.

(4) Work on biogenic production of trace gases by aquatic plants other than phytoplankton suggests that nutrient availability can have an effect on isoprene emissions [4, 48]. Preliminary results from Evans and Mak [38] suggest that isoprene production by *Thalassiosira pseudonana* decreased with reductions of provided phosphate, nitrate, and silica. The importance of this relationship between nutrients and emissions requires further investigation.

(5) Due to their high SOA forming potential, and the very high initial estimates of emission rates recently published, additional field and lab work on marine monoterpene emissions is warranted.

(6) For the assessment of water column isoprene losses, information on both chemical and biological consumption is needed. However, as several studies have suggested that ocean emission rates cannot always account for air mixing ratios in the marine boundary layer, these loss processes may be much more important in estuaries and near coastal regions than in the open oceans.

(7) Additional measurements of isoprene-specific tracers in areas of higher isoprene emissions and air mixing ratios could help to constrain assessments of impact on SOA.

## 10. Conclusions

Isoprene and terpene emissions are of interest in remote marine environments as sources of SOA, contributors to photooxidant chemistry, and as biogenic tracers. The amounts and impacts of these emissions on the atmosphere is not well constrained, but may be potentially important for future climate and air quality research. These uncertainties associated with marine isoprene emissions and its effects on local photochemistry and SOA formation can only be answered with additional data from a variety of sources including laboratory, field, and modeling studies. All three approaches should continue concurrently, with a focus on phytoplankton speciation, nutrient-dependence, chemical and biological water-column loss, and other factors that can affect emissions. Because of the complex nature of this water-air-biological system, it is important to make trace gas measurement in air and water phases in concert with a suite of detailed biological and environmental measurements such as aerosol chemical composition and size distribution, meteorological parameters (e.g., light, wind, and temperature), physical water parameters, pigment concentrations, and cell counts of dominant phytoplankton species.

## Acknowledgement

N. Meskhidze would like to acknowledge the support by the Office of Science (BER), U.S. Department of Energy, Grant no. DE-FG02-08ER64508.

## References

[1] A. Guenther, T. Karl, P. Harley, C. Wiedinmyer, P. I. Palmer, and C. Geron, "Estimates of global terrestrial isoprene emissions using MEGAN (Model of Emissions of Gases and Aerosols from Nature)," *Atmospheric Chemistry and Physics*, vol. 6, no. 11, pp. 3181–3210, 2006.

[2] B. Bonsang, C. Polle, and G. Lambert, "Evidence for marine production of isoprene," *Geophysical Research Letters*, vol. 19, no. 11, pp. 1129–1132, 1992.

[3] W. J. Broadgate, P. S. Liss, and S. A. Penkett, "Seasonal emissions of isoprene and other reactive hydrocarbon gases from the ocean," *Geophysical Research Letters*, vol. 24, no. 21, pp. 2675–2678, 1997.

[4] A. Ekberg, A. Arneth, H. Hakola, S. Hayward, and T. Holst, "Isoprene emission from wetland sedges," *Biogeosciences*, vol. 6, no. 4, pp. 601–613, 2009.

[5] G. P. Ayers, R. W. Gillett, H. Granek, C. De Serves, and R. A. Cox, "Formaldehyde production in clean marine air," *Geophysical Research Letters*, vol. 24, no. 4, pp. 401–404, 1997.

[6] N. Carslaw, D. J. Creasey, D. E. Heard, et al., "Modeling OH, $HO_2$, and $RO_2$ radicals in the marine boundary layer 1. Model construction and comparison with field measurements," *Journal of Geophysical Research Atmospheres*, vol. 104, no. D23, pp. 30241–30255, 1999.

[7] A. C. Lewis, K. D. Bartle, D. E. Heard, J. B. McQuaid, M. J. Pilling, and P. W. Seakins, "In situ, gas chromatographic measurements of non-methane hydrocarbons and dimethyl sulfide at a remote coastal location (Mace Head, Eire) July-August 1996," *Journal of the Chemical Society, Faraday Transactions*, vol. 93, no. 16, pp. 2921–2927, 1997.

[8] A. C. Lewis, L. J. Carpenter, and M. J. Pilling, "Nonmethane hydrocarbons in Southern Ocean boundary layer air," *Journal of Geophysical Research Atmospheres*, vol. 106, no. D5, pp. 4987–4994, 2001.

[9] E. Liakakou, M. Vrekoussis, B. Bonsang, Ch. Donousis, M. Kanakidou, and N. Mihalopoulos, "Isoprene above the Eastern Mediterranean: seasonal variation and contribution to the oxidation capacity of the atmosphere," *Atmospheric Environment*, vol. 41, no. 5, pp. 1002–1010, 2007.

[10] M. Claeys, B. Graham, G. Vas et al., "Formation of secondary organic aerosols through photooxidation of isoprene," *Science*, vol. 303, no. 5661, pp. 1173–1176, 2004.

[11] J. H. Kroll and J. H. Seinfeld, "Chemistry of secondary organic aerosol: formation and evolution of low-volatility organics in the atmosphere," *Atmospheric Environment*, vol. 42, no. 16, pp. 3593–3624, 2008.

[12] S. Platnick and S. Twomey, "Determining the susceptibility of cloud albedo to changes in droplet concentration with the advanced very high resolution radiometer," *Journal of Applied Meteorology*, vol. 33, no. 5, pp. 334–347, 1994.

[13] P. G. Falkowski, Y. Kim, Z. Kolber, C. Wilson, C. Wirick, and R. Cess, "Natural versus anthropogenic factors affecting low-level cloud albedo over the North Atlantic," *Science*, vol. 256, no. 5061, pp. 1311–1313, 1992.

[14] R. Boers, G. P. Ayers, and J. L. Gras, "Coherence between seasonal variation in satellite-derived cloud optical depth and boundary layer CCN concentrations at a mid- latitude Southern Hemisphere station," *Tellus, Series B*, vol. 46, no. 2, pp. 123–131, 1994.

[15] R. Boers, J. R. Acarreta, and J. L. Gras, "Satellite monitoring of the first indirect aerosol effect: retrieval of the droplet concentration of water clouds," *Journal of Geophysical Research Atmospheres*, vol. 111, no. 22, Article ID D22208, 2006.

[16] S. M. Vallina, R. Simó, and S. Gassó, "What controls CCN seasonality in the Southern Ocean? A statistical analysis based on satellite-derived chlorophyll and CCN and model-estimated OH radical and rainfall," *Global Biogeochemical Cycles*, vol. 20, no. 1, Article ID GB1014, 2006.

[17] N. Meskhidze and A. Nenes, "Phytoplankton and cloudiness in the Southern Ocean," *Science*, vol. 314, no. 5804, pp. 1419–1423, 2006.

[18] Y. Hu, M. Vaughan, C. McClain et al., "Global statistics of liquid water content and effective number concentration of water clouds over ocean derived from combined CALIPSO and MODIS measurements," *Atmospheric Chemistry and Physics*, vol. 7, no. 12, pp. 3353–3359, 2007.

[19] C. Hoose, J. E. Kristjánsson, T. Iversen, A. Kirkevåg, ∅. Seland, and A. Gettelman, "Constraining cloud droplet number concentration in GCMs suppresses the aerosol indirect effect," *Geophysical Research Letters*, vol. 36, no. 12, Article ID L12807, 2009.

[20] W. J. Broadgate, G. Malin, F. C. Küpper, A. Thompson, and P. S. Liss, "Isoprene and other non-methane hydrocarbons from seaweeds: a source of reactive hydrocarbons to the atmosphere," *Marine Chemistry*, vol. 88, no. 1-2, pp. 61–73, 2004.

[21] S. L. Shaw, S. W. Chisholm, and R. G. Prinn, "Isoprene production by Prochlorococcus, a marine cyanobacterium, and other phytoplankton," *Marine Chemistry*, vol. 80, no. 4, pp. 227–245, 2003.

[22] B. Gantt, N. Meskhidze, and D. Kamykowski, "A new physically-based quantification of marine isoprene and primary organic aerosol emissions," *Atmospheric Chemistry and Physics*, vol. 9, pp. 4915–4927, 2009.

[23] O. W. Wingenter, K. B. Haase, P. Strutton et al., "Changing concentrations of CO, $CH_4$, $C_5H_8$, $CH_3Br$, $CH_3I$, and dimethyl sulfide during the Southern Ocean Iron Enrichment Experiments," *Proceedings of the National Academy of Sciences of the United States of America*, vol. 101, no. 23, pp. 8537–8541, 2004.

[24] R. M. Moore and L. Wang, "The influence of iron fertilization on the fluxes of methyl halides and isoprene from ocean to atmosphere in the SERIES experiment," *Deep-Sea Research*, vol. 53, no. 20–22, pp. 2398–2409, 2006.

[25] P. J. Milne, D. D. Riemer, R. G. Zika, and L. E. Brand, "Measurement of vertical distribution of isoprene in surface seawater, its chemical fate, and its emission from several phytoplankton monocultures," *Marine Chemistry*, vol. 48, no. 3-4, pp. 237–244, 1995.

[26] A. R. Baker, S. M. Turner, W. J. Broadgate et al., "Distribution and sea-air fluxes of biogenic trace gases in the eastern Atlantic Ocean," *Global Biogeochemical Cycles*, vol. 14, no. 3, pp. 871–886, 2000.

[27] S. Matsunaga, M. Mochida, T. Saito, and K. Kawamura, "In situ measurement of isoprene in the marine air and surface seawater from the western North Pacific," *Atmospheric Environment*, vol. 36, no. 39-40, pp. 6051–6057, 2002.

[28] L. Acuna-Alvarez, D. A. Exton, K. N. Timmis, D. J. Suggett, and T. J. McGenity, "Characterization of marine isoprene-degrading communities," *Environmental Microbiology*, vol. 11, no. 12, pp. 3280–3291, 2009.

[29] D. J. Erickson III and J. L. Hernandez, "A global, high resolution, satellite-based model of air-sea isoprene flux," in *Gas Transfer at Water Surfaces*, vol. 127 of *Geophysical Monograph*, American Geophysical Union, 2002.

[30] N. Meskhidze and A. Nenes, "Reply to comment on "Phytoplankton and cloudiness in the Southern Ocean"," *Science*, vol. 317, no. 5834, pp. 42–43, 2007.

[31] O. W. Wingenter, "Isoprene, cloud droplets, and phytoplankton," *Science*, vol. 317, no. 5834, pp. 42–43, 2007.

[32] M. Ratte, O. Bujok, A. Spitzy, and J. Rudolph, "Photochemical alkene formation in seawater from dissolved organic carbon: results from laboratory experiments," *Journal of Geophysical Research Atmospheres*, vol. 103, no. D5, pp. 5707–5717, 1998.

[33] R. M. Moore, D. E. Oram, and S. A. Penkett, "Production of isoprene by marine phytoplankton cultures," *Geophysical Research Letters*, vol. 21, no. 23, pp. 2507–2510, 1994.

[34] A. Colomb, N. Yassaa, J. Williams, I. Peeken, and K. Lochte, "Screening volatile organic compounds (VOCs) emissions from five marine phytoplankton species by head space gas chromatography/mass spectrometry (HS-GC/MS)," *Journal of Environmental Monitoring*, vol. 10, no. 3, pp. 325–330, 2008.

[35] N. Yassaa, I. Peeken, E. Zöllner et al., "Evidence for marine production of monoterpenes," *Environmental Chemistry*, vol. 5, no. 6, pp. 391–401, 2008.

[36] W. A. McKay, M. F. Turner, B. M. R. Jones, and C. M. Halliwell, "Emissions of hydrocarbons from marine phytoplankton—some results from controlled laboratory experiments," *Atmospheric Environment*, vol. 30, no. 14, pp. 2583–2593, 1996.

[37] S. R. Arnold, D. V. Spracklen, J. Williams, et al., "Evaluation of the global oceanic isoprene source and its impacts on marine organic carbon aerosol," *Atmospheric Chemistry and Physics*, vol. 9, pp. 1253–1262, 2009.

[38] T. Evans and J. E. Mak, "Biological Volatile Organic Compounds (BVOCs) emissions from the planktonic diatom Thalassiosira pseudonana," in *Proceedings of the American Geophysical Union, Fall Meeting*, 2009, abstract no. A11B-0089.

[39] V. Sinha, J. Williams, M. Meyerhöfer, U. Riebesell, A. I. Paulino, and A. Larsen, "Air-sea fluxes of methanol, acetone, acetaldehyde, isoprene and DMS from a Norwegian fjord following a phytoplankton bloom in a mesocosm experiment," *Atmospheric Chemistry and Physics*, vol. 7, no. 3, pp. 739–755, 2007.

[40] B. Gantt, N. Meskhidze, Y. Zhang, and J. Xu, "The effect of marine isoprene emissions on secondary organic aerosol and ozone formation in the coastal United States," *Atmospheric Environment*, vol. 44, no. 1, pp. 115–121, 2010.

[41] P. I. Palmer and S. L. Shaw, "Quantifying global marine isoprene fluxes using MODIS chlorophyll observations," *Geophysical Research Letters*, vol. 32, no. 9, Article ID L09805, 5 pages, 2005.

[42] G. Luo and F. Yu, "A numerical evaluation of global oceanic emissions of $\alpha$-pinene and isoprene," *Atmospheric Chemistry and Physics*, vol. 10, no. 4, pp. 2007–2015, 2010.

[43] A. B. Guenther, R. K. Monson, and R. Fall, "Isoprene and monoterpene emission rate variability: observations with eucalyptus and emission rate algorithm development," *Journal of Geophysical Research Atmospheres*, vol. 96, no. D6, pp. 10799–10808, 1991.

[44] N. Gist and A. C. Lewis, "Seasonal variations of dissolved alkenes in coastal waters," *Marine Chemistry*, vol. 100, no. 1-2, pp. 1–10, 2006.

[45] S. Haapanala, J. Rinne, K.-H. Pystynen, H. Hellén, H. Hakola, and T. Riutta, "Measurements of hydrocarbon emissions from a boreal fen using the REA technique," *Biogeosciences*, vol. 3, no. 1, pp. 103–112, 2006.

[46] H. Hellén, H. Hakola, K.-H. Pystynen, J. Rinne, and S. Haapanala, "C2-C10 hydrocarbon emissions from a boreal wetland and forest floor," *Biogeosciences*, vol. 3, no. 2, pp. 167–174, 2006.

[47] P. Tiiva, R. Rinnan, T. Holopainen, S. K. Mörsky, and J. K. Holopainen, "Isoprene emissions from boreal peatland microcosms; effects of elevated ozone concentration in an open field experiment," *Atmospheric Environment*, vol. 41, no. 18, pp. 3819–3828, 2007.

[48] S. Fares, F. Brilli, I. Noguès et al., "Isoprene emission and primary metabolism in Phragmites australis grown under different phosphorus levels," *Plant Biology*, vol. 10, no. 1, pp. 38–43, 2008.

[49] H. K. Lichtenthaler, "The 1-deoxy-D-xylulose-5-phosphate pathway of isoprenoid biosynthesis in plants," *Annual Review of Plant Physiology and Plant Molecular Biology*, vol. 50, pp. 47–65, 1999.

[50] A. C. Lewis, J. B. McQuaid, N. Carslaw, and M. J. Pilling, "Diurnal cycles of short-lived tropospheric alkenes at a north Atlantic coastal site," *Atmospheric Environment*, vol. 33, no. 15, pp. 2417–2422, 1999.

[51] J. P. Greenberg, A. B. Guenther, and A. Turnipseed, "Marine organic halide and isoprene emissions near Mace Head, Ireland," *Environmental Chemistry*, vol. 2, no. 4, pp. 291–294, 2005.

[52] I. E. Galbally, S. J. Lawson, I. A. Weeks et al., "Volatile organic compounds in marine air at Cape Grim, Australia," *Environmental Chemistry*, vol. 4, no. 3, pp. 178–182, 2007.

[53] Y. Yokouchi, H.-J. Li, T. Machida, S. Aoki, and H. Akimoto, "Isoprene in the marine boundary layer (Southeast Asian Sea, eastern Indian Ocean, and Southern Ocean): comparison with dimethyl sulfide and bromoform," *Journal of Geophysical Research Atmospheres*, vol. 104, no. D7, pp. 8067–8076, 1999.

[54] A. Colomb, V. Gros, S. Alvain et al., "Variation of atmospheric volatile organic compounds over the Southern Indian Ocean (30–49 S)," *Environmental Chemistry*, vol. 6, no. 1, pp. 70–82, 2009.

[55] B. Gantt, N. Meskhidze, and A. G. Carlton, "The impact of marine organics on the air quality of the western United States," *Atmospheric Chemistry and Physics Discussions*, vol. 10, no. 3, pp. 6257–6278, 2010.

[56] M. E. Hay and W. Fenical, "Marine plant-herbivore interactions: the ecology of chemical defense," *Annual Review of Ecology and Systematics*, vol. 19, pp. 111–145, 1988.

[57] M. L. Wise, "Monoterpene biosynthesis in marine algae," *Phycologia*, vol. 42, no. 4, pp. 370–377, 2003.

[58] J. H. Sartin, C. J. Halsall, B. Davison, S. Owen, and C. N. Hewitt, "Determination of biogenic volatile organic compounds (C8–C16) in the coastal atmosphere at Mace Head, Ireland," *Analytica Chimica Acta*, vol. 428, no. 1, pp. 61–72, 2001.

[59] C. Wiedinmyer, A. Guenther, P. Harley, et al., "Global organic emissions from vegetation," in *Emissions of Atmospheric Trace Compounds*, C. Granier, P. Artaxo, and C. E. Reeves, Eds., Kluwer Academic Publishers, Dordrecht, The Netherlands, 2004.

[60] D. K. Button, "Evidence for a terpene-based food chain in the Gulf of Alaska," *Applied and Environmental Microbiology*, vol. 48, no. 5, pp. 1004–1011, 1984.

[61] A. Guenther, C. N. Hewitt, D. Erickson, et al., "A global model of natural volatile organic compound emissions," *Journal of Geophysical Research Atmospheres*, vol. 100, no. D5, pp. 8873–8892, 1995.

[62] S. Alvain, C. Moulin, Y. Dandonneau, and F. M. Bréon, "Remote sensing of phytoplankton groups in case 1 waters from global SeaWiFS imagery," *Deep-Sea Research Part I*, vol. 52, no. 11, pp. 1989–2004, 2005.

[63] D. Kamykowski, S.-J. Zentara, J. M. Morrison, and A. C. Switzer, "Dynamic global patterns of nitrate, phosphate, silicate, and iron availability and phytoplankton community composition from remote sensing data," *Global Biogeochemical Cycles*, vol. 16, no. 4, Article ID 1077, 2002.

[64] D. V. Spracklen, S. R. Arnold, J. Sciare, K. S. Carslaw, and C. Pio, "Globally significant oceanic source of organic carbon aerosol," *Geophysical Research Letters*, vol. 35, no. 12, Article ID L12811, 2008.

[65] G. J. Roelofs, "A GCM study of organic matter in marine aerosol and its potential contribution to cloud drop activation," *Atmospheric Chemistry and Physics*, vol. 8, no. 3, pp. 709–719, 2008.

[66] J. R. Hopkins, I. D. Jones, A. C. Lewis, J. B. McQuaid, and P. W. Seakins, "Non-methane hydrocarbons in the Arctic boundary layer," *Atmospheric Environment*, vol. 36, no. 20, pp. 3217–3229, 2002.

[67] D. E. Heard, K. A. Read, J. Methven et al., "The North Atlantic Marine Boundary Layer Experiment (NAMBLEX). Overview of the campaign held at Mace Head, Ireland, in summer 2002," *Atmospheric Chemistry and Physics*, vol. 6, no. 8, pp. 2241–2272, 2006.

[68] B. Langmann, C. Scannell, and C. O'Dowd, "New directions: organic matter contribution to marine aerosols and cloud condensation nuclei," *Atmospheric Environment*, vol. 42, no. 33, pp. 7821–7822, 2008.

[69] P. Vaattovaara, P. E. Huttunen, Y. J. Yoon et al., "The composition of nucleation and Aitken modes particles during coastal nucleation events: evidence for marine secondary organic contribution," *Atmospheric Chemistry and Physics*, vol. 6, no. 12, pp. 4601–4616, 2006.

[70] R. L. Modini, Z. D. Ristovski, G. R. Johnson et al., "New particle formation and growth at a remote, sub-tropical coastal location," *Atmospheric Chemistry and Physics*, vol. 9, no. 19, pp. 7607–7621, 2009.

[71] M. Claeys, W. Wang, R. Vermeylen et al., "Chemical characterisation of marine aerosol at Amsterdam Island during the austral summer of 2006-2007," *Journal of Aerosol Science*, vol. 41, no. 1, pp. 13–22, 2010.

Hindawi Publishing Corporation
Advances in Meteorology
Volume 2010, Article ID 830846, 7 pages
doi:10.1155/2010/830846

*Research Article*

# Wind Speed Influences on Marine Aerosol Optical Depth

**Colin O'Dowd,[1] Claire Scannell,[1,2] Jane Mulcahy,[1,3] and S. Gerard Jennings[1]**

[1] *School of Physics & Centre for Climate and Air Pollution Studies, Environmental Change Institute, National University of Ireland Galway, University Road, Galway, Ireland*
[2] *Université Paris 6, LATMOS/IPSL, CNRS/INSU, 75005 Paris, France*
[3] *Global Model Evaluation and Development, Met Office, Exeter, Devon EX1 3PB, UK*

Correspondence should be addressed to Colin O'Dowd, colin.odowd@nuigalway.ie

Received 18 February 2010; Revised 18 July 2010; Accepted 21 August 2010

Academic Editor: David Kieber



The Mulcahy (Mulcahy et al., 2008) power-law parameterization, derived at the coastal Atlantic station Mace Head, between clean marine aerosol optical depth (AOD) and wind speed is compared to open ocean MODIS-derived AOD versus wind speed. The reported AOD versus wind speed (U) was a function of $\sim U^2$. The open ocean MODIS-derived AOD at 550 nm and 860 nm wavelengths, while in good agreement with the general magnitude of the Mulcahy parameterization, follows a power-law with the exponent ranging from 0.72 to 2.47 for a wind speed range of 2–18 m s$^{-1}$. For the four cases examined, some MODIS cases underestimated AOD while other cases overestimated AOD relative to the Mulcahy scheme. Overall, the results from MODIS support the general power-law relationship of Mulcahy, although some linear cases were also encountered in the MODIS dataset. Deviations also arise between MODIS and Mulcahy at higher wind speeds (>15 m s$^{-1}$), where MODIS-derived AOD returns lower values as compared to Mulcahy. The results also support the suggestion than wind generated sea spray, under moderately high winds, can rival anthropogenic pollution plumes advecting out into marine environments with wind driven AOD contributing to AOD values approaching 0.3.

## 1. Introduction

Sea spray aerosol is one of the largest natural contributors to the global aerosol loading and thus plays an important role in the global radiative budget [1, 2]. Submicron size aerosols are especially relevant in terms of cloud condensation nuclei [3], while both sub- and supermicron sizes contribute to aerosol scattering [4] and to aerosol optical depth [5]. Both of these effects suggest that sea spray aerosol plays an important role in the global radiative budget, contributing to the aerosol climate effect [6, 7].

Mulcahy et al. [5] established that under moderate to high wind speed conditions, AOD associated with sea spray followed a power-law wind-speed dependency with an exponent of ~2. At moderately high wind speeds, sea spray-derived AOD reached the order of 0.35, often exceeding AOD associated with pollution plumes over oceanic regions. The relationship of Mulcahy et al. [5] has recently been compared to model-predicted AOD from sea spray sources by Madry et al. [8]. In the latter study, they found that model-derived AOD also followed a wind speed square function, and that the formulation proposed by Mulcahy et al. [5] was highly correlated to the modeled-derived AOD values.

Mulchay et al. [5] report AOD values for clean marine air which are significantly higher than those previously reported (e.g., Smirnov et al. [9]), most likely due to a wider wind speed range in Mulcahy et al. [5] along with extensive filtering and analysis procedures used; however, the Mulcahy et al. [5] data were taken in the coastal environment, and apart from the aforementioned modeling study, they have not been compared to open-ocean measurements of AOD. In this study, we compare the Mulcahy et al. [5] AOD-wind speed relationship to MODIS-derived AOD versus wind speed. The comparison is done for two remote open ocean regions.

## 2. MODIS AOD and Wind Speed Data

Clean air masses are essential to ensure that the only contribution to the AOD is from natural aerosols, in this

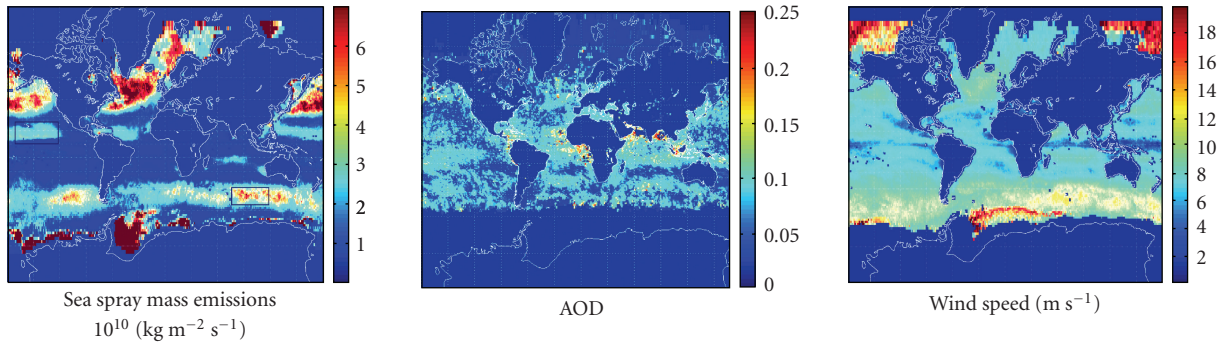


Figure 1: (a) depicts a global sea spray mass emissions map scheme illustrating areas for which AOD was examined in the North Pacific and Southern oceans, (b) illustrates global annual average AOD for June 2006, and (c) shows the average monthly wind speed.

case sea spray aerosols. This is achieved by choosing remote marine locations away from large land masses, by examining the air mass trajectories over each location and choosing only those days for which the air mass has not passed over land in the five days previous. These periods were chosen based on clean marine air systems observed using HYSPLIT back trajectories over two specific grids for 2006. The HYSPLIT or HYbrid Single Particle Lagrangian Integrated Trajectory model run by NOAA can compute simple forward or backward air parcel trajectories from any starting or finishing grid point. It can run complex dispersion and deposition simulations and compute the advection of an ensemble of pollutants or the advection of a single pollutant. For this work, its ability to compute multiple and single backward air mass trajectories from a particular location was utilised to determine the direction of approaching air mass trajectories. For further information see [10].

For this analysis, $1^\circ \times 1^\circ$ resolution *C005* MODIS daily AOD data taken from the Ocean level 3 MODIS Atmosphere Daily Global Product for 2006 at 550 nm and 860 nm were utilised. Two grid areas were chosen in remote marine locations (Figure 1): one in the north Pacific (0° N–20° N and 180° W–110° W) and one in the Southern ocean (40° S–60° S and 120° E–80° E), denoted hereafter as Grid 1 and Grid 2. Shown in the figure is a sea spray mass emission rate along with MODIS-derived AOD. The additional criteria used for selection of the grids were as follows: only clean air masses were examined as determined by back-trajectory analysis; there must be no cloud contamination; there must be variable wind speeds during the period. Grid 1 and grid 2 were analysed for January and December 2006 and July and December 2006, respectively. The areas chosen coincided with areas of high sea spray aerosol concentrations. Such large areas were chosen in order to sample a complete range of wind speeds under the strict criteria that were utilized. AOD and wind speed data were retrieved daily for the month long periods outlined for both grids. Wind speed data was retrieved from the SeaWinds instrument on the QuickSCAT satellite. SeaWinds is a microwave radar that measures near-surface wind speed and direction with a swath resolution of $0.25^\circ \times 0.25^\circ$. It was launched into a polar, sun-synchronous orbit with 98.6° inclination and with a local equator crossing time at the ascending node of 6:00 am ± 30 mins and the descending node of 18:00 ± 30 mins. Data is available in daily, weekly, and monthly formats. For this analysis, wind speed was interpolated to a $1^\circ \times 1^\circ$ grid to compare to a $1^\circ \times 1^\circ$ AOD grid, and each wind speed data point was matched to its corresponding AOD data point at each time and location. Since the ascending equatorial crossing time of MODIS AQUA is approximately 1:30 am, 4.5 hours prior to QuikSCAT, care was taken in choosing times and locations where wind speed variability was minimal. Between 2000 and 5000 AOD data points were binned according to wind speed intervals for each month for each grid.

Clouds are characterised by high optical depths, and AOD measurements cannot be made in areas of cloud cover. Therefore, it is imperative for accurate AOD measurements that firstly, areas of cloud be clearly identified and secondly, a maximum number of successive cloud-free days be employed in the analysis. MODIS level 2 *C005* data has a stringent cloud screening process based on algorithms by Martins et al. [11] in which pixels classified as being fully or partially contaminated by cloud are "flagged" out of the data set. For a full description of the cloud masking procedure see Remer et al. [12]. Finally, for complete insurance that there is no residual contamination by clouds, an extra filter is utilised whereby pixels are "flagged" as cloudy if AOD in the infrared channel (1640 nm) exceeds 3 [13]. Additionally, it is desirable that wind speeds range from high to low, typically 4–20 m s$^{-1}$ to provide a wind speed range comparable with Mulcahy et al. [5].

There are a number of uncertainties associated with satellite measurements, for example, the presence of clouds which are not removed by the filtering process, and whitecaps at high wind speeds lead to emissivity effects which can affect the quality of the retrieved MODIS AOD. More details can be read in Tanre et al. [14]. Other uncertainties arise as the two instruments are not collocated temporally or spatially. MODIS aqua has an equatorial crossing time 4.5 hours prior to that of QuikSCAT. Also interpolating the QuikSCAT grid from 0.25° to 1° can cause an uncertainty of up to 5%. However, we aimed to reduce such uncertainties with

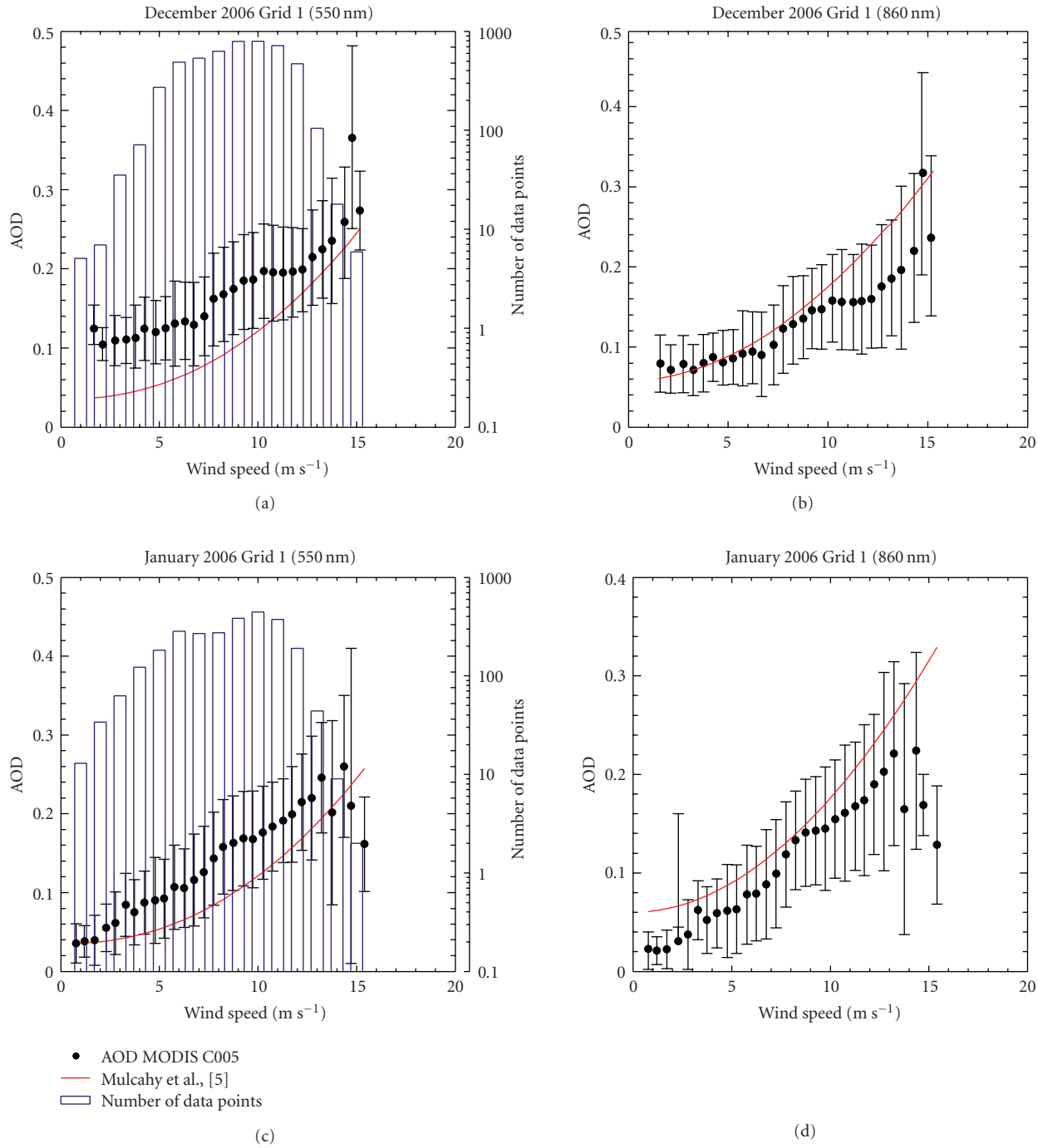


Figure 2: This Figure compares MODIS C005 AOD data at 550 nm and 860 nm (together with the standard deviation of AOD data within each bin) for Grid 1 during December and January 2006 with the Mulcahy et al. [5] AOD-wind speed relationship. Also shown is the number of data points per wind speed average bin.

the strict criteria with which our data was chosen. For all satellite instruments, calibration errors can lead to biases in the retrieved data. For MODIS aqua, Guenthar et al. [15] demonstrated a calibration error of between 1.8%-1.9%; however, this impact was deemed to be negligible on optical depth retrievals. The uncertainty in wind speed derived from QuikSCAT was shown to be approximately 1 m s$^{-1}$, [16]. Sun glint and reflectance from whitecaps do result in a positive bias of 1%–10% for the MODIS AOD data which is within an acceptable degree of accuracy, [17].

## 3. Evaluation of Satellite-Derived AOD versus Wind Speed

Figures 2 and 3 present a comparison between AOD at 550 nm and 860 nm with wind speed for the two selected

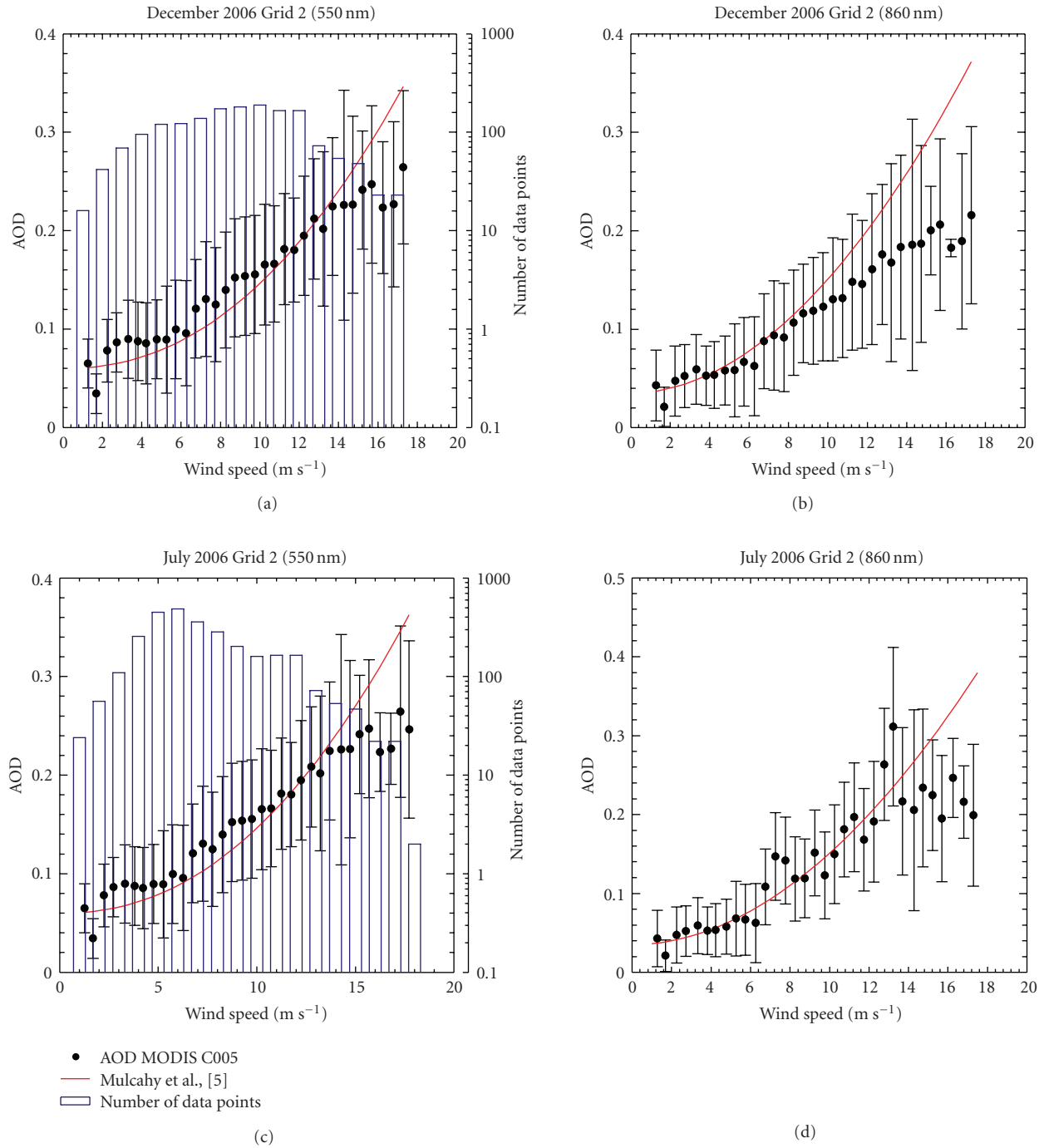


FIGURE 3: This Figure compares MODIS C005 AOD data at 550 nm and 860 nm (together with the standard deviation of AOD data within each bin) for Grid 2 during December and July 2006 with the Mulcahy et al. [5] AOD-wind speed relationship.

grids and for the two selected periods associated with each grid. Although not shown in the figures, the data were fitted using power-law regression equations, the parameters, and correlation coefficients which are given in Table 1.

## 4. Results

The results for Grid 1 during December and January 2006 are shown in Figure 2 and cover a wind speed range of 2 m s$^{-1}$ to 15 m s$^{-1}$. For December, the 550 nm MODIS AOD is higher than the Mulcahy scheme for the lower wind speeds, increasing up to 10 m s$^{-1}$ where it levels out between 10 and 13 m s$^{-1}$, after which AOD increased again. For the 860 nm wavelength, there is excellent agreement with Mulcahy up to 10 m s$^{-1}$, after which AOD levels out till it starts to increase with wind speed above 13 m s$^{-1}$. For the January case, a similar trend is seen where in the 550 nm case, AOD is higher than that reported by Mulcahy, and for 860 nm, AOD is

Table 1: Power-law fits for MODIS AOD versus wind speed for Grid 1 and Grid 2.

| Grid | 550 nm | 860 nm |
|---|---|---|
| December Grid 1 | $\text{AOD} = 0.114 + 2.2 \times 10^{-4}\,\text{U}^{2.47}$, $r^2 = 0.89$ | $\text{AOD} = 0.077 + 2.9 \times 10^{-4}\,\text{U}^{2.36}$, $r^2 = 0.91$ |
| January Grid 1 | $\text{AOD} = -0.004 + 0.033\,\text{U}^{0.72}$, $r^2 = 0.91$ | $\text{AOD} = -0.018 + 0.029\,\text{U}^{0.77}$, $r^2 = 0.88$ |
| December Grid 2 | $\text{AOD} = 0.042 + 9.7 \times 10^{-4}\,\text{U}^{1.09}$, $r^2 = 0.97$ | $\text{AOD} = 0.019 + 0.077\,\text{U}^{1.40}$, $r^2 = 0.97$ |
| July Grid 2 | $\text{AOD} = 0.0395 + 0.011\,\text{U}^{1.04}$, $r^2 = 0.95$ | $\text{AOD} = 0.0387 + 0.117\,\text{U}^{1.015}$, $r^2 = 0.83$ |

marginally lower than that in the Mulcahy parameterization. Between 9 and 13 m s$^{-1}$, there is a slight reduction in the slope of the AOD-wind speed relationship, although not as drastic as the December case where it more or less levels off. The fitted power-law relationship for the December 550 nm case possessed an exponent of 2.47, and for the 860 nm wavelength, the exponent was 2.36. These exponents are slightly higher than the Mulcahy exponents (2.2 for 500 nm and 1.95 for the 832 nm wavelengths). For the January case, the exponents are significantly lower with a value of 0.72 for the 550 nm wavelength and 0.77 for the 860 nm wavelength. For these four relationships, the correlation coefficient ($r^2$) was between 0.88 and 0.91.

For Grid 2, shown in Figure 3, AOD values are observed over a wind speed range of 2 to 18 m s$^{-1}$. For the December 550 nm case, excellent agreement between MODIS and Mulcahy is observed up to ~16 m s$^{-1}$, after which the MODIS AOD levels off as Mulcahy continues to increase. For 860 nm, excellent agreement is seen up to 9-10 m s$^{-1}$, after which MODIS AOD levels off.

For July, the Grid 2 550 nm data shows very good agreement with Mulcahy, although MODIS produces slightly higher AOD values at lower wind speeds and slightly lower values at the higher wind speeds. For 860 nm, the July data agree very well up to 15 m s$^{-1}$, after which it levels off as the Mulcahy parameterization continues to rise with rising wind speed.

The fitted relationships for the December case between MODIS AOD and the Mulcahy scheme reflect a power law with an exponent of 1.09 for the 550 nm wavelength and 1.40 for the 860 nm wavelength. For the July case, the respective exponents are 1.04 and 1.02. The correlation coefficient for these 4 cases ranges from 0.83 to 0.97.

## 5. Discussion

The MODIS-derived AOD-wind speed relationships follow a power law with an exponent ranging from below unity (0.72) to values greater than 2 (up to 2.47), with three out of the 8 cases have, more or less, a linear relationship with an exponent of ~1. As mentioned, Mulcahy found an exponent of ~2.2 for 500 nm and ~2 for 832 nm. The variability of the MODIS values could be due to a number of reasons. In Grid 1, the December 550 nm case, relative to Mulcahy, reflects higher AOD at low wind speeds. There are three possibilities for these higher values: there is a significant fraction of secondary marine aerosol associated with these cases, thus contributing to enhanced AOD; there are high conditions of relative humidity, thus increasing the aerosol scattering potential; or the cases examined were influenced by long-range transport of anthropogenic aerosols, thus also contributing to the elevated AOD levels. The excellent agreement at low-to-moderate wind speeds for the 860 nm wavelength combined with the 550 nm date would suggest a significant fraction of submicron particles, either natural or anthropogenic, rather than an increase in relative humidity. As mentioned above, in this case, there was a levelling off in AOD at 10–13 m s$^{-1}$, before continuing to increase above 13 m s$^{-1}$. It is not clear what causes this trend; however, in most cases, at the highest wind speeds above 15 m s$^{-1}$, the MODIS-derived AOD is less than that in the Mulcahy parameterization. For wind speeds less than 15 m s$^{-1}$, there is more often than not very good agreement between the two datasets, although there is still some variability in overestimation and underestimation by MODIS relative to Mulcahy. Our results should also be compared to some recent satellite-derived AOD-wind speed relationships. Huang et al. [18] found a linear relationship between AOD and wind speed ranging from ~0.08-0.09 at zero m s$^{-1}$ to ~0.15–0.175 at 20 m s$^{-1}$. It should be noted that, for the same wavelength, Mulcahy estimates a lower wind speed AOD value of 0.04 or less, and at the highest wind speed measured by Mulcahy (18 m s$^{-1}$), AOD is greater (~0.35). By comparison, Lehahn et al. [19] found similarly low wind speed values as Mulcahy (0.04 or less) and values of about 0.18 at a wind speed of 14 m s$^{-1}$ compared to values of ~0.24 [5], but with a significantly lower correlation coefficient ($R \sim 0.45$–$0.5$). The Huang et al. [18] satellite AOD study, relative to the Mulcahy ground-based AOD study, tends to overestimate AOD by about 100% under conditions of zero wind speed and underestimate AOD at the higher wind speeds of 18–20 m s$^{-1}$ by a similar amount. Lehahn et al. [19] provide better agreement with Mulcahy at the lower wind speeds (less than ~12 m s$^{-1}$); however, at their maximum reported wind speeds of less than 15 m s$^{-1}$, their AOD values are about 25% less than that reported by Mulcahy et al. [5].

It should be noted that AOD derived from the precision filter radiometer is a more direct measurement, and many more assumptions are required in the MODIS retrieval

algorithm than in the precision filter radiometer. Consequently, one would expect the radiometer data to reflect the more accurate AOD-wind speed relationship. In addition, and as stated in the introduction, a detailed modeling study of sea spray production and associated AOD also concluded a power law with an exponent of 2 [8]. Finally, meteorological effects such as increased deposition rates may be associated with stable boundary layers would reduce the spray residence time, thus reducing its AOD impact; variations in precipitation rates or long-range transport of anthropogenic aerosols can all contribute to the variability in the MODIS cases. Nevertheless, the main conclusions arrived at by Mulcahy et al. [5] still hold, namely, that sea spray contributions to marine AOD can approach or even exceed values of 0.3 and that natural sea spray under moderately high wind speed regimes can rival that of many anthropogenic plumes advecting out into marine environments.

## 6. Conclusions

MODIS-derived AOD for clean, remote maritime conditions are analysed as a function of wind speeds ranging from 2 to 18 m s$^{-1}$. The relationships observed followed a power law with exponents ranging from 0.72 to 2.47 for 550 nm wavelengths and from 0.75 to 2.40 for the 860 nm wavelength. The MODIS-derived AOD was compared to the Mulcahy parameterization derived from a precision filter radiometer at a coastal NE Atlantic station (Mace Head). Generally, good agreement was found between the two datasets, although, on a case by case basis, sometimes MODIS overestimated and sometimes underestimated relative to Mulcahy. Mostly, MODIS-delivered lower AOD values at higher wind speeds (>15 m s$^{-1}$) when compared to Mulcahy, and at times, overestimated at lower wind speeds, resulting in an exponent close to 1, producing a linear relationship between AOD and wind speed at times. There are a number of reasons for the variability in the MODIS derived AOD-wind speed exponent. These include the possibility of variability in meteorology (i.e., precipitation and stability) which may reduce sea spray residence time, long range transport of anthropogenic aerosol, secondary marine aerosol production, and variability in relative humidity fields, altering aerosol scattering efficiency. While there is variability in MODIS-derived AOD versus wind speed, with the parameterized exponent deviating from the Mulcahy squared power law dependency, there is no reason to suggest that a power law with an exponent of 2.2 for 500 nm, and 2 for 860 nm is not a robust parameterization. The results also support the suggestion that wind-generated sea spray, under moderately high winds, can rival anthropogenic pollution plumes advecting out into marine environments with wind driven AOD contributing to AOD values approaching 0.3.

## Acknowledgments

This work was supported by the Irish Environmental Protection Agency. The authors also wish to acknowledge the World Optical Depth Research and Calibration Centre (WORCC) and Senior Scientist Christoph Wehrli and his team for facilitation of the quality-controlled PFR AOD data at Mace Head.

## References

[1] S. Solomon, D. Qin, M. Manning et al., *Climate Change 2007: The Physical Science Basis. Contribution of Working Group 1 to the Fourth Assessment Report of the Intergovernmental Panel on Climate Change*, Cambridge University Press, Cambridge, UK, 2007.

[2] C. D. O'Dowd and G. De Leeuw, "Marine aerosol production: a review of the current knowledge," *Philosophical Transactions of the Royal Society A*, vol. 365, no. 1856, pp. 1753–1774, 2007.

[3] C. D. O'Dowd, J. A. Lowe, M. H. Smith, and A. D. Kaye, "The relative importance of non-sea-salt sulphate and sea-salt aerosol to the marine cloud condensation nuclei population: an improved multi-component aerosol-cloud droplet parametrization," *Quarterly Journal of the Royal Meteorological Society*, vol. 125, no. 556, pp. 1295–1313, 1999.

[4] C. Kleefeld, C. D. O'Dowd, S. O'Reilly et al., "Relative contribution of submicron and supermicron particles to aerosol light scattering in the marine boundary layer," *Journal of Geophysical Research D*, vol. 107, no. 19, article 8103, 2002.

[5] J. P. Mulcahy, C. D. O'Dowd, S. G. Jennings, and D. Ceburnis, "Significant enhancement of aerosol optical depth in marine air under high wind conditions," *Geophysical Research Letters*, vol. 35, no. 16, Article ID L16810, 2008.

[6] C. D. O'Dowd, M. C. Facchini, F. Cavalli et al., "Biogenically driven organic contribution to marine aerosol," *Nature*, vol. 431, no. 7009, pp. 676–680, 2004.

[7] T. S. Bates, T. L. Anderson, T. Baynard et al., "Aerosol direct radiative effects over the northwest Atlantic, northwest Pacific, and North Indian Oceans: estimates based on in-situ chemical and optical measurements and chemical transport modeling," *Atmospheric Chemistry and Physics*, vol. 6, no. 6, pp. 1657–1732, 2006.

[8] W. L. Madry, O. B. Toon, and C. D. O'Dowd, "Modeled optical thickness of the sea salt aerosol over the world ocean," submitted to *Journal of Geophysical Research*.

[9] A. Smirnov, B. N. Holben, Y. J. Kaufman et al., "Optical properties of atmospheric aerosol in maritime environments," *Journal of the Atmospheric Sciences*, vol. 59, no. 3, pp. 501–523, 2002.

[10] R. R. Draxler and G. D. Hess, "An overview of the HYSPLIT_4 modelling system for trajectories, dispersion and deposition," *Australian Meteorological Magazine*, vol. 47, no. 4, pp. 295–308, 1998.

[11] J. V. Martins, D. Tanré, L. Remer, Y. Kaufman, S. Mattoo, and R. Levy, "MODIS cloud screening for remote sensing of aerosols over oceans using spatial variability," *Geophysical Research Letters*, vol. 29, no. 12, Article ID 8009, 4 pages, 2002.

[12] L. A. Remer, Y. J. Kaufman, D. Tanré et al., "The MODIS aerosol algorithm, products, and validation," *Journal of the Atmospheric Sciences*, vol. 62, no. 4, pp. 947–973, 2005.

[13] A. Smirnov, B. N. Holben, T. F. Eck, O. Dubovik, and I. Slutsker, "Cloud-screening and quality control algorithms for the AERONET database," *Remote Sensing of Environment*, vol. 73, no. 3, pp. 337–349, 2000.

[14] D. Tanré, Y. J. Kaufman, M. Herman, and S. Mattoo, "Remote sensing of aerosol properties over oceans using the MODIS/EOS spectral radiances," *Journal of Geophysical Research D*, vol. 102, no. 14, pp. 16971–16988, 1997.

[15] B. Guenther, X. Xiong, V. V. Salomonson, W. L. Barnes, and J. Young, "On-orbit performance of the Earth observing system moderate resolution imaging spectroradiometer; first year of data," *Remote Sensing of Environment*, vol. 83, no. 1-2, pp. 16–30, 2002.

[16] W. T. Liu, "Progress in scatterometer application," *Journal of Oceanography*, vol. 58, no. 1, pp. 121–136, 2002.

[17] L. A. Remer, D. Tanre, and Y. J. Kaufman, "Algorithm theoretical basis document (ATBD): algorithm for remote sensing of tropospheric aerosol from MODIS," Collection 5, Product ID: MOD04/MYD04, 2006.

[18] H. Huang, G. E. Thomas, and R. G. Grainger, "Relationship between wind speed and aerosol optical depth over remote ocean," *Atmospheric Chemistry and Physics*, vol. 10, no. 13, pp. 5943–5950, 2010.

[19] Y. Lehahn, I. Koren, E. Boss, Y. Ben-Ami, and O. Altaratz, "Estimating the maritime component of aerosol optical depth and its dependency on surface wind speed using satellite data," *Atmospheric Chemistry and Physics*, vol. 10, no. 14, pp. 6711–6720, 2010.

Hindawi Publishing Corporation
Advances in Meteorology
Volume 2010, Article ID 301395, 9 pages
doi:10.1155/2010/301395

*Research Article*

# Ocean Emission Effects on Aerosol-Cloud Interactions: Insights from Two Case Studies

**Armin Sorooshian[1,2] and Hanh T. Duong[1]**

[1] *Department of Chemical and Environmental Engineering, University of Arizona, P.O. Box 210011, Tucson, AZ 85721, USA*
[2] *Department of Atmospheric Sciences, University of Arizona, P.O. Box 210081, Tucson, AZ 85721, USA*

Correspondence should be addressed to Armin Sorooshian, armin@email.arizona.edu

Received 9 January 2010; Revised 28 February 2010; Accepted 24 April 2010

Academic Editor: Markus D. Petters



Two case studies are discussed that evaluate the effect of ocean emissions on aerosol-cloud interactions. A review of the first case study from the eastern Pacific Ocean shows that simultaneous aircraft and space-borne observations are valuable in detecting links between ocean biota emissions and marine aerosols, but that the effect of the former on cloud microphysics is less clear owing to interference from background anthropogenic pollution and the difficulty with field experiments in obtaining a wide range of aerosol conditions to robustly quantify ocean effects on aerosol-cloud interactions. To address these limitations, a second case was investigated using remote sensing data over the less polluted Southern Ocean region. The results indicate that cloud drop size is reduced more for a fixed increase in aerosol particles during periods of higher ocean chlorophyll A. Potential biases in the results owing to statistical issues in the data analysis are discussed.

## 1. Introduction

Since oceans cover ~70% of the earth surface, they represent a massive source of gaseous and aerosol emissions that mix with ship and continental emissions to form a highly complex soup of marine aerosol particles. Aerosols directly interact with solar radiation via scattering and absorption of light, and they also serve as cloud condensation nuclei (CCN) and influence cloud properties and reflectivity. Attention to the importance of aerosols in cloud and rain formation can be traced back several decades ago to observations that maritime clouds exhibit lower droplet concentrations than similar clouds influenced by anthropogenic emissions over continental areas, and that the maritime clouds often rain in less than 30 minutes [1–3]. Since that time, research has pointed to two critical pieces of information linking aerosols to warm clouds: (i) more numerous subcloud aerosol particles result in more reflective clouds (all else being fixed) because of more abundant and smaller cloud droplets [4] and (ii) for more numerous and smaller cloud droplets, suppressed droplet collision-coalescence results in less precipitation [5]. But observational and modeling studies often provide conflicting results with regard to the magnitude and even the sign of aerosol effects on clouds and precipitation [6]. Furthermore, aerosol-cloud interactions represent the largest uncertainty in assessments of the total anthropogenic radiative forcing [7].

As shown in Figure 1 (see red arrows), aerosols are at the heart of the effect of ocean emissions on cloud properties. The sources and nature of marine aerosols are influenced by some combination of ocean emissions, ship exhaust, and transported continental emissions. The task of characterizing the optically and CCN-relevant properties of marine aerosols is overwhelming owing to the difficulty in their measurement, their short atmospheric lifetime in the marine atmosphere, their spatial inhomogenieties, and the complexity of their composition. Just the organic fraction of aerosols alone is thought to comprise over thousands of species that are virtually impossible to speciate altogether [8]. While it has long been known that ocean-emitted dimethylsulfide (DMS) plays a major role in influencing the marine CCN budget [9–11], recent studies have pointed to the importance of other trace gas emissions such as isoprene [12–15] and organic amines [16, 17], which can partition

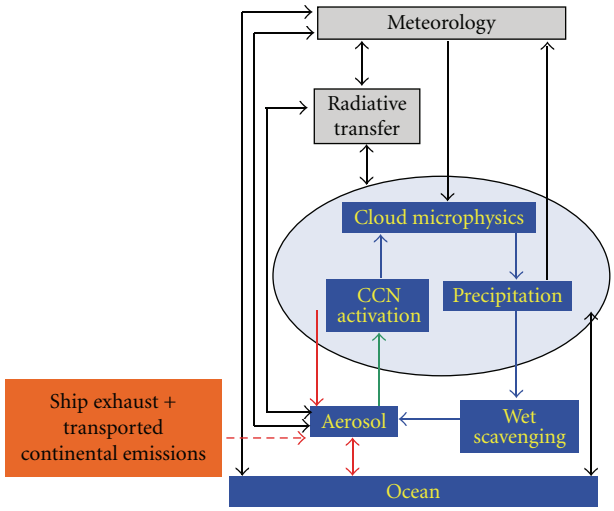


FIGURE 1: Illustration of the interactive processes between oceans, aerosols, clouds, meteorology, and radiation in the marine atmosphere. The red arrows represent the sources of aerosols and the green and blue arrows collectively encompass the microphysical processes associated with aerosol-cloud-precipitation interactions.

into the aerosol phase via secondary formation mechanisms [18–31]. Also, the importance of primary emissions of sea spray aerosols has long been recognized, but the significance of primary biological aerosol particles is becoming more evident as they have been shown to influence marine atmospheric processes more than previously assumed [32–41]. Although more will be learned about the physicochemical properties of marine aerosols with advances in instrumentation, a remaining uncertainty is the extent to which various aerosol physicochemical properties affect the cloud microphysical and radiative response of clouds.

The effect of aerosols on clouds begins with the process of cloud drop activation (Figure 1, green arrow). Observational and modeling studies suggest that aside from dynamic effects (e.g., cloud base updraft velocity), the most important aerosol physicochemical parameter governing cloud drop number concentration ($N_d$) is the aerosol size distribution [42–46], while aerosol composition is argued to be of secondary importance [45]. However, under certain conditions related to the degree of aerosol abundance or updraft velocity strength, chemical effects have been shown to rival the aerosol size distribution with regard to the value of $N_d$ [47]. The current understanding of the drop activation process has benefited from both aerosol-CCN (e.g., [48–52]) and aerosol/CCN-$N_d$ closure studies (e.g., [44, 53–55]). Although past closure studies have been met with limited success, one study in particular, that carried out an aerosol-$N_d$ closure analysis using a cloud parcel model and aircraft measurements from a single platform [44], showed that $N_d$ within adiabatic cloud regions was within 15% (on average) of predictions. The accuracy of the drop activation process in models will continue to benefit from future studies of this nature using improved experimental techniques.

In addition to drop activation, the overall microphysical response of clouds (e.g., drop size) to aerosols is highly uncertain owing to the difficulty in untangling aerosol effects on clouds in a buffered system [56]. Observational studies face the challenging task of relating aerosol perturbations to cloud microphysical responses (Figure 1, green and blue arrows) while removing meteorological effects. A failure to account for such meteorological factors, which refer to large-scale thermodynamic and dynamic parameters that dictate cloud properties on a larger scale, will yield misleading results. The introduction of state-of-the-art observational tools such as NASA's A-Train constellation of satellites [57] has provided valuable information related to aerosol and cloud properties with a high degree of spatial and temporal coverage that cannot be obtained with dedicated field studies. Therefore, although there are many holes in the current knowledge related to marine aerosols and their effect on clouds and climate, new observational platforms are providing an unprecedented view of ocean-aerosol-cloud interactions.

The goal of this work is twofold: (i) present two case studies that examine ocean effects on aerosol-cloud interactions, specifically examining the steps leading from ocean emissions to a change in cloud drop size and (ii) discuss how results from these case studies can improve future attempts to quantify the links between oceans, aerosol particles, and clouds. Experimental methods used in this work are first briefly summarized. Then results are highlighted from a recent case study in the eastern Pacific Ocean region, where the drawbacks of that work are used to motivate a second case study in the Southern Ocean region that is subsequently described in detail.

## 2. Experimental Methods

Two case studies are presented below to explore ocean effects on aerosol-cloud interactions. In both case studies, ocean chlorophyll A data are used from the Sea-viewing Wide Field-of-view Sensor (Sea-WiFS; 8-day averaged data). Chlorophyll A is a proxy measurement of phytoplankton biomass and caution must be exercised when interpreting it as a proxy for primary production (i.e., biota emissions). The first case study focusing on the eastern Pacific Ocean region (35.5° N–37° N, 122° W–123.5° W) is described in detail elsewhere [17], but is revisited here to highlight findings that motivate the second case study. Briefly, aerosol, cloud, and meteorological measurements were carried out on-board the Center for Interdisciplinary Remotely-Piloted Aircraft Studies (CIRPAS) Twin Otter as part of the Marine Stratus/Stratocumulus Experiment (MASE II) in July 2007. The relevant instrumentation ([17, see Table 1]) included a forward scattering spectrometer probe (cloud drop distribution), a particle-into-liquid sampler (water-soluble composition) [58], a differential mobility analyzer (aerosol size distribution), and a continuous flow thermal gradient cloud condensation nuclei counter [59].

The second case study examines the spatial domain in the Southern Ocean region encompassed by the following

Table 1: Summary of correlative relationships ($r^2$) between ocean chlorophyll A, marine aerosols, and stratocumulus clouds during the three-week MASE II field campaign in July 2007, during which chlorophyll A levels ranged between 1.01–3.58 mg m$^{-3}$. Owing to the short duration of the study and limited measurements of chlorophyll A ($n = 3$), all data have been averaged to correspond to the time durations corresponding to each chlorophyll A measurement. Details related to the mean, standard deviation, and range of values of these parameters are discussed in detail by Sorooshian et al. [17]. (Chl A = chlorophyll A; DEA = diethylamine; MSA = methanesulfonate; $N_d$ = cloud drop number concentration; TKE = turbulent kinetic energy).

| | Chl A | DEA | MSA | Particle Conc. | CCN (0.3%) | $N_d$ | TKE |
|---|---|---|---|---|---|---|---|
| DEA | 0.99 | | | | | | |
| MSA | 1.00 | 0.98 | | | | | |
| Particle Conc. | 0.10 | 0.05 | 0.07 | | | | |
| CCN (0.3%) | 0.59 | 0.69 | 0.65 | 0.13 | | | |
| $N_d$ | 0.97 | 0.92 | 0.95 | 0.23 | 0.42 | | |
| TKE | 0.97 | 1.00 | 0.99 | 0.02 | 0.75 | 0.89 | |
| Wind speed | 0.78 | 0.86 | 0.94 | 0.03 | 0.96 | 0.62 | 0.95 |

coordinates: 42° S–60° S, 180° W–180° E. Cloud and aerosol parameters are obtained from the Moderate Resolution Imaging Spectroradiometer (MODIS), specifically the 1° gridded aerosol index (Level 3, MODIS Collection 5) [60] and the drop effective radius (Level 2, 1-km resolution) [61]. Aerosol index (AI) is taken as the product of the 0.55 $\mu$m aerosol optical depth $\times$ 0.55/0.867 $\mu$m Ångstrom exponent, where the latter parameter accounts for the aerosol size distribution. MODIS is also used to derive cloud liquid water path (LWP; a product of the drop effective radius and cloud optical depth). Lower tropospheric static stability (LTSS = potential temperature difference between 700 hPa and 1000 hPa) estimates are derived from the European Centre for Medium Range Weather Forecasts (ECMWF) analyses. This parameter serves as a proxy for the thermodynamic state of the atmosphere [62]. A detailed screening procedure using data from the CloudSat cloud profiling radar, ECMWF-AUXiliary analysis (ECMWF-AUX), and MODIS is used to isolate only warm clouds for this case study analysis [63].

## 3. Case Study in the Eastern Pacific Ocean Region

A recent study off the coast of California pointed to the advantage of simultaneously using multiple platforms of analysis to study ocean-aerosol-cloud interactions, while also highlighting experimental limitations to studying these interactive processes in the coupled ocean-atmosphere system [17]. Table 1 presents a reanalysis of data from that study, specifically summarizing the degree of correlation between Sea-WiFS-derived chlorophyll A, meteorological parameters, and aerosol and cloud properties. Biogenic tracers were detected in the boundary layer aerosols during periods of enhanced ocean emissions, including methanesulfonate (MSA, a dimethylsulfide oxidation product) and diethylamine (DEA). These two species were highly correlated with both chlorophyll A and low-level wind speed ($r^2 > 0.86$). Amines were shown to be a source of secondary organic aerosol in the marine atmosphere, which together with MSA accounted for as high as 14% of the mass of sulfate during the peak chlorophyll A period. It is argued that rather than predominantly being produced via new particle formation or being primarily emitted, that amines partitioned to the aerosol phase by condensation onto preexisting aerosols; this is supported by the lack of a correlation between particle concentration and either DEA/MSA/chlorophyll A ($r^2 \leq 0.1$), and with independent field [16, 64] and laboratory measurements [65] related to particulate amine production.

Subsaturated aerosol hygroscopic growth measurements indicated that the organic component during periods of high chlorophyll A and wind speed exhibited considerable water uptake ability. However, a critical limitation of the study was the inability to distinguish between the effect of ocean-derived organics and other organics (e.g., ship emissions) on overall hygroscopicity. Enhanced CCN activity was also observed, which was attributed to both size distribution and chemical effects, but again it was not possible to confidently attribute the change in CCN activity to the ocean-derived organics owing to the region of analysis.

Although in Table 1 it is shown that MSA/DEA/ chlorophyll A are highly correlated with $N_d$ ($r^2 \geq 0.92$), other meteorological proxies such as turbulent kinetic energy ($r^2 = 0.89$) are also highly correlated with $N_d$. In order to quantify the cloud microphysical response to an aerosol perturbation, it is necessary to account for meteorological conditions. In other words, clouds with similar LWP (or some closely-related proxy) should be compared when determining how cloud droplet size varies with the subcloud aerosol concentration. Short-term field studies are faced with the challenge of obtaining a significant range of aerosol variability in bins of cloud LWP to afford a robust calculation of an aerosol effect on cloud properties. For example, after removing data clearly influenced by anthropogenic pollution (using particle concentration data and back-trajectory analysis) in the current case study, only three events can be identified exhibiting a narrow range of meteorological conditions (turbulent kinetic energy was used as the meteorological proxy) to compare subcloud CCN to $N_d$ ($r^2 = 0.41$). Similarly, only three events were isolated with a narrow range of subcloud CCN concentration to correlate the turbulent kinetic energy to $N_d$ ($r^2 = 0.95$). Therefore, the limited dataset indicates that meteorology influenced $N_d$ to a greater extent than aerosol effects, and that aerosol perturbations as

a result of higher chlorophyll A and wind speed may have had a secondary effect on $N_d$.

Two key limitations in this case study included the region of analysis and the difficulty in obtaining a sufficiently wide range of aerosol conditions with surface- and aircraft-based measurements to robustly quantify links between aerosol perturbations and cloud microphysical responses at fixed meteorological conditions (i.e., LWP). The region off the coast of California is characterized by a significant amount of background anthropogenic pollution, which makes it difficult to identify a causal relationship between ocean emissions and cloud properties (i.e., change in drop size). Generally speaking, targeting links between ocean emissions and aerosol and cloud properties may be difficult in many regions of the globe where field studies are carried out owing to the significant amount of background pollution in the form of aged ship emissions and transported continental emissions. A region that likely qualifies as a better ambient laboratory to study the effects of marine biota emissions on cloud properties is the Southern Ocean, which is the focus of the next case study that leverages satellite data. Limitations in data from dedicated field campaigns, as noted above, strongly motivate the use of satellite data, which afford greater temporal and spatial coverage (i.e., greater chance of achieving a wide range of aerosol conditions as a function of cloud regime).

## 4. Case Study in the Southern Ocean Region

This case study is motivated by previous work based on satellite-based observations in the Southern Ocean region, which indicated that a link exists between phytoplankton and cloudiness [13]. More specifically, cloud drop effective radius was shown to be reduced during periods of enhanced chlorophyll A, suggesting that enhanced phytoplankton emissions lead to higher $N_d$. However, there is uncertainty as to whether the inverse correlation between chlorophyll A and drop effective radius is a robust relationship in different global regions [17, 66].

The cloud microphysical response to aerosol perturbations is quantified in this analysis using the following Aerosol-Cloud Interaction metric [67]:

$$\mathrm{ACI}_r = -\frac{\partial \ln r_e}{\partial \ln \alpha} \quad (\text{range} = 0\text{–}0.33), \tag{1}$$

where $r_e$ is the drop effective radius (at cloud top using MODIS), $\alpha$ is a subcloud CCN proxy (AI in this analysis), and the partial derivative is evaluated with meteorological conditions held fixed (i.e., LWP). A higher value of $\mathrm{ACI}_r$ can be interpreted as meaning that for a fixed increase in AI, drop radius decreases more (all else fixed). The analysis is conducted for 11 LWP bins between 50 and 350 g m$^{-2}$ and for varying degrees of atmospheric stability, where data are separated into conditions of relatively low stability (LTSS < 15°C) and high stability (LTSS > 18°C). While the data are stratified into meteorological bins, it is noted that there still is room for meteorological variability owing to measurement uncertainties and because the bins still exhibit a finite range of values. Satellite-derived $\mathrm{ACI}_r$ values are reported only when they statistically significant with 95% confidence (1-tailed T distribution).

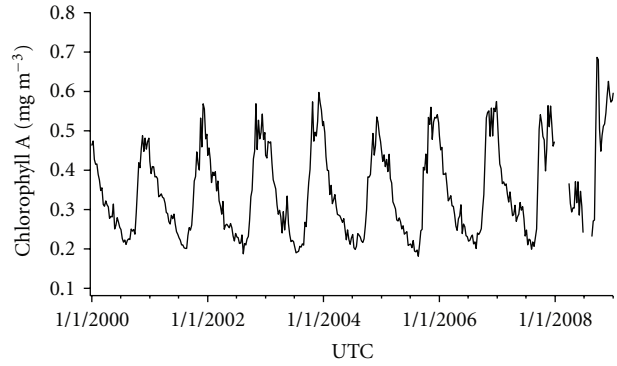


Figure 2: Time series of 8-day averaged Sea-WiFS chlorophyll A concentration in Southern Ocean region (42° S–60° S, 180° W – 180° E).

Figure 2 displays the time series of chlorophyll A, where it is clearly evident that there are periods of enhanced phytoplankton biomass, usually between October and February. Previous field-based studies have also identified clear seasonal differences in CCN and $N_d$, with increases during summer months (e.g., January and February) [68, 69], but the enhancement is less pronounced for $N_d$ [69]. Although higher values of ocean chlorophyll A exist in smaller spatial domains in the Southern Ocean, this analysis is carried out for a large area to ensure there is a sufficient amount of data to provide a robust calculation of $\mathrm{ACI}_r$ in the numerous macrophysical bins employed. In order to compare $\mathrm{ACI}_r$ during periods of relatively low and high chlorophyll A, data is split into three time periods ranging between October–February (>0.3 mg m$^{-3}$), March–September (<0.3 mg m$^{-3}$), and April–August (<0.3 mg m$^{-3}$). The latter two time periods represent low chlorophyll A conditions, but differ in time range to demonstrate the biasing effect of varying sample sizes on the absolute magnitude of $\mathrm{ACI}_r$. Although the data from April and August were removed for the results reported here, the conclusions of the sample size comparison are robust regardless of which months of data are removed.

Figure 3 summarizes the results of the $\mathrm{ACI}_r$ analysis. For low LTSS conditions (<15°C), $\mathrm{ACI}_r$ ranges in value between 0.06–0.19 over the LWP range studied, while for more stable conditions (LTSS > 18°C) the values range between 0.04–0.05. All of the $\mathrm{ACI}_r$ values are contained within the expected range of values for $\mathrm{ACI}_r$ [0–0.33; 67, 70] and are consistent with values obtained in other satellite-based studies [62, 70–72]. A peculiar feature of these data is that much fewer data points are statistically significant for more stable conditions; furthermore, those statistically significant values at high LTSS exhibit the smallest overall $\mathrm{ACI}_r$ values. This is hypothesized to be due to the difficulty in observing the $\mathrm{ACI}_r$ signal in clouds with greater dynamical suppression. The striking result of this analysis is that the majority of data points exhibit higher $\mathrm{ACI}_r$ during periods of higher chlorophyll A. The difference in $\mathrm{ACI}_r$ is even greater when using the wider time range to represent low chlorophyll

Table 2: Statistical summary of the $ACI_r$ analysis shown in Figure 3. The numbers reported below represent ratios of a particular parameter between periods of relatively high chlorophyll A (>0.3 mg m$^{-3}$; October–February) versus low chlorophyll A (<0.3 mg m$^{-3}$; April–August). The average and standard deviation calculations are based on 11 values representing individual LWP bins between 50 and 350 g m$^{-2}$. These results represent 27 months of data starting in June 2006 for the Southern Ocean region (42° S–60° S, 180° W–180° E). (AI = aerosol index; AOD = aerosol optical depth; ANG = Ångstrom exponent; $r_e$ = cloud drop effective radius; min = minimum value; max = maximum value).

| | AI (min) | AI (max) | AI (range) | AOD (min) | AOD (max) | AOD (range) | ANG (min) | ANG (max) | ANG (range) | $r_e$ (min) | $r_e$ (max) | $r_e$ (range) |
|---|---|---|---|---|---|---|---|---|---|---|---|---|
| Average | 3.46 | 1.69 | 1.55 | 1.51 | 1.20 | 1.19 | 2.57 | 1.39 | 1.33 | 1.15 | 0.99 | 0.94 |
| Std. Dev. | 0.77 | 0.38 | 0.39 | 0.47 | 0.37 | 0.39 | 1.18 | 0.34 | 0.34 | 0.38 | 0.03 | 0.14 |

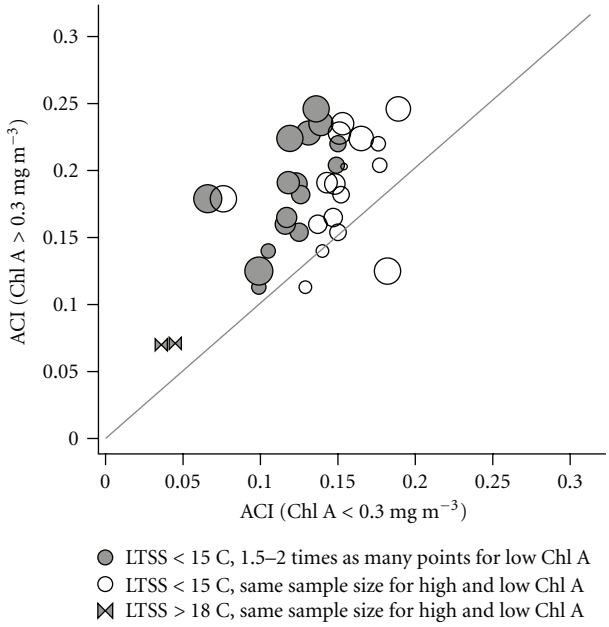


Figure 3: Comparison of $ACI_r$ values (1) for periods of relatively high and low chlorophyll A concentration in the Southern Ocean region based on data over a span of 27 months starting in June 2006. Marker sizes are proportional to LWP between 50 and 350 g m$^{-2}$ (11 total LWP bins).

A conditions; this is presumably a result of larger sample sizes (greater by a factor of ~1.5–2), and consequently a dampening of the $ACI_r$ signal owing to a greater likelihood of mixing different macrophysical conditions. To emphasize that using a larger sample size at similar chlorophyll A conditions will reduce the $ACI_r$ signal, $ACI_r$ is larger during the April–August time frame by a factor of 1.35 ± 0.28 as compared to the March–September period.

When comparing comparable sample sizes for conditions of high chlorophyll A and low chlorophyll A (April–August), the value of $ACI_r$ during the former period is greater by a factor of 1.3 ± 0.3. This result suggests that during periods of higher phytoplankton biomass a fixed increase in aerosol particles more strongly suppresses $r_e$ because of more droplets for a fixed amount of cloud water. If this is the case, a potential explanation for these results is that those marine aerosols during periods of higher chlorophyll A may exhibit more favorable physicochemical properties (i.e., size distribution and chemical properties) with regard to droplet activation. However, cautionary notes apply with regard to this conclusion owing to measurement and statistical uncertainties. Table 2 highlights the issue of whether a "fair" statistical comparison was conducted during the identified periods of high and low chlorophyll A conditions; it is hypothesized that a wider dynamic range in AI during periods of high chlorophyll A results in a more pronounced ACI signal using satellite data. Several ratios (minimum, maximum, range) are reported between periods of high versus low chlorophyll A for AI, AOD, Ångstrom exponent, and $r_e$. It is shown that during periods of higher chlorophyll A, the minimum, maximum, and overall range of AI values was larger than those for low chlorophyll A conditions. Of the two AI subcomponents (AOD and Ångstrom exponent), the range in the Ångstrom exponent was larger (~1.33) as compared to AOD (1.19) during high chlorophyll A periods versus low chlorophyll A periods. (It is noted that using AOD as the subcloud CCN proxy in (1) results in an $ACI_r$ enhancement of 1.23 ± 0.66, which is slightly less than that when using AI.) No enhancement was evident for cloud drop effective radius (when analyzed in bins of cloud LWP), which was relatively similar for the two chlorophyll A conditions. Owing to the wider range of AI (and higher overall absolute values) during the period of enhanced chlorophyll A, it is suspected that the $ACI_r$ signal is more pronounced. The likely reason that the $r_e$ values were more similar as compared to AI (and its subcomponents) is that marine aerosols are more closely linked physically to ocean emissions than clouds (Figure 1). Therefore, although a link between higher chlorophyll A and enhanced AI values seems to be evident, the effect on cloud properties cannot be identified with high confidence using this dataset owing at least partly to statistical factors in this analysis.

## 5. Conclusions

Two case studies were discussed that explore ocean effects on aerosol-cloud interactions in regions with different levels of background anthropogenic pollution: off the California coast and the Southern Ocean. The first study that is reviewed briefly in this work off the California coast [17] leveraged simultaneous satellite and field measurements to show a direct link between ocean emissions and aerosol

physicochemical properties during periods of enhanced chlorophyll A and low-level wind speed, which otherwise would not have been identified with any one measurement platform alone. That work also pointed to the advantage of each individual platform of analysis (ground, airborne, satellite); for example, the aircraft measurements provided unique insight into the detailed aerosol physicochemical properties and their vertical atmospheric profiles. But a drawback with the aircraft and ground-based measurements was the difficulty in obtaining a wide range of aerosol conditions at fixed meteorological conditions to robustly quantify the cloud microphysical response to aerosol perturbations during periods of varying ocean productivity. Furthermore, that region is characterized by a significant amount of background anthropogenic pollution, which made it challenging to isolate the effect of ocean biota emissions on cloud properties.

Owing to the ambiguity of the results related to ocean emissions on aerosol-cloud interactions in the first case study, a second investigation was carried out for the Southern Ocean region owing to its lower amount of background anthropogenic pollution. In order to examine aerosol effects on clouds in this area during periods of relatively low and high chlorophyll A conditions, $ACI_r$ (1) was quantified while accounting for macrophysical factors such as atmospheric stability and cloud LWP. The cloud microphysical response to aerosol perturbations was stronger (higher $ACI_r$) during periods of higher chlorophyll A. This indicates that cloud drop size experiences a greater reduction for a fixed increase in aerosol concentration, potentially as a result of aerosols with more favorable physicochemical properties for droplet activation. But a causal relationship is difficult to establish owing to biasing factors in the datasets. It is shown that during periods of higher chlorophyll A, the range and minimum/maximum values of AI and its subcomponents (AOD and Ångstrom exponent) are higher than those during low-chlorophyll A periods. Although this points to higher aerosol concentrations during times characterized by enhanced phytoplankton biomass, it also suggests that the $ACI_r$ signal may be more pronounced owing to the wider range in AI. It is argued that this does not allow for a "fair" comparison and it points to the need to consider such issues in future studies. Another factor shown to bias $ACI_r$ values is sample size, where an increase in the amount of data led to a reduction in $ACI_r$ for conditions of low chlorophyll A presumably owing to a greater likelihood of mixing data across a wider range of meteorological and cloud conditions.

The topic of ocean-aerosol-cloud interactions will benefit from future analyses with more extensive datasets at higher spatial resolution. Field measurements are needed in addition to satellite observations to quantify the physicochemical properties of marine aerosols (e.g., size and composition) and to probe more detailed issues such as the role of surface-active and directly-emitted aerosol particles [73–78] in influencing $N_d$ and cloud albedo. In addition, complementary modeling-based studies (e.g., [79–84]), are essential in advancing predictions of marine aerosol emissions and their impacts on clouds and climate.

## Acknowledgments

We acknowledge support from Office of Naval Research grant N00014-10-1-0811. The authors acknowledge Matt Lebsock for assistance with satellite data. Ocean chlorophyll A data used in this study were acquired using the GES-DISC Interactive Online Visualization ANd aNalysis Infrastructure (Giovanni) as part of the NASA's Goddard Earth Sciences (GES) Data and Information Services Center (DISC).

## References

[1] P. Squires, "The microstructure of cumuli in maritime and continental air," *Tellus*, vol. 8, pp. 443–444, 1956.

[2] P. Squires, "Penetrative downdraughts in cumuli," *Tellus*, vol. 10, pp. 381–389, 1958.

[3] P. Squires and S. Twomey, "A comparison of cloud nucleus measurements over central north america and caribbean sea," *Journal of the Atmospheric Sciences*, vol. 23, pp. 401–404, 1966.

[4] S. Twomey, "Influence of pollution on shortwave albedo of clouds," *Journal of the Atmospheric Sciences*, vol. 34, pp. 1149–1152, 1977.

[5] B. A. Albrecht, "Aerosols, cloud microphysics, and fractional cloudiness," *Science*, vol. 245, no. 4923, pp. 1227–1230, 1989.

[6] A. P. Khain, "Notes on state-of-the-art investigations of aerosol effects on precipitation: a critical review," *Environmental Research Letters*, vol. 4, no. 1, Article ID 015004, 2009.

[7] IPCC, "Summary for policymakers," in *Climate Change 2007: The Physical Science Basis. Contribution of Working Group I to the Fourth Assessment Report of the Intergovernmental Panel on Climate Change*, S. Solomon, D. Qin, M. Manning, et al., Eds., Cambridge University Press, New York, NY, USA, 2007.

[8] A. H. Goldstein and I. E. Galbally, "Known and unexplored organic constituents in the earth's atmosphere," *Environmental Science and Technology*, vol. 41, no. 5, pp. 1514–1521, 2007.

[9] M. O. Andreae and H. Raemdonck, "Dimethyl sulfide in the surface ocean and the marine atmosphere: a global view," *Science*, vol. 221, no. 4612, pp. 744–747, 1983.

[10] G. E. Shaw, "Bio-controlled thermostasis involving the sulfur cycle," *Climatic Change*, vol. 5, no. 3, pp. 297–303, 1983.

[11] R. J. Charlson, J. E. Lovelock, M. O. Andreae, and S. G. Warren, "Oceanic phytoplankton, atmospheric sulphur, cloud albedo and climate," *Nature*, vol. 326, no. 6114, pp. 655–661, 1987.

[12] M. Claeys, B. Graham, G. Vas et al., "Formation of secondary organic aerosols through photooxidation of isoprene," *Science*, vol. 303, no. 5661, pp. 1173–1176, 2004.

[13] N. Meskhidze and A. Nenes, "Phytoplankton and cloudiness in the southern ocean," *Science*, vol. 314, no. 5804, pp. 1419–1423, 2006.

[14] S. R. Arnold, D. V. Spracklen, J. Williams et al., "Evaluation of the global oceanic isoprene source and its impacts on marine organic carbon aerosol," *Atmospheric Chemistry and Physics*, vol. 9, no. 4, pp. 1253–1262, 2009.

[15] S. Ekström, B. Nozière, and H.-C. Hansson, "The cloud condensation nuclei (CCN) properties of 2-methyltetrols and $C_3$-$C_6$ polyols from osmolality and surface tension measurements," *Atmospheric Chemistry and Physics*, vol. 9, no. 3, pp. 973–980, 2009.

[16] M. C. Facchini, S. Decesari, M. Rinaldi et al., "Important source of marine secondary organic aerosol from biogenic amines," *Environmental Science and Technology*, vol. 42, no. 24, pp. 9116–9121, 2008.

[17] A. Sorooshian, L. T. Padró, A. Nenes, et al., "On the link between ocean biota emissions, aerosol, and maritime clouds: airborne, ground, and satellite measurements off the coast of California," *Global Biogeochemical Cycles*, vol. 23, no. 4, Article ID GB4007, p. 15, 2009.

[18] C. D. O'Dowd and G. de Leeuw, "Marine aerosol production: a review of the current knowledge," *Philosophical Transactions of the Royal Society A*, vol. 365, no. 1856, pp. 1753–1774, 2007.

[19] J. Liggio, S.-M. Li, and R. McLaren, "Heterogeneous reactions of glyoxal on particulate matter: identification of acetals and sulfate esters," *Environmental Science and Technology*, vol. 39, no. 6, pp. 1532–1541, 2005.

[20] R. Volkamer, P. J. Ziemann, and M. J. Molina, "Secondary organic aerosol formation from acetylene (C2H 2): seed effect on SOA yields due to organic photochemistry in the aerosol aqueous phase," *Atmospheric Chemistry and Physics*, vol. 9, no. 4, pp. 1907–19028, 2009.

[21] A. L. Corrigan, S. W. Hanley, and D. O. De Haan, "Uptake of glyoxal by organic and inorganic aerosol," *Environmental Science and Technology*, vol. 42, no. 12, pp. 4428–4433, 2008.

[22] C. J. Hennigan, M. H. Bergin, J. E. Dibb, and R. J. Weber, "Enhanced secondary organic aerosol formation due to water uptake by fine particles," *Geophysical Research Letters*, vol. 35, no. 18, Article ID L18801, 5 pages, 2008.

[23] J. D. Blando and B. J. Turpin, "Secondary organic aerosol formation in cloud and fog droplets: a literature evaluation of plausibility," *Atmospheric Environment*, vol. 34, no. 10, pp. 1623–1632, 2000.

[24] P. Warneck, "In-cloud chemistry opens pathway to the formation of oxalic acid in the marine atmosphere," *Atmospheric Environment*, vol. 37, no. 17, pp. 2423–2427, 2003.

[25] K. K. Crahan, D. Hegg, D. S. Covert, and H. Jonsson, "An exploration of aqueous oxalic acid production in the coastal marine atmosphere," *Atmospheric Environment*, vol. 38, no. 23, pp. 3757–3764, 2004.

[26] B. Ervens, G. Feingold, G. J. Frost, and S. M. Kreidenweis, "A modeling of study of aqueous production of dicarboxylic acids: 1. Chemical pathways and speciated organic mass production," *Journal of Geophysical Research*, vol. 109, no. 15, Article ID D15205, 20 pages, 2004.

[27] J. Z. Yu, X.-F. Huang, J. Xu, and M. Hu, "When aerosol sulfate goes up, so does oxalate: implication for the formation mechanisms of oxalate," *Environmental Science and Technology*, vol. 39, no. 1, pp. 128–133, 2005.

[28] A. Sorooshian, V. Varutbangkul, F. J. Brechtel et al., "Oxalic acid in clear and cloudy atmospheres: analysis of data from international consortium for atmospheric research on transport and transformation 2004," *Journal of Geophysical Research*, vol. 111, no. 23, Article ID D23S45, 17 pages, 2006.

[29] A. Sorooshian, M.-L. Lu, F. J. Brechtel et al., "On the source of organic acid aerosol layers above clouds," *Environmental Science and Technology*, vol. 41, no. 13, pp. 4647–4654, 2007.

[30] A. G. Carlton, B. J. Turpin, K. E. Altieri et al., "Atmospheric oxalic acid and SOA production from glyoxal: results of aqueous photooxidation experiments," *Atmospheric Environment*, vol. 41, no. 35, pp. 7588–7602, 2007.

[31] K. E. Altieri, S. P. Seitzinger, A. G. Carlton, B. J. Turpin, G. C. Klein, and A. G. Marshall, "Oligomers formed through in-cloud methylglyoxal reactions: chemical composition, properties, and mechanisms investigated by ultra-high resolution FT-ICR mass spectrometry," *Atmospheric Environment*, vol. 42, no. 7, pp. 1476–1490, 2008.

[32] M. L. Wells and E. D. Goldberg, "Occurrence of small colloids in sea water," *Nature*, vol. 353, no. 6342, pp. 342–344, 1991.

[33] M. L. Wells and E. D. Goldberg, "Colloid aggregation in seawater," *Marine Chemistry*, vol. 41, no. 4, pp. 353–358, 1993.

[34] R. Benner, J. D. Pakulski, M. McCarthy, J. I. Hedges, and P. G. Hatcher, "Bulk chemical characteristics of dissolved organic matter in the ocean," *Science*, vol. 255, no. 5051, pp. 1561–1564, 1992.

[35] M. L. Wells, "Marine colloids—a neglected dimension," *Nature*, vol. 391, no. 6667, pp. 530–531, 1998.

[36] E. K. Bigg, C. Leck, and L. Tranvik, "Particulates of the surface microlayer of open water in the central Arctic Ocean in summer," *Marine Chemistry*, vol. 91, no. 1–4, pp. 131–141, 2004.

[37] C. Leck and E. K. Bigg, "Biogenic particles in the surface microlayer and overlaying atmosphere in the central Arctic Ocean during summer," *Tellus, Series B*, vol. 57, no. 4, pp. 305–316, 2005.

[38] C. Leck and E. K. Bigg, "Source and evolution of the marine aerosol—a new perspective," *Geophysical Research Letters*, vol. 32, no. 19, Article ID L19803, 4 pages, 2005.

[39] R. Jaenicke, "Abundance of cellular material and proteins in the atmosphere," *Science*, vol. 308, no. 5718, 73 pages, 2005.

[40] E. K. Bigg, "Sources, nature and influence on climate of marine airborne particles," *Environmental Chemistry*, vol. 4, no. 3, pp. 155–161, 2007.

[41] V. R. Després, J. F. Nowoisky, M. Klose, R. Conrad, M. O. Andreae, and U. Pöschl, "Characterization of primary biogenic aerosol particles in urban, rural, and high-alpine air by DNA sequence and restriction fragment analysis of ribosomal RNA genes," *Biogeosciences*, vol. 4, no. 6, pp. 1127–1141, 2007.

[42] J. W. Fitzgerald, "Effect of aerosol composition on cloud droplet size distribution—numerical study," *Journal of the Atmospheric Sciences*, vol. 31, pp. 1358–1367, 1974.

[43] G. Feingold, "Modeling of the first indirect effect: analysis of measurement requirements," *Geophysical Research Letters*, vol. 30, no. 19, pp. 7–4, 2003.

[44] W. C. Conant, T. M. VanReken, T. A. Rissman et al., "Aerosol-cloud drop concentration closure in warm cumulus," *Journal of Geophysical Research*, vol. 109, no. 13, Article ID D13204, 12 pages, 2004.

[45] B. Ervens, G. Feingold, and S. M. Kreidenweis, "Influence of water-soluble organic carbon on cloud drop number concentration," *Journal of Geophysical Research*, vol. 110, no. 18, Article ID D18211, 14 pages, 2005.

[46] U. Dusek, G. P. Frank, L. Hildebrandt et al., "Size matters more than chemistry for cloud-nucleating ability of aerosol particles," *Science*, vol. 312, no. 5778, pp. 1375–1378, 2006.

[47] A. Nenes, R. J. Charlson, M. C. Facchini, M. Kulmala, A. Laaksonen, and J. H. Seinfeld, "Can chemical effects on cloud droplet number rival the first indirect effect?" *Geophysical Research Letters*, vol. 29, no. 17, article 1848, 4 pages, 2002.

[48] T. M. VanReken, T. A. Rissman, G. C. Roberts et al., "Toward aerosol/cloud condensation nuclei (CCN) closure during CRYSTAL-FACE," *Journal of Geophysical Research*, vol. 108, no. D20, article 4633, 18 pages, 2003.

[49] P. S. K. Liu, W. R. Leaitch, C. M. Banic, S.-M. Li, D. Ngo, and W. J. Megaw, "Aerosol observations at chebogue point during the 1993 North Atlantic regional experiment: relationships among cloud condensation nuclei, size distribution, and chemistry," *Journal of Geophysical Research*, vol. 101, no. 22, pp. 28971–28990, 1996.

[50] D. S. Covert, J. L. Gras, A. Wiedensohler, and F. Stratmann, "Comparison of directly measured CCN with CCN modeled from the number-size distribution in the marine boundary layer during ACE 1 at Cape Grim, Tasmania," *Journal of Geophysical Research*, vol. 103, no. 13, pp. 16597–16608, 1998.

[51] W. Cantrell, G. Shaw, G. R. Cass et al., "Closure between aerosol particles and cloud condensation nuclei at kaashidhoo climate observatory," *Journal of Geophysical Research*, vol. 106, no. 22, pp. 28711–28718, 2001.

[52] J. R. Snider, S. Guibert, J.-L. Brenguier, and J.-P. Putaud, "Aerosol activation in marine stratocumulus clouds: 2. Köhler and parcel theory closure studies," *Journal of Geophysical Research*, vol. 108, no. 15, article 8629, 23 pages, 2003.

[53] S. Twomey and J. Warner, "Comparison of measurements of cloud droplets and cloud nuclei," *Journal of the Atmospheric Sciences*, vol. 24, pp. 702–703, 1967.

[54] J. W. Fitzgerald and P. Spyers-Duran, "Changes in cloud nucleus concentration and cloud droplet size distribution associated with pollution from St. Louis," *Journal of Applied Meteorology*, vol. 30, pp. 511–516, 1973.

[55] J. R. Snider and J.-L. Brenguier, "Cloud condensation nuclei and cloud droplet measurements during ACE-2," *Tellus, Series B*, vol. 52, no. 2, pp. 828–842, 2000.

[56] B. Stevens and G. Feingold, "Untangling aerosol effects on clouds and precipitation in a buffered system," *Nature*, vol. 461, no. 7264, pp. 607–613, 2009.

[57] G. L. Stephens, D. G. Vane, R. J. Boain et al., "The cloudsat mission and the a-train: a new dimension of space-based observations of clouds and precipitation," *Bulletin of the American Meteorological Society*, vol. 83, no. 12, pp. 1771–1742, 2002.

[58] A. Sorooshian, F. J. Brechtel, Y. L. Ma, et al., "Modeling and characterization of a particle-into-liquid sampler (PILS)," *Aerosol Science and Technology*, vol. 40, pp. 396–409, 2006.

[59] G. C. Roberts and A. Nenes, "A continuous-flow streamwise thermal-gradient CCN chamber for atmospheric measurements," *Aerosol Science and Technology*, vol. 39, no. 3, pp. 206–221, 2005.

[60] L. A. Remer, Y. J. Kaufman, D. Tanré et al., "The MODIS aerosol algorithm, products, and validation," *Journal of the Atmospheric Sciences*, vol. 62, no. 4, pp. 947–973, 2005.

[61] S. Platnick, M. D. King, S. A. Ackerman et al., "The MODIS cloud products: algorithms and examples from terra," *IEEE Transactions on Geoscience and Remote Sensing*, vol. 41, no. 2, pp. 459–473, 2003.

[62] S. A. Klein and D. L. Hartmann, "The seasonal cycle of low stratiform clouds," *Journal of Climate*, vol. 6, no. 8, pp. 1587–1606, 1993.

[63] M. D. Lebsock, G. L. Stephens, and C. Kummerow, "The seasonal cycle of low stratiform clouds," *Journal of Geophysical Research*, vol. 113, no. 8, Article ID D15205, 12 pages, 2008.

[64] A. Sorooshian, S. M. Murphy, S. Hersey et al., "Comprehensive airborne characterization of aerosol from a major bovine source," *Atmospheric Chemistry and Physics*, vol. 8, no. 17, pp. 5489–5520, 2008.

[65] S. M. Murphy, A. Sorooshian, J. H. Kroll, et al., "Secondary aerosol formation from atmospheric reactions of aliphatic amines," *Atmospheric Chemistry and Physics*, vol. 7, no. 9, pp. 2313–2337, 2007.

[66] M. A. Miller and S. E. Yuter, "Lack of correlation between chl A and cloud droplet effective radius in shallow marine clouds," *Geophysical Research Letters*, vol. 35, Article ID L13807, 7 pages, 2008.

[67] G. Feingold, L. A. Remer, J. Ramaprasad, and Y. J. Kaufman, "Analysis of smoke impact on clouds in Brazilian biomass burning regions: an extension of Twomey's approach," *Journal of Geophysical Research*, vol. 106, no. 19, pp. 22907–22922, 2001.

[68] G. P. Ayers and J. L. Gras, "Seasonal relationship between cloud condensation nuclei and aerosol methanesulphonate in marine air," *Nature*, vol. 353, no. 6347, pp. 834–835, 1991.

[69] S. S. Yum and J. G. Hudson, "Wintertime/summertime contrasts of cloud condensation nuclei and cloud microphysics over the Southern Ocean," *Journal of Geophysical Research*, vol. 109, no. 6, Article ID D06204, 14 pages, 2004.

[70] F.-M. Bréon, D. Tanré, and S. Generoso, "Aerosol effect on cloud droplet size monitored from satellite," *Science*, vol. 295, no. 5556, pp. 834–838, 2002.

[71] T. Matsui, H. Masunaga, R. A. Pielke Sr., and W.-K. Tao, "Impact of aerosols and atmospheric thermodynamics on cloud properties within the climate system," *Geophysical Research Letters*, vol. 31, no. 6, Article ID L06109, 4 pages, 2004.

[72] J. Quaas, O. Boucher, and F.-M. Bréon, "Aerosol indirect effects in POLDER satellite data and the laboratoire de Météorologie dynamique-zoom (LMDZ) general circulation model," *Journal of Geophysical Research*, vol. 109, no. 8, Article ID D08205, 9 pages, 2004.

[73] E. J. Hoffman and R. A. Duce, "Factors influencing the organic carbon content of marine aerosols: a laboratory study," *Journal of Geophysical Research*, vol. 81, no. 21, pp. 3667–3670, 1976.

[74] R. M. Gershey, "Characterization of seawater organic-matter carried by bubble-generated aerosols," *Limnology and Oceanography*, vol. 28, pp. 309–319, 1983.

[75] D. C. Blanchard, "The ejection of drops from the sea and their enrichment with bacteria and other materials: a review," *Estuaries*, vol. 12, no. 3, pp. 127–137, 1989.

[76] R. S. Tseng, J. T. Viechnicki, R. A. Skop, and J. W. Brown, "Sea-to-air transfer of surface-active organic compounds by bursting bubbles," *Journal of Geophysical Research*, vol. 97, no. 4, pp. 5201–5206, 1992.

[77] A. M. Middlebrook, D. M. Murphy, and D. S. Thomson, "Observations of organic material in individual marine particles at cape grim during the first aerosol characterization experiment (ACE 1)," *Journal of Geophysical Research*, vol. 103, no. 13, pp. 16475–16483, 1998.

[78] C. D. O'Dowd, M. C. Facchini, F. Cavalli et al., "Biogenically driven organic contribution to marine aerosol," *Nature*, vol. 431, no. 7009, pp. 676–680, 2004.

[79] G. J. Roelofs, "A GCM study of organic matter in marine aerosol and its potential contribution to cloud drop activation," *Atmospheric Chemistry and Physics*, vol. 8, no. 3, pp. 709–719, 2008.

[80] D. V. Spracklen, S. R. Arnold, J. Sciare, K. S. Carslaw, and C. Pio, "Globally significant oceanic source of organic carbon aerosol," *Geophysical Research Letters*, vol. 35, no. 12, Article ID L12811, 5 pages, 2008.

[81] B. Langmann, C. Scannell, and C. O'Dowd, "New directions: organic matter contribution to marine aerosols and cloud condensation nuclei," *Atmospheric Environment*, vol. 42, no. 33, pp. 7821–7822, 2008.

[82] C. D. O'Dowd, B. Langmann, S. Varghese, C. Scannell, D. Ceburnis, and M. C. Facchini, "A combined organic-inorganic sea-spray source function," *Geophysical Research Letters*, vol. 35, no. 1, Article ID L01801, 5 pages, 2008.

[83] B. Gantt, N. Meskhidze, and D. Kamykowki, "A new physically-based quantification of isoprene and primary organic aerosol emissions from the world's oceans," *Atmospheric Chemistry and Physics*, vol. 9, pp. 4915–4927, 2009.

[84] B. Gantt, N. Meskhidze, Y. Zhang, and J. Xu, "The effect of marine isoprene emissions on secondary organic aerosol and ozone formation in the coastal United States," *Atmospheric Environment*, vol. 44, no. 1, pp. 115–121, 2009.

Hindawi Publishing Corporation
Advances in Meteorology
Volume 2010, Article ID 239808, 13 pages
doi:10.1155/2010/239808

*Research Article*

# Effects of Ocean Ecosystem on Marine Aerosol-Cloud Interaction

**Nicholas Meskhidze[1] and Athanasios Nenes[2,3]**

[1] *Department of Marine, Earth and Atmospheric Sciences, North Carolina State University, Raleigh, NC 27695, USA*
[2] *School of Earth and Atmospheric Sciences, Georgia Institute of Technology, Atlanta, GA 30332, USA*
[3] *School of Chemical and Biomolecular Engineering, Georgia Institute of Technology, Atlanta, GA 30332, USA*

Correspondence should be addressed to Nicholas Meskhidze, nmeskhidze@ncsu.edu

Received 1 March 2010; Accepted 12 May 2010

Academic Editor: Charles R. McClain



Using satellite data for the surface ocean, aerosol optical depth (AOD), and cloud microphysical parameters, we show that statistically significant positive correlations exist between ocean ecosystem productivity, the abundance of submicron aerosols, and cloud microphysical properties over different parts of the remote oceans. The correlation coefficient for remotely sensed surface chlorophyll *a* concentration ([Chl-*a*]) and liquid cloud effective radii over productive areas of the oceans varies between $-0.2$ and $-0.6$. Special attention is given to identifying (and addressing) problems from correlation analysis used in the previous studies that can lead to erroneous conclusions. A new approach (using the difference between retrieved AOD and predicted sea salt aerosol optical depth, $AOD_{diff}$) is developed to explore causal links between ocean physical and biological systems and the abundance of cloud condensation nuclei (CCN) in the remote marine atmosphere. We have found that over multiple time periods, 550 nm $AOD_{diff}$ (sensitive to accumulation mode aerosol, which is the prime contributor to CCN) correlates well with [Chl-*a*] over the productive waters of the Southern Ocean. Since [Chl-*a*] can be used as a proxy of ocean biological productivity, our analysis demonstrates the role of ocean ecology in contributing CCN, thus shaping the microphysical properties of low-level marine clouds.

## 1. Introduction

Aerosols influence the planetary radiation balance directly by scattering and absorbing sunlight, and indirectly by modifying cloud microphysical properties [1–4]. Marine aerosols are particularly important, as they contribute considerably to the global aerosol load, are emitted from a large surface area, and have an ability to strongly influence reflective properties and lifetime of marine stratiform clouds [5]. Marine aerosols could be especially important for understanding the cloud-mediated effects of aerosols on climate, because cloud properties are most sensitive to the addition of particles when the background concentration is low [6]. Factors that regulate the concentration of marine aerosols, and thus the reflectivity of low-level marine clouds, can strongly affect the whole climate system [7, 8]. Cloud droplet number concentration (CDNC) over the remote oceans ranges from a few tens per $cm^3$ in biologically inactive regions (seasons) to a few hundred per $cm^3$ under biologically active conditions [9]. Despite recognizing their crucial role, the source strength and chemical composition of marine aerosols remain poorly quantified [10, 11].

Aerosols over the remote oceans consist of a mixture of sea salt particles, organics, and sulfates from the oxidation of biogenic dimethyl sulfide (DMS), with certain contribution from mineral dust and smoke from wildfires [9]. Sea salt is a major component of marine aerosol over regions with high wind speeds and/or when other aerosol sources are weak [12–16]. In addition to sea salt, the biological sulfur cycle has also been proposed as a major source of CCN over biologically active regions of the oceans [17, 18]. In recent years, significant abundances of organic carbon (OC) aerosols (in addition to sea salt and DMS oxidation products) have been identified in marine environments [19–23]. The concentrations of marine-source OC aerosols are particularly high over regions of enhanced oceanic biological activity [24]. These organic aerosols have been proposed to have two distinctly different sources which can be broadly classified as primary and secondary [25]. Bubble bursting processes that emit sea salt aerosols into marine boundary layer also

transfer marine primary organic matter (POM), which is composed of biogenic secretions and bacterial/viral debris [24, 26–29]. Secondary organic aerosols (SOAs) over remote marine regions were proposed to be formed from phytoplankton emitted different types of biogenic volatile organic compounds (BVOCs) [30–34]. Because of their enhanced fine-mode concentration and surface active nature, these organic particles could act synergistically with the established mechanisms of DMS and sea salt, influencing both number concentration and CCN activity of remote marine aerosols [24, 32, 35]. Overall, analyses of marine aerosol chemical composition show that over the productive waters of the ocean the majority of submicron mass of sea spray aerosols can be organic [24, 36–38].

The importance of marine biogenic source contribution to CCN number has motivated numerous studies (using remote sensing products, in situ measurements or modeling) to examine the relationship between ocean productivity and shallow marine cloud properties. Although the link between ocean productivity and CCN has been shown to be mediated through a range of intermediate species that are subject to considerable variability over different timescales, most studies suggest a strong correlation between remotely sensed surface Chlorophyll *a* ([Chl-*a*]) and liquid cloud effective radii ($r_e$) [32, 39–47]. An exception is the study of Miller and Yuter [48] (hereon MY08), who did not find a correlation between [Chl-*a*] and $r_e$ and questioned the conclusions of previous studies. This diversity of conclusions reflects the complexity of studying marine biogenic aerosol-cloud interactions. Owing to the dynamic nature of oceanic aerosol sources, large signal-to-noise ratio and coarse spatial resolution of remote sensing products, unraveling the links between ocean ecosystems, aerosols, and clouds requires a carefully-thought statistical analysis method.

This study has two goals. First, to identify sources of uncertainty in studying the correlation between [Chl-*a*] and $r_e$ and provide guidelines on the optimum selection of statistical methods, time periods and oceanic regions. These guidelines are then applied to study the correlation between [Chl-*a*] and $r_e$ over different regions and time periods (including those in the MY08 study). Second, we present a novel approach for separating sea salt and nonsea salt (nss) components of aerosol optical depth (AOD) over the ocean and its application to determining the effect of ocean primary productivity on marine CCN.

## 2. Methods

The remotely sensed data used in this study include the Sea-viewing Wide Field-of-view Sensor (SeaWiFS) 8 day averaged ~9 km resolution [Chl-*a*] data, Quick Scatterometer (QuikSCAT) derived daily ocean surface wind speed ($U_{10}$) at 0.25° × 0.25° spatial resolution, and Moderate Resolution Imaging Spectroradiometer (MODIS/Terra) Collection 5 (C5) Level-3 global quality assured-(QA-) weighted daily averaged liquid cloud (i.e., cloud cover, thermodynamic phase, liquid water path, and optical depth) and AOD products gridded at 1° × 1° spatial resolution. To be consistent between different satellite sensors all the data for the years 2002–2008 were area-averaged and regridded to 1° × 1° resolution. The MODIS aerosol algorithm was designed to minimize cloud contamination by using a sensitive cloud detection algorithm [49, 50]. In addition, aerosol data with AOD > 0.8 were removed from the analysis to avoid misclassification of clouds and aerosols [51]. Nevertheless it has been shown that the MODIS AOD retrievals may still contain residual artifacts introduced by clouds [52, 53], by 3D effects near clouds [54, 55] and by physical changes to the "aerosol" in the vicinity of clouds [56].

Table 1: Regression statistics for ss-AOD versus surface wind speed.

| Correlation | $r^2$ | Source |
|---|---|---|
| $\text{ss-AOD}_{500} = 0.0068^{*}U + 0.056$ | 0.14 | [57] |
| $\text{ss-AOD}_{1020} = 0.0093^{*}U + 0.018$ | 0.27 | [57] |
| $\text{ss-AOD}_{500} = 0.00055^{*}U^{2.195} + 0.06$ | 0.97* | [58] |
| $\text{ss-AOD}_{555} = 0.00016^{*}U^{2.3} + 0.036$ | 0.36 | [59] |

* $r^2$ values are based on 17 wind speed bins (between 5 $\text{ms}^{-1}$ and 18 $\text{ms}^{-1}$). See Mulcahy et al. [58] for more details.

To derive the relationship between sea salt AOD (ss-AOD) and $U_{10}$ we have chosen the linear function of Smirnov et al. [57] and the power law of Mulcahy et al. [58] and Glantz et al. [59]. Marine background AOD regression statistics for the relationship of Smirnov et al. [57] was derived using 10 years of the Aerosol Robotic Network (AERONET) data collected at Midway Islands (Sand Island) in the northern Pacific Ocean at (28.2°N and 177.4°W). Visual inspection of the global [Chl-*a*] distribution shows that Sand Island is surrounded by ocean waters with very low productivity (see Figure 1 in Supplementary Material available online at doi:10.1155/2010/239808). It is therefore expected that marine aerosols at Sand Island will not be influenced considerably by primary productivity. In addition, anthropogenic contribution to AOD in this remote oceanic region is also very low [60], suggesting that AOD-wind relationship derived at Midway Islands can be used to estimate the ss-AOD. Measurements of Mulcahy et al. [58] were carried out from January 2002 to December 2004 at the Mace Head global atmosphere watch (GAW) research station on the west coast of Ireland (53.3°N, 9.9°W). The study was strictly limited to winter periods (November–March) and clean marine air masses, where sea salt aerosol is expected to dominate AOD. Sea salt dominated all aerosol size ranges during wintertime with little influence of biogenically produced inorganic and organic matter to the marine aerosol mass [22, 24]. The relationship between ss-AOD and the $U_{10}$ offered by Glantz et al. [59] was estimated by combining SeaWiFS AOD with surface wind speed obtained from the European Centre for Medium-Range Weather Forecasts (ECMWF). The regression statistics from all three studies are summarized in Table 1.

The contribution of ss-AOD to total remotely sensed AOD over the ocean are examined using different satellites with different equatorial crossing times. SeaWiFS is in

descending sun-synchronous near-polar circular orbit with ~12 : 20 LT equator crossing time, MODIS/Terra is in a descending node with ~10 : 30 LT equator crossing time, the $U_{10}$ was derived as average of both ascending (~6 : 00 LT) and descending (~18 : 00 LT) paths of QuikSCAT. Such approach is not expected to introduce any significant errors in our analysis as the characteristic time scale of [Chl-$a$] variability is about a week [61] and the correlation time between the surface winds and the marine aerosol (away from the continents) is sufficient for MODIS and QuikSCAT retrievals to be connected [62].

## 3. The Statistical Analysis

An approach to evaluate the spatial correlation between phytoplankton abundance ([Chl-$a$]) and marine cloud properties (e.g., $r_e$) by contrasting cloud properties over the "blooms" (defined as a subset of grid boxes with average [Chl-$a$] above some threshold, for example, [Chl-$a$] > 1 mg m$^{-3}$ used in MY08) against "nonbloom" grid boxes can lead to erroneous conclusions as shown below. The correlation coefficient, $R_{[\text{Chl-}a],r_e}$, between [Chl-$a$] and $r_e$ can be written as

$$R_{[\text{Chl-}a],r_e} = \frac{\sum_{i=1}^{n} [\text{Chl-}a]_i r_{e_i} - n\overline{[\text{Chl-}a]}\,\overline{r_e}}{\sqrt{\left(\sum_{i=1}^{n} [\text{Chl-}a]_i^2 - n\overline{[\text{Chl-}a]}^2\right)\left(\sum_{i=1}^{n} r_{e_i}^2 - n\overline{r_e}^2\right)}}, \quad (1)$$

where $\overline{[\text{Chl-}a]}$ and $\overline{r_e}$ are sample means, $[\text{Chl-}a]_i$ and $r_{ei}$ are the sample dataset, and $n$ is the sample size. From (1) it follows that conditional sampling of the data (set by the arbitrary bloom threshold [Chl-$a$]) can alter the magnitude of $R_{[\text{Chl-}a],r_e}$. An example that illustrates this is presented in Table 2, which shows that positive, negative or no correlation between [Chl-$a$] and $r_e$ can be obtained by changing the [Chl-$a$] threshold values for the dataset. Table 2 also reveals that such "bloom area" criteria can reduce sample size to <5% of available data, making the results statistically unreliable.

The above example illustrates that in correlation analysis between [Chl-$a$] and $r_e$ bloom and nonbloom regions should not be considered separately; instead *all* data-points should be included. Moreover, depending on ambient conditions, maximum [Chl-$a$] in a bloom can vary considerably (e.g., from 0.6 to 23, [63]). This relativity of the bloom strength makes it difficult to define a universal threshold for [Chl-$a$] value and can lead to biased conclusions. Overall, the usage of a [Chl-$a$] threshold should be avoided in statistical analyses.

## 4. Selection of Spatial Resolution for Remotely Sensed Data

When examining the relationship between ocean ecosystem and overlying clouds it is typical to use specific oceanic regions and time periods. Although the effect of ocean productivity on marine clouds does not scale linearly with [Chl-$a$], it is desirable to examine the possible relationship between [Chl-$a$] and $r_e$ for periods with extensive blooms and the regions where cloud properties are not dominated by other types of aerosol interactions (e.g., strong dust or biomass burning plumes). The areas of elevated ocean primary productivity downwind of East Asia and West African Coast may not be ideal for detecting biogenic signals in $r_e$, as these regions are known to be strongly impacted by anthropogenic and mineral dust aerosol [64, 65]. This, in conjunction with the threshold-based statistical approach, may explain the lack of correlation between [Chl-$a$] and $r_e$ reported by MY08. Indeed, the area-averaged monthly mean MODIS retrieved AOD values at 550 nm ($\text{AOD}_{\text{M}}^{550}$) for the regions used in MY08 analysis were larger than 0.3 and the area-averaged daily $\text{AOD}_{\text{M}}^{550}$ values often reached 0.5 (not shown). Under such high (non-biogenic) aerosol loadings it will be difficult, if not impossible, to identify the biogenic effects on marine cloud properties.

Owing to its unique spatial location and circumpolar nature, the Southern Ocean (SO) remains an ideal place for examining the effects of marine productivity on liquid clouds using remotely sensed data. Primary productivity in the SO is peaking during the austral summer and gradually declining with a minimum in winter. Waters in the SO can support massive phytoplankton blooms [32, 66, 67], with [Chl-$a$] more than an order of magnitude higher than the background levels [68, 69]. The SO is characterized with minimal influence by mineral dust and also remains to be one of the most pristine regions of the globe with little impact from anthropogenic pollution. The surface [Chl-$a$] in this area can be used as a reliable proxy for the primary production [66, 70]. Strong and persistent westerlies with weak latitudinal component [71] make it possible to examine cloud properties upwind and downwind of the bloom. Although it is practically impossible to fully separate the effects of aerosols and meteorology on cloud microphysical properties, studies have shown [32, 44] that over the Southern Ocean CCN concentration does not correlate well with surface wind speed, precipitation, or sea surface temperature (SST). The periodic nature of the blooms (with distinct intraseasonal and interannual variability often out of phase from other periodic signals that may affect cloud properties) is ideal for exploring the temporal relationship between ocean productivity and regional clouds. When examining the correlation between marine productivity and cloud properties with remote sensing, it is important to properly select the spatial resolution for the data averaging. For example, the effect of secondary aerosols, which are the outcome of gas-to-particle processes, should generally appear not over the bloom, but farther downwind. Modeling results of Woodhouse et al. [72] show that DMS oxidation could influence condensational growth of existing particles not over the bloom, but ~100 km downwind, although the effect on CCN number may occur several thousand kilometers downwind of the bloom. The effect of marine primary organic aerosols generated at the sea surface through wind driven processes should be more centered in near the bloom region. Based on the lifetime of (1-2 hrs) for some of the phytoplankton produced VOCs over the SO [73] and the mean wind speed of ~40 km/hr [74], the effect of marine-SOA on clouds should appear ~100 km downwind

Table 2: Correlations of [Chl-*a*] and $r_e$ for the events chosen in MY08, using different threshold values of [Chl-*a*] that define the phytoplankton "bloom."

| Location (Date Range) | [Chl-*a*] threshold mg m$^{-3}$ | $R_{[\text{Chl-}a],r_e}$ [(a)] | $R_{\text{lim}}$ [(b)] | Sample size | Percent of data points satisfying the [Chl-*a*] threshold (%) |
|---|---|---|---|---|---|
| Southern Atlantic—48°S to 56°S, 55°W to 21°W (11 Dec. 2001–8 Jan. 2002) | No cutoff | −0.25 | −0.32<br>−0.17 | 645 | 97 |
| | >0.5 | −0.38 | −0.49<br>−0.26 | 211 | 32 |
| | >1.0 | −0.55 (−0.67) | −0.71<br>−0.36 | 64 | 10 |
| | >1.5 | −0.29 | −0.59<br>0.08 | 31 | 5 |
| | >2.0 | −0.17 | −0.58<br>0.31 | 20 | 3 |
| | >2.5 | +0.08 | −0.47<br>0.59 | 15 | 2.3 |
| | <1.0 | −0.1 (−0.02) | −0.18<br>−0.02 | 582 | 88 |
| Sea of Okhotsk—57°N to 52°N and 146°E to 152°E (26 June 2003–27 July 2003) | No cutoff | 0.14 | −0.18<br>0.42 | 43 | 100 |
| | >1.0 | 0.13 (−0.02) | −0.35<br>0.55 | 20 | 48 |
| | <1.0 | −0.17 (−0.13) | −0.55<br>0.26 | 24 | 55 |
| Northwest Atlantic—42°N to 60°N and 55°W to 21°W) (5 Aug. 2003– 4 Sep. 2004) | No cutoff | −0.51 | −0.57<br>−0.46 | 658 | 99 |
| | >1.0 | **−0.21** (**−0.09**) | −0.52<br>0.16 | 32 | 5 |
| | <1.0 | **−0.56** (**−0.18**) | −0.61<br>−0.5 | 627 | 94 |
| West African Coast—4°N to 14°S and 20°W to 14°E (1 Jan. 2002–1 Feb. 2002) | No cutoff | −0.03 | −0.12<br>0.06 | 449 | 68 |
| | >1.0 | −0.09 (0.02) | −0.41<br>0.24 | 38 | 6 |
| | <1.0 | 0.13 (0.13) | 0.04<br>0.23 | 412 | 62 |
| Bering Sea—52°N to 70°N and 176°E to 150°W (6 Apr. 2004–7 May 2004) | No cutoff | −0.45 | −0.53<br>−0.35 | 326 | 49 |
| | >1.0 | **−0.42** (**−0.13**) | −0.55<br>−0.27 | 139 | 21 |
| | <1.0 | 0.04 (−0.1) | −0.11<br>0.18 | 188 | 28 |

[(a)] Values in parenthesis are from MY08; highlighted values are the episodes when discrepancies between our and MY08 results were outside the 95% confidence intervals.
[(b)] The 95% confidence limits (the upper and lower bounds of a 95% confidence interval).

from the bloom. This distance may vary in different parts of the oceans based on chemical loss rates of VOCs and potential aid of organic vapors (from the oxidation products of marine sources of VOCs) to the nucleation events and growth of ultrafine particles [75, 76]. Therefore, when examining the relationship between ocean productivity and physical properties of shallow marine clouds over the SO using remotely sensed data, best correlation is likely to be achieved at $2^\circ \times 2^\circ$ averaged grid boxes (roughly 100–150 km $\times$ 220 km in the SO).

## 5. Negative Correlation between [Chl-$a$] and $r_e$

Figures 1 and 2 show correlation between [Chl-$a$] and $r_e$ over the Northwest Atlantic and the Bering Sea regions for the same time periods and the datasets used in MY08 (see Table 2). Figure 1 demonstrates that during the bloom period, out of all variables examined, $r_e$ is primarily correlated with [Chl-$a$] with $R_{[\text{Chl-}a],r_e} \sim -0.5$ (see Table 2). Figure 2 shows that over the low [Chl-$a$] regions of the Bering Sea, monthly averaged cloud effective radii is ~15 to 18 $\mu$m, with sharp decrease (~10 $\mu$m) in the vicinity of the bloom region. Considerable negative correlation ($R_{[\text{Chl-}a],r_e} \sim -0.4$) was also obtained for this episode with large discrepancies (highlighted values) between our results and the ones reported in MY08 (Table 2). Additional case studies over the Southern Indian Ocean and South Atlantic Ocean (Figure 3, Table 3) also show significant negative correlations between [Chl-$a$] and $r_e$; $R_{[\text{Chl-}a],r_e}$ values inside ($-0.45$, $-0.38$ and $-0.22$) and outside ($-0.09$, $-0.29$ and $-0.07$) the bloom regions of Figure 3 are significantly different, suggesting that marine biota could influence shallow marine cloud properties.

## 6. Retrieved AOD not Associated with Sea Salt

A major issue for quantifying the climatic effects of marine biogenic aerosols with the use of satellite data is the dominance of aerosol mass loading over the oceans by sea salt and aerosols of terrestrial origin. Detection of ocean biologically generated aerosols is further complicated due to their small size and low scattering efficiency. Here we employ a novel approach by examining the differences between MODIS-AOD and ss-AOD ($\text{AOD}_{\text{diff}}$) at different wavelengths. If sea salt aerosols were the only ones affecting observed top of the atmosphere (TOA) reflectances over the oceans, one expects to see very low and uniform values for $\text{AOD}_{\text{diff}}$. On the other hand, if aerosols other than sea salt can be important, $\text{AOD}_{\text{diff}}$ is expected to highlight the regions where nss-aerosols contribute to the observed reflectances. Figures 4(a) and 4(b) show large regions of Atlantic Ocean (east of Africa), Pacific Ocean (downwind from east Asia), Indian Ocean (west of Singapore and Indonesia), Arabian sea and Bay of Bengal, with sizable positive values for the $\text{AOD}_{\text{diff}}$ at 550 nm ($\text{AOD}_{\text{diff}}^{550}$). These figures show that the regions highlighted by warm colors on Figure 4(b) (positive difference between MODIS-AOD and ss-AOD) are typically associated with mineral dust and/or anthropogenic aerosol

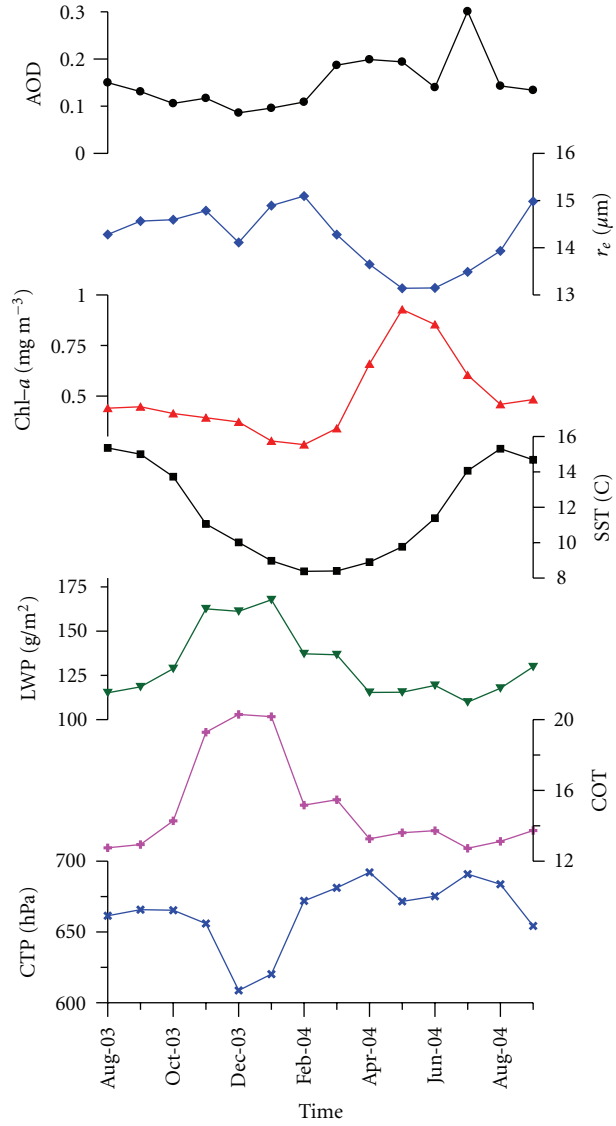


Figure 1: Time series of the area-averaged MODIS Aerosol optical depth (AOD), liquid cloud effective radii ($r_e$), sea surface temperature (SST), liquid water path (LWP), liquid cloud optical thickness (COT), liquid cloud top pressure (CTP) and SeaWiFS [Chl-$a$] in Northwest Atlantic (42°N to 60°N and 55°W to 21°W).

(i.e., biomass burning, industrial emissions). Interestingly, Figure 4(b) also shows positive values for $\text{AOD}_{\text{diff}}^{550}$ over the SO, the region characterized by minor contribution from both anthropogenic aerosols and mineral dust. Variations in size distribution of various aerosol types have been shown to strongly influence the radiative properties of the aerosols such as the scattering phase function, single scattering albedo and spectral variation of AOD [77]. AOD retrieved from sensing at shorter wavelengths are more sensitive to accumulation mode aerosol, while the larger wavelengths are more sensitive to coarse particles. Therefore, the $\text{AOD}_{\text{diff}}$ can be used to infer the relative importance of aerosol generation processes. Figure 4(c) shows the difference between MODIS-AOD and ss-AOD at wavelength

Table 3: Correlations of [Chl-$a$] and $r_e$ for different events of Figure 3.

| Location (date range) | | | Correlation coefficient between [Chl-$a$] and $r_e$ |
|---|---|---|---|
| Southern Indian (25 November 2006–31 December 2006) | 46°S to 52°S, 65°E to105°E | Inside the boom | −0.45 |
| | 42°S to 46°S, 65°E to105°E; 52°S to 60°S, 65°E to105°E | Outside the bloom | −0.09 |
| Southern Atlantic (10 December 2004–08 January 2005) | 50°S to 54°S, 55°W to 21°W | Inside the boom | −0.38 |
| | 42°S to 50°S, 55°W to 21°W; 54°S to 60°S, 55°W to 21°W | Outside the bloom | −0.29 |
| Southern Atlantic (11 December 2002–08 January 2003) | 50°S to 56°S, 55°W to 21°W | Inside the boom | −0.22 |
| | 42°S to 50°S, 55°W to 21°W 56°S to 60°S, 55°W to 21°W | Outside the bloom | −0.07 |

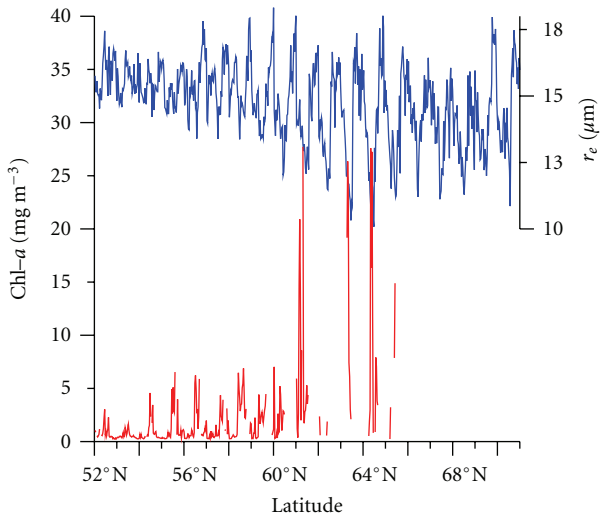


Figure 2: The 1°× 1° square monthly averaged SeaWiFS-observed [Chl-$a$] (red) and MODIS cloud effective radii (blue) over the Bering Sea. Between every tick marker on the $x$-axis, there are 35 data points corresponding to the starting point of the next west-to-east row in the longitudinal direction (176°E to 150°W). The large portion of the [Chl-$a$] data is missing due to the inclusion of continental regions.

of 1020 nm ($AOD_{diff}^{1020}$). When compared against $AOD_{diff}^{550}$ shown on Figure 4(b), $AOD_{diff}^{1020}$ is generally smaller, and effectively zero in pollution-dominated oceanic regions (e.g., downwind from eastern North America, east Asia and Indonesia). This is expected, as aerosol in these regions is dominated by submicron particles that scatter more effectively at shorter wavelengths. Comparison of Figures 4(b) and 4(c) also reveals smaller $AOD_{diff}^{1020}$ than $AOD_{diff}^{550}$ over the SO, suggesting that an accumulation mode aerosol is ubiquitous over the SO. It should be noted that these AOD differences over the SO are statistically significant, as they represent long-term averages with values much larger than the uncertainties in MODIS retrievals over the oceans [78].

To elucidate the role of ocean biology in the observed $AOD_{diff}^{550}$, we examined the time series of [Chl-$a$] and $AOD_{diff}^{550}$ in seven SO regions (Figure 4(a)) characterized by massive phytoplankton blooms during the austral summer and one in the central South Pacific gyre known as "the Earth's largest oceanic desert" [79]. The $AOD_{diff}^{550}$ were derived using three different ss-AOD parameterizations of Smirnov et al. [57], Mulcahy et al. [58] and Glantz et al. [59]. Figure 5 shows temporal correlations between $AOD_{diff}^{550}$ and [Chl-$a$] for selected oceanic regions, which are statistically significant at the 95% confidence level (Table 4). Figure 5 shows that during the austral summer similar patterns are seen in the SO between ocean surface productivity and the abundance of accumulation mode aerosol not associated with sea salt (Figure 5 and Table 4). During the high wind season (austral winter), the $AOD_{diff}^{550}$ turns negative (particularly using the Mulcahy et al. [58] regression), indicating potential overestimation of sea salt contribution to observed AOD. Unlike other stations, however, the [Chl-$a$] and $AOD_{diff}$ data from Station 8 (Figure 5(h); Table 4) show negative correlations, suggesting that the source of accumulation mode aerosol may differ between high and low productivity regions. Although aerosol measurements made over the high ocean productivity regions suggest using [Chl-$a$] as a proxy for the emissions of marine organic matter [80, 81], recent study by Russell et al. [82] indicates that dissolved organic carbon (DOC) and particulate organic carbon (POC) concentrations in the sea surface microlayer may provide the source of organic aerosols in the Arctic and north Atlantic regions, respectively. It is interesting to notice, that the surface waters near the Station 8 have some of the highest levels of DOC in the entire South Pacific Ocean [83], and therefore can explain the absence of correlation between [Chl-$a$] and $AOD_{diff}$. All together, this evidence suggests a robust link between marine productivity and accumulation mode aerosol (i.e., CCN) over the oceans and in particular the SO.

To address potential bias in aerosol retrievals from "cloud contamination", we have removed all aerosol data with AOD > 0.8 (Removal of *all* aerosol retrievals that may be influenced from clouds could leads to complete loss of aerosol-cloud interaction information [84]). This analysis, nevertheless, does include several imperfections. The satellite signal is a combination of radiation from the atmosphere as well as from the surface. MODIS observed reflectances

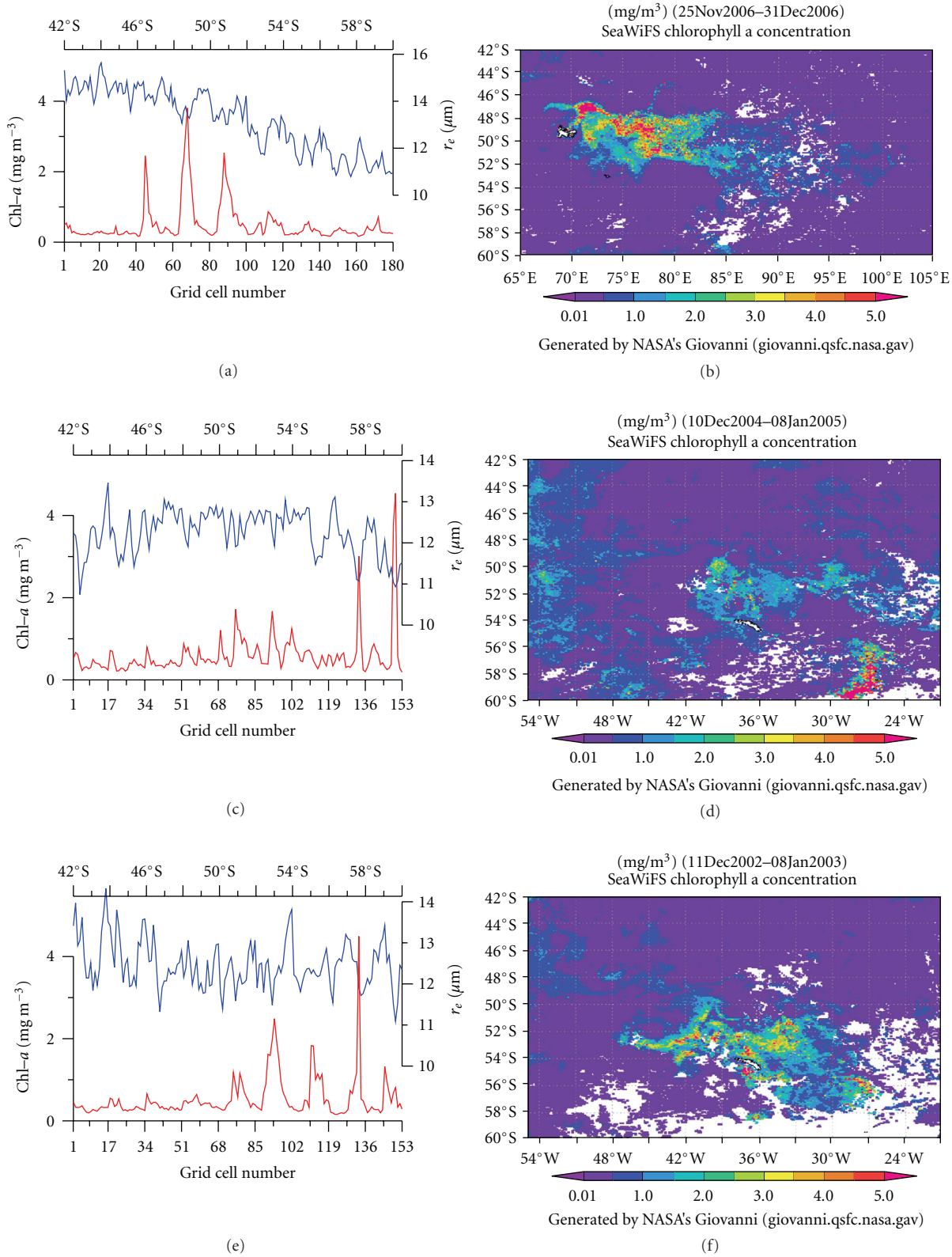


FIGURE 3: The 2° × 2° square monthly averaged [Chl -*a*] and $r_e$ data for Southern Indian Ocean for (a), (b) 25 November 2006–31 November 2006; Southern Atlantic Ocean for (c), (d) 10 December 2004–08 January 2005; and Southern Atlantic Ocean for (e),(f) 11 December 2002–08 January 2003. The white color over the ocean denotes the missing data due to clouds. The Kerguelen Island (49.25°S–69.58°E) and the South Georgia Island (54.25°S, 36.75°W) are shown by black contours. The method is adopted from Meskhidze and Nenes [32]. The images and data used in this figure were acquired using the GES-DISC Interactive Online Visualization ANd aNalysis Infrastructure (Giovanni) as part of the NASA's Goddard Earth Sciences (GES) Data and Information Services Center (DISC).

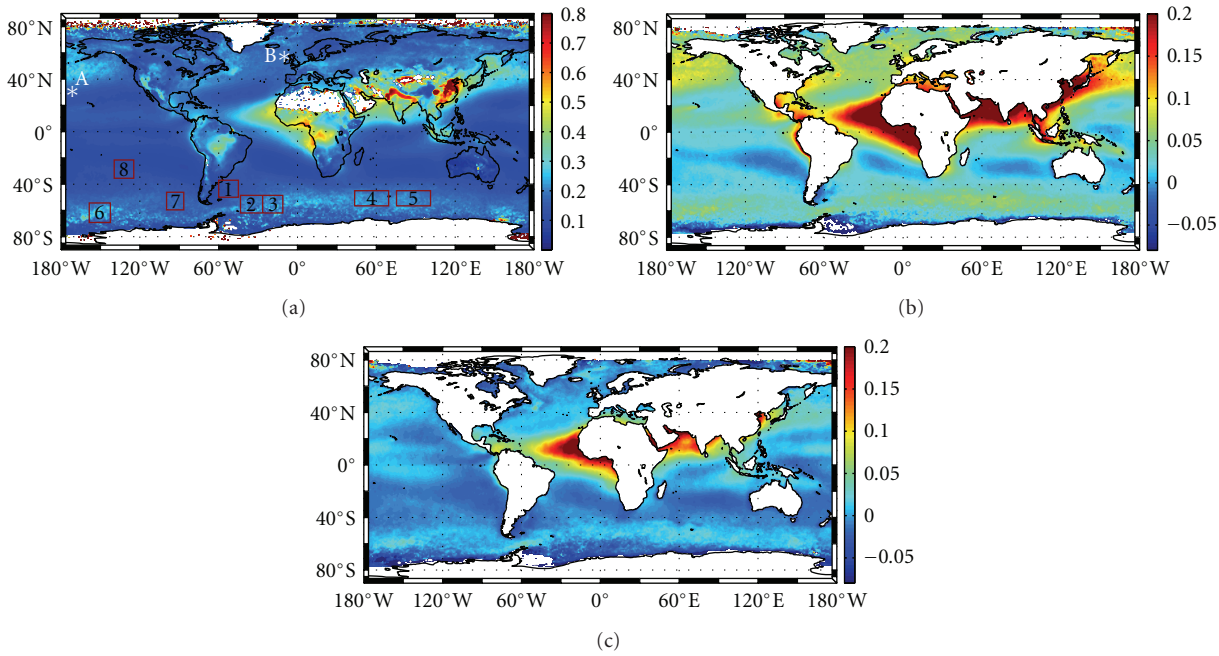


Figure 4: Seven-year (2002–2008) averaged daily data for (a) MODIS AOD at 550 nm and the differences between MODIS AOD and parameterized ss-AOD at (b) 550 nm and (c)1020 nm. The ss-AOD is calculated using Smirnov et al. [57] regression. Red boxes on Figure 4(a) indicate seven regions where time series analyses are carried out. Position of each boxes (latitude and longitude) are given in Table 4. Letters A and B denote locations of previous study areas of Smirnov et al. [57] at Midway Islands (28.2°N and 177.4°W) and Mulchay et al. [58] at the Mace Head station (53.3°N, 9.9°W), respectively. The study region of Glantz et al. [59] encompassed large areas of the North Pacific Ocean, roughly from 180°W to 160°W and 15°N to 45°N.

Table 4: Correlations of [Chl-*a*] and $AOD_{diff}$ for time series of Figure 5[(1)].

| Location (Date Range) | [Chl-*a*] and $AOD_{diff}^{550(2)}$ | [Chl-*a*] and $AOD_{diff}^{1020(3)}$ | [Chl-*a*] and $AOD_{diff}^{550(4)}$ | [Chl-*a*] and $AOD_{diff}^{550(5)}$ |
|---|---|---|---|---|
| Southern Atlantic | 0.60 (0.52) | 0.41 (0.30) | 0.60 (0.52) | 0.59 (0.50) |
| Box #1 (39°S to 47°S, 57°W to 47°W) | (0.66) | (0.50) | (0.67) | (0.65) |
| Southern Atlantic | 0.57 (0.48) | 0.31 (0.18) | 0.59 (0.48) | 0.58 (0.45) |
| Box #2 (48°S to 58°S, 43°W to 31°W) | (0.65) | (0.41) | (0.68) | (0.68) |
| Southern Atlantic | 0.54 (0.44) | 0.30 (0.15) | 0.56 (0.44) | 0.35 (0.23) |
| Box #3 (48°S to 58°S, 31°W to 20°W) | (0.61) | (0.44) | (0.66) | (0.47) |
| Southern Indian | 0.65 (0.55) | 0.41 (0.30) | 0.65 (0.55) | 0.66 (0.52) |
| Box #4 (48°S to 55°S, 44°E to 64°E) | (0.70) | (0.51) | (0.71) | (0.72) |
| Southern Indian | 0.40 (0.28) | 0.18 (0.07) | 0.49 (0.38) | 0.43 (0.32) |
| Box #5 (47°S to 55°S, 71°E to 91°E) | (0.49) | (0.33) | (0.54) | (0.54) |
| Southern Pacific | 0.35 (0.21) | 0.03 (−0.13) | 0.42 (0.29) | 0.37 (0.23) |
| Box #6 (55°S to 67°S, 159°W to 145°W) | (0.45) | (0.14) | (0.48) | (0.48) |
| Southern Pacific | 0.34 (0.23) | 0.18 (0.11) | 0.34 (0.18) | 0.37 (0.26) |
| Box #7 (46°S to 56°S, 100°W to 90°W) | (0.42) | (0.32) | (0.37) | (0.47) |
| Southern Pacific | −0.25 (−0.36) | −0.15 (−0.23) | −0.38 (−0.42) | −0.21 (−0.31) |
| Box #8 (25°S to 35°S, 135°W to 125°W) | (−0.15) | (−0.05) | (−0.23) | (−0.12) |

(1) Numbers in parenthesis show the upper and lower bounds of a 95% confidence interval.
(2) ss-AOD at 500 nm was calculated using Smirnov et al. [57] parameterization.
(3) ss-AOD at 1020 nm was calculated using Smirnov et al. [57] parameterization.
(4) ss-AOD at 500 nm was calculated using Mulcahy et al. [58] parameterization.
(5) ss-AOD at 555 nm was calculated using Glantz et al. [59] parameterization.

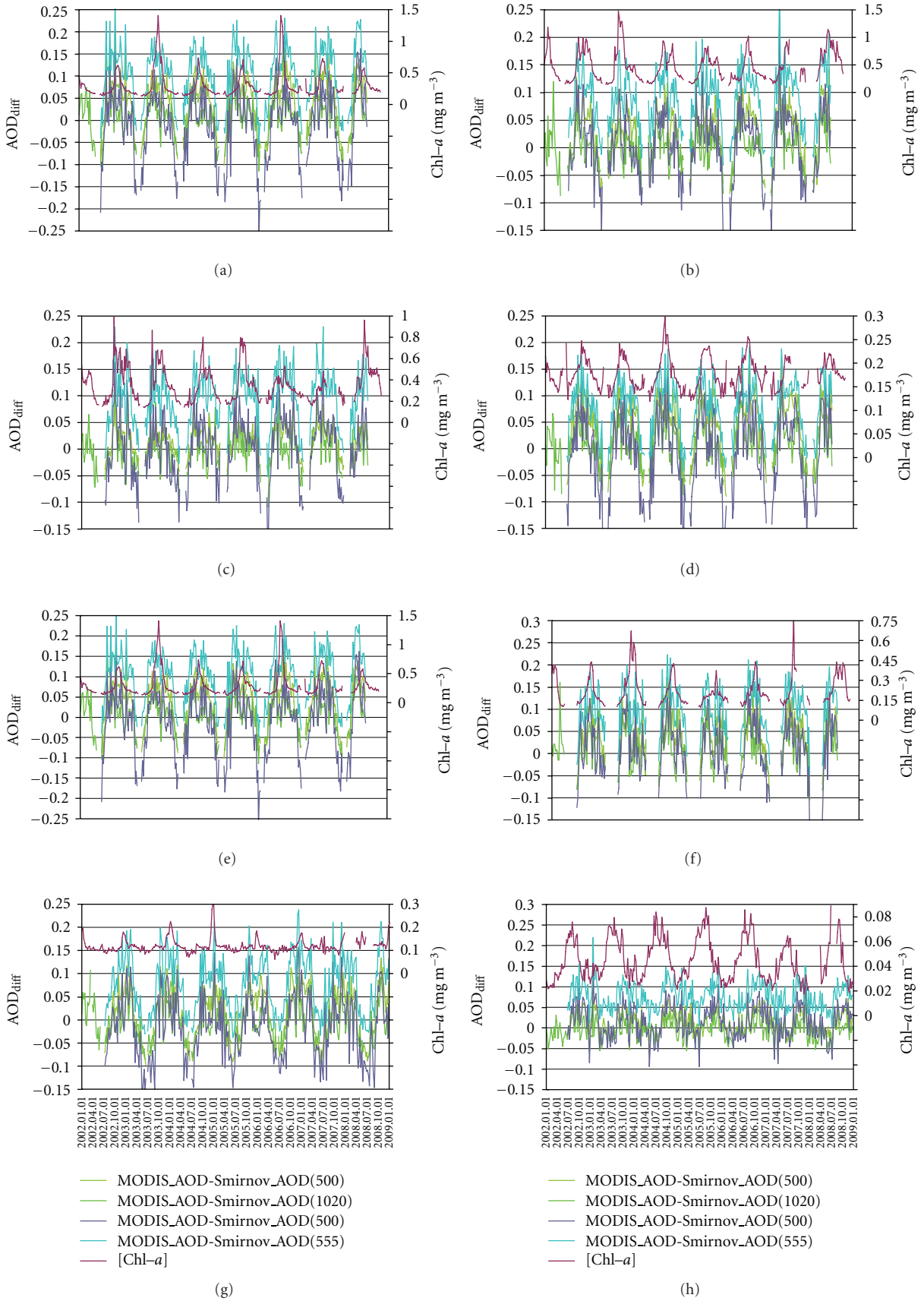


FIGURE 5: (a)–(h) Time series of the area-averaged $AOD_{diff}$ (right axis) and [Chl-$a$] (left axis) for the boxes 1–8 shown on Figure 4. The daily differences in AOD values were averaged over 8 days.

are then converted to AODs using nine tropospheric aerosol models [85]. The atmospheric contribution includes multiple scattering by gas and aerosol, as well as reflection of the atmosphere by the sea surface. The ocean surface calculation includes Sun glint reflection off the surface waves [86], reflection by whitecaps [87] and Lambertian reflectance from underwater scattering (sediments, chlorophyll, etc). For the current version of the lookup table, reflectances are calculated using a surface wind of 6.0 m/s. Zero water-leaving radiance is assumed at all six compared wavelengths, except for at 550 nm, where a fixed reflectance of 0.005 is used [85]. Although this may lead to spurious correlations between AOD and [Chl-*a*] at high special resolution, it is not expected to have sizable influence when averaged over the large area as ones used in this study.

## 7. Conclusion

The use of remote sensing products is very valuable for studying marine biota-cloud links. Statistical analyses however must be carried out very carefully, using as much *a priori* knowledge as possible. We show that conditional sampling, and using periods and locations where aerosol from ocean biota are dwarfed by other sources can lead to biased conclusions. We propose guidelines that address these potential issues, and show that there is statistically significant negative correlation between warm cloud effective radii and surface ocean productivity in different parts of the ocean and different time periods. A novel approach, based on MODIS retrieved total aerosol optical depth and predicted sea salt aerosol optical depth ($AOD_{diff}$), is proposed to study the link between ocean biological productivity and submicron aerosols over the oceans. By employing different wavelength for estimating $AOD_{diff}$, it was proposed that the large summertime discrepancies between MODIS retrieved AODs and parameterized ss-AODs over the Southern Ocean are mainly related to accumulation model aerosols and cannot be explained by mere variations in column abundance of sea salt. Since the SO is characterized with minimal influence of anthropogenic pollution and mineral dust, summertime positive values in $AOD_{diff}^{550}$ are most likely related to marine primary organic aerosols and secondary aerosols associated with biogenic trace gas emissions from the ocean.

Today it is widely accepted that the ocean ecosystem (particularly over the biologically active regions) can significantly influence CCN over the remote oceans. It has also been suggested that correct characterization of marine biogenic aerosols and factors that regulate their emissions could be essential for the accurate modeling of climate forcing assessments. However, satellite remote sensing alone cannot ascertain causal mechanism for the relationship between ocean ecosystem and properties of marine shallow clouds. Future studies through the combination of laboratory measurements, in situ data, satellite remote sensing and models are required to establish a comprehensive mechanism for this highly complex and interactive system of aerosol-ocean ecosystems-cloud interactions with multiple forcings and feedbacks.

## Acknowledgments

This research was supported by the Office of Science (BER), US Department of Energy, Grant no. DE-FG02-08ER64508. The authors greatly appreciate the help in data processing by Brett Gantt.

## References

[1] S. Twomey, "The influence of pollution on the shortwave albedo of clouds," *Journal of Atmospheric Science*, vol. 34, pp. 1149–1152, 1977.

[2] B. A. Albrecht, "Aerosols, cloud microphysics, and fractional cloudiness," *Science*, vol. 245, no. 4923, pp. 1227–1230, 1989.

[3] R. J. Charlson, S. E. Schwartz, J. M. Hales et al., "Climate forcing by anthropogenic aerosols," *Science*, vol. 255, no. 5043, pp. 423–430, 1992.

[4] IPCC, "Summary for policy makers," in *Climate Change 2007: The Physical Science Basis. Contribution of Working Group I to the Fourth Assessment Report of the Intergovernmental Panel on Climate Change*, S. Solomon, D. Qin, and M. Manning, Eds., Cambridge University Press, Cambridge, UK, 2007.

[5] S. A. Klein and D. L. Hartmann, "The seasonal cycle of low stratiform clouds," *Journal of Climate*, vol. 6, no. 8, pp. 1587–1606, 1993.

[6] S. Platnick and S. Twomey, "Determining the susceptibility of cloud albedo to changes in droplet concentration with the Advanced Very High Resolution Radiometer," *Journal of Applied Meteorology*, vol. 33, no. 5, pp. 334–347, 1994.

[7] D. A. Randell, J. A. Coakley Jr., C. W. Fairall, R. A. Kropfli, and D. H. Lenschow, "Outlook for research on subtropical marine stratiform clouds," *Bulletin—American Meteorological Society*, vol. 65, no. 12, pp. 1290–1301, 1984.

[8] B. Stevens, G. Vali, K. Comstock et al., "Pockets of open cells and drizzle in marine stratocumulus," *Bulletin of the American Meteorological Society*, vol. 86, no. 1, pp. 51–57, 2005.

[9] M. O. Andreae, "Aerosols before pollution," *Science*, vol. 315, no. 5808, pp. 50–51, 2007.

[10] C. D. O'Dowd and G. De Leeuw, "Marine aerosol production: a review of the current knowledge," *Philosophical Transactions of the Royal Society A*, vol. 365, no. 1856, pp. 1753–1774, 2007.

[11] M. O. Andreae and D. Rosenfeld, "Aerosol-cloud-precipitation interactions. Part 1. The nature and sources of cloud-active aerosols," *Earth-Science Reviews*, vol. 89, no. 1-2, pp. 13–41, 2008.

[12] C. D. O'Dowd, M. H. Smith, I. E. Consterdine, and J. A. Lowe, "Marine aerosol, sea-salt, and the marine sulphur cycle: a short review," *Atmospheric Environment*, vol. 31, no. 1, pp. 73–80, 1997.

[13] D. M. Murphy, J. R. Anderson, P. K. Quinn, et al., "Influence of sea-salt on aerosol radiative properties in the Southern Ocean marine boundary layer," *Nature*, vol. 392, no. 6671, pp. 62–65, 1998.

[14] P. K. Quinn, D. J. Coffman, V. N. Kapustin, T. S. Bates, and D. S. Covert, "Aerosol optical properties in the marine boundary layer during the first aerosol Characterization Experiment (ACE 1) and the underlying chemical and physical aerosol properties," *Journal of Geophysical Research D*, vol. 103, no. 13, pp. 16547–16563, 1998.

[15] C. Kleefeld, C. D. O'Dowd, S. O'Reilly et al., "Relative contribution of submicron and supermicron particles to aerosol light scattering in the marine boundary layer," *Journal of Geophysical Research D*, vol. 107, no. 19, article 8103, 2002.

[16] T. S. Bates, P. K. Quinn, D. J. Coffman, J. E. Johnson, and A. M. Middlebrook, "Dominance of organic aerosols in the marine boundary layer over the Gulf of Maine during NEAQS 2002 and their role in aerosol light scattering," *Journal of Geophysical Research D*, vol. 110, no. 18, pp. 1–14, 2005.

[17] G. E. Shaw, "Bio-controlled thermostasis involving the sulfur cycle," *Climatic Change*, vol. 5, no. 3, pp. 297–303, 1983.

[18] R. J. Charlson, J. E. Lovelock, M. O. Andreae, and S. G. Warren, "Oceanic phytoplankton, atmospheric sulphur, cloud albedo and climate," *Nature*, vol. 326, no. 6114, pp. 655–661, 1987.

[19] T. Novakov, C. E. Corrigan, J. E. Penner, C. C. Chuang, O. Rosario, and O. L. Mayol Bracero, "Organic aerosols in the Caribbean trade winds: a natural source?" *Journal of Geophysical Research D*, vol. 102, no. 17, pp. 21307–21313, 1997.

[20] J.-P. Putaud, R. Van Dingenen, M. Mangoni et al., "Chemical mass closure and assessment of the origin of the submicron aerosol in the marine boundary layer and the free troposphere at Tenerife during ACE-2," *Tellus, Series B*, vol. 52, no. 2, pp. 141–168, 2000.

[21] F. Cavalli, M. C. Facchini, S. Decesari et al., "Advances in characterization of size-resolved organic matter in marine aerosol over the North Atlantic," *Journal of Geophysical Research D*, vol. 109, no. 24, pp. 1–14, 2004.

[22] Y. J. Yoon, D. Ceburnis, F. Cavalli et al., "Seasonal characteristics of the physicochemical properties of North Atlantic marine atmospheric aerosols," *Journal of Geophysical Research D*, vol. 112, no. 4, Article ID D04206, 2007.

[23] C. A. Pio, M. Legrand, T. Oliveira et al., "Climatology of aerosol composition (organic versus inorganic) at nonurban sites on a west-east transect across Europe," *Journal of Geophysical Research D*, vol. 112, no. 23, Article ID D23S02, 2007.

[24] C. D. O'Dowd, M. C. Facchini, F. Cavalli et al., "Biogenically driven organic contribution to marine aerosol," *Nature*, vol. 431, no. 7009, pp. 676–680, 2004.

[25] D. Ceburnis, C. D. O'Dowd, G. S. Jennings et al., "Marine aerosol chemistry gradients: elucidating primary and secondary processes and fluxes," *Geophysical Research Letters*, vol. 35, no. 7, Article ID L07804, 2008.

[26] D. C. Blanchard and A. H. Woodcock, "Bubble formation and modification in the sea and its meteorological significance," *Tellus*, vol. 9, pp. 145–158, 1957.

[27] A. M. Middlebrook, D. M. Murphy, and D. S. Thomson, "Observations of organic material in individual marine particles at Cape Grim during the First Aerosol Characterization Experiment (ACE I)," *Journal of Geophysical Research D*, vol. 103, no. 13, pp. 16475–16483, 1998.

[28] C. Leck and E. K. Bigg, "Source and evolution of the marine aerosol—a new perspective," *Geophysical Research Letters*, vol. 32, no. 19, Article ID L19803, pp. 1–4, 2005.

[29] C. Leck and E. K. Bigg, "Biogenic particles in the surface microlayer and overlaying atmosphere in the central Arctic Ocean during summer," *Tellus, Series B*, vol. 57, no. 4, pp. 305–316, 2005.

[30] B. Bonsang, C. Polle, and G. Lambert, "Evidence for marine production of isoprene," *Geophysical Research Letters*, vol. 19, no. 11, pp. 1129–1132, 1992.

[31] S. L. Shaw, S. W. Chisholm, and R. G. Prinn, "Isoprene production by Prochlorococcus, a marine cyanobacterium, and other phytoplankton," *Marine Chemistry*, vol. 80, no. 4, pp. 227–245, 2003.

[32] N. Meskhidze and A. Nenes, "Phytoplankton and cloudiness in the southern ocean," *Science*, vol. 314, no. 5804, pp. 1419–1423, 2006.

[33] N. Yassaa, I. Peeken, E. Zöllner et al., "Evidence for marine production of monoterpenes," *Environmental Chemistry*, vol. 5, no. 6, pp. 391–401, 2008.

[34] G. Luo and F. Yu, "A numerical evaluation of global oceanic emissions of $\alpha$-pinene and isoprene," *Atmospheric Chemistry and Physics*, vol. 10, no. 4, pp. 2007–2015, 2010.

[35] C. Leck and E. K. Bigg, "Comparison of sources and nature of the tropical aerosol with the summer high Arctic aerosol," *Tellus, Series B*, vol. 60, no. 1, pp. 118–126, 2008.

[36] W. C. Keene, H. Maring, J. R. Maben et al., "Chemical and physical characteristics of nascent aerosols produced by bursting bubbles at a model air-sea interface," *Journal of Geophysical Research D*, vol. 112, no. 21, Article ID D21202, 2007.

[37] M. C. Facchini, M. Rinaldi, S. Decesari et al., "Primary submicron marine aerosol dominated by insoluble organic colloids and aggregates," *Geophysical Research Letters*, vol. 35, no. 17, Article ID L17814, 2008.

[38] S. R. Zorn, F. Drewnick, M. Schott, T. Hoffmann, and S. Borrmann, "Characterization of the South Atlantic marine boundary layer aerosol using an aerodyne aerosol mass spectrometer," *Atmospheric Chemistry and Physics*, vol. 8, no. 16, pp. 4711–4728, 2008.

[39] D. Hegg, L. Radke, and P. Hobbs, "Measurements of Aitken nuclei and cloud condensation nuclei in the marine atmosphere and their relationship to the DMS-cloud-climate hypothesis," *Journal of Geophysical Research*, vol. 96, pp. 18727–18733, 1991.

[40] M. O. Andreae, W. Elbert, and S. J. de Mora, "Biogenic sulfur emissions and aerosols over the tropical South Atlantic. 3. Atmospheric dimethylsulfide, aerosols and cloud condensation nuclei," *Journal of Geophysical Research*, vol. 100, no. 6, pp. 335–356, 1995.

[41] P. G. Falkowski, Y. Kim, Z. Kolber, C. Wilson, C. Wirick, and R. Cess, "Natural versus anthropogenic factors affecting low-level cloud albedo over the North Atlantic," *Science*, vol. 256, no. 5061, pp. 1311–1313, 1992.

[42] R. Boers, G. P. Ayers, and J. L. Gras, "Coherence between seasonal cycles in satellite observed cloud optical depth and boundary layer CCN concentration at a mid-latitude Southern Hemispheric site," *Tellus, Series B*, vol. 46, pp. 123–131, 1994.

[43] R. Boers, J. R. Acarreta, and J. L. Gras, "Satellite monitoring of the first indirect aerosol effect: retrieval of the droplet concentration of water clouds," *Journal of Geophysical Research D*, vol. 111, no. 22, Article ID D22208, 2006.

[44] S. M. Vallina, R. Simó, and S. Gassó, "What controls CCN seasonality in the Southern Ocean? A statistical analysis based on satellite-derived chlorophyll and CCN and model-estimated OH radical and rainfall," *Global Biogeochemical Cycles*, vol. 20, no. 1, Article ID GB1014, 2006.

[45] Y. Hu, M. Vaughan, C. McClain et al., "Global statistics of liquid water content and effective number concentration of water clouds over ocean derived from combined CALIPSO and MODIS measurements," *Atmospheric Chemistry and Physics*, vol. 7, no. 12, pp. 3353–3359, 2007.

[46] M. G. Lawrence, "An empirical analysis of the strength of the phytoplankton- dimethylsulfide-cloud-climate feedback cycle," *Journal of Geophysical Research*, vol. 98, no. 11, pp. 663–673, 1993.

[47] G. J. Roelofs, "A GCM study of organic matter in marine aerosol and its potential contribution to cloud drop activation," *Atmospheric Chemistry and Physics*, vol. 8, no. 3, pp. 709–719, 2008.

[48] M. A. Miller and S. E. Yuter, "Lack of correlation between chlorophyll a and cloud droplet effective radius in shallow marine clouds," *Geophysical Research Letters*, vol. 35, no. 13, Article ID L13807, 2008.

[49] J. V. Martins, D. Tanré, L. Remer, Y. Kaufman, S. Mattoo, and R. Levy, "MODIS cloud screening for remote sensing of aerosols over oceans using spatial variability," *Geophysical Research Letters*, vol. 29, no. 12, Article ID 8009, 2002.

[50] B.-C. Gao, Y. J. Kaufman, D. Tanre, and R.-R. Li, "Distinguishing tropospheric aerosols from thin cirrus clouds for improved aerosol retrievals using the ratio of 1.38-$\mu$m and 1.24-$\mu$m channels," *Geophysical Research Letters*, vol. 29, no. 18, Article ID 1890, 2002.

[51] J. I. Brennan, Y. J. Kaufman, I. Koren, and R. R. Li, "Aerosol-cloud interaction—misclassification of MODIS clouds in heavy aerosol," *IEEE Transactions on Geoscience and Remote Sensing*, vol. 43, no. 4, pp. 911–915, 2005.

[52] Y. J. Kaufman, I. Koren, L. A. Remer, D. Rosenfeld, and Y. Rudich, "The effect of smoke, dust, and pollution aerosol on shallow cloud development over the Atlantic Ocean," *Proceedings of the National Academy of Sciences of the United States of America*, vol. 102, no. 32, pp. 11207–11212, 2005.

[53] J. Zhang, J. S. Reid, and B. N. Holben, "An analysis of potential cloud artifacts in MODIS over ocean aerosol optical thickness products," *Geophysical Research Letters*, vol. 32, no. 15, Article ID L15803, 2005.

[54] A. Marshak, S. Platnick, T. Varnai, G. Wen, and R. F. Cahalan, "Impact of 3D radiative effects on satellite retrievals of cloud droplet sizes," *Journal of Geophysical Research*, vol. 111, Article ID D09207, 2006.

[55] G. Wen, A. Marshak, R. F. Cahalan, L. A. Remer, and R. G. Kleidman, "3D aerosol-cloud radiative interaction observed in collocated MODIS and ASTER images of cumulus cloud fields," *Journal of Geophysical Research*, vol. 112, Article ID D13204, 2007.

[56] J. L. Tackett and L. Di Girolamo, "Enhanced aerosol backscatter adjacent to tropical trade wind clouds revealed by satellite-based lidar," *Geophysical Research Letters*, vol. 36, no. 14, Article ID L14804, 2009.

[57] A. Smirnov, B. N. Holben, T. F. Eck, O. Dubovik, and I. Slutsker, "Effect of wind speed on columnar aerosol optical properties at Midway Island," *Journal of Geophysical Research D*, vol. 108, no. 24, Article ID 4802, 2003.

[58] J. P. Mulcahy, C. D. O'Dowd, S. G. Jennings, and D. Ceburnis, "Significant enhancement of aerosol optical depth in marine air under high wind conditions," *Geophysical Research Letters*, vol. 35, no. 16, Article ID L16810, 2008.

[59] P. Glantz, E. D. Nilsson, and W. von Hoyningen-Huene, "Estimating a relationship between aerosol optical thickness and surface wind speed over the ocean," *Atmospheric Research*, vol. 92, no. 1, pp. 58–68, 2009.

[60] N. Bellouin, O. Boucher, J. Haywood, and M. S. Reddy, "Global estimate of aerosol direct radiative forcing from satellite measurements," *Nature*, vol. 438, no. 7071, pp. 1138–1141, 2005.

[61] B. M. Uz and J. A. Yoder, "High frequency and mesoscale variability in SeaWiFS chlorophyll imagery and its relation to other remotely sensed oceanographic variables," *Deep-Sea Research Part II*, vol. 51, no. 10-11, pp. 1001–1017, 2004.

[62] Y. Lehahn, I. Koren, E. Boss, Y. Ben-Ami, and O. Altaratz, "Estimating the maritime component of aerosol optical depth and its dependency on surface wind speed using MODIS and QuikSCAT data," *Atmospheric Chemistry and Physics Discussions*, vol. 10, no. 1, pp. 1983–2003, 2010.

[63] P. W. Boyd, T. Jickells, C. S. Law et al., "Mesoscale iron enrichment experiments 1993–2005: synthesis and future directions," *Science*, vol. 315, no. 5812, pp. 612–617, 2007.

[64] Y. J. Kaufman, D. Tanré, and O. Boucher, "A satellite view of aerosols in the climate system," *Nature*, vol. 419, no. 6903, pp. 215–223, 2002.

[65] Y. J. Kaufman, O. Boucher, D. Tanré, M. Chin, L. A. Remer, and T. Takemura, "Aerosol anthropogenic component estimated from satellite data," *Geophysical Research Letters*, vol. 32, no. 17, Article ID L17804, 2005.

[66] R. E. Korb, M. J. Whitehouse, and P. Ward, "SeaWiFS in the southern ocean: spatial and temporal variability in phytoplankton biomass around South Georgia," *Deep-Sea Research Part II*, vol. 51, no. 1–3, pp. 99–116, 2004.

[67] N. Meskhidze, A. Nenes, W. L. Chameides, C. Luo, and N. Mahowald, "Atlantic Southern Ocean productivity: fertilization from above or below?" *Global Biogeochemical Cycles*, vol. 21, no. 2, Article ID GB2006, 2007.

[68] J. H. Martin and S. E. Fitzwater, "Iron-deficiency limits phytoplankton growth in the north-east pacific subarctic," *Nature*, vol. 331, no. 6154, pp. 341–343, 1988.

[69] P. W. Boyd, A. J. Watson, C. S. Law et al., "A mesoscale phytoplankton bloom in the polar Southern Ocean stimulated by iron fertilization," *Nature*, vol. 407, no. 6805, pp. 695–702, 2000.

[70] M. P. Meredith, J. L. Watkins, E. J. Murphy, et al., "An anticyclonic circulation above the Northwest Georgia Rise, Argentina," *Geophysical Research Letters*, vol. 30, no. 2061, p. 5, 2003.

[71] S. T. Gille, "Statistical characterization of zonal and meridional ocean wind stress," *Journal of Atmospheric and Oceanic Technology*, vol. 22, no. 9, pp. 1353–1372, 2005.

[72] M. T. Woodhouse, G. W. Mann, K. S. Carslaw, and O. Boucher, "New directions: the impact of oceanic iron fertilisation on cloud condensation nuclei," *Atmospheric Environment*, vol. 42, no. 22, pp. 5728–5730, 2008.

[73] I. E. Galbally, S. J. Lawson, I. A. Weeks et al., "Volatile organic compounds in marine air at Cape Grim, Australia," *Environmental Chemistry*, vol. 4, no. 3, pp. 178–182, 2007.

[74] X. Yuan, "High-wind-speed evaluation in the Southern Ocean," *Journal of Geophysical Research D*, vol. 109, no. 13, Article ID D13101, 2004.

[75] P. Vaattovaara, P. E. Huttunen, Y. J. Yoon et al., "The composition of nucleation and Aitken modes particles during coastal nucleation events: evidence for marine secondary organic contribution," *Atmospheric Chemistry and Physics*, vol. 6, no. 12, pp. 4601–4616, 2006.

[76] R. L. Modini, Z. D. Ristovski, G. R. Johnson et al., "New particle formation and growth at a remote, sub-tropical coastal location," *Atmospheric Chemistry and Physics*, vol. 9, no. 19, pp. 7607–7621, 2009.

[77] T. F. Eck, B. N. Holben, J. S. Reid et al., "Wavelength dependence of the optical depth of biomass burning, urban, and desert dust aerosols," *Journal of Geophysical Research D*, vol. 104, no. 24, pp. 31333–31349, 1999.

[78] L. A. Remer, Y. J. Kaufman, D. Tanré et al., "The MODIS aerosol algorithm, products, and validation," *Journal of the Atmospheric Sciences*, vol. 62, no. 4, pp. 947–973, 2005.

[79] H. Claustre and S. Maritorena, "The many shades of ocean blue," *Science*, vol. 302, no. 5650, pp. 1514–1515, 2003.

[80] C. D. O'Dowd, B. Langmann, S. Varghese, C. Scannell, D. Ceburnis, and M. C. Facchini, "A combined organic-inorganic sea-spray source function," *Geophysical Research Letters*, vol. 35, no. 1, Article ID L07804, 2008.

[81] D. Ceburnis, C. D. O'Dowd, G. S. Jennings et al., "Marine aerosol chemistry gradients: elucidating primary and secondary processes and fluxes," *Geophysical Research Letters*, vol. 35, no. 7, Article ID L07804, 2008.

[82] L. M. Russell, L. N. Hawkins, A. A. Frossard, P. K. Quinn, and T. S. Bates, "Carbohydrate-like composition of submicron atmospheric particles and their production from ocean bubble bursting," *Proceedings of the National Academy of Sciences of the United States of America*, vol. 107, no. 15, pp. 6652–6657, 2010.

[83] D. Hansell, C. A. Carlson, D. J. Repeta, and R. Schlitzer, "Dissolved organic matter in the ocean: a controversy stimulates new insights," *Oceanography*, vol. 22, no. 4, pp. 202–211, 2009.

[84] I. Koren, G. Feingold, and L. A. Remer, "The invigoration of deep convective clouds over the Atlantic: aerosol effect, meteorology or retrieval artifact?" *Atmospheric Chemistry and Physics Discussions*, vol. 10, no. 2, pp. 3893–3936, 2010.

[85] R. C. Levy, L. A. Remer, D. Tanré et al., "Evaluation of the moderate-resolution imaging spectroradiometer (MODIS) retrievals of dust aerosol over the ocean during PRIDE," *Journal of Geophysical Research D*, vol. 108, no. 8594, 2003.

[86] C. Cox and W. Munk, "Measurements of the roughness of the sea surface from photographs of the sun's glitter," *Journal of the Optical Society of America*, vol. 44, pp. 838–850, 1954.

[87] P. Koepke, "Effective reflectance of oceanic whitecaps," *Applied Optics*, vol. 23, no. 11, pp. 1816–1824, 1984.

Hindawi Publishing Corporation
Advances in Meteorology
Volume 2010, Article ID 939171, 16 pages
doi:10.1155/2010/939171

*Research Article*

# Global Modeling of the Oceanic Source of Organic Aerosols

**Stelios Myriokefalitakis,[1] Elisabetta Vignati,[2] Kostas Tsigaridis,[3,4] Christos Papadimas,[5] Jean Sciare,[6] Nikolaos Mihalopoulos,[1] Maria Cristina Facchini,[7] Matteo Rinaldi,[7] Frank J. Dentener,[2] Darius Ceburnis,[8] Nikos Hatzianastasiou,[5] Colin D. O'Dowd,[8] Michiel van Weele,[9] and Maria Kanakidou[1]**

[1] *Environmental Chemical Processes Laboratory, Department of Chemistry, University of Crete, 71003, Heraklion, Greece*
[2] *Institute for Environment and Sustainability, European Commission, Joint Research Centre, 21027, Ispra, Italy*
[3] *NASA Goddard Institute for Space Studies, New York, NY 10025, USA*
[4] *Center for Climate Systems Research, Columbia University, New York, NY 10025, USA*
[5] *Department of Physics, University of Ioannina, 54110, Ioannina, Greece*
[6] *LSCE, CNRS/CEA, 91190, Gif sur Yvette, France*
[7] *Institute of Atmospheric Sciences and Climate, CNR, 40129, Bologna, Italy*
[8] *School of Physics and Environmental Change Institute, National University of Ireland, Galway, Ireland*
[9] *Royal Netherlands Meteorological Institute (KNMI), P.O. Box 201, 3730 AE, De Bilt, The Netherlands*

Correspondence should be addressed to Maria Kanakidou, mariak@chemistry.uoc.gr

Received 16 February 2010; Revised 11 May 2010; Accepted 15 June 2010

Academic Editor: Nicholas Meskhidze



The global marine organic aerosol budget is investigated by a 3-dimensional chemistry-transport model considering recently proposed parameterisations of the primary marine organic aerosol (POA) and secondary organic aerosol (SOA) formation from the oxidation of marine volatile organic compounds. MODIS and SeaWiFS satellite data of Chlorophyll-a and ECMWF solar incoming radiation, wind speed, and temperature are driving the oceanic emissions in the model. Based on the adopted parameterisations, the SOA and the submicron POA marine sources are evaluated at about 5 Tg $yr^{-1}$ (~1.5 Tg C $yr^{-1}$) and 7 to 8 Tg $yr^{-1}$ (~4 Tg C $yr^{-1}$), respectively. The computed marine SOA originates from the dimethylsulfide oxidation (~78%), the potentially formed dialkyl amine salts (~21%), and marine hydrocarbon oxidation (~0.1%). Comparison of calculations with observations indicates an additional marine source of soluble organic carbon that could be partially encountered by marine POA chemical ageing.

## 1. Introduction

Organic aerosol (OA) attracts the attention of the scientific community due to their climate and health relevance [1–4]. Marine OA components are considered as important natural aerosol constituents, which significantly contribute to the global aerosol burden and affect Earth's climate. Observations of OA in the marine atmosphere have shown the existence of significant amounts of primary organic carbon of marine origin [5, 6] in the submicron sea-spray, as well as a small relative contribution to the coarse mode sea-spay [7], over the ocean that seem to be related with the biological activity in the ocean [8].

The ocean also emits a complex mixture of organic gases (VOC) like alkenes, dimethyl sulphide (DMS) [5, 9–11], isoprene, monoterpenes [12–15], and aliphatic amines [7]. A few decades ago, DMS emissions from the oceans have been suggested to control cloudiness in the clean marine environment via sulphate ($SO_4^=$) aerosol formation (CLAW hypothesis [16]). DMS oxidation is known to produce $SO_4^=$ and methane sulphonate ($MS^-$), both present in the aerosol phase, at proportions that depend on the meteorological conditions and oxidant levels in the marine environment [17, 18]. Vallina et al. [19] attributed between 35% and 80% of cloud condensation nuclei (CCN) in the Southern Ocean to biogenics of marine origin. They supported the

central role of biogenic DMS emissions in controlling both number and variability of CCN over the remote ocean. $MS^-$ containing both sulphur and carbon atoms is also a component of organic aerosol. Other VOCs with identified marine sources that are involved in secondary organic aerosol (SOA) formation are monoterpenes [15] and isoprene [12, 13, 20]. The marine source of monoterpenes has been recently identified [15], but this source requires further investigations for accurate evaluation of its global strength and distribution. Isoprene has been shown to produce secondary organic aerosol both via gas-phase reactions followed by gas-to-particle partitioning of its semivolatile products [21, 22] and cloud processing of organic matter [23, 24]. Isoprene, one of the most important biogenic volatile organic compound (VOC) with large terrestrial emissions ~600 Tg $yr^{-1}$ [25], has a comparatively small oceanic source that is highly uncertain and varies from 0.2–1.4 Tg $yr^{-1}$. Despite its small intensity, this source is expected to have an impact on the marine boundary layer gas-phase chemistry because of isoprene's high reactivity [26, 27].

The formation of SOA over oceans, although expected to be smaller than over land [28, 29], triggers scientific interest due to the potential involvement of SOA in the formation of clouds in the remote marine atmosphere [30] especially where aerosol levels of other components are low. Recently, several studies investigated the intensity of marine sources of OA, with estimates varying by more than an order of magnitude (2–75 Tg C $yr^{-1}$ [20, 31–34]).

In order to evaluate the marine organic aerosol contribution to the atmosphere, we used the 3-dimensional global chemistry transport model TM4-ECPL. We computed the SOA formation from marine emissions of isoprene, monoterpenes, DMS, and amines, together with the primary organic aerosol (POA) marine emissions. Both primary and secondary OA distributions are calculated online driven by wind speed, temperature, solar radiation, and ocean productivity (represented by chlorophyll-a), as well as atmospheric oxidant levels that are also calculated online [35]. Marine SOA from isoprene, monoterpenes and DMS are formed via gas phase oxidation followed by gas-to-particle conversion and via multiphase chemical processes. As summarized by Ervens et al. [24] and references therein, isoprene chemistry can form SOA via cloud processing that consists of partitioning of isoprene oxygenated products like glyoxal, methylglyoxal, and pyruvic acid to the cloud water and subsequent in cloud oxidation to form glycolic, glyoxylic and oxalic acids. These mechanisms are parameterized in our model based on the linearized relationship recently published by Ervens et al. [24] for stratiform clouds, using the cloud occurrence and lifetime, the liquid water content of clouds, isoprene concentration, and the VOC/NOx conditions in each grid and assuming one SOA product from all in-cloud reactions. The participation of aerosol water on gas-to-particle partitioning and multiphase chemistry is not taken into account in the present study. Potential contribution to SOA of amine salts produced by reactions of dimethyl and diethyl amines of marine origin with sulphuric acid is also investigated. The POA submicron marine source is parameterised in the model based on recently published parameterisations derived from experimental data [8] as described in Vignati et al. [34]. Model results are evaluated against observations in the marine environment.

## 2. Model Description

For the present study, the well documented offline chemistry-transport global model TM4 is used. The model version applied here (TM4-ECPL) contains a comprehensive gas phase chemistry as described by Myriokefalitakis et al. [35] and aerosol parameterisations from Tsigaridis et al. [36] and Tsigaridis and Kanakidou [29] with improvements as described in Section 2.3. TM4-ECPL runs on 31 vertical hybrid layers from the surface to 10 hPa and in two different horizontal resolutions, the low resolution of $4^\circ \times 6^\circ$ in latitude and longitude and the high resolution of $2^\circ \times 3^\circ$. For the present study, the low resolution version of the model with time-step of 1 hour for the chemistry calculations has been used. The model's input meteorology comes from the ECMWF (European Centre for Medium-Range Weather Forecasts) operational forecast data for the period from 2000 to 2008 and is updated every 6 hours.

A complete overview of emissions used in this study can be found in the supplemental material by Myriokefalitakis et al. [35]. Here below, we provide information on the emissions of particular interest for the present study. For the biogenic and anthropogenic VOC, nitrogen oxides ($NO_x$), carbon monoxide (CO), and all biomass burning trace gas emissions, TM4-ECPL uses the $1^\circ \times 1^\circ$ gridded emission distributions from the POET database [37] that correspond to the year 2000.

The adopted emissions of primary particles (carbonaceous aerosols, dust, and a small fraction of sulphate −2.5%) in TM4-ECPL are presented in detail in Tsigaridis et al. [36] and Tsigaridis and Kanakidou [29]. Biomass burning emissions of carbonaceous aerosols and black carbon for the respective year are adopted from the Global Fire Emissions Database version 2 [38]. Primary OA from the oceans is parameterised in the model as outlined in Section 2.2.

For most simulations performed for the present study, the sea-salt source has been calculated online driven by the ECMWF wind speed at every time-step, parameterized as suggested by Gong [39] and fitted for accumulation and coarse modes taken into account in TM4-ECPL as described in detail in Vignati et al. [34]. The thus calculated total sea-salt emissions account almost 6290 Tg $yr^{-1}$ (31 Tg $yr^{-1}$ in the fine mode) on a global basis for the year 2006, that is slightly higher than the upper limit of the IPCC-TAR fluxes of $3340 \pm 80\%$ Tg $yr^{-1}$, but lower than the AEROCOM (Aerosol Comparisons between Observations and Models) inventory of about 7925 Tg $yr^{-1}$ (96.5 Tg $yr^{-1}$ in the fine mode) for the year 2000 [40]. The AEROCOM 2000 inventory has been also used to evaluate uncertainties. Sea-salt is considered to be present in 2 modes in the online wind driven method (accumulation and coarse) and in 3 modes when using the AEROCOM inventories (Aitken, accumulation, and coarse), while dust is present in 2 modes (accumulation and coarse), which come from the AEROCOM emissions (as described in

Table 1: Annual emissions of oceanic species adopted in the model.

| Oceanic tracer | Emissions ($Tg\,yr^{-1}$) |
|---|---|
| Isoprene | 1.0 |
| Monoterpenes | 0.2 |
| POA | 7-8* |
| DMS | 19.5** |
| $C_2H_2$ | 1.0 |
| $C_2H_4$ | 1.2 |
| $C_3H_6$ | 1.3 |
| $C_3H_8$ | 1.1 |
| Sea-Salt | 6290* |
| Amines | 0.8# |

* Calculated by the model for 2006; ** Tg S $yr^{-1}$; # Tg N $yr^{-1}$.

Tsigaridis et al. [36]) updated to interannual dust inventory for the years 2000–2007. All other aerosol components are considered to be present in the accumulation mode only.

*2.1. VOC Marine Emissions.* Annual mean distribution of light alkenes marine emissions (Table 1) are taken from POET database in 1°× 1° grid [37]. DMS, isoprene, and monoterpenes oceanic emissions, which are of particular interest for the present study as secondary sources of OA in the marine environment, are parameterized interactively as a product of piston velocity and surface seawater concentration. Piston velocity is calculated as a function of wind speed, temperature and the Schmidt number [45]. DMS surface seawater concentration distribution is taken from Kettle et al. [11]. For isoprene and monoterpenes their surface seawater distributions are assumed proportional to the product of chlorophyll-a (Chl-a) distribution and the logarithm of the square of the incoming solar radiation at the earth's surface. The incoming solar radiation at surface is taken from the ECMWF data and is used as substitute for the ambient light intensity that has been suggested by Gantt et al. [20] to drive the isoprene emission rates in the marine environment. However, our approach does not account for different phytoplankton groups that have been shown to produce biogenic volatile organic compounds at different rates [13–15, 20]. Chl-a is taken from observations by the satellite-based sensors moderate resolution imaging spectroradiometer (MODIS) (Figure 1) and sea-viewing wide field-of-view sensor (SeaWiFS). SeaWiFS and MODIS global monthly data products have been generated by the NASA ocean biology processing group (OBPG) and ingested into the GES-DISC interactive online visualization and analysis infrastructure (Giovanni) system, developed by the Goddard Earth Sciences Data and Information Services Center (GES DISC/DAAC) [46]. There are missing data in the MODIS/SeaWifs Chl-a daily products on high spatial resolution (9 km × 9 km) that have been neglected when producing the 1°× 1° monthly product. The 1°× 1° daily products have been produced as the composite of the high resolution daily 9 km × 9 km data. They have been further averaged over a calendar month to provide the monthly data at 1°× 1° on a global scale [47, 48]. Absence of data at the 1° × 1° monthly constructed database, as is the case for polar regions, is translated by the model to absence of chl-a in the corresponding model grid. The thus derived substitute of the isoprene emissions is scaled to the global value of 1 Tg $yr^{-1}$ for the year 2006 that is a central in the range of published global marine isoprene source estimates ([12, 13, 20] and references therein). The distribution of isoprene emission rates in the model is depicted in Figures 1(c) and 1(d). Driven by wind speed, Chl-a and solar incoming radiation, isoprene emissions in TM4-ECPL show high levels in the extratropics and particularly during summer-time as well as in the tropical region where incoming solar radiation maximizes. This pattern is similar with the more accurate computations by Gantt et al. [20]. Based on the measured emission rates from various studied phytoplankton species of monoterpenes (0.3 to 225.9 nmol g-$[Chl\text{-}a]^{-1}$ $day^{-1}$ [15]) and of isoprene (1.21–9.66 $\mu$mol g-$[Chl\text{-}a]^{-1}$ $day^{-1}$ [13] or even up to 24 $\mu$mol g-$[Chl\text{-}a]^{-1}$ $day^{-1}$, measured for diatoms at high light intensity [20]), annual global marine emissions of monoterpenes of up to 0.4 $Tg\,yr^{-1}$ are derived. In the present study 0.2 $Tg\,yr^{-1}$ of monoterpenes marine emissions have been adopted and distributed as those of isoprene.

Observations in the marine environment indicate that dimethyl and diethyl ammonium salts of biogenic origin are present in the marine OA and could account for about 20% of the observed nitrogen in the inorganic form of ammonium [7]. On the other hand, Gibb et al. [49] evaluated a net flux of methylamines from the atmosphere into the sea water in the NW Arabian Sea based on atmospheric and sea water observations. They mentioned, however, that this observation should not be extrapolated to the global ocean. Therefore, in the present study, we also explore the amines contribution to the marine SOA. For this, amines emissions are arbitrary taken to about one tenth of the ammonia emissions from the oceans as distributed in the GEIA database (http://www.mnp.nl/geia/data/Ammonia/ [50]). Thus, the marine amines emissions of 0.8 TgN $yr^{-1}$ are adopted for this explorative simulation.

*2.2. Primary Marine Organic Aerosol Emissions.* The oceanic source of primary submicron OA has been calculated based on the parameterisation proposed by O'Dowd et al. [8] and updated by Vignati et al. [34] that provides the POA as a mass fraction of the submicron sea-salt aerosol source, based on the surface ocean Chl-a.

In the present study, the monthly average oceanic Chl-a concentrations are derived from satellite-based MODIS observations in 1° × 1° horizontal grid resolution (Figures 1(a) and 1(b) for two different seasons). Alternatively, we calculated this fraction based on SeaWiFS Chl-a product as in Vignati et al. [34]. Sea-salt emissions are parameterized as detailed in Vignati et al. [34] accounting for particles radius increases with Chl-a due to added organic material from the oceans.

In TM4-ECPL, marine submicron POA is considered to be emitted entirely as insoluble but internally mixed with sea-salt as determined by O'Dowd et al. [8], in contrast to terrestrial POA from combustion and fossil fuel sources that

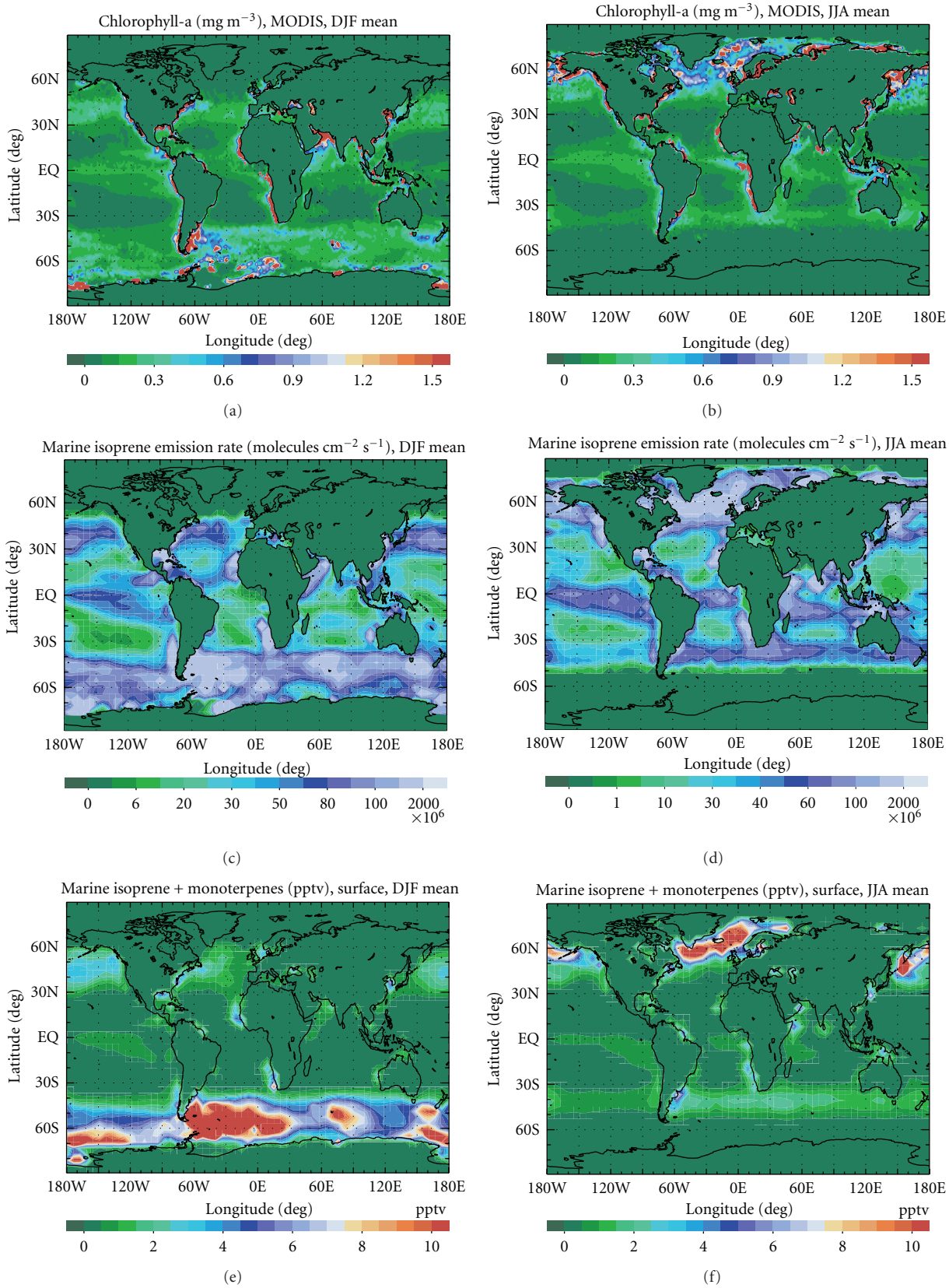


Figure 1: Seasonal mean surface distribution of Chl-a in mg m$^{-3}$ as retrieved from MODIS (see text) (a) for DJF and (b) for JJA; Marine isoprene emission rate in molecule cm$^{-2}$ s$^{-1}$ (c) for DJF (d) for JJA; Sum of marine isoprene and monoterpenes concentrations in pptv computed by the model (e) for DJF and (f) for JJA; for the year 2006.

are considered to be emitted by 50% as hydrophilic [51]. Ageing of insoluble POA of continental origin is taken into account as described by Tsigaridis and Kanakidou [28] and corresponds to a global mean turnover time of about 1 day. Finally, based on Facchini et al. [52], we adopted coarse mode marine POA source as suggested by Gantt et al. [20].

*2.3. Secondary Organic Aerosol Formation Pathways Considered in the Model.* TM4-ECPL considers sulphur and ammonia chemistry and the oxidation of $C_1$–$C_5$ volatile organic compounds (VOC) including isoprene, glyoxal as well as a highly simplified terpenes and aromatic chemistry, described in detail by Myriokefalitakis et al. [35]. All major aerosol components including secondary ones (sulphate, nitrates, methane sulphonate, and other organics) are computed online together with the gas-phase chemistry and aerosol associated water; details are given in Tsigaridis et al. [36] and references therein.

Compared to earlier OA modelling studies [13, 32, 33], the marine POA and SOA are calculated at every model time-step. Precisely, marine SOA is produced from the oxidation of isoprene and monoterpenes of marine origin and from DMS oxidation by hydroxyl radicals (with methanesulfonate ($MS^-$) being a minor oxidation product). A potential reaction of amines of marine origin with sulphuric acid [7, 53] has been also investigated. Thus, for isoprene and DMS, explicit oxidation schemes are considered in TM4-ECPL that affect oxidants and organic compound levels at every model time-step. $MS^-$, that is also a SOA component, is considered to be produced via both gas and aqueous phase reactions based on the parameterisation of Mihalopoulos et al. [54].

For the SOA formation from isoprene and monoterpenes, the gas-phase oxidation two-product model has been adopted. In addition to the earlier studies by Tsigaridis and Kanakidou [29] and references therein, the applied updated SOA two-product yield parameterisation also accounts for the NOx-dependent SOA formation from isoprene oxidation. This parameterisation is based on VOC/NOx threshold values proposed in literature as indicated in Table 3 together with the input parameters adopted for these parameterisations. This approach for simplification purposes assumes that only hydrogen peroxy ($HO_2$)/organic peroxy ($RO_2$) or NO reactions occur depending on the VOC/NOx ratio [55]. Unpublished results by Tsigaridis and coworkers indicate that an overestimate by less than 10% in the low $NO_x$ environment, as is the case of the marine atmosphere, is associated with this approach. In the model, isoprene is also considered to produce SOA via cloud processing, parameterized based on the linearised relationship recently published by Ervens et al. [24] for stratiform clouds.

Finally, in an explorative simulation on the role of amines, biogenic marine amines are represented in the model by one gas-phase surrogate species considered to be a 50 : 50 mixture of dimethyl and diethyl amines with average properties. For simplicity, their oxidation by OH radical is assumed to produce only gas phase products, namely formic and acetic acids, formaldehyde, and acetaldehyde and to proceed with a rate of $K_{OH} = 3.5\times10^{-12}$ molecules$^{-1}$ cm$^3$ s$^{-1}$ (mean between ethylamine and dimethylamine reaction rates with OH radical [49, 64]). Also, for simplicity, reactions with $O_3$ which are at least 5 times less effective than those with OH in removing dimethyl amine from the gas phase have been neglected here. This assumption can lead to less than 20% overestimate of the importance of the amines reactions with OH radical. In the absence of available kinetic and thermodynamic data [7], dialkyl amines uptake on sulphate aerosol is assumed to proceed similarly to ammonia. Note that recently amines of biogenic origin in the nucleation mode in the marine environment have been suggested to enhance sulphuric acid water nucleation by Kurtén et al. [65]. Although largely uncertain, our simulations will provide a first estimate of the order of magnitude of the levels of the potentially formed amine salts that are here represented by one particulate phase surrogate species. SOA formation in the troposphere from other amine oxidation pathways [53] has been neglected in the present study. A Henry law coefficient of 39 M atm$^{-1}$ given by Sander [66] for diethylamine has been adopted.

*2.4. The Simulations.* In order to investigate the oceanic source of OA and especially the distribution and global budget of secondary and primary components, we performed various TM4-ECPL simulations. The two simulations discussed here are Simulation S1 and Simulation S2.

Simulation S1, used as the base case, accounts for marine SOA formation from isoprene, monoterpenes and DMS oxidation and tentatively by amines reactions with sulphuric acid as described in Section 2.3. The levels of each marine SOA component are individually computed and stored to allow detailed SOA budget analysis. The model also takes into account Chl-a monthly distributions from MODIS retrievals and computes on line the sea-salt emissions in the accumulation and coarse modes and POA marine emissions in the sub micron mode as a fraction [34] of sea-salt emissions in the accumulation mode. Simulation S1 has been performed for the period 2000–2008.

Simulation S2 is as S1, but it is based on monthly distributions of Chl-a from SeaWiFS retrievals and is used to evaluate uncertainties associated in the OA submicron source with the adopted Chl-a retrievals. This simulation has been performed for 2006.

## 3. Results and Discussion

*3.1. Global Distributions and Seasonal Variability.* The computed global distributions of marine POA, SOA from marine isoprene and monoterpenes, $MS^-$ from DMS oxidation and potentially formed amine sulfates are calculated by TM4-ECPL every time-step, monthly mean values are stored and analyzed here below. The annual mean surface distributions of the respective marine OA components for the first model level (simulation S1) for the year 2006 are shown in Figures 2(c)–2(g) together with the sea-salt distribution in the accumulation mode (Figure 2(b)). The computed annual mean distribution of the fraction of marine POA (%OA)

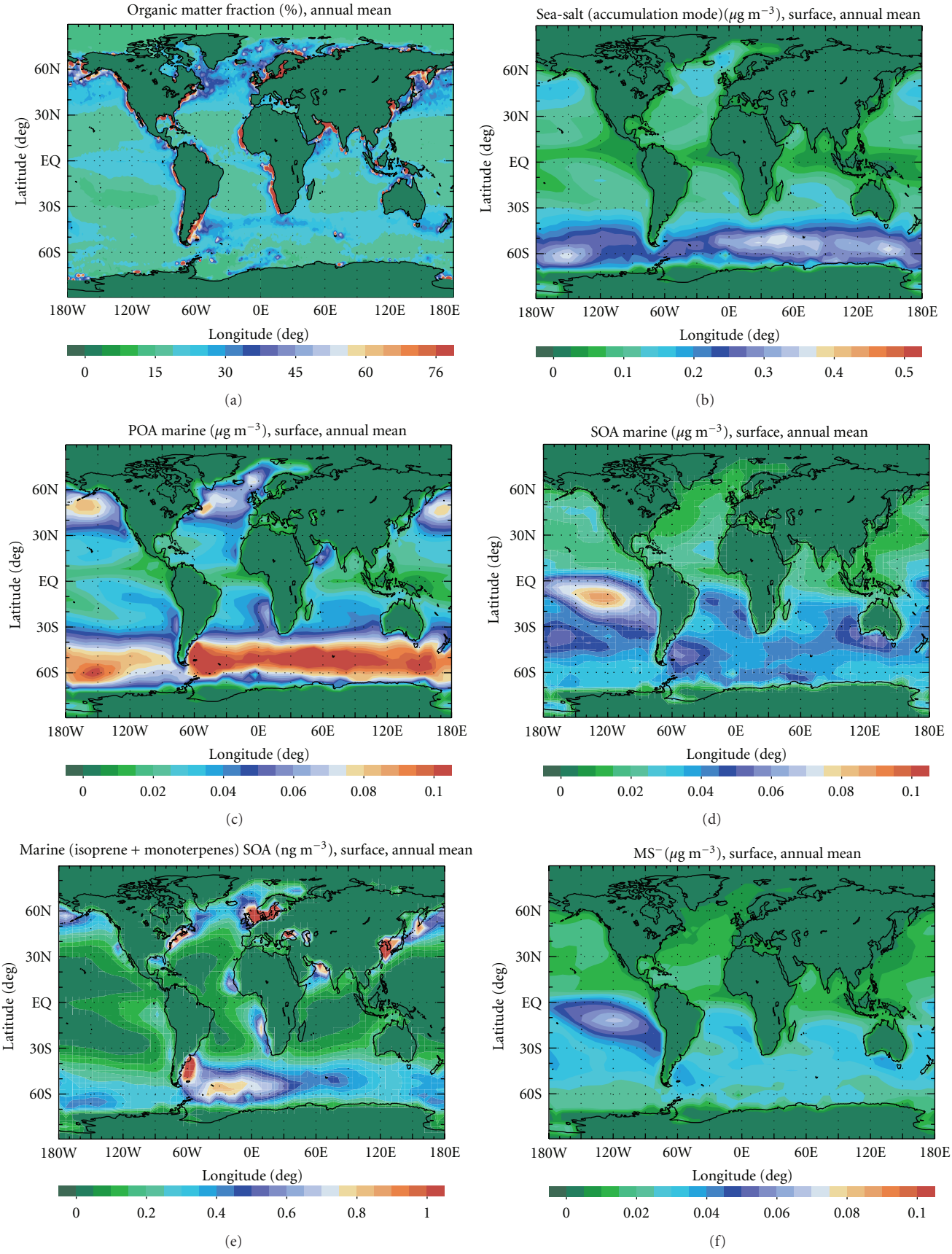


Figure 2: Continued.

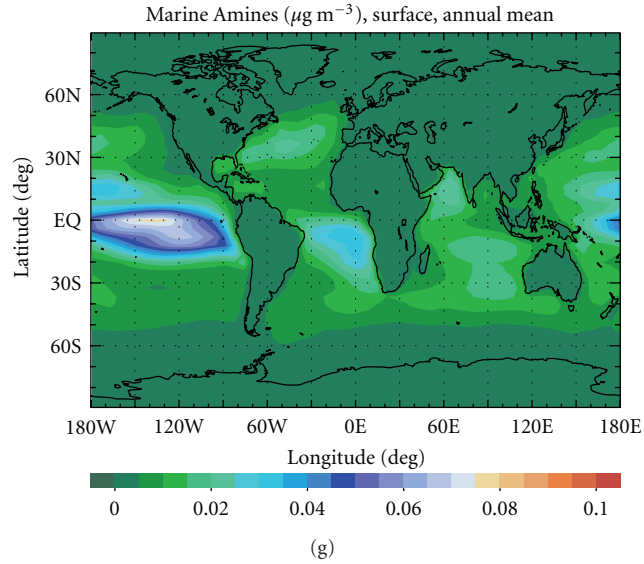


Figure 2: Annual mean surface distributions of (a) mass fraction of Marine OA to submicron sea-spray aerosol (in percent) calculated based on Chl-a as described by Vignati et al. [34]; (b) sea-salt in the accumulation mode; (c) Marine POA; (d) total marine SOA (from $MS^{-}$, isoprene and monoterpenes); (e) SOA from marine isoprene and monoterpenes; (f) SOA from $MS^{-}$, (g) SOA from marine Amines. Aerosol components are given in $\mu$g m$^{-3}$, except for SOA from marine isoprene and monoterpenes which is given in ng m$^{-3}$.

Table 2: Isoprene and monoterpene surface concentrations (in pptv) in the marine boundary layer Comparison between observations and TM4-ECPL monthly mean model results in the corresponding 4° × 6° (latitude × longitude) model grid.

| Location | Month | Model (pptv) | Observations (pptv) | Reference |
|---|---|---|---|---|
| | | Isoprene | | |
| N. Atlantic Ocean | Jul. 2004 | 0.06 | 2.8 ± 0.8 | [56] |
| Norwegian Sea | Aug. 1999 | 2.4 | 1.9 ± 0.8 | [57] |
| NW Pacific Ocean | May 2001 | 2.5 | 7.2–110 | [58] |
| Indian Ocean (50°S–20°S & 50°E–80°E) | Dec. 2004 | 2–9 | 20–340 | [59] |
| Southern Ocean* (69°S, 39°35′E–45°S, 105°E) | Dec. 1997 | 1.4 | 13 (< 0.1–57) | [60] |
| Straits of Florida (24°N, 80°W) | Sep. 1993 | 127 | 5–11 | [61] |
| Hao atoll (18°S, 140°W) | Jun. 1990 | 0.6 | <2 | [12] |
| Syowa Station (69°00′S, 39°35′E) | Dec. 1997 | 0.2 | 0.1–57 | [60] |
| Southern Ocean | Jan.-Feb. 2007 | 10.4 | 26–187* | [15] |
| | | Monoterpenes | | |
| Southern Ocean | Jan.-Feb. 2007 | 1.4 ± 0.9 | 5 − 125* | [15] |
| Indian Ocean (50°S–20°S & 50°E–80°E) | Dec. 2004 | 23 | 56 ± 20 | [59] |

* Range of average observations for far away before the bloom and in situ bloom cases, 35°49′ S, 20°22′ E to 52°17′ S, 67°73′W.

associated with the submicron sea-salt aerosol is depicted in Figure 2(a) and maximizes near the coasts at upwelling areas as well as in the north and south Atlantic midlatitudes and in the southern Indian Ocean. The marine POA submicron source distribution (Figure 2(c)) is the product of the distributions of submicron sea-salt (Figure 2(b)) and of %OA fraction. Whereas the marine submicron POA maximizes over the oceans in the 30°–60° latitude band in both hemispheres with the highest levels calculated for the southern hemisphere, SOA from isoprene and monoterpenes exhibit high levels in the high productivity regions mainly in the northern hemisphere and at the south east coast of South America as well as secondary marine maxima in the southern tropics. It is worth mentioning that the few pptv isoprene calculated by the model for the remote marine boundary layer are close to the low values of the observations summarized in Table 2. The concentrations of isoprene reflect its emission distribution and its oxidation by hydroxyl and nitrate radicals and ozone. Thus, they maximize over the extra-tropical oceans (Figures 1(e) and 1(f)) and present secondary maxima over the tropics in areas of relatively high Chl-a exposed to intensive incoming solar radiation. The monthly mean calculated marine isoprene concentrations near the surface are in general lower than the observed levels that correspond to a short (a few minutes to <1 h) daytime period (Table 2), like for instance the

Table 3: Properties of the SOA species used by the two-product model for SOA formation.

| [1]$SOA_i$ | $\alpha_i$ | $K_i$ ($m^3\,\mu g^{-1}$) | $\Delta H$ ($kJ\ mol^{-1}$) | Reference |
|---|---|---|---|---|
| isoprene-p1N | 0.0021 | 1.6200 | 42 | [22] |
| isoprene-p2N | 0.4975 | 0.0086 | 42 | [22] |
| isoprene-p1H | 0.0288 | 1.6200 | 42 | [22] |
| isoprene-p2H | 0.2320 | 0.0086 | 42 | [22] |
| a-pinene-p1N | 0.0138 | 0.0637 | 38 | [62] |
| a-pinene-p2N | 0.4610 | 0.0026 | 38 | [62] |
| a-pinene-p1H | 0.1920 | 0.0637 | 38 | [62] |
| a-pinene-p2H | 0.2150 | 0.0026 | 38 | [62] |
| b-pinene-p1N | 0.0260 | 0.1950 | 40 | [62] |
| b-pinene-p2N | 0.4580 | 0.0030 | 40 | [62] |
| b-pinene-p1H | 0.3617 | 0.1950 | 40 | [62] |
| b-pinene-p2H | 0.2262 | 0.0030 | 40 | [62] |
| toluene-p1N | 0.0348 | 0.0403 | 40 | [63] |
| toluene-p2N | 0.1178 | 0.0010 | 40 | [63] |
| toluene-p1H | 0.0710 | 0.0530 | 40 | [63] |
| toluene-p2H | 0.1380 | 0.0019 | 40 | [63] |
| xylene-p1N | 0.0240 | 0.2290 | 60 | [63] |
| xylene-p2N | 0.1520 | 0.0040 | 60 | [63] |
| xylene-p1H | 0.0490 | 0.3010 | 60 | [63] |
| xylene-p2H | 0.1780 | 0.0080 | 60 | [63] |

[1] Nomenclature of species was chosen as follows: first 3 or 4 capital letters denote the parent VOC. The letter "p", followed by the number 1 or 2, denotes the product number. In case there is an additional letter "N" or "H", it denotes formation under low and high VOC/NOx ratio conditions, respectively. For the intermediate case of aromatic oxidation (5.5 < VOC/NOx < 8 in ppbC/ppb; [63]), the average parameters of high-to-low VOC/NOx were used.

100–200 pptv observed in the Indian Ocean during summer by Colomb et al. [59]. Differences between model results and observations like those shown in Table 2 are expected and justified both by the low spatial resolution of our model as well as the expected high temporal and spatial variability of isoprene and monoterpenes concentrations in the marine environment.

$MS^-$ shows a smoother geographical distribution with high levels all over the southern ocean and a regional maximum in the tropical Pacific. The highest levels of amine sulphates, tentatively calculated, seem to occur over the tropical oceans (Figure 2(g)) following the adopted ocean emission distribution of gaseous amines and the surface concentrations of sulphuric acid.

Figures 3(a), 3(b), 3(c), and 3(d) depict the seasonality of marine POA and SOA (excluding the amine salt contribution), respectively, as calculated by the model for simulation S1. Both primary and secondary OA sources are computed to exhibit a strong seasonality driven by biological activity, represented in the model by Chl-a, and wind speed (both for SOA and POA) as well as surface solar radiation, temperature and oxidant levels (for SOA). In Figures 3(e) and 3(f), the fraction of marine OA to the marine submicron aerosol mass is depicted and indicates contributions of at least 10% over the oceans that maximise in the tropics to about 20%–25% (attributed to the SOA patterns) and in the extratropical oceans with more than 50% contribution mainly attributed to the marine POA. As expected, the OA contribution to the sub micron marine aerosol exhibits large seasonal patterns in the extra tropical areas.

The relative importance between primary and secondary marine submicron OA source can be seen from Figures 4(a) and 4(b) that depict the contribution of marine POA and marine SOA to the marine OA (sum of the two components), respectively, on an annual mean basis. These figures clearly demonstrate the dominance of SOA in the tropics compared to the POA that dominates the marine OA in the extra-tropical oceans.

The ratio of marine OA to total (marine and terrestrial) OA at surface is depicted in Figure 4(c). According to TM4-ECPL model calculations, marine OA is a significant fraction of surface OA concentrations over the oceans with the greatest contribution to the total OA load in the North Atlantic, North Pacific, and the Southern Ocean (between 30° and 60°S). At this latitude zone, marine SOA is also the major component of total SOA (Figure 4(d)). Regions of continental outflow are subject to less than 40% marine contribution to the total OA whereas in the Southern Ocean's this fraction reaches 90%. The relative importance of marine OA to the other marine fine aerosol components, the sea-salt in the accumulation mode and the marine sulphate are depicted in Figures 4(e) and 4(f), respectively. These figures indicate the dominance of marine SOA over the sea-salt submicron aerosol in the tropics and that of marine POA over sulphate aerosol in the extratropical oceanic regions.

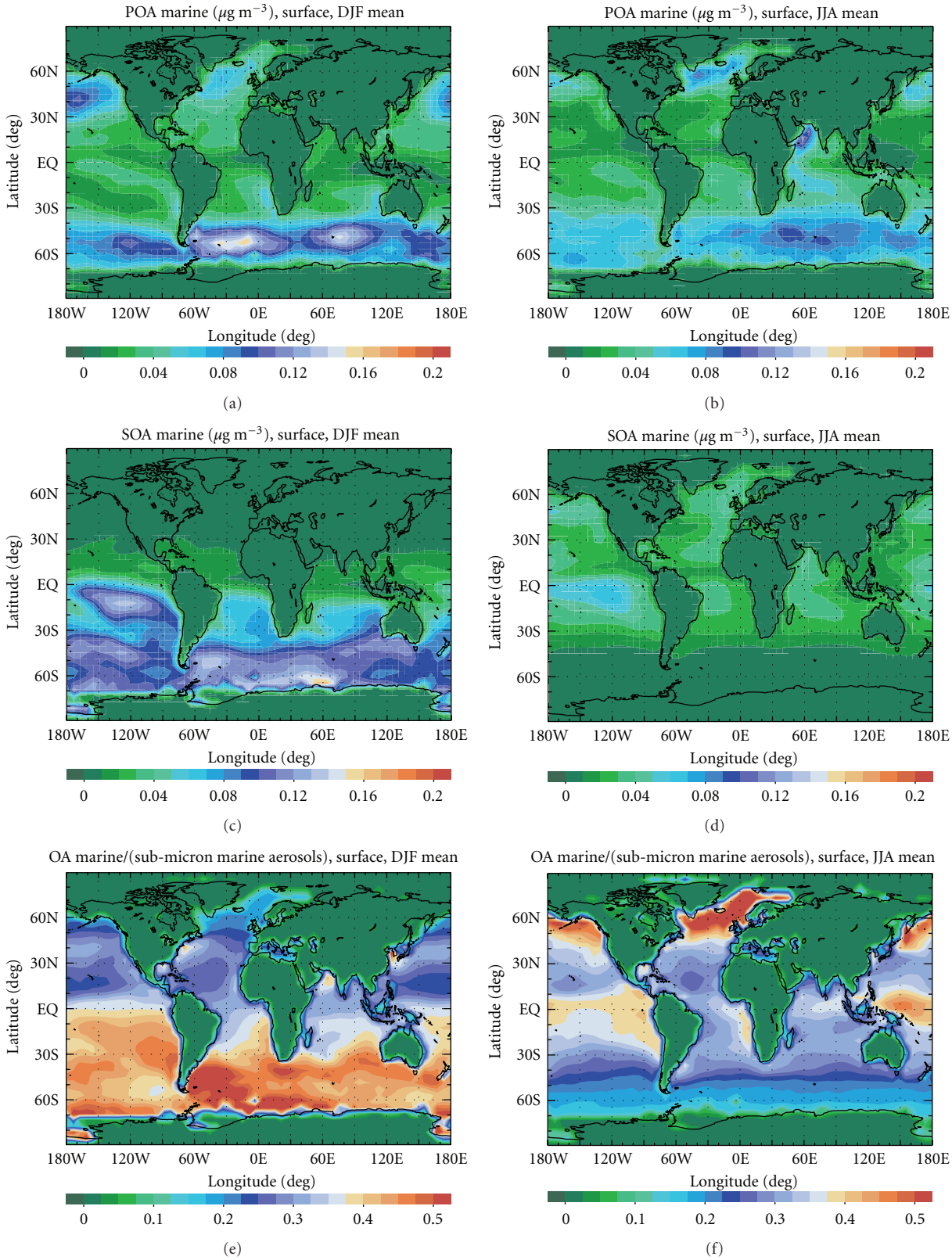


Figure 3: Calculated mean surface distributions for S1 of ((a), (b)) marine submicron POA ((c), (d)) marine SOA in $\mu$g m$^{-3}$; ((e), (f)) mass ratio of marine OA (POA+SOA) to marine sub micron aerosol (sum of OA, $SO_4^=$ and sea-salt in the accumulation mode) for DJF ((a), (b), and (c)) and JJA ((b), (d), and (f)) 2006.

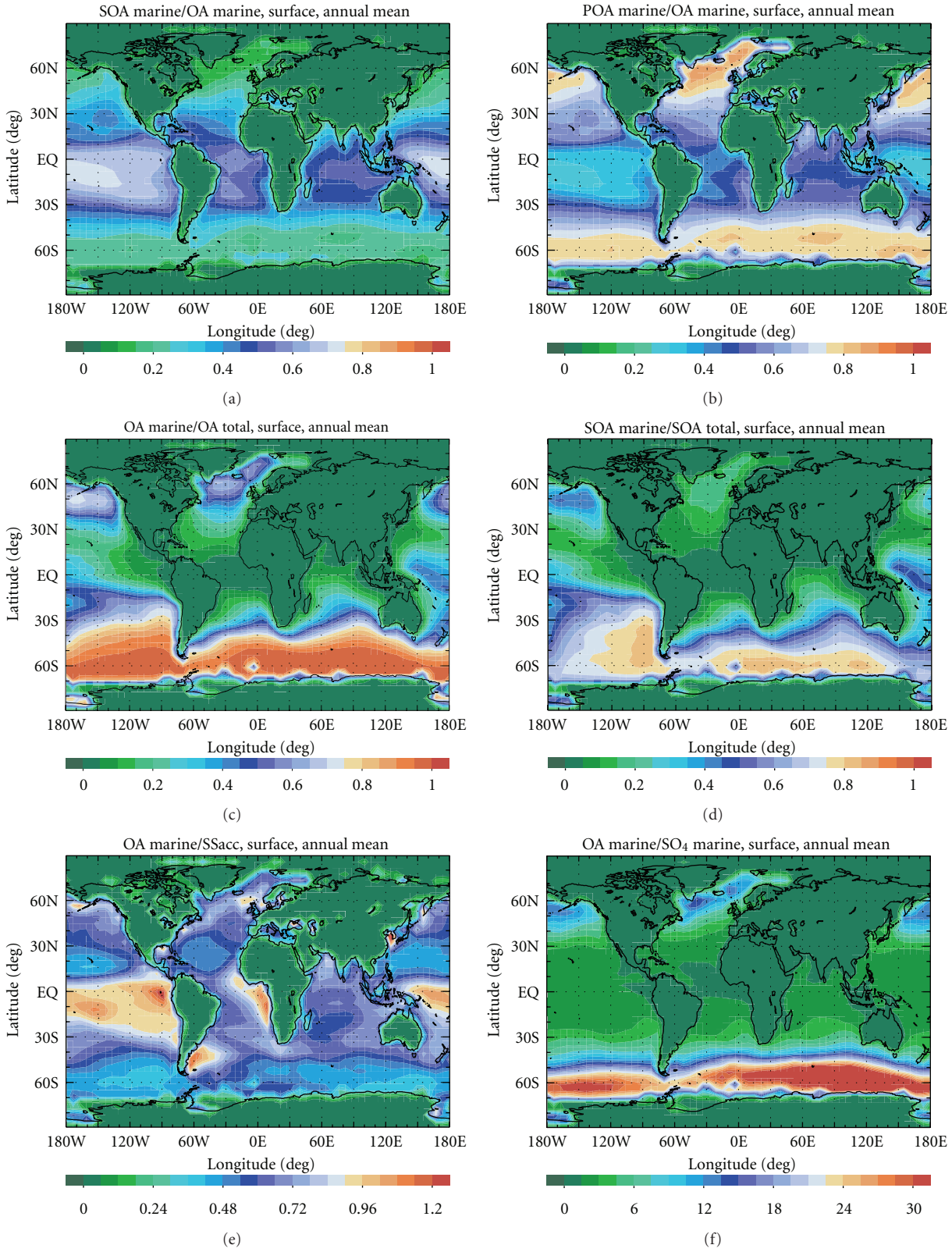


Figure 4: Calculated mean fraction of (a) marine SOA to total marine OA, (b) marine POA to total marine OA, (c) marine OA to total OA, (d) marine SOA to total SOA, (e) marine OA to sea-salt in the accumulation mode, (f) marine OA to marine sulphate. For clarity values over entirely land covered model grids have been omitted.

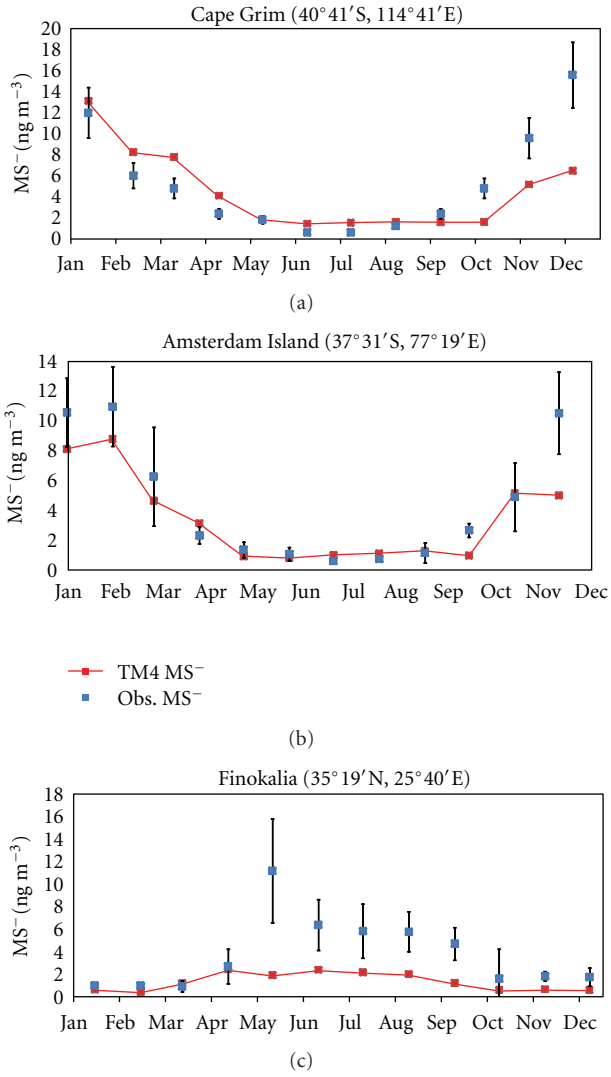


FIGURE 5: Comparison of methanesulphonate ($MS^-$) observations with model results. Observed (filled squares with standard deviation bars) and model $MS^-$ (solid line red squares) at: (a) Cape Grim (40°41′S, 114°41′E; [17]) (b) Amsterdam Island (37°31′S, 77°19′E; [41]), (c) Finokalia (35°19′N, 25°40′ E; [42]). All values are in ng $m^{-3}$.

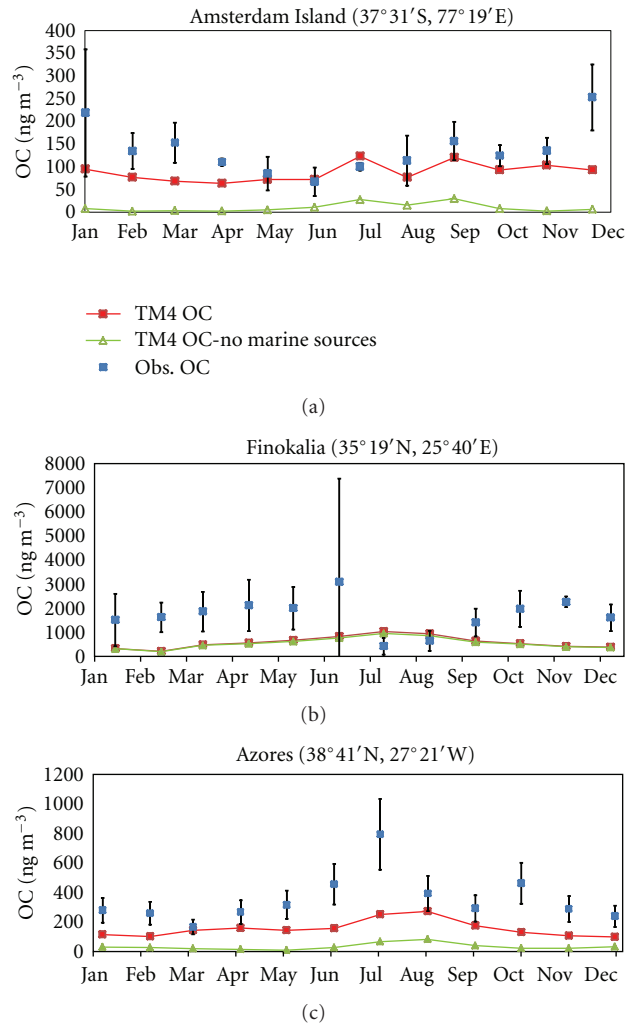


FIGURE 6: Comparison of particulate Organic Carbon (OC) observations with model results. Observed OC (blue squares with standard deviation bars), modelled OC-S1 accounting for the oceanic sources of OA (red line—squares), and neglecting the marine OA sources (green line—triangles) at marine locations. (a) Amsterdam Island (37°31′S, 77°19′E; [41]) and (b) Finokalia (35°19′N, 25°40′E; [42] and [43]), (c) Azores (38°41′N, 27°21′W; from Pio et al. [44]. All values are in ng $m^{-3}$.

*3.2. Comparison of Aerosol Simulations with Observations.* Model results are compared with few recent observations of organic aerosol and particulate $MS^-$ over oceanic locations available in literature.

Figure 5 depicts the comparison between model results and observed annual cycle of $MS^-$. TM4-ECPL is able to reasonably simulate concentrations and seasonal variation of $MS^-$ at these oceanic locations. The concentrations of $MS^-$ show strong seasonal dependence with the maximum values of $MS^-$ observed during the warm season. At Amsterdam Island [41] and Cape Grim [17] sites, both of them located in the South Hemisphere, the maximum $MS^-$ concentrations are observed and calculated during December to February (~12 ng $cm^{-3}$ in February and ~16 ng $cm^{-3}$ in December, respectively). At Finokalia station located in the eastern Mediterranean the maximum concentrations are observed [42] and calculated during May and October (with maximum value of ~14 ng $cm^{-3}$), when the oxidation of $MS^-$ precursors (DMSO, gaseous MSA, DMS) by OH radicals in the aqueous phase is significant and wet removal is low. Comparing Figures 5(b) and 7(a), it appears that $MS^-$ contributes less than 15% to the observed WSOC in the remote marine atmosphere.

Figure 6 compares the observed concentrations of organic aerosols with model results from simulation S1 (all sources) when the oceanic components of OA are neglected. TM4-ECPL underpredicts the observed OC concentrations at various oceanic stations (see figure caption for details). At these sites the highest concentrations are observed during summer, but the model best simulates the OC concentrations

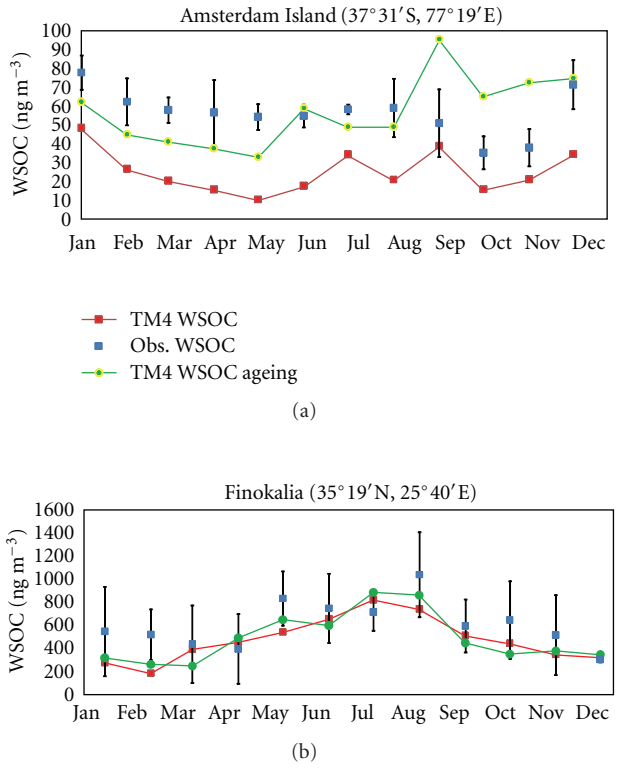


Figure 7: Comparison of water-soluble organic carbon (WSOC) observations with model results. Observed WSOC (blue squares with standard deviation bars) and modelled WSOC-S1 (red line—squares) and WSOC when ageing of marine POA is taken into account (circles and green line) at (a) Amsterdam Island (37°31′S, 77°19′E) [41] and (b) Finokalia (35°19′N, 25°40′ E) [42]. All values are in ng m$^{-3}$.

during winter. In order to investigate the uncertainties of marine sources on OC concentrations, the measured values are compared with the OC concentrations computed when accounting and when neglecting the oceanic source of OA. Based on these comparisons, among the studied locations, Amsterdam Island is the station the most affected by the marine OA source (Figure 6(a)). We find that a wintertime mean background level of about 25 ng cm$^{-3}$ of OC at Amsterdam island can be attributed to other sources of OC than the ocean that corresponds to about 10% of the total OA in agreement with our calculations depicted in Figure 4. Note, however, that Amsterdam Island is located at the north edge of a highly biologically active zone over the Southern Ocean. The underestimation of OC concentrations by the model might be associated either with the coarse resolution of the model that prohibits accounting for the sharp latitudinal gradients in the biological activity in the surrounding area or with a possible underestimation of marine sources associated with the specific phytoplankton species distribution. The contribution of the various SOA components (from isoprene and monoterpenes, MS$^-$ and amine salts) that are part of the water soluble organic carbon (WSOC) has been further investigated for this location. Figure 7 compares the WSOC observations with TM4-ECPL model results. It appears that although the model simulates reasonably well the observations of OC at Amsterdam island (Figure 6(a)), the model underestimate WSOC observations at this remote ocean monitoring station as shown in Figure 7(a). This could indicate a potentially missing marine source of WSOC in our model. This is not the case for the remote coastal monitoring station of Finokalia in the Mediterranean (Figure 7(b)) where model results compare well with observations, indicating that for continentally affected marine locations the model captures well the WSOC since any potentially missing marine sources of WSOC would be minor contributors to the observed WSOC. To further investigate potentially missing formation pathways for WSOC, we have performed an additional simulation considering that the marine POA is subject to chemical ageing as in the case of anthropogenic POA [28], converted thus to WSOC. Because marine POA is associated with the short lived sea-salt aerosol and thus experiences a short lifetime, this conversion is not expected to significantly affect total marine OA but mainly increase WSOC levels. Indeed, as shown in Figure 7(a) for Amsterdam island, observed and modeled WSOC agree reasonably well when ageing of marine POA is taken into account. These results point to the chemical ageing of marine POA as a significant source of WSOC in the remote marine atmosphere.

The model aerosol optical depth (AOD) derived as explained in Tsigaridis et al. [36] has been confronted with MODIS retrievals for AOD in the fine mode. The selected oceanic regions for this comparison are shown in Figure 8(a) and the annual mean computed AOD are compared with the MODIS AOD in Figure 8(b). On average, the model AOD distribution presents similar pattern with the MODIS retrievals except over the Pacific tropical oceanic regions (30° N–30° S) where the model underestimates the fine fraction of AOD by a factor of 2. This underestimate over the tropical Pacific Ocean might be related to missing secondary organic aerosol sources in our model. Indeed, as shown in Figures 3(e) and 3(f) organic aerosols tend to significantly contribute to fine aerosol values over these marine regions. Furthermore, Figure 4 shows that the major contribution of marine SOA (Figure 4(a)) is at the tropic regions (30° N–30° S) and that of marine POA (Figure 4(b)) in the extratropics.

In addition to the direct interactions with radiation, aerosols affect climate via their impact on CCN. CCN activity is characterised by the critical size to which a particle activates and depends among other on the mass of the particle that affects its size, on the hygroscopicity and the surface tension of its components. Thus, OA mass of marine origin, if not contributing to new nuclei as suggested by Kurtén et al. [65] for amine salts, will increase the existing submicron particles helping them to reach a critical size faster than in the absence of these OA. In this respect, the insoluble organic fraction of the aerosol is expected to provide droplet growth kinetic delays [67] whereas the water soluble organic mass is behaving approximately similar to sulphate aerosols.

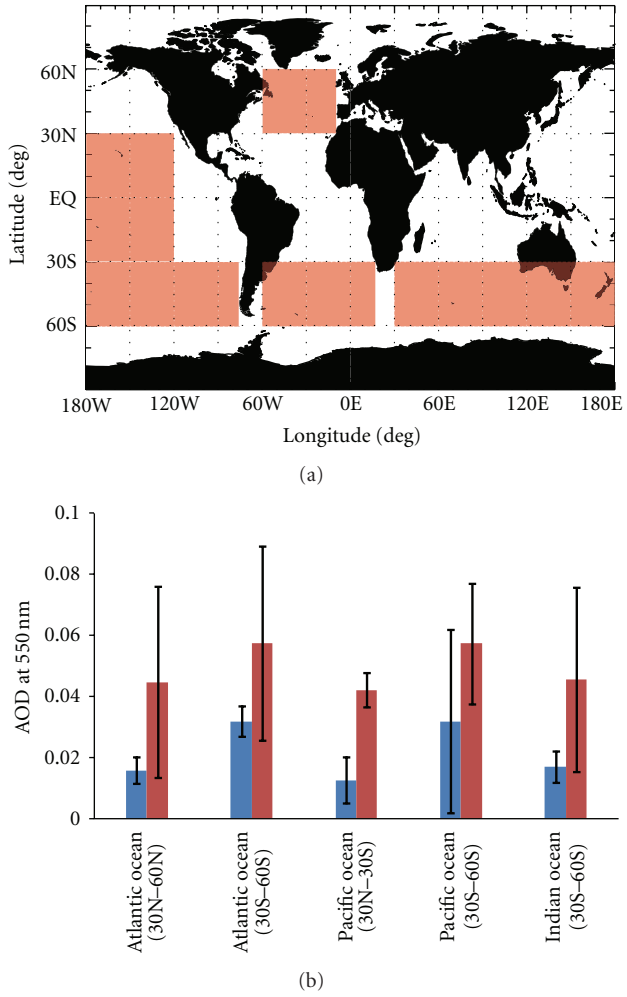


Figure 8: Comparison of MODIS AOD retrievals with model results. Retrieved MODIS AOD (red bars), modeled total AOD-S1 (blue bars), at selected marine locations: Atlantic Ocean (60 N,60 W–0 N,10 W), Atlantic Ocean (30 S,60 W–60 S,15 E), Pacific Ocean (30 S,180 W–60 S,75 W), Pacific Ocean (30 N,180 W–30 S,120 W) and Indian Ocean (30 S,30 E–60 S,180 E).

*3.3. Budget Calculations.* Based on the adopted parameterizations of marine sources of DMS, marine amines, isoprene and monoterpenes emissions as well as the parameterizations of SOA formation from the oxidation of these marine precursors TM4-ECPL evaluates the marine SOA global annual chemical production at about 5.1 Tg $yr^{-1}$. Approximately, 0.1 Tg $yr^{-1}$ originate from oceanic monoterpenes and isoprene oxidation, 4.0 Tg $yr^{-1}$ from $MS^{-}$ and 1.0 Tg $yr^{-1}$ in case of from marine amines when they are taken into account for SOA production. Marine SOA is removed via dry and wet deposition. As a result the global annual burden on marine SOA in the model domain equals about 0.06 Tg $yr^{-1}$ for SOA mainly (78%) from $MS^{-}$.

The global annual oceanic POA emissions in the accumulation mode are calculated to be 7 Tg $yr^{-1}$ based on MODIS Chl-a retrievals for the year 2006. By adopting Chl-a distribution retrieved from SeaWiFS observations in the model leads to about 1 Tg $yr^{-1}$ higher marine source of POA than estimated based on the MODIS Chl-a retrievals. As discussed in Vignati et al. [34] the calculated POA marine emissions are associated with an uncertainty of about a factor of 4, mainly attributed to that in the submicron sea-salt emissions. In addition, at least an overall 45% of uncertainty is associated with low spatial resolution estimates of POA source; the low resolution always overestimates the POA source compared to the high resolution simulation. Comparison of model results with observations indicates an additional marine source of soluble organic carbon that could be partially encountered by marine POA chemical ageing.

A large fraction of oceanic OA is removed from the atmosphere through wet (9.7 Tg $yr^{-1}$) and dry (2.4 Tg $yr^{-1}$) deposition. A small fraction of marine sub-micron POA is also removed via sedimentation, following the fate of sea-salt aerosols. The global annual burden of marine OA equals 0.12 Tg with a lifetime of about 4 days. Note, however, that the model POA emissions from terrestrial sources in the model domain, amount 42 Tg $yr^{-1}$ for the year 2006. That is about 8 times higher than the marine sources estimated in the present study. Moreover, the SOA formation from terrestrial sources in the model domain amounts about 42 Tg $yr^{-1}$, which is about 8 times higher than marine SOA production.

## 4. Conclusions

The global 3-dimensional chemistry/transport model TM4-ECPL has been adapted to simulate the temporal and spatial distribution of primary and secondary marine organic aerosols. The annual global source of marine SOA is estimated at about 5.1 Tg $yr^{-1}$. Monoterpenes and isoprene oxidation is calculated to produce about 0.1 Tg $yr^{-1}$, $MS^{-}$ contribution to SOA is 4 Tg $yr^{-1}$ and in the case of taking into account marine alkyl amine salts marine SOA production is increasing by 1 Tg $yr^{-1}$. On the global scale, most of marine SOA (~78%) originates from the dimethylsulfide oxidation to methanesulfonic acid seconded by alkyl amines salts (~21%). Note that these results depend on the adopted parameterisations of marine sources of DMS, marine amines, and marine volatile organic compounds as well as the parameterizations of SOA formation from the oxidation of these marine precursors. For instance, if the oceanic source of isoprene and monoterpenes is one and two orders of magnitude larger, respectively, as evaluated by Luo and Yu [68], then the contribution of these compounds to the marine SOA formation could be significant. The annual global marine source of POA is evaluated at about 7 to 8 Tg POA $yr^{-1}$ with an additional uncertainty of a factor of 4 associated with our calculations. The lowest estimates are issued when the sea-salt source is calculated on line by TM4 driven by wind speed whereas about 4 times higher estimates are derived using the AEROCOM derived sea-salt emission inventory [40] that differs from the online estimates to the size distribution of the emissions. In addition, Chlorophyll-a distributions derived from MODIS lead to slightly lower (~1 Tg $yr^{-1}$) marine POA emission estimates than those

from SeaWiFS. The primary marine source estimate is about 10% the terrestrial POA emissions. Primary submicron and secondary OA sources are calculated to be of about the same order of magnitude in terms of mass. DMS is strongly contributing to the SOA source from known precursors on global scale. However, regionally and seasonally, isoprene and monoterpenes could significantly contribute to marine SOA formation. According to our model simulations that are based on the present understanding of marine SOA formation, organosulfates are the major marine SOA components. Unidentified potential source of VOC or missing SOA formation processes, like for instance aerosol water chemistry that is here neglected, in the marine atmosphere could account for additional marine SOA.

The present study elucidates the importance of interactions between nitrogen, sulphur, and carbon cycle for the organic aerosol mass in the atmosphere. Further investigations are needed to improve our knowledge on such processes and in particular to properly account for organic nitrogen formation and amines which appear to be a large fraction of marine organic aerosols.

## Acknowledgments

This work was supported by the EU Project MAP and its presentation has been facilitated by the ACCENT European Network of Excellence. S. Myriokefalitakis and C. Papadimas acknowledge support by PENED 03ED373 Grants. K. Tsigaridis was supported by an appointment to the NASA Postdoctoral Program at the Goddard Institute for Space Studies, administered by Oak Ridge Associated Universities through a contract with NASA. The authors thank the reviewers for their constructive comments.

## References

[1] M. Kanakidou, J. H. Seinfeld, S. N. Pandis et al., "Organic aerosol and global climate modelling: a review," *Atmospheric Chemistry and Physics*, vol. 5, no. 4, pp. 1053–1123, 2005.

[2] U. Pöschl, "Atmospheric aerosols: composition, transformation, climate and health effects," *Angewandte Chemie International Edition*, vol. 44, no. 46, pp. 7520–7540, 2005.

[3] S. Fuzzi, M. O. Andreae, B. J. Huebert et al., "Critical assessment of the current state of scientific knowledge, terminology, and research needs concerning the role of organic aerosols in the atmosphere, climate, and global change," *Atmospheric Chemistry and Physics*, vol. 6, no. 7, pp. 2017–2038, 2006.

[4] S. Solomon, D. Qin, M. Manning, et al., "Summary for policymakers," in *Climate Change 2007: The Physical Science Basis. Contribution of Working Group I to the Fourth Assessment Report of the Intergovernmental Panel on Climate Change*, Cambridge University Press, Cambridge, UK, 2007, http://www.ipcc.ch/pdf/assessment-report/ar4/wg1/ar4-wg1-spm.pdf.

[5] R. A. Duce, P. S. Liss, J. T. Merrill, et al., "The atmospheric input of trace species to the World ocean," *Global Biogeochemical Cycles*, vol. 5, no. 3, pp. 193–259, 1991.

[6] C. D. O'Dowd, M. C. Facchini, F. Cavalli et al., "Biogenically driven organic contribution to marine aerosol," *Nature*, vol. 431, no. 7009, pp. 676–680, 2004.

[7] M. C. Facchini, M. Rinaldi, S. Decesari et al., "Primary submicron marine aerosol dominated by insoluble organic colloids and aggregates," *Geophysical Research Letters*, vol. 35, no. 17, Article ID L17814, 2008.

[8] C. D. O'Dowd, B. Langmann, S. Varghese, C. Scannell, D. Ceburnis, and M. C. Facchini, "A combined organic-inorganic sea-spray source function," *Geophysical Research Letters*, vol. 35, no. 1, Article ID L01801, 2008.

[9] B. Bonsang, M. Kanakidou, G. Lambert, and P. Monfray, "The marine source of C2-C6 aliphatic hydrocarbons," *Journal of Atmospheric Chemistry*, vol. 6, no. 1-2, pp. 3–20, 1988.

[10] M. Kanakidou, B. Bonsang, J. C. Le Roulley, G. Lambert, D. Martin, and G. Sennequier, "Marine source of atmospheric acetylene," *Nature*, vol. 333, no. 6168, pp. 51–52, 1988.

[11] A. J. Kettle, M. O. Andreae, D. Amouroux et al., "A global database of sea surface dimethylsulfide (DMS) measurements and a procedure to predict sea surface DMS as a function of latitude, longitude, and month," *Global Biogeochemical Cycles*, vol. 13, no. 2, pp. 399–444, 1999.

[12] B. Bonsang, C. Polle, and G. Lambert, "Evidence for marine production of isoprene," *Geophysical Research Letters*, vol. 19, no. 11, pp. 1129–1132, 1992.

[13] S. R. Arnold, D. V. Spracklen, J. Williams et al., "Evaluation of the global oceanic isoprene source and its impacts on marine organic carbon aerosol," *Atmospheric Chemistry and Physics*, vol. 9, no. 4, pp. 1253–1262, 2009.

[14] W. J. Broadgate, G. Malin, F. C. Küpper, A. Thompson, and P. S. Liss, "Isoprene and other non-methane hydrocarbons from seaweeds: a source of reactive hydrocarbons to the atmosphere," *Marine Chemistry*, vol. 88, no. 1-2, pp. 61–73, 2004.

[15] N. Yassaa, I. Peeken, E. Zllner et al., "Evidence for marine production of monoterpenes," *Environmental Chemistry*, vol. 5, no. 6, pp. 391–401, 2008.

[16] R. J. Charlson, J. E. Lovelock, M. O. Andreae, and S. G. Warren, "Oceanic phytoplankton, atmospheric sulphur, cloud albedo and climate," *Nature*, vol. 326, no. 6114, pp. 655–661, 1987.

[17] G. P. Ayers and J. L. Gras, "Seasonal relationship between cloud condensation nuclei and aerosol methanesulphonate in marine air," *Nature*, vol. 353, no. 6347, pp. 834–835, 1991.

[18] I. Barnes, J. Hjorth, and N. Mihalapoulos, "Dimethyl sulfide and dimethyl sulfoxide and their oxidation in the atmosphere," *Chemical Reviews*, vol. 106, no. 3, pp. 940–975, 2006.

[19] S. M. Vallina, R. Simó, and S. Gassó, "What controls CCN seasonality in the Southern Ocean? A statistical analysis based on satellite-derived chlorophyll and CCN and model-estimated OH radical and rainfall," *Global Biogeochemical Cycles*, vol. 20, no. 1, Article ID GB1014, 2006.

[20] B. Gantt, N. Meskhidze, and D. Kamykowski, "A new physically-based quantification of isoprene and primary organic aerosol emissions from the world's oceans ," *Atmospheric Chemistry and Physics*, vol. 9, no. 1, pp. 2933–2965, 2009.

[21] M. Claeys, B. Graham, G. Vas et al., "Formation of secondary organic aerosols through photooxidation of isoprene," *Science*, vol. 303, no. 5661, pp. 1173–1176, 2004.

[22] D. K. Henze and J. H. Seinfeld, "Global secondary organic aerosol from isoprene oxidation," *Geophysical Research Letters*, vol. 33, no. 9, Article ID L09812, 2006.

[23] H.-J. Lim, A. G. Carlton, and B. J. Turpin, "Isoprene forms secondary organic aerosol through cloud processing: model simulations," *Environmental Science and Technology*, vol. 39, no. 12, pp. 4441–4446, 2005.

[24] B. Ervens, A. G. Carlton, B. J. Turpin, K. E. Altieri, S. M. Kreidenweis, and G. Feingold, "Secondary organic aerosol yields from cloud-processing of isoprene oxidation products," *Geophysical Research Letters*, vol. 35, no. 2, Article ID L02816, 2008.

[25] A. Guenther, T. Karl, P. Harley, C. Wiedinmyer, P. I. Palmer, and C. Geron, "Estimates of global terrestrial isoprene emissions using MEGAN (Model of Emissions of Gases and Aerosols from Nature)," *Atmospheric Chemistry and Physics*, vol. 6, no. 11, pp. 3181–3210, 2006.

[26] E. Liakakou, M. Vrekoussis, B. Bonsang, Ch. Donousis, M. Kanakidou, and N. Mihalopoulos, "Isoprene above the Eastern Mediterranean: seasonal variation and contribution to the oxidation capacity of the atmosphere," *Atmospheric Environment*, vol. 41, no. 5, pp. 1002–1010, 2007.

[27] P. I. Palmer and S. L. Shaw, "Quantifying global marine isoprene fluxes using MODIS chlorophyll observations," *Geophysical Research Letters*, vol. 32, no. 9, Article ID L09805, 5 pages, 2005.

[28] K. Tsigaridis and M. Kanakidou, "Global modelling of secondary organic aerosol in the troposphere: a sensitivity analysis," *Atmospheric Chemistry and Physics*, vol. 3, no. 5, pp. 1849–1869, 2003.

[29] K. Tsigaridis and M. Kanakidou, "Secondary organic aerosol importance in the future atmosphere," *Atmospheric Environment*, vol. 41, no. 22, pp. 4682–4692, 2007.

[30] N. Meskhidze and A. Nenes, "Phytoplankton and cloudiness in the southern ocean," *Science*, vol. 314, no. 5804, pp. 1419–1423, 2006.

[31] B. Langmann, C. Scannell, and C. O'Dowd, "New directions: organic matter contribution to marine aerosols and cloud condensation nuclei," *Atmospheric Environment*, vol. 42, no. 33, pp. 7821–7822, 2008.

[32] G. J. Roelofs, "A GCM study of organic matter in marine aerosol and its potential contribution to cloud drop activation," *Atmospheric Chemistry and Physics*, vol. 8, no. 3, pp. 709–719, 2008.

[33] D. V. Spracklen, S. R. Arnold, J. Sciare, K. S. Carslaw, and C. Pio, "Globally significant oceanic source of organic carbon aerosol," *Geophysical Research Letters*, vol. 35, no. 12, Article ID L12811, 2008.

[34] E. Vignati, M. C. Facchini, M. Rinaldi et al., "Global scale emission and distribution of sea-spray aerosol: sea-salt and organic enrichment," *Atmospheric Environment*, vol. 44, no. 5, pp. 670–677, 2010.

[35] S. Myriokefalitakis, M. Vrekoussis, K. Tsigaridis et al., "The influence of natural and anthropogenic secondary sources on the glyoxal global distribution," *Atmospheric Chemistry and Physics*, vol. 8, no. 16, pp. 4965–4981, 2008.

[36] K. Tsigaridis, M. Krol, F. J. Dentener et al., "Change in global aerosol composition since preindustrial times," *Atmospheric Chemistry and Physics*, vol. 6, no. 12, pp. 5143–5162, 2006.

[37] C. Granier, A. Guenther, J. F. Lamarque, et al., "POET, a database of surface emissions of ozone precursors," 2005, http://www.aero.jussieu.fr/projet/ACCENT/POET.php.

[38] G. R. van der Werf, J. T. Randerson, L. Giglio, G. J. Collatz, P. S. Kasibhatla, and A. F. Arellano Jr., "Interannual variability in global biomass burning emissions from 1997 to 2004," *Atmospheric Chemistry and Physics*, vol. 6, no. 11, pp. 3423–3441, 2006.

[39] S. L. Gong, "A parameterization of sea-salt aerosol source function for sub- and super-micron particles," *Global Biogeochemical Cycles*, vol. 17, no. 4, pp. 8–1, 2003.

[40] F. Dentener, S. Kinne, T. Bond et al., "Emissions of primary aerosol and precursor gases in the years 2000 and 1750 prescribed data-sets for AeroCom," *Atmospheric Chemistry and Physics*, vol. 6, no. 12, pp. 4321–4344, 2006.

[41] J. Sciare, O. Favez, R. Sarda-Estève, K. Oikonomou, H. Cachier, and V. Kazan, "Long-term observations of carbonaceous aerosols in the Austral Ocean atmosphere: evidence of a biogenic marine organic source," *Journal of Geophysical Research D*, vol. 114, no. 15, Article ID D15302, 2009.

[42] N. Mihalopoulos,unpublished.

[43] E. Koulouri, S. Saarikoski, C. Theodosi et al., "Chemical composition and sources of fine and coarse aerosol particles in the Eastern Mediterranean," *Atmospheric Environment*, vol. 42, no. 26, pp. 6542–6550, 2008.

[44] C. A. Pio, M. Legrand, T. Oliveira et al., "Climatology of aerosol composition (organic versus inorganic) at nonurban sites on a west-east transect across Europe," *Journal of Geophysical Research D*, vol. 112, no. 23, Article ID D23S02, 2007.

[45] P. Liss and L. Merlivat, "Air-sea gas exchange rates: introduction and synthesis," in *The Role of Air-Sea Exchange in Geochemical Cycling*, P. Buat-Menard, Ed., pp. 113–127, D. Reidel, Norwell, Mass, USA, 1986.

[46] J. G. Acker and G. Leptoukh, "Online analysis enhances use of NASA Earth Science Data," *Eos, Transactions, American Geophysical Union*, vol. 88, no. 2, pp. 14–17, 2007.

[47] W. E. Esaias, M. R. Abbott, I. Barton et al., "An overview of MODIS capabilities for ocean science observations," *IEEE Transactions on Geoscience and Remote Sensing*, vol. 36, no. 4, pp. 1250–1265, 1998.

[48] M. D. King, W. P. Menzel, Y. J. Kaufman et al., "Cloud and aerosol properties, precipitable water, and profiles of temperature and water vapor from MODIS," *IEEE Transactions on Geoscience and Remote Sensing*, vol. 41, no. 2, pp. 442–458, 2003.

[49] S. W. Gibb, R. F. C. Mantoura, and P. S. Liss, "Ocean-atmosphere exchange and atmospheric speciation of ammonia and methylamines in the region of the NW Arabian Sea," *Global Biogeochemical Cycles*, vol. 13, no. 1, pp. 161–178, 1999.

[50] A. F. Bouwman, D. S. Lee, W. A. H. Asman, F. J. Dentener, K. W. van der Hoek, and J. G. J. Olivier, "A global high-resolution emission inventory for ammonia," *Global Biogeochemical Cycles*, vol. 11, no. 4, pp. 561–587, 1997.

[51] W. F. Cooke, C. Liousse, H. Cachier, and J. Feichter, "Construction of a $1^\circ \times 1^\circ$ fossil fuel emission data set for carbonaceous aerosol and implementation and radiative impact in the ECHAM4 model," *Journal of Geophysical Research D*, vol. 104, no. D18, pp. 22137–22162, 1999.

[52] M. C. Facchini, S. Decesari, M. Rinaldi et al., "Important source of marine secondary organic aerosol from biogenic amines," *Environmental Science and Technology*, vol. 42, no. 24, pp. 9116–9121, 2008.

[53] S. M. Murphy, A. Sorooshian, J. H. Kroll et al., "Secondary aerosol formation from atmospheric reactions of aliphatic amines," *Atmospheric Chemistry and Physics*, vol. 7, no. 9, pp. 2313–2337, 2007.

[54] N. Mihalopoulos, V. M. Kerminen, M. Kanakidou, H. Berresheim, and J. Sciare, "Formation of particulate sulfur species (sulfate and methanesulfonate) during summer over the Eastern Mediterranean: a modelling approach," *Atmospheric Environment*, vol. 41, no. 32, pp. 6860–6871, 2007.

[55] T. E. Lane, N. M. Donahue, and S. N. Pandis, "Simulating secondary organic aerosol formation using the volatility basis-set approach in a chemical transport model," *Atmospheric Environment*, vol. 42, no. 32, pp. 7439–7451, 2008.

[56] A. C. Lewis, M. J. Evans, J. Methven et al., "Chemical composition observed over the mid-Atlantic and the detection of pollution signatures far from source regions," *Journal of Geophysical Research D*, vol. 112, no. 10, Article ID D10S39, 2007.

[57] J. R. Hopkins, I. D. Jones, A. C. Lewis, J. B. McQuaid, and P. W. Seakins, "Non-methane hydrocarbons in the Arctic boundary layer," *Atmospheric Environment*, vol. 36, no. 20, pp. 3217–3229, 2002.

[58] S. Matsunaga, M. Mochida, T. Saito, and K. Kawamura, "In situ measurement of isoprene in the marine air and surface seawater from the western North Pacific," *Atmospheric Environment*, vol. 36, no. 39-40, pp. 6051–6057, 2002.

[59] A. Colomb, V. Gros, S. Alvain et al., "Variation of atmospheric volatile organic compounds over the Southern Indian Ocean (30–49°S)," *Environmental Chemistry*, vol. 6, no. 1, pp. 70–82, 2009.

[60] Y. Yokouchi, H.-J. Li, T. Machida, S. Aoki, and H. Akimoto, "Isoprene in the marine boundary layer (Southeast Asian Sea, eastern Indian Ocean, and Southern Ocean): comparison with dimethyl sulfide and bromoform," *Journal of Geophysical Research D*, vol. 104, no. 7, pp. 8067–8076, 1999.

[61] P. J. Milne, D. D. Riemer, R. G. Zika, and L. E. Brand, "Measurement of vertical distribution of isoprene in surface seawater, its chemical fate, and its emission from several phytoplankton monocultures," *Marine Chemistry*, vol. 48, no. 3-4, pp. 237–244, 1995.

[62] A. A. Presto, K. E. Huff-Hartz, and N. M. Donahue, "Secondary organic aerosol production from terpene ozonolysis. 2. Effect of NOx concentration," *Environmental Science and Technology*, vol. 39, no. 18, pp. 7046–7054, 2005.

[63] C. Song, K. Na, and D. R. Cocker III, "Impact of the hydrocarbon to $NO_x$ ratio on secondary organic aerosol formation," *Environmental Science and Technology*, vol. 39, no. 9, pp. 3143–3149, 2005.

[64] R. Atkinson, R. A. Perry, and J. N. Pitts Jr., "Rate constants for the reactions of the OH radical with $(CH_3)_2NH$, $(CH_3)_3N$, and $C_2H_5NH_2$ over the temperature range 298–426∘K," *The Journal of Chemical Physics*, vol. 68, no. 4, pp. 1850–1853, 1977.

[65] T. Kurtén, V. Loukonen, H. Vehkamäki, and M. Kulmala, "Amines are likely to enhance neutral and ion-induced sulfuric acid-water nucleation in the atmosphere more effectively than ammonia," *Atmospheric Chemistry and Physics*, vol. 8, no. 14, pp. 4095–4103, 2008.

[66] R. Q. Sander, "Compilation of Henry's Law Constants for Inorganic and Organic Species of Potential Importance in Environmental Chemistry, Version 3," April 1999, http://www.mpch-mainz.mpg.de/~sander/res/henry.html.

[67] A. Asa-Awuku, G. J. Engelhart, B. H. Lee, S. N. Pandis, and A. Nenes, "Relating CCN activity, volatility, and droplet growth kinetics of $\beta$-caryophyllene secondary organic aerosol," *Atmospheric Chemistry and Physics*, vol. 9, no. 3, pp. 795–812, 2009.

[68] G. Luo and F. Yu, "A numerical evaluation of global oceanic emissions of $\alpha$-pinene and isoprene," *Atmospheric Chemistry and Physics*, vol. 10, no. 4, pp. 2007–2015, 2010.

Hindawi Publishing Corporation
Advances in Meteorology
Volume 2010, Article ID 482603, 10 pages
doi:10.1155/2010/482603

*Research Article*

# Contribution of Isoprene Oxidation Products to Marine Aerosol over the North-East Atlantic

**Tatu Anttila,[1] Baerbel Langmann,[2] Saji Varghese,[3] and Colin O'Dowd[3]**

[1] *Finnish Meteorological Institute, Research and Development, Climate and Global Change, P.O. BOX 503, 00101 Helsinki, Finland*
[2] *Institute of Geophysics, University of Hamburg, KlimaCampus, Bundesstrasse 55, 20146 Hamburg, Germany*
[3] *School of Physics, Centre for Climate & Air Pollution Studies, Environmental Change Institute, National University of Ireland Galway, University Road, Galway, Ireland*

Correspondence should be addressed to Tatu Anttila, tatu.anttila@fmi.fi

Received 15 February 2010; Revised 14 May 2010; Accepted 21 June 2010

Academic Editor: Olaf Stetzer



Secondary organic aerosol (SOA) formation through isoprene oxidation was investigated with the regional-scale climate model REMOTE. The applied modeling scheme includes a treatment for marine primary organic aerosol emissions, aerosol microphysics, and SOA formation through the gas/particle partitioning of semivolatile, water-soluble oxidation products. The focus was on SOA formation taking place over the North-East Atlantic during a period of high biological activity. Isoprene SOA concentrations were up to ~5 ng $m^{-3}$ over North Atlantic in the base case model runs, and isoprene oxidation made a negligible contribution to the marine organic aerosol (OA) mass. In particular, isoprene SOA did not account for the observed water-soluble organic carbon (WSOC) concentrations over North Atlantic. The performed model calculations, together with results from recent field measurements, imply a missing source of SOA over remote marine areas unless the isoprene oxidation products are considerably less volatile than the current knowledge indicates.

## 1. Introduction

Marine aerosols influence the global climate system directly by scattering incoming solar radiation and indirectly by acting as nuclei on which cloud droplets are formed [1, 2]. The magnitude of these effects depend on both the physical and chemical properties of marine aerosols. These properties are tied to the aerosol formation mechanisms which can be classified as primary, such as mechanical production driven by wind interactions at the ocean surface, and secondary which refers to gas-to-particle conversion (including heterogeneous reactions) resulting from the gas phase oxidation of volatile compounds [3]. Recently, considerable research effort has been put into characterizing the contribution of organic compounds to the marine aerosol [4–6]. The research has been motivated by the work of O'Dowd et al. [7] who found significant amounts of both water soluble and water insoluble organic aerosol mass in clean marine air. However, the sources of organic carbon are not fully characterized at the present and hence also the relative contributions of primary and secondary processes remain to be evaluated. In this regard, it has been suggested that a potentially important aerosol source is the formation of secondary organic aerosol (SOA) via isoprene oxidation [8].

Several studies have investigated the importance of the SOA formation to the marine aerosol by employing modeling and remote sensing techniques along with laboratory measurements [9–11]. Meskhidze and Nenes [9] suggested that SOA formation resulting from isoprene oxidation affects the cloudiness over oceans even though the authors initially overestimated isoprene emissions. On the other hand, Arnold et al. [10] argued that SOA formation has negligible influence on organic carbon (OC) concentrations over oceans while the results of Gantt et al. [11] show that isoprene SOA may contribute to the submicron marine aerosol mass notably over the tropical oceanic regions. Here it is worth noting that these studies focus on global estimates and also treat the SOA formation in a simplified manner by assuming a constant yield for the secondary organic mass.

We have addressed the above-mentioned gaps in the current research by employing a regional climate model REMOTE which includes aerosol microphysics and a mechanistic treatment of the isoprene-driven SOA formation. Our goal is to investigate the net and relative contributions of isoprene oxidation products to the marine aerosol mass over the model domain covering Europe and Northern Atlantic in particular. Furthermore, we focus on a high biological activity period from June to August. We also investigate the sensitivity of the results to the current uncertainties in mechanisms underlying isoprene SOA formation.

## 2. Methods

*2.1. Model Set-Up.* We use the regional three-dimensional on-line climate-chemistry/aerosol model REMOTE (Regional Model with Tracer Extension) [12, 13] with the physical parameterisations of the global ECHAM-4 model [14]. After being released in the atmosphere, gas phase and aerosol phase trace species undergo transport processes (horizontal and vertical advection, transport in convective clouds, vertical turbulent diffusion—for more details see [12]) and are removed from the atmosphere by sedimentation and dry and wet deposition.

For the determination of aerosol dynamics and thermodynamics we use the M7 module, which is described in detail in [15, 16]. The aerosol dynamical processes in M7 include nucleation, coagulation, and condensation. The aerosol size spectrum is represented by the superposition of seven log-normal distributions subdivided into a soluble and an insoluble coarse, accumulation and Aitken mode, and an additional soluble nucleation mode. The five aerosol components considered in the standard M7 are sulfate (SO4), black carbon (BC), organic carbon (OC), sea salt (SS), and mineral dust (DU). These components have either negligible or low solubility or are treated as an internal mixture of insoluble and soluble compounds. Mixed particles are formed from insoluble particles by coagulation and condensation. Each mode can be described by three moments: aerosol number $N$, number median radius $r$, and standard deviation $\sigma$. Standard deviations are prescribed in M7 [15], so that the median radius of each mode can be calculated from the corresponding aerosol number and aerosol mass, which are transported as 25 tracers.

REMOTE is applied with 19 vertical layers of increasing thickness between the Earth's surface and the 10 hPa pressure level using terrain following hybrid pressure-sigma coordinates. The model domain covers Europe and the North-East Atlantic and is subdivided into 81 × 91 grid boxes of 0.5° resolution (approximately 55 km) on a rotated latitude/longitude grid. The model covers an area from about 10° W to 30° E at the southern boundary of about 30° N and from about 40° W to 60° E in the north at about 70° N. A model time step of 5 minutes is chosen. REMOTE is initialised at the first time step using meteorological analysis data of the European Centre for Medium Range Weather Forecast (ECMWF), which are updated at the lateral boundaries every 6 hours. Trace species concentration at the lateral boundaries is prescribed and held constant throughout the simulation period.

*2.2. Emissions.* Anthropogenic emissions obtained from the EMEP emission inventory (http://webdab.emep.int/) are prescribed as monthly fluxes. For coarse mode sea salt, we use the same approach as described in [16] with a table look-up for wind speeds between 1 and 40 m/s. An organic-inorganic source function for the mixture of POC and sea salt aerosols is used for the net accumulation sea-spray flux [17].

The marine isoprene flux has been estimated dependent on the ocean chlorophyll-a concentration which is used as proxy for the marine biological activity. Based on [9] we assume that the average isoprene seawater concentration in nM is proportional to chlorophyll-a concentration in mg/m$^3$ as measured from SeaWiFs. The air-sea flux of isoprene is determined as the product of the isoprene seawater concentration and a gas exchange coefficient according to [18] where the gas exchange coefficient is dependent on 10 m wind speed and Schmidt number which in turn depends on surface temperature. In addition, terrestrial biogenic terpene and isoprene emissions from forests [12] are considered.

*2.3. SOA Formation Scheme.* Gas-phase oxidation of isoprene leads to a large number of semivolatile compounds capable of partitioning into the particle phase [8]. Here the semivolatile compounds are lumped into two model compounds $G_1$ and $G_2$ that represent the high- and low-yield reaction products, respectively. These compounds are produced in the gas phase as follows:

$$\text{Isoprene} + \text{OH} \longrightarrow \alpha_1 G_1 + \alpha_2 G_2 \tag{1}$$

where $\alpha_1$ and $\alpha_2$ are the stoichiometric coefficients for $G_1$ and $G_2$, respectively. No other reaction channels are considered because the SOA formation via other channels (e.g., oxidation driven by $O_3$ or $NO_3$) is not well characterized at the present [8]. The values of $\alpha_1$ and $\alpha_2$ are displayed in Table 1 and they were chosen according to the summary of experimental data presented in the recent review [8]. Please note that the values correspond to low $NO_x$ conditions which reflect the conditions of our study.

The gas/particle partitioning of $G_1$ and $G_2$ is calculated using Henry's Law equilibrium [19]. This approach was chosen because it is suitable for treating water-soluble compounds and because available information on semivolatile oxidation products of isoprene suggests that many of the compounds are highly water-soluble [8]. Furthermore, marine aerosols contain relatively large amount of water which absorbs soluble compounds [19]. According to Henry's Law, the equilibrium partitioning of a water-soluble compound $X$ between the gas and aqueous phase is given by the following equation:

$$C_{X,\text{aq}} = K_X(T) \times C_{X,\text{gas}}, \tag{2}$$

where $C_{X,\text{aq}}$ and $C_{X,\text{gas}}$ are the aqueous- and gas-phase concentrations of $X$, respectively, $K_X$ is Henry's Law constant for $X$, and $T$ is the temperature. Here it is assumed that $G_1$

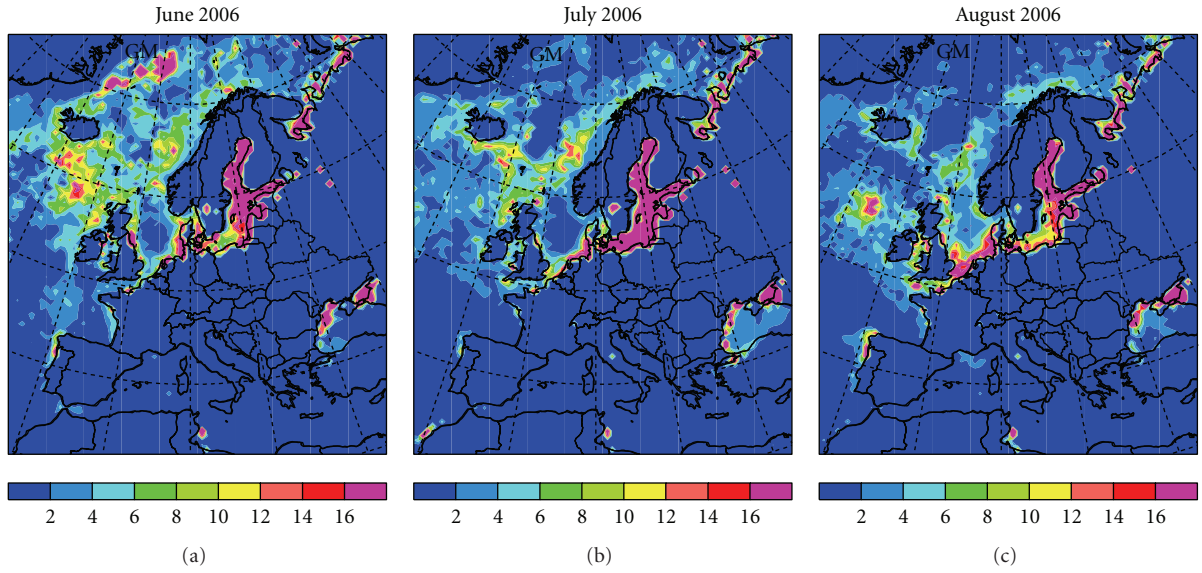


Figure 1: Monthly averaged marine isoprene fluxes. Latitudes are shown every 10° from 40° N to 70° N. Longitudes are also shown every 10° with Greenwhich (0°) indicated with GM in the figures.

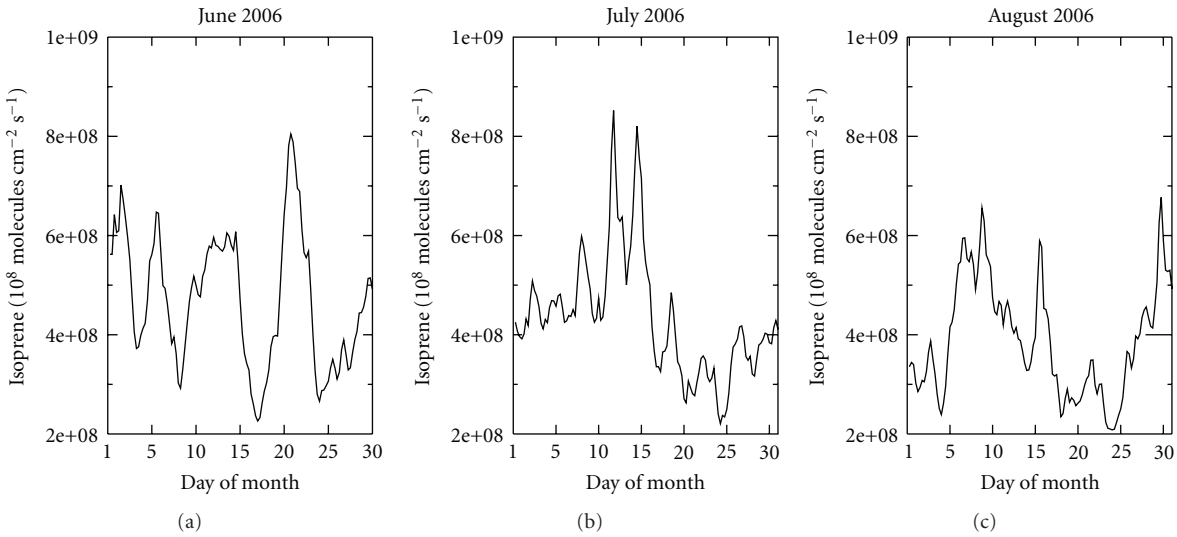


Figure 2: Time series of isoprene emission fluxes over water. For the areas covered by water, see, for example, Figure 1.

and $G_2$ behave ideally and thus no activity coefficients are introduced into (2). Furthermore, the temperature dependency of Henry's Law constant is accounted for through the Clausius-Clapeyron equation under the assumption that the enthalpy of vaporization for $X$, $\Delta H_X$, does not depend on the temperature. Finally, the gas/particle partitioning is calculated by neglecting the cloud water as cloud droplet formation is not treated explicitly in the model.

In order to maintain consistency, we have chosen the physicochemical properties of $G_1$ and $G_2$ using 1,3-propanediol and 1,2,4-butanetriol as model compounds. Both of these compounds are highly water-soluble polyols which have been suggested to contribute to the atmospheric SOA [21], and their properties are relatively well known. Furthermore, polyols are known to form as a result of isoprene oxidation, diols being among the first-generation products while triols result from further oxidation [8]. This is also consistent with $G_1$ and $G_2$ being the high- and low-yield reaction products, respectively. Table 1 displays the chosen values for the needed physicochemical parameters. Even though the model compounds are less volatile than most of the isoprene oxidation products [8], recent studies have suggested that compounds containing multiple OH groups (diols, triols, and tetrols, e.g.) contribute substantially to the isoprene SOA [22–24] and therefore $G_1$ and $G_2$ can be considered as representative of compounds making up the isoprene SOA. For the sake of comparison, the saturation vapour pressures, $P_{sat}$, corresponding to Henry's

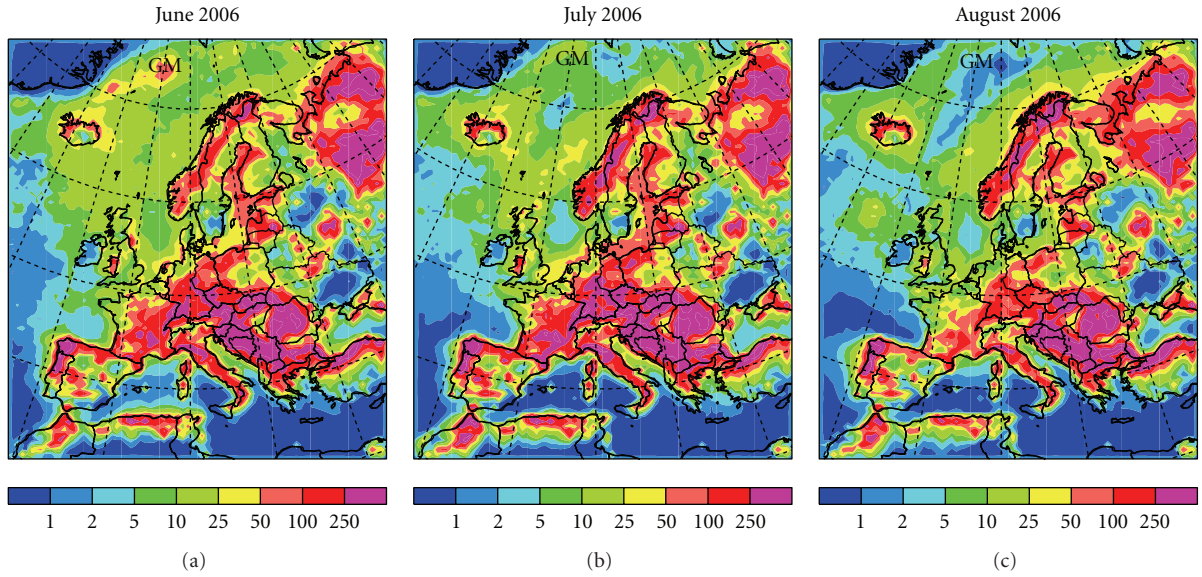


Figure 3: Monthly mean isoprene surface concentrations over surface for June, July, and August 2006. See caption of Figure 1 for more information about latitudes and longitudes.

Table 1: The properties of the semivolatile isoprene oxidation products $G_1$ and $G_2$. The references are given below the table. Here is $\rho_i$ the density of $G_i$.

| Compound | $\alpha_i$ | $MW_i$[a] (g/mol) | $K_i$ (298 K)[b] (M/atm) | $\Delta H_i$ (kJ/mol) | $\rho_i$[c] (g/cm$^3$) |
|---|---|---|---|---|---|
| $G_1$ | 0.28 | 76.1 | 9.1e5 | 72.4[a] | 1.0 |
| $G_2$ | 0.032 | 106.0 | 3e11 | 90.0[c] | 1.0 |

[a]Based on data presented in [20].
[b]Sander, R.,1999. http://www.mpch-mainz.mpg.de/~sander/res/henry.html.
[c]No data were found; estimated on the basis of data presented in [20] for structurally similar compounds.

Law constants of $G_1$ and $G_2$ are around 6.1e-5 and 1.9e-10 atm at 298 K, respectively, assuming ideal conditions at the infinite dilution limit (the equation relating to Henry's Law constant and $P_{sat}$ can be found from, e.g., [21]). Conversely, the values for the gas/particle partitioning constants $K_{om.1}$ and $K_{om.2}$ recommended in [8] for low NOx conditions would correspond to $P_{sat}$ values of around 4.6e-8 and 2.2e-10 atm, respectively, at 298 K. The conversion was done by assuming ideal conditions and that the average molecular weight of the organics making up the organic phase is 120 g/mol [25].

The SOA formation scheme used here differs from the widely used treatment for SOA formation where the equilibrium partitioning is calculated assuming that the particle-phase organics constitute the absorbing medium rather than water [8, 25]. In this regard, our approach is complimentary to the previous studies and thus gives new insight to the potential of isoprene oxidation to contribute to the marine SOA formation.

*2.4. Extension of M7.* It is assumed that aerosols present in any mode containing water can absorb the isoprene oxidation products excluding the nucleation mode. Because isoprene oxidation products were modeled with two compounds, six new aerosol components were thus added to M7 which corresponds to two new compounds present in Aitken, accumulation and coarse modes. Nucleation mode was not included because it makes up only a small fraction of the aerosol volume capable of absorbing semivolatile compounds. Moreover, the amount of isoprene SOA present in each mode is calculated according to the fractional contribution of the mode to the total particle water content.

It is expected that semivolatile isoprene oxidation products, being water-soluble, contribute to the particle water content. This is accounted for by applying the ZSR relation according to which solutes take up water independently of each other [19]. This is also consistent with the treatment of the particle water uptake in M7 [15]. The needed water activity data are taken from the literature [26], and the model compounds for $G_1$ and $G_2$ were 1,3-propanediol and 1,2,4-butanetriol, respectively, consistently with the treatment described in the previous section. In other regards, the new components were treated similarly as the existing aerosol components in M7.

## 3. Results

*3.1. Isoprene Fluxes and Surface Concentrations.* Monthly mean modeled marine isoprene emission fluxes for June, July, and August 2006 are displayed in Figure 1, and emission time series over water are displayed in Figure 2. As seen, the mean fluxes range between $\sim 10^8$-$10^9$ cm$^{-2}$ s$^{-1}$ over the North-East Atlantic. This range compares well with the modeling and measurement results presented by Palmer and

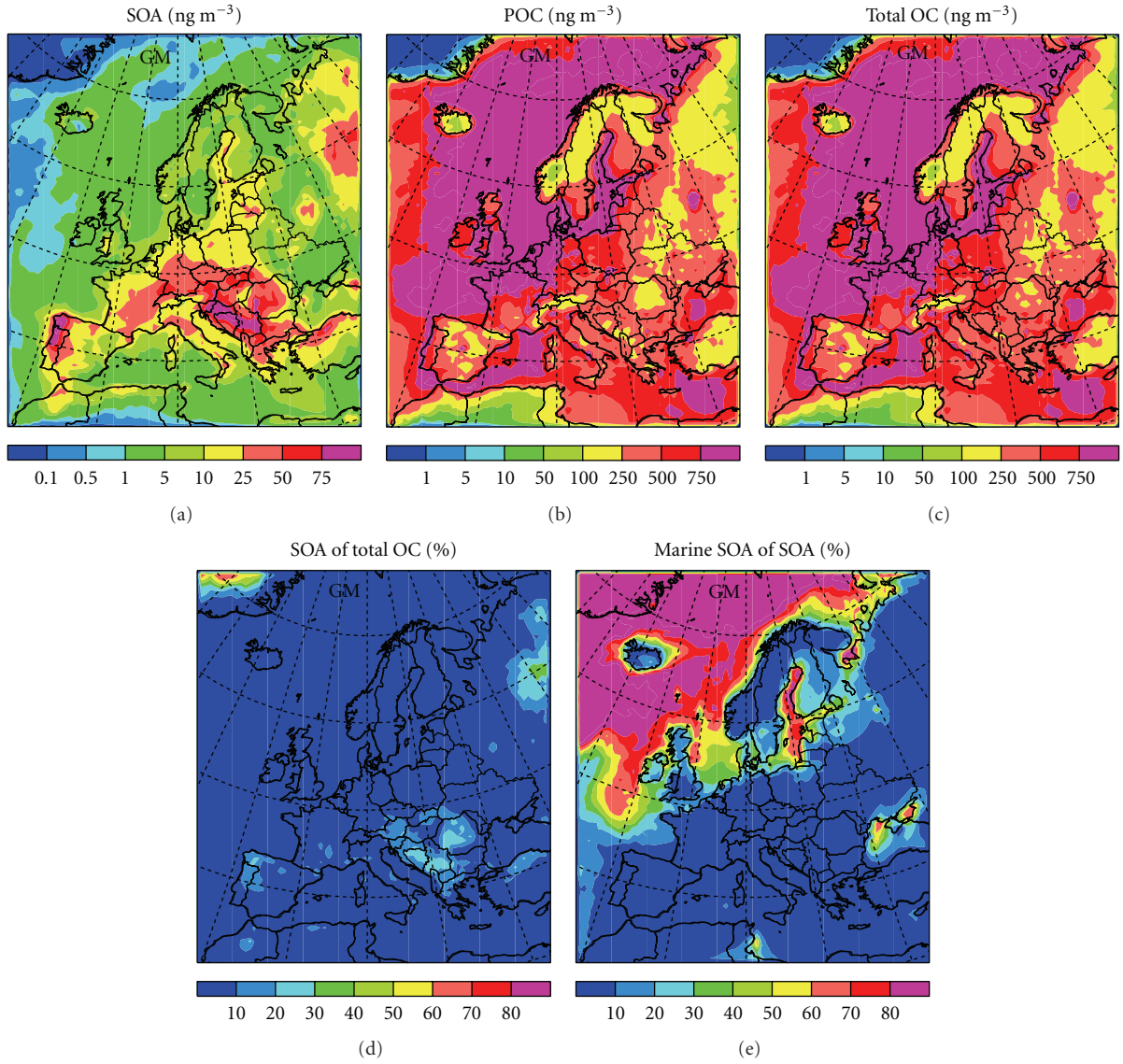


Figure 4: Time-averaged organic aerosol surface concentrations for June 2006. Here "SOA" refers to secondary organic aerosol, "POC" to the primary organic carbon, and "total OC" to the total organic carbon. Also, "% SOA" refers to the relative contribution of isoprene SOA to the total organic aerosol mass (in percents) and "% marine SOA of SOA" to the relative contribution of marine SOA to the total SOA (in percents). The relative contributions are derived on the mass basis. See caption of Figure 1 for more information about latitudes and longitudes.

Shaw [18] and Gantt et al. [11]. Figure 2 shows the six-hour average variation of isoprene fluxes over water. The daily variation is mainly caused by variation in the wind speed, and the average fluxes were $4.7 \times 10^8$, $4.4 \times 10^8$, and $3.9 \times 10^8$ molecules cm$^{-2}$ s$^{-1}$ for June, July, and August, respectively.

Surface isoprene concentrations, shown in Figure 3, exhibit a considerable contrast in the land/sea distribution with considerably more isoprene over land areas. This is due to differences in biogenic activity, and the contrast is comparable with the results of Arnold et al. [10]. Regarding results for noncoastal marine boundary layer, the isoprene concentrations reach values of up to a few ten ppt while being typically between 1 and 5 ppt which is in agreement with the results of Arnold et al. [10]. Also, comparison of Figures 1 and 3 shows that the isoprene emissions are reflected in the isoprene surface concentrations as expected. Monthly mean surface isoprene concentrations over the NE Atlantic are the highest in June 2006 correlated with the highest chlorophyll-a concentrations during this period. In addition to the chlorophyll-a concentration, wind speed is limiting the isoprene fluxes and hence also the isoprene gas-phase concentrations in particular during August.

*3.2. Marine Organic Carbon: Primary versus Secondary Sources.* Figure 4 shows the monthly mean surface concentrations of SOA, primary organic carbon and total organic carbon (TOC), the relative contribution of SOA to TOC, and

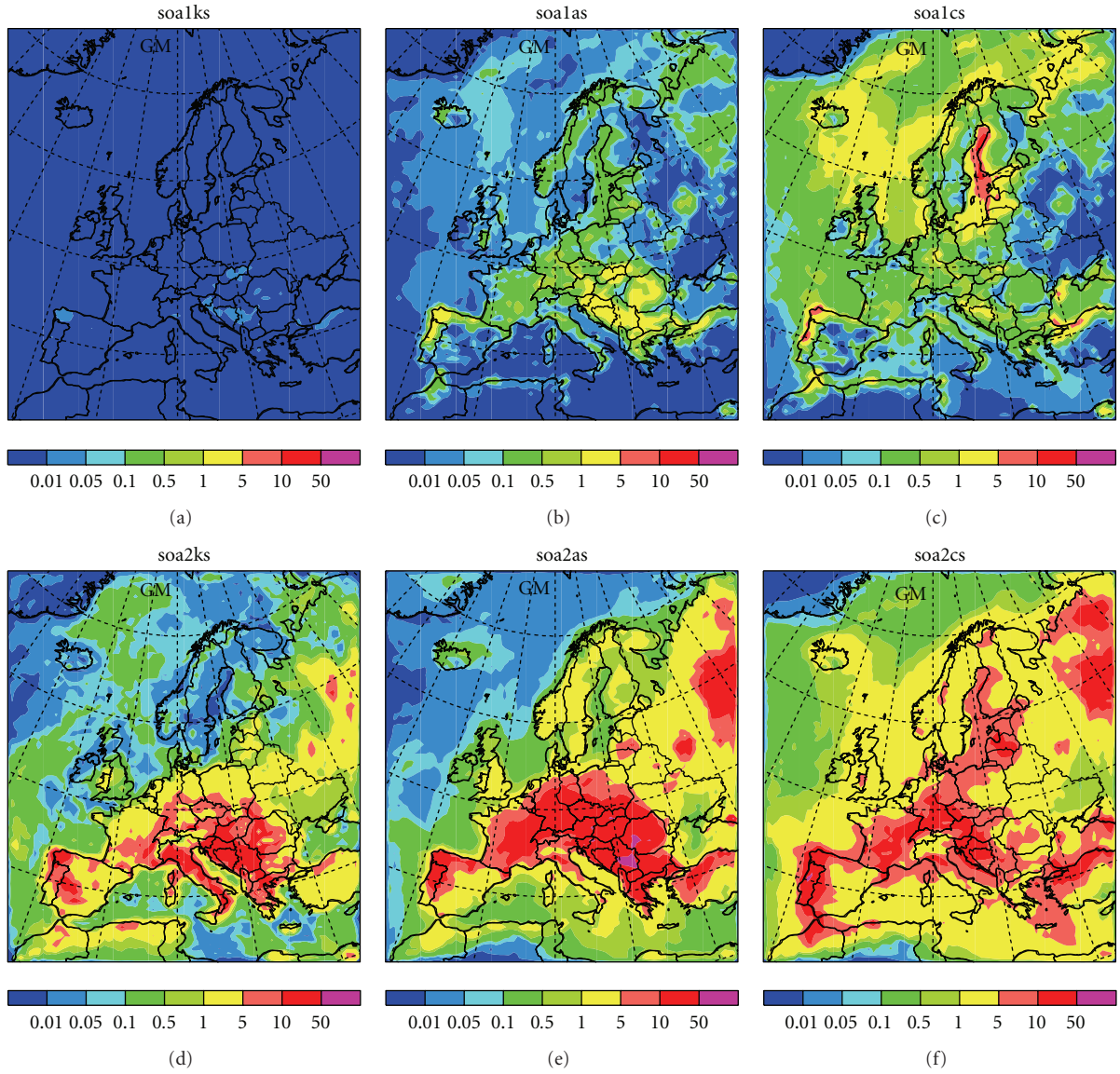


Figure 5: Average particle-phase concentrations over surface of isoprene oxidation products $G_1$ (above) and $G_2$ (below) for June 2006. The concentrations results are shown separately for Aitken (left), accumulation (middle), and coarse aerosol modes (right). See caption of Figure 1 for more information about latitudes and longitudes.

the relative contribution of marine SOA to the total SOA for June 2006. As seen, isoprene SOA makes only a marginal contribution to the TOC over the remote marine boundary layer, the SOA concentration being up to $\sim 5\,\mathrm{ng\,m^{-3}}$. SOA comprises thus only <1% of the TOC, and a similar estimate was reached also in the study of Arnold et al. [10]. As expected, the highest contribution of marine SOA to the total SOA occurs over ocean water, the contribution of SOA with marine origin being close to 100% over remote marine areas. Mode-fractionated aerosol-phase concentrations of $G_1$ and $G_2$ in Aitken, accumulation and coarse modes are shown in Figure 5 for June 2006. A comparison of the contributions of $G_1$ and $G_2$ reveals that the less volatile $G_2$ accounts for most of the simulated SOA mass despite the lower stoichiometric yield (see Table 1). Over remote marine areas, largest SOA concentrations are found generally in the coarse mode because the mode contains largest concentration of particulate water (not shown here). The submicron SOA concentrations remain below one $\mathrm{ng\,m^{-3}}$ over North Atlantic; that is, the contribution of isoprene oxidation to submicron aerosol mass is negligible.

The measured WSOC concentrations of North Atlantic marine aerosols ranged between $\sim 0.1$–$0.15\,\mu\mathrm{gC\,m^{-3}}$ during the summer months [5]. Using a ratio of 2.1 for the average organic molecular weight per carbon weight [27], the maximum modeled isoprene SOA concentrations over North-East Atlantic (around $5\,\mathrm{ng\,m^{-3}}$ see above) were around $2.4\,\mathrm{ngC\,m^{-3}}$. Keeping in mind that the primary organic aerosol is treated as insoluble whereas SOA is assumed to be entirely water-soluble in the model, it can be

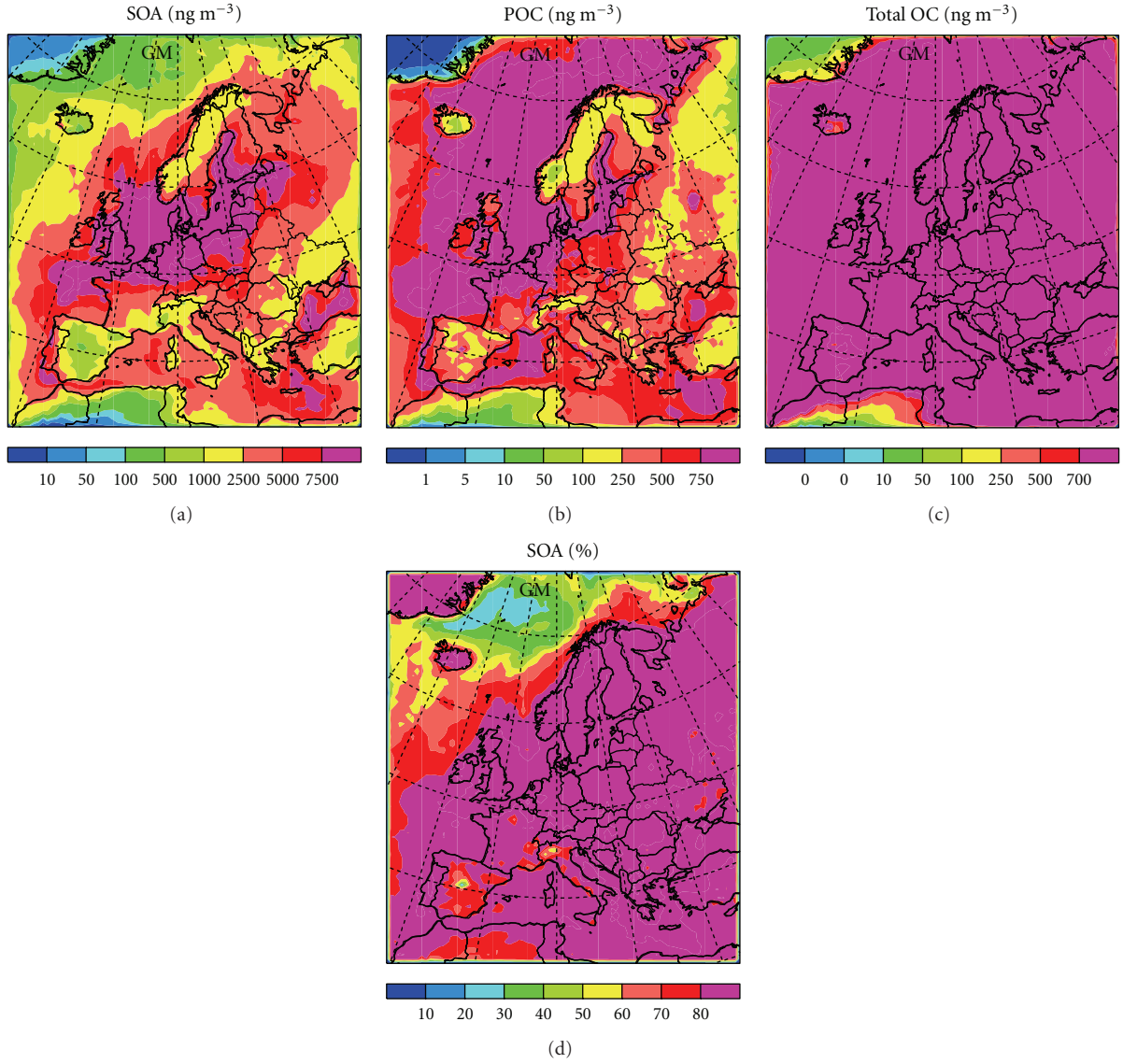


Figure 6: Time-averaged organic aerosol surface concentrations for June 2006 with $K_1$ = 9.1e6 M/atm. Here "SOA" refers to secondary organic aerosol, "POC" to the primary organic carbon, and "total OC" to the total organic carbon. Also, "% SOA" refers to the relative contribution of isoprene SOA to the total organic aerosol mass (in percents). The relative contribution is derived on the mass basis. See caption of Figure 1 for more information about latitudes and longitudes.

thus concluded that isoprene SOA cannot account for the observed WSOC concentrations. Moreover, recent studies of Ceburnis et al. [28] and Facchini et al. [6] suggest that marine WIOC is mainly of primary origin and that WSOC originates mainly from secondary sources. Consequently, the performed simulations suggest that SOA formation resulting from isoprene oxidation does not explain the observed WSOC concentrations, but other secondary sources need to be investigated.

As further seen from Figure 4, TOC concentrations were around 1 $\mu$g m$^{-3}$ over the North Atlantic. Using the above-mentioned conversion factor, this would correspond to TOC concentrations of around 0.48 $\mu$gC m$^{-3}$. This can be compared with the measurement results from the Mace Head station according to which TOC concentrations varied between ~0.4–0.6 $\mu$gC m$^{-3}$ for the period from June to August [29]. To conclude with, the model reproduces the observed TOC concentrations relatively well but underestimates the observed contribution of WSOC to the marine aerosol.

*3.3. Sensitivity Studies.* Key model parameters in determining the amount of SOA formed are Henry's Law constants for the oxidation products G1 and G2, K1 and K2, respectively (see Section 2.3). Given the current uncertainties in isoprene SOA formation, we repeated the above-described model simulations with increased values of $K_1$ and $K_2$ at 298 K in order to investigate whether increased partitioning of $G_1$ and $G_2$ into the particle phase may alter the conclusions

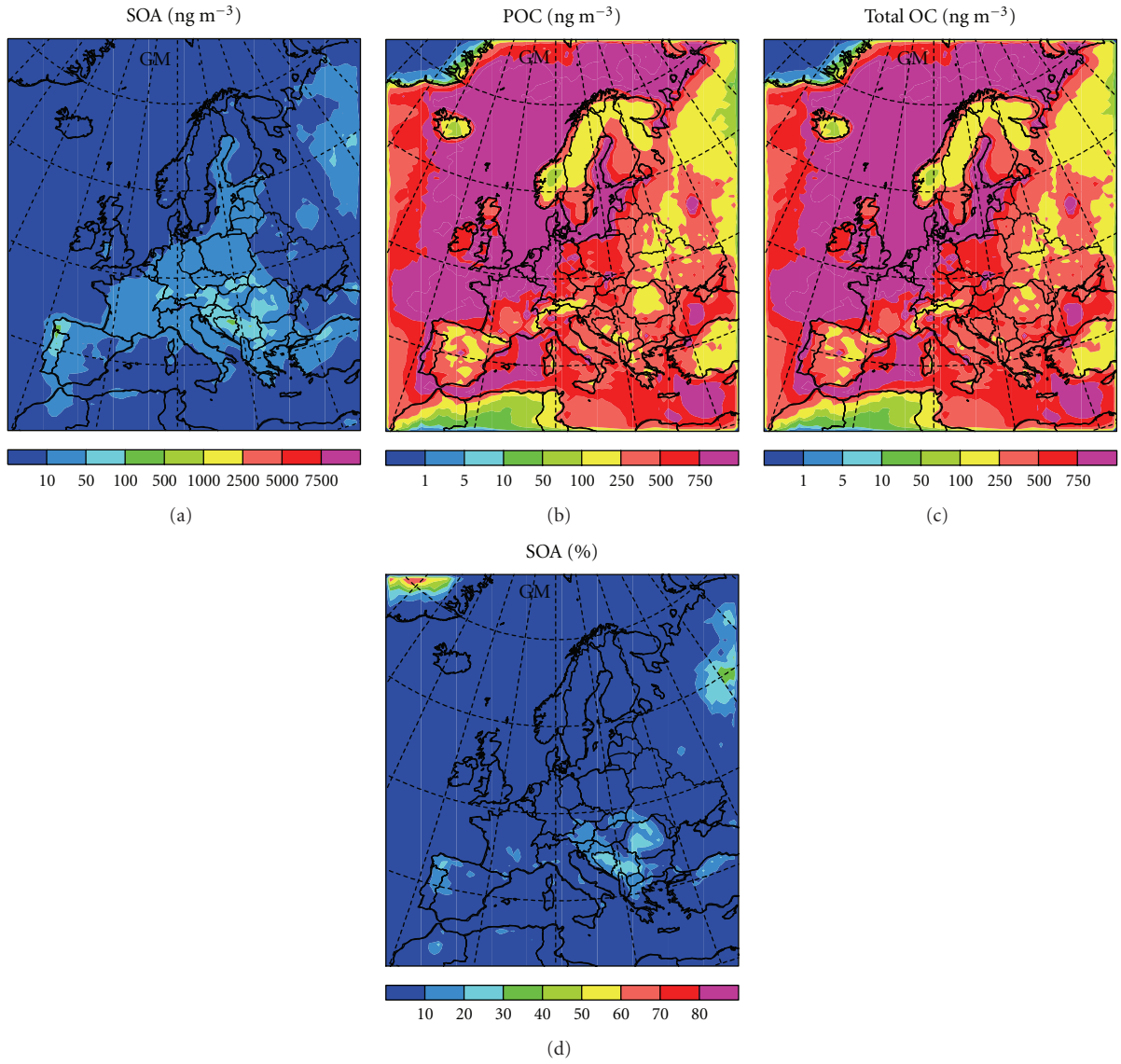


Figure 7: Same as Figure 6 but for the model runs with $K_2$ = 3e11 M/atm.

based on the base case simulations. Here the focus was on marine SOA concentrations close to the surface level. As in the base simulations, the main source of marine SOA was mainly isoprene oxidation taking place over oceans rather than oxidation of terrestrial emissions (not shown). In the first sensitivity run, the value of $K_1$ was increased by an order of magnitude (Figure 6). As seen, the increased partitioning of $G_1$ leads to considerable increases in the isoprene SOA masses such that isoprene SOA accounts for up to ~80–90% of the total organic aerosol mass over North Atlantic. In the second sensitivity run, the value of $K_2$ was increased by an order of magnitude (Figure 7). Because $G_2$ is produced with smaller yield in the gas phase (Table 1), increased partitioning into the aerosol phase does not lead to notable increases in the SOA concentrations. Even though $G_2$ made dominant contribution to the isoprene SOA in the base case simulations, the results are more sensitive to the properties of more volatile compound $G_1$. Accordingly, the contribution of isoprene SOA to the marine organic carbon is sensitive to the amount of semivolatile reaction products that are formed with relatively large yield.

## 4. Summary and Conclusions

Contribution of isoprene oxidation products to the marine organic aerosol was investigated with a regional climate model REMOTE. The aerosol microphysics module of REMOTE, M7, was extended to treat gas/particle partitioning of semivolatile, water-soluble isoprene oxidation products. Here it is worth noting that the applied isoprene SOA formation scheme differs from those applied in the previous studies where the semivolatile reaction products were assumed to partition into the particle organic phase

rather than into the aqueous phase. Furthermore, the focus was on SOA formation taking place over the North-East Atlantic during a period of high biological activity.

Isoprene SOA concentrations were up to $\sim 5\,\mathrm{ng\,m^{-3}}$ over North Atlantic in the base case model runs, and the SOA was formed almost entirely over water. Isoprene oxidation made a negligible contribution to the marine organic aerosol (OA) mass. In particular, isoprene SOA did not account for the observed concentrations of water-soluble organic carbon (WSOC) over North Atlantic. The performed model calculations, together with results from recent field measurements, imply a missing source of WSOC over remote marine areas unless the isoprene oxidation products are considerably less volatile than the current knowledge indicates. A possible source is also conversion of water-insoluble compounds into WSOC through heterogeneous reactions taking place in the aqueous phase of particles and cloud droplets [29, 30]. In order to elucidate the origin of WSOC in marine aerosols, isoprene oxidation mechanisms in both the gas and aerosol phase need to be elucidated further along with investigating the potential of other volatile organic compounds (such as monoterpenes; see, e.g., [31]) to form SOA over marine areas.

## Acknowledgments

The authors would like to acknowledge Environmental Protection Agency of Ireland, Enterprise Ireland, and the European Commission (MAP project, http://macehead.nuigalway.ie/map). One of the authors (T. Anttila) acknowledges financial support from the ACCENT network (Atmospheric Composition Change—European Network of Excellence, http://www.accent-network.org/) and from the Emil Aaltonen Foundation.

## References

[1] S. Twomey, "Aerosols, clouds and radiation," *Atmospheric Environment, Part A*, vol. 25, no. 11, pp. 2435–2442, 1991.

[2] U. Lohmann and J. Feichter, "Global indirect aerosol effects: a review," *Atmospheric Chemistry and Physics*, vol. 5, no. 3, pp. 715–737, 2005.

[3] C. D. O'Dowd and G. De Leeuw, "Marine aerosol production: a review of the current knowledge," *Philosophical Transactions of the Royal Society A*, vol. 365, no. 1856, pp. 1753–1774, 2007.

[4] F. Cavalli, M. C. Facchini, S. Decesari et al., "Advances in characterization of size-resolved organic matter in marine aerosol over the North Atlantic," *Journal of Geophysical Research D*, vol. 109, no. 24, Article ID D24215, 14 pages, 2004.

[5] Y. J. Yoon, D. Ceburnis, F. Cavalli et al., "Seasonal characteristics of the physicochemical properties of North Atlantic marine atmospheric aerosols," *Journal of Geophysical Research D*, vol. 112, no. 4, Article ID D04206, 2007.

[6] M. C. Facchini, M. Rinaldi, S. Decesari et al., "Primary submicron marine aerosol dominated by insoluble organic colloids and aggregates," *Geophysical Research Letters*, vol. 35, no. 17, Article ID L17814, 2008.

[7] C. D. O'Dowd, M. C. Facchini, F. Cavalli et al., "Biogenically driven organic contribution to marine aerosol," *Nature*, vol. 431, no. 7009, pp. 676–680, 2004.

[8] A. G. Carlton, C. Wiedinmyer, and J. H. Kroll, "A review of Secondary Organic Aerosol (SOA) formation from isoprene," *Atmospheric Chemistry and Physics*, vol. 9, no. 14, pp. 4987–5005, 2009.

[9] N. Meskhidze and A. Nenes, "Phytoplankton and cloudiness in the southern ocean," *Science*, vol. 314, no. 5804, pp. 1419–1423, 2006.

[10] S. R. Arnold, D. V. Spracklen, J. Williams et al., "Evaluation of the global oceanic isoprene source and its impacts on marine organic carbon aerosol," *Atmospheric Chemistry and Physics*, vol. 9, no. 4, pp. 1253–1262, 2009.

[11] B. Gantt, N. Meskhidze, and D. Kamykowski, "A new physically-based quantification of marine isoprene and primary organic aerosol emissions," *Atmospheric Chemistry and Physics*, vol. 9, no. 14, pp. 4915–4927, 2009.

[12] B. Langmann, "Numerical modelling of regional scale transport and photochemistry directly together with meteorological processes," *Atmospheric Environment*, vol. 34, no. 21, pp. 3585–3598, 2000.

[13] B. Langmann, S. Varghese, E. Marmer et al., "Aerosol distribution over Europe: a model evaluation study with detailed aerosol microphysics," *Atmospheric Chemistry and Physics*, vol. 8, no. 6, pp. 1591–1607, 2008.

[14] E. Roeckner, K. Arpe, L. Bengtsson, et al., "The atmospheric general circulation model ECHAM-4: model description and simulation of present-day climate," Tech. Rep. 218, Max Planck Institute for Meteorology, Hamburg, Germany, 1996.

[15] E. Vignati, J. Wilson, and P. Stier, "M7: an efficient size-resolved aerosol microphysics module for large-scale aerosol transport models," *Journal of Geophysical Research D*, vol. 109, no. 22, Article ID D22202, 17 pages, 2004.

[16] P. Stier, J. Feichter, S. Kinne et al., "The aerosol-climate model ECHAM5-HAM," *Atmospheric Chemistry and Physics*, vol. 5, no. 4, pp. 1125–1156, 2005.

[17] E. Vignati, M. C. Facchini, M. Rinaldi et al., "Global scale emission and distribution of sea-spray aerosol: sea-salt and organic enrichment," *Atmospheric Environment*, vol. 44, no. 5, pp. 670–677, 2010.

[18] P. I. Palmer and S. L. Shaw, "Quantifying global marine isoprene fluxes using MODIS chlorophyll observations," *Geophysical Research Letters*, vol. 32, no. 9, Article ID GL022592, 5 pages, 2005.

[19] J. H. Seinfeld and S. N. Pandis, *Atmospheric Chemistry and Physics: From Air Pollution to Climate Change*, John Wiley & Sons, New York, NY, USA, 1998.

[20] J. A. Dean, *Lange's Handbook on Chemistry*, McGraw-Hill, New York, NY, USA, 13th edition, 1985.

[21] P. Saxena and L. M. Hildemann, "Water-soluble organics in atmospheric particles: a critical review of the literature and application of thermodynamics to identify candidate compounds," *Journal of Atmospheric Chemistry*, vol. 24, no. 1, pp. 57–109, 1996.

[22] M. Claeys, B. Graham, G. Vas et al., "Formation of secondary organic aerosols through photooxidation of isoprene," *Science*, vol. 303, no. 5661, pp. 1173–1176, 2004.

[23] E. O. Edney, T. E. Kleindienst, M. Jaoui et al., "Formation of 2-methyl tetrols and 2-methylglyceric acid in secondary organic aerosol from laboratory irradiated isoprene/$NO_X$/$SO_2$/air mixtures and their detection in ambient $PM_{2.5}$ samples collected in the eastern United States," *Atmospheric Environment*, vol. 39, no. 29, pp. 5281–5289, 2005.

[24] I. Kourtchev, T. Ruuskanen, W. Maenhaut, M. Kulmala, and M. Claeys, "Observation of 2-methyltetrols and related photooxidation products of isoprene in boreal forest aerosols from

Hyytiälä, Finland," *Atmospheric Chemistry and Physics*, vol. 5, no. 10, pp. 2761–2770, 2005.

[25] J. F. Pankow, "An absorption model of the gas/aerosol partitioning involved in the formation of secondary organic aerosol," *Atmospheric Environment*, vol. 28, no. 2, pp. 189–193, 1994.

[26] C. Marcolli and T. Peter, "Water activity in polyol/water systems: new UNIFAC parameterization," *Atmospheric Chemistry and Physics*, vol. 5, no. 6, pp. 1545–1555, 2005.

[27] B. J. Turpin and H.-J. Lim, "Species contributions to PM2.5 mass concentrations: revisiting common assumptions for estimating organic mass," *Aerosol Science and Technology*, vol. 35, no. 1, pp. 602–610, 2001.

[28] D. Ceburnis, C. D. O'Dowd, G. S. Jennings et al., "Marine aerosol chemistry gradients: elucidating primary and secondary processes and fluxes," *Geophysical Research Letters*, vol. 35, no. 7, Article ID L07804, 2008.

[29] H.-J. Lim, A. G. Carlton, and B. J. Turpin, "Isoprene forms secondary organic aerosol through cloud processing: model simulations," *Environmental Science and Technology*, vol. 39, no. 12, pp. 4441–4446, 2005.

[30] A. Limbeck, M. Kulmala, and H. Puxbaum, "Secondary organic aerosol formation in the atmosphere via heterogeneous reaction of gaseous isoprene on acidic particles," *Geophysical Research Letters*, vol. 30, no. 19, Article ID GL017738, 6 pages, 2003.

[31] N. Yassaa, I. Peeken, E. Zöllner et al., "Evidence for marine production of monoterpenes," *Environmental Chemistry*, vol. 5, no. 6, pp. 391–401, 2008.

Hindawi Publishing Corporation
Advances in Meteorology
Volume 2010, Article ID 689763, 9 pages
doi:10.1155/2010/689763

*Research Article*

# Simulating Marine New Particle Formation and Growth Using the M7 Modal Aerosol Dynamics Modal

**Ciaran Monahan,[1] Henri Vuollekoski,[2] Markku Kulmala,[2] and Colin O'Dowd[1]**

[1] *Centre for Climate and Air Pollution Studies, National University of Ireland Galway, Galway, Ireland*
[2] *Department of Physics, University of Helsinki, 00014 Helsinki, Finland*

Correspondence should be addressed to Colin O'Dowd, colin.odowd@nuigalway.ie

Received 12 April 2010; Revised 26 August 2010; Accepted 22 September 2010

Academic Editor: Nicholas Meskhidze



A modal atmospheric aerosol model (M7) is evaluated in terms of predicting marine new particle formation and growth. Simulations were carried out for three different nucleation schemes involving (1) kinetic self-nucleation of OIO (2) nucleation *via* OIO activation by $H_2SO_4$ and (3) nucleation *via* OIO activation by $H_2SO_4$ plus condensation of a low-volatility organic vapour. Peak OIO and $H_2SO_4$ vapour concentrations were both limited to $6 \times 10^6$ molecules $cm^{-3}$ at noontime while the peak organic vapour concentration was limited to $12 \times 10^6$ molecules $cm^{-3}$. All simulations produced significant concentrations of new particles in the Aitken mode. From a base case particle concentration of 222 $cm^{-3}$ at radii >15 nm, increases in concentrations to 366 $cm^{-3}$ were predicted from the OIO-OIO case, 722 $cm^{-3}$ for the OIO-$H_2SO_4$ case, and 1584 $cm^{-3}$ for the OIO-$H_2SO_4$ case with additional condensing organic vapours. The results indicate that open ocean new particle production is feasible for clean conditions; however, new particle production becomes most significant when an additional condensable organic vapour is available to grow the newly formed particles to larger sizes. Comparison to sectional model for a typical case study demonstrated good agreement and the validity of using the modal model.

## 1. Introduction

Aerosols are ubiquitous in the Earth atmosphere and have measurable impacts on climate, atmospheric chemistry, and human health [1]. Marine aerosols are thought to have a potentially significant role in future climate change through biogeochemical feedback processes [2]. The aforementioned studies focussed on biogenic DMS-derived sulphate driving marine new particle formation and subsequent growth into cloud condensation nuclei (CCN) sizes ($r > 35$–$50$ nm).

Detailed modelling studies [3] have, however, demonstrated that while sulphuric acid is present in sufficient concentrations to promote nucleation, the concentration is insufficient to grow these nucleated clusters into aerosol particles operationally defined as $D > 3$ nm.

An increase in marine aerosol concentration, providing the increased aerosol population is water soluble, can potentially lead to an increase in CCN; however, there are three stages to growth. The first stage involves nucleation of stable or critical clusters; the second stage involves the growth of clusters into pseudostationary aerosol particles where they can survive significantly longer than clusters (e.g., if a particle grows to 6 nm in size, it has the potential to survive at least 100 times longer than a cluster of 0.5 nm [4]; the third stage is continued growth to CCN sizes. There has been little evidence to date demonstrating that these growth processes can be achieved through the sulphur cycle. Furthermore, oceanic new particle production events are difficult to quantify in comparison to terrestrial events. Coastal zones, in contrast, provide typically stronger biogenic signals and possibly are scalable to, and indicative of, difficult-to-detect open ocean processes. A case and example of this is the formation of new particles in the tidal and/or coastal where macro algae biogenic gas emissions are the strongest [4–7]. O'Dowd and Hoffmann [7] provide an informed overview of coastal new particle production driven by the release of molecular iodine and its subsequent photolysis and oxidation by ozone.

More recently, a number of studies have been carried out on the nucleation and growth capabilities of iodine oxides [8, 9] where it has been found that iodine oxides have the potential to make significant contribution to the formation of new particles as well as contributing to a considerable increase in growth rates of newly formed stable clusters. More recently, simulations using a sectional model on iodine dioxide nucleation in coastal and open ocean marine environments found that particle production driven by iodine compounds is possible, but by OIO and $H_2SO_4$ alone, only few particles are likely to reach detectable sizes without an additional low volatility vapour, owing to the scavenging by coagulation processes with the existing aerosol population [10].

In the examination of the nucleation mechanisms relating to iodine oxides presented in this work, three parameterisations from Vuollekoski et al. [10], that include both iodine oxide and an additional nonnucleating organic condensable vapour, are investigated. The M7 [11] atmospheric microphysics aerosol module has been used to incorporate firstly iodine oxide (OIO) self-nucleation, secondly iodine oxide—sulphuric acid nucleation, and thirdly, iodine oxide—sulphuric acid nucleation with additional condensation of a low volatility organic vapour. The iodine oxide self-nucleation is a kinetic mechanism while the iodine oxide—sulphuric acid mechanism represents activation of iodine oxide by sulphuric acid vapours.

Recent results from the NE Atlantic reported the occurrence of open ocean particle production and growth events [12–14]. The latter study points to a condensable vapour source concentration of the order of $1.2\times10^7$ molecules $cm^{-3}$ to explain typical growth rates of 0.8 nm $hour^{-1}$ observed. This study builds on the aforementioned sectional modelling sensitivity studies by Vuollekoski et al. [10] and the new experimental data to evaluate the ability of the M7 modal model to reproduce the experimental observations and to simulate these with the same skill as a detailed sectional model.

## 2. Model Setup

The model used to perform the simulations in this study was the M7 atmospheric microphysics aerosol box model [11]. The M7 module was designed to be coupled with general circulation models and chemistry transport models. In M7 the aerosol populations is divided into two groups: mixed (water-soluble) particles, and insoluble particles. The model separates the aerosol populations into seven classes according to the dry radius size of the particles.

A "pseudomodal" approach is used to describe the aerosol populations and to determine the aerosol dynamics. The mixed aerosol size distribution over different size ranges is represented by four lognormal modes: nucleation (0.5–5 nm), Aitken (5 nm–50 nm), accumulation (50 nm–500 nm), and coarse modes (>500 nm), while the rate constants for coagulation and condensation are calculated for the average mode radius rather than the integral over the mode. The geometric standard deviations of these modes are 1.59 for the nucleation, Aitken, and accumulation modes, both soluble and insoluble, while the coarse have a geometric standard deviation of 2.0 for the soluble and insoluble modes [11].

The aerosol species considered in the M7 module are mineral dust, black carbon (BC) and primary organic carbon, sulphate, and sea salt. The aerosol dynamic processes in M7 include nucleation, coagulation, and condensation of sulphuric acid. Mixed (or soluble) particles are formed from insoluble particles by coagulation and condensation.

In the M7 model, it is assumed that the mixed particles are a water-soluble mixture of insoluble and soluble material. The separation of the aerosol populations into these two populations allows for the representation of the evolution of the hygroscopic properties of the initially insoluble compounds, on which their atmospheric lifetimes and also their interaction with clouds depend.

For this study, the box model was modified to include two new vapour species, iodine oxide along with a low-volatility organic vapour species, and also the aerosol processes adapted to allow for the condensation of both these vapours, as well as the nucleation of iodine oxide and activation nucleation of iodine oxide by sulphuric acid. For the duration of each simulation, clear sky conditions were assumed.

Both OIO and condensing organic vapour are treated as $H_2SO_4$, but with an alternative molar mass and molecular density. The OIO is considered to possess a molar mass of 158.90 g/mol with a molecular density of 4.98 g/mol, while the organic vapour is considered to have more sulphur-derived properties, having a molar mass and molecular density of 98.08 g $mol^{-1}$ and 1.84 g/$cm^3$, respectively. The transfer of sulfate, OIO, and the condensable organic vapour to the particles is based on Fuchs [15]. Mass transfer from the vapour species to the soluble and insoluble particles are distinguished by different mass accommodation coefficients, 1.0 for soluble and 0.3 for insoluble modes. The change in the mass due to nucleation and condensation of the vapour compounds are integrated over each time step. The vapour species are assumed to condense on all modes, resulting in a net increase of the mean modal radius.

Simulations were carried out to simulate nucleation occurring in typical marine conditions, using two of the parameterized nucleation schemes presented in Vuollekoski et al. [10] iodine-driven kinetic nucleation ($K_1 \times [\mathrm{OIO}] \times [\mathrm{OIO}]$) and particle formation deriving from sulfuric acid—iodine-driven activation nucleation ($K_2 \times [\mathrm{H_2SO_4}] \times [\mathrm{OIO}]$) [10]. The values for the kinetic parameters $K_1$ and $K_2$ were estimated by simulation of the observed aerosol formation bursts in the vicinity of Mace Head research station with an aerosol dynamical box model. The recommended values of these parameters are $3 \times 10^{-12}$ ($3.5 \times 10^{-13} - -3.5 \times 10^{-10}$) $cm^3\ s^{-1}$ for $K_1$ and $3 \times 10^{-10}$ $cm^3\ s^{-1}$ for $K_2$.

In the presented simulations, the new particle formation arising from the contribution of the iodine oxides was assumed to occur during daylight hours, when marine halogen emissions were exposed to incoming solar radiation. Due to the lack of information on the quantities or the timescales involved in biogenic precursor gas emissions, it was assumed that emissions would be at a minimum at sunrise and

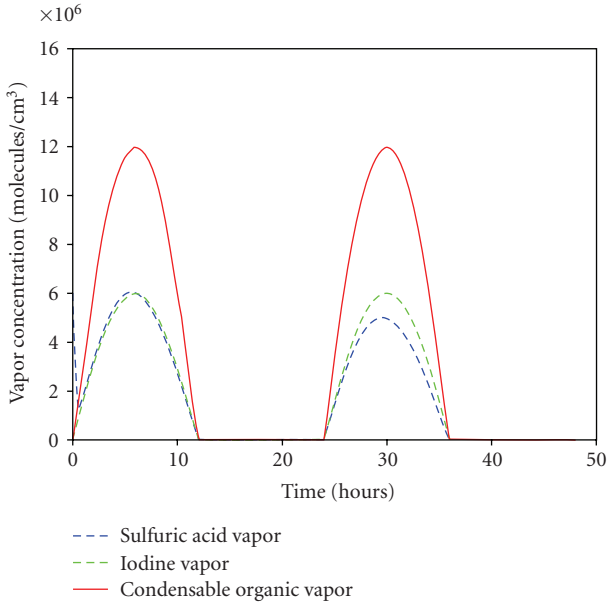


Figure 1: Concentrations of vapour species taken over 48 hours of simulation time.

sunset, reaching a peak around midday when incoming solar radiation is at its maximum. In the simulations where a condensable organic vapor is also present, its concentration, presented in Figure 1, was assumed to follow the same scheme, as this gas is also assumed to come about from biological production.

Throughout all simulations presented in this study, the peak sulphuric acid vapor concentration was $6 \times 10^6$ molecules $cm^{-3}$, [16] with the peak iodine oxide vapor also being $6 \times 10^6$ molecules $cm^{-3}$, while the peak concentration of the additional organic vapor, when present, was $1.2 \times 10^7$ molecules $cm^{-3}$. The iodine oxide peak value is taken somewhat as arbitrary, noting that sensitivities were evaluated in Vuollekoski et al. [10]. The organic vapour concentration estimate is taken from [14].

The initial aerosol populations were also setup so as to describe typical clean marine background concentrations. While no particles were assumed to be present in the nucleation mode (0.5 nm–5 nm), the initial loadings of the other size ranges were 200 particles $cm^{-3}$ for the Aitken (5 nm–50 nm) size range, 100 particles $cm^{-3}$ for the accumulation (50 nm–500 nm) size range, and 2 particles $cm^{-3}$ for the coarse (larger than 500 nm) size range. All of the mass in the coarse mode is assumed to be sea salt, corresponding to a wind speed of approximately 7 $m \cdot s^{-1}$. In the smaller size ranges, aerosol composition was assumed to be sulfate. For these parameters, the Aitken mode was initially centered ~16 nm, the accumulation mode ~75 nm, and the coarse mode around ~700 nm.

For comparison, the sectional model used by Vuollekoski et al. [10] was setup to run with the assumptions used in this paper. The model is based on the UHMA model (University of Helsinki Multicomponent Aerosol model, [17]), which is a size-segregated box model incorporating all basic aerosol dynamical processes: nucleation, condensation, coagulation and dry deposition.

## 3. Results

*3.1. General Simulations.* Simulations were conducted over a 48-hour time period. The first simulation was carried out for condensing sulphuric acid and no nucleation as a base case scenario. This base case was completed with final concentrations of 171 particles $cm^{-3}$ for the Aitken mode, 105 particles $cm^{-3}$ for the accumulation, and 2 particles $cm^{-3}$ for the coarse modes, reflecting some coagulation loss in the Aitken mode along with growth of Aitken mode sizes into the accumulation mode over the 48-hour period. The contour plot of the size distribution over the period is shown in Figure 2. The number concentrations at sizes larger than 15, 25, 35 and 50 nm radius were 222, 150, 121, and 110 $cm^{-3}$, respectively (Table 1). The second simulation related to iodine oxide self-nucleation ($K_1 \times [OIO] \times [OIO]$). The size distribution evolution is shown in Figure 2, and the nucleation mode and Aitken mode particle concentrations are shown in Figure 3(a) where it can be seen that the simulation resulted in moderately high-number concentrations in the nucleation mode, reaching a maximum of 7000 $cm^{-3}$ during the first day, and 5000 $cm^{-3}$ on the second day. For the Aitken mode, peak concentrations of 260 $cm^{-3}$ are seen on the first day, rising to 430 $cm^{-3}$ on the second day. Number concentrations larger than 15, 25, 35, and 50 nm radius were 366, 196, 134, and 110 $cm^{-3}$, respectively (Table 1).

Model runs using the sulfuric acid-iodine-driven nucleation ($K_2 \times [H_2SO_4] \times [OIO]$) exhibited higher number concentrations compared to the OIO-OIO simulations. The evolving size distribution is shown in Figure 2, and the nucleation mode and Aitken mode concentrations are shown in Figure 3(b). The nucleation mode peaks at about 46,000 $cm^{-3}$ on the first day, and on the second day the peak is just below 42,000 $cm^{-3}$. The Aitken mode after the mid day peak in the production of OIO, with peak concentrations reaching 900 $cm^{-3}$ on the first day, increased to 1568 $cm^{-3}$ on the second day. By the end of the simulation, the number concentrations at sizes larger than 15, 25, 35, and 50 nm radius were 722, 243, 136 and 110 $cm^{-3}$, respectively (Table 1).

The final simulation was for $H_2SO_4$-OIO plus a condensing organic vapour. Again, the evolving size distribution is illustrated in Figure 2 and the nucleation mode and Aitken mode concentrations are shown in Figure 3(c). For this simulation, similar peak nucleation concentrations were seen to the $H_2SO_4$-OIO case on day one and slightly less on day two. The Aitken mode, in contrast, shows significantly higher peak concentrations with >2500 $cm^{-3}$ achieved on day one and 3026 $cm^{-3}$ on day 2. By the end of the simulation, the number concentration at sizes larger than 15, 25, 35, and 50 nm radius were 1585, 556, 230, and 126 $cm^{-3}$, respectively.

The change in the Aitken mode radius for the three simulations involving nucleation is shown in Figure 4. At the start of the simulation, the mode radius is 15.8 nm and increases to approximately 18 nm in all three cases.

Table 1: Comparison of absolute particle number concentrations increases for particles of radii more than 50, 35, 25, and 15 nm, using the different nucleation schemes, taken over 48 hours at vapor concentrations of $6 \times 10^6$ molec·cm$^{-3}$ for the sulphuric acid and iodine along with $12 \times 10^6$ molec·cm$^{-3}$ for the nonnucleating organic vapor.

| Radius (nm) | Number concentration (cm$^{-3}$) $H_2SO_4$ only (no nucleation) | Number concentration (cm$^{-3}$) OIO-OIO | Number concentration (cm$^{-3}$) $H_2SO_4$-OIO | Number concentration (cm$^{-3}$) $H_2SO_4$-OIO-COV |
|---|---|---|---|---|
| >15 | 221.5 | 366.1 | 722.3 | 1584.5 |
| >25 | 150.4 | 196.0 | 243.1 | 556.3 |
| >35 | 121.0 | 133.5 | 135.9 | 229.6 |
| >50 | 109.5 | 111.2 | 110.0 | 125.6 |
| Radius (nm) | Percentage increase $H_2SO_4$ only (No nucleation) | Percentage increase OIO-OIO | Percentage increase $H_2SO_4$-OIO | Percentage increase $H_2SO_4$-OIO-COV |
| >15 | — | 65% | 226% | 615% |
| >25 | — | 30% | 62% | 270% |
| >35 | — | 10% | 12% | 90% |
| >50 | — | 2% | 0.5% | 15% |

The OIO-OIO simulation takes the longest time to reach 18 nm while, as expected, the most rapid initial growth is seen for the case with the condensing organic vapour. After the mode reaches 18 nm, there is a sudden drop to approximately 12 nm in all cases, albeit at different rates. The drop results from the nucleation mode growing into the Aitken mode and reducing the mean or modal radius. Thereafter, the Aitken mode grows continuously to the end of the simulations with peak growth rates observed for all simulations during the rise in concentration of vapours associated with the second day's photochemical cycle.

For the accumulation mode, there is a marginal decrease in mode radius; however, as stated above, there is still a significant increase (15%) in particle concentration at sizes >50 nm and 90% at sizes larger than 35 nm. For the base case without nucleation but with $H_2SO_4$-driven growth, maximum growth rates, in daylight hours, of 0.11 nm hour$^{-3}$ is achieved. By comparison, with OIO nucleation and growth, combined with $H_2SO_4$ growth, growth rates achieved are 0.17 nm hour$^{-1}$. For the $H_2SO_4$ activation of OIO, subsequent growth reaches 0.3 nm hour$^{-1}$, while the final case with additional condensable vapors, the maximum growth rate achieved, is 0.48 nm hour$^{-1}$. Night time growth rates range from 0.002 nm hour$^{-1}$ for the base case to 0.072 nm hour$^{-1}$ for the organic vapor case.

The nucleation scheme involving sulfuric acid and iodine in the presence of organic condensable vapor is, not surprisingly, the most effective particle formation scheme, yielding particle concentrations of more than 3000 cm$^{-3}$ in the Aitken mode. This scheme also produces the higher growth rates for both particles in the nucleation and Aitken modes. This increased particle number concentration and growth rates are due to the growth rate enhancement triggered by the additional organic vapor, allowing nucleation mode particles to grow more rapidly to larger and more stable size ranges. This also leads to an initial low Aitken mean modal radius as new particles grow from the nucleation mode.

The OIO-OIO scheme exhibits the smallest peak particle number concentration compared to either of the other schemes, primarily due to the most rapid depletion of OIO, leaving much less vapour to condense on newly nucleated clusters and to grow them to stable sizes. This is also evident in a detailed examination of the mean particle radius for various size ranges within the Aitken mode.

## 4. Comparison of Modal and Sectional Models

A particular case study of an extended growth event is presented by way of comparison between modelled events and those measured. The presented event illustrates growth over a time exceeding 24 hours from JD236 to JD238. Particles with a modal peak at ~15 nm are deleted at the beginning of JD236 and continue to grow throughout the following 48 hours to almost 25 nm in radius. This well-defined episode, characterised by very high concentrations of nucleation mode particles in the 1.5–3 nm range, is in the absence of either anthropogenic modification or coastal nucleation events. Analysing this extended growth period, suitable numbers can be acquired to reproduce this event from a modelling approach.

Recent open ocean nucleation studies have pointed to a lifetime of approximately 15 hours before detection [14]. A nucleation event was therefore simulated using the $H_2SO_4$-OIO-COV scheme beginning 15 hours before detection time in order to test the validity of the model. Modal radii and concentration were then compared. Peak vapour concentrations of $6 \times 10^6$, $6 \times 10^6$, and $1.8 \times 10^7$ molec·cm$^{-3}$ were used for the concentration of $H_2SO_4$, OIO, and the COV respectively. A vapour concentration of $1.8 \times 10^7$ molec·cm$^{-3}$ was used in this case study as this was found to better simulate the growth of the open ocean plume case study than the $1.2 \times 10^7$ molec·cm$^{-3}$ value used in initial simulations. This differs from the value calculated by O'Dowd et al. [14]

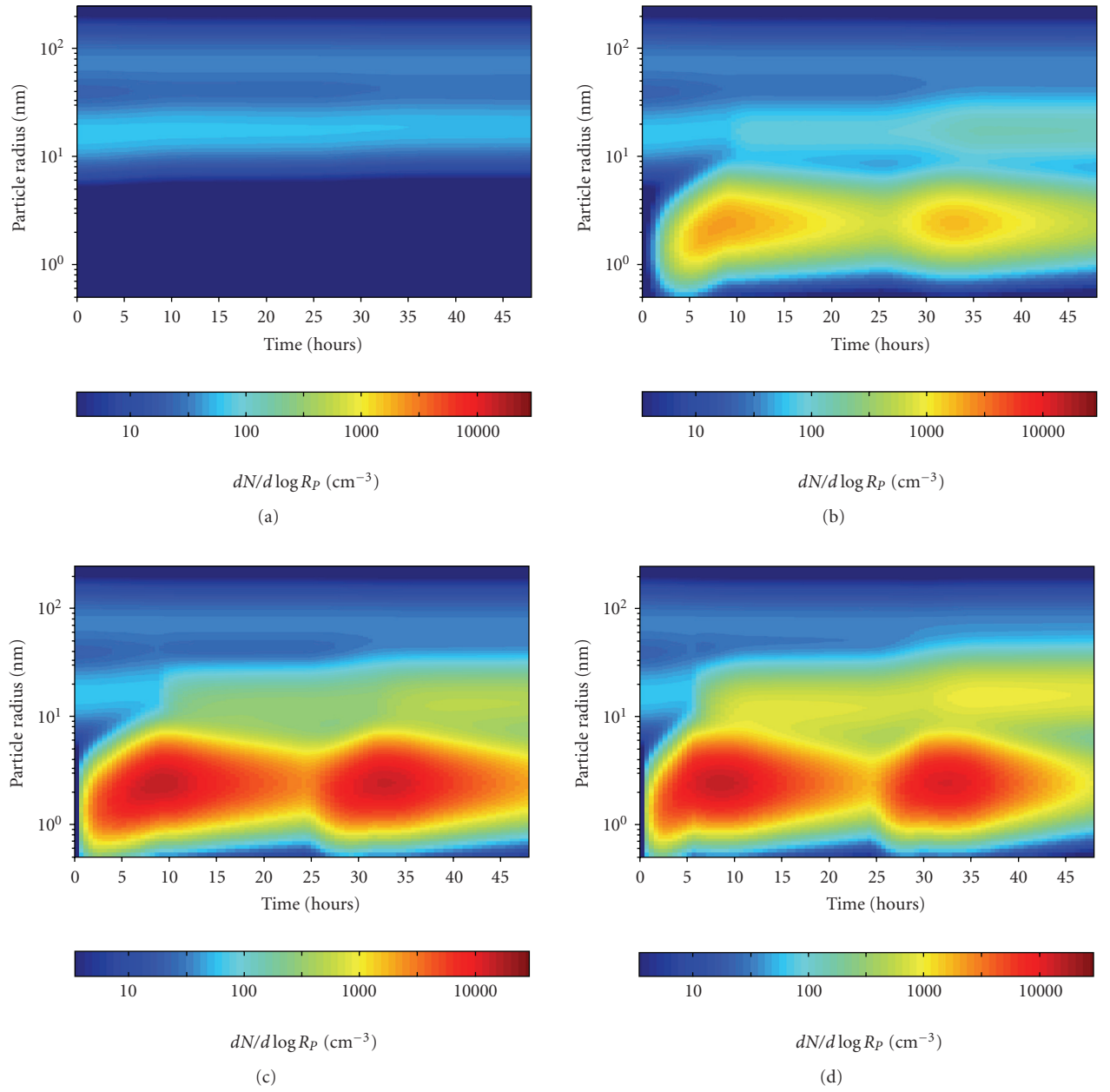


FIGURE 2: (a) Base case of $H_2SO_4$ growth without nucleation (b) kinetic self (OIO) nucleation and growth (c) $H_2SO_4$-OIO nucleation and (d) $H_2SO_4$-OIO nucleation plus condensation of organic vapours.

($1.2 \times 10^7$ molecules cm$^{-3}$) marginally and can be attributed to differences in the measured and modelled size distribution condensation sinks. Vapour concentrations were assumed to have a daily sinusoidal concentration as in previous simulations.

The developing size distributions are shown in Figure 5, and some key differences in the modal and sectional approaches are evident. The modal model will transfer particles from one mode to the adjacent mode if the lognormal size distribution has grown a sufficient amount so as to intersect the adjacent mode. This process is evident in Figure 5(b) in which we see an increases in the Aitken mode concentration during a growth period, but a decrease in the mean mode radius of the nucleation mode as the larger particles are transferred to the Aitken mode. The sectional model in contrast has a steady growth of the nucleation mode into the Aitken size range.

The Aitken mode concentration and mode radius are compared in Figure 6. The modal model's Aitken mode concentration is lower in comparison with the sectional model; however there is a higher degree of correlation between the modal model and that measured. The sectional

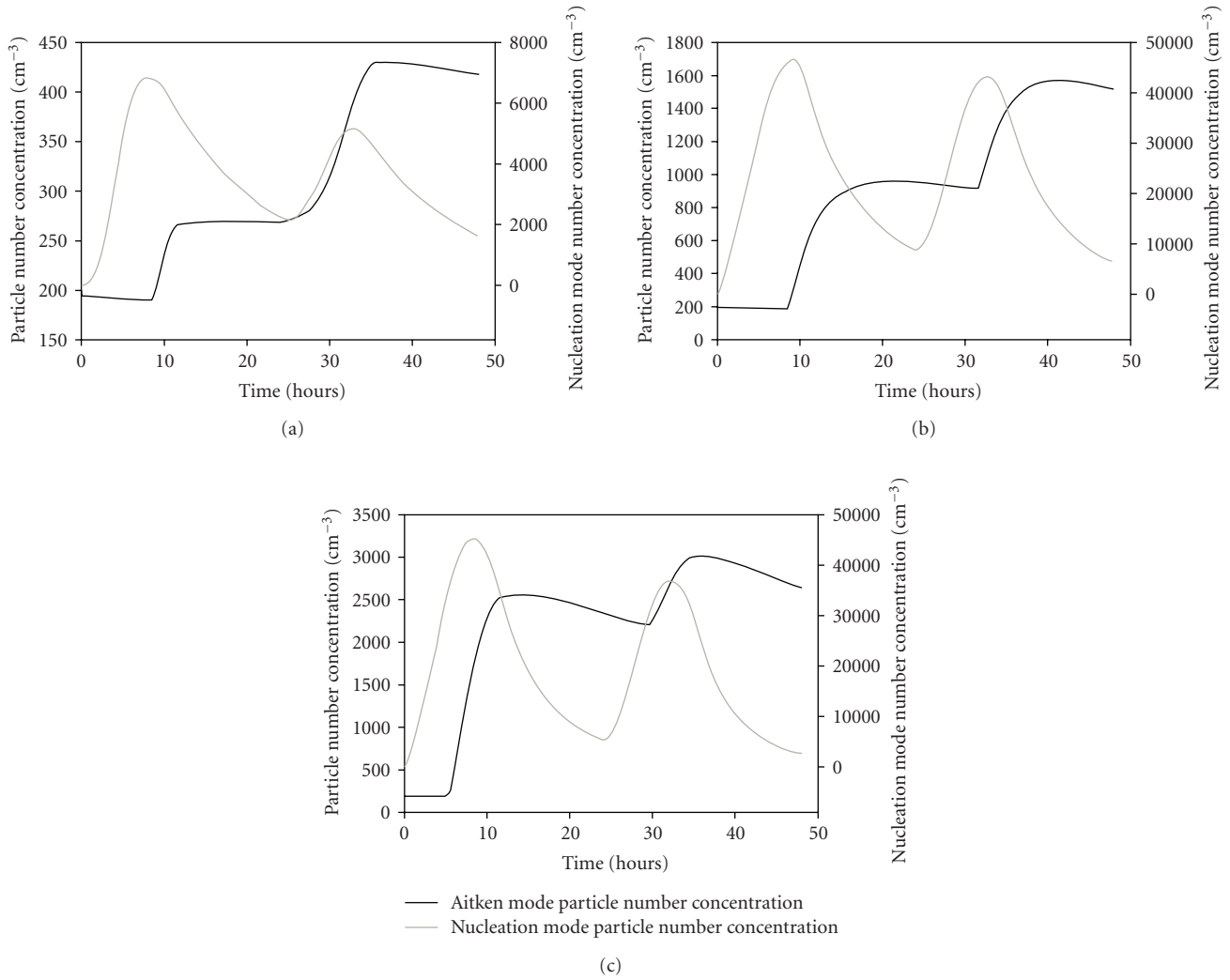


Figure 3: (a) Particle concentrations from the iodine oxide self-nucleation scheme nucleation scheme taken over 48 hours at maximum OIO vapor concentrations of $6 \times 10^6$ molecules cm$^{-3}$. (b) Particle concentrations from the sulfuric acid-iodine-driven nucleation schemes taken over 48 hours at maximum vapor concentrations of $6 \times 10^6$ molecules cm$^{-3}$ for both vapors. (c) Particle concentrations of sulfuric acid-iodine-based nucleation scheme in the presence of organic condensable vapor nucleation schemes taken over 48 hours at maximum vapor concentrations of $6 \times 10^6$ molecules cm$^{-3}$ for the sulphuric acid and iodine, along with a maximum of $12 \times 10^6$ molecules cm$^{-3}$ for the nonnucleating organic vapor.

model has a higher Aitken mode concentration due to a more constant growth of nucleation mode particles. Examining Figure 6(b) it can be seen that there was reasonably good correlation between the mode radii of the modal and sectional models. Both models however exhibit a larger mode radius than that of measured events, with radii at the end of the simulation of 16 nm, 23 nm, and 27 nm for the measured, modal and sectional plumes, respectively. There is a somewhat higher modal radius in the sectional model results over the measurement period; however this is mainly due to the merging of the nucleation and Aitken mode when the nucleation mode particle population has grown to comparable sizes. The modal model results show lower numbers during the measurement period mainly due to the aforementioned differences in the modal and sectional techniques, leading to lower numbers of instances of modal merging.

## 5. Discussion

These findings are in qualitative agreement with those of Vuollekoski et al. [10] who also found, using a sectional aerosol model and some different assumptions relating to the environmental conditions that iodine oxide nucleation did lead to significant nucleation, but very few of the newly formed particles grow to large sizes without the presence of a low-volatility organic vapor. Vuollekoski et al. [10] suggested that condensable vapours with concentrations of the order of $10^6$ molecules cm$^{-3}$ were sufficient for noteable particle production. The current results suggest that concentrations as low as $\sim 10^7$ molecules cm$^{-3}$ can still have a modest but notable (10%) increase in particle concentrations larger that 50 nm radius and 90% for sizes larger than 35%. Vuollekoski et al. [10] also suggested that iodine oxides were likely to lead to cloud condensation nuclei sizes if air had advected

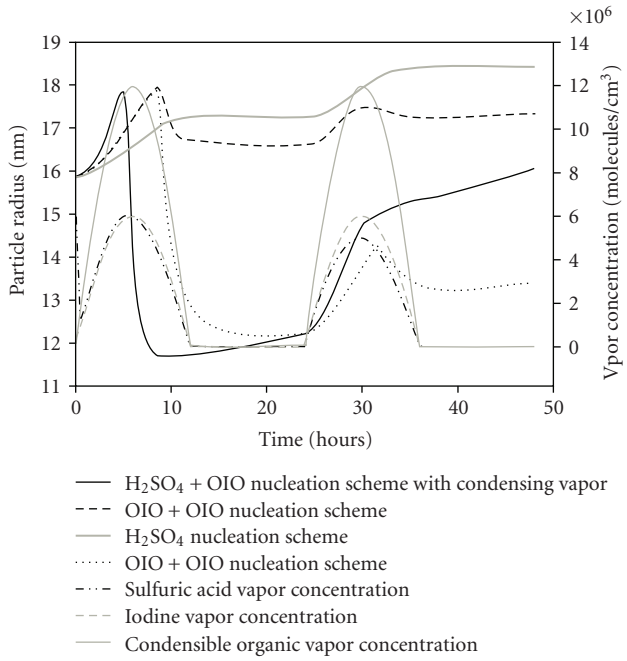


Figure 4: Comparison between aitken mode particle radii of the different nucleation schemes (on the left)

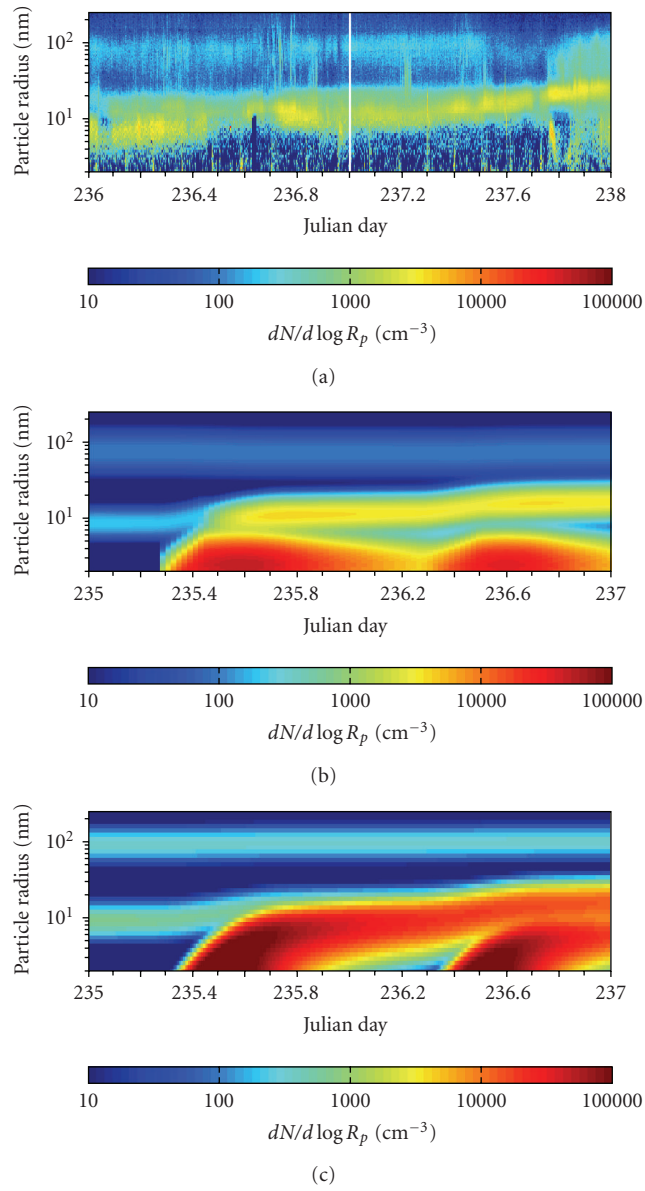


Figure 5: (a) Recorded open ocean nucleation event, (b) a modeled nucleation event beginning 15 hours before plume detection using modal model, and (c) a modeled nucleation event beginning 15 hours before plume detection using sectional model.

over large plankton blooms extending over hundreds of kilometres where sustained iodine oxide production could prevail. While the OIO concentrations in this study have been arbitrarily chosen, they represent the concentration fields required to have a noninsignificant impact on the marine aerosol population, particularly at sizes larger that 35 nm and 50 nm radius where they can contribute to the marine cloud condensation nuclei population.

Recent work has revealed that open-ocean new particle formation and growth events are not uncommon over biologically-rich oceans such as the North East Atlantic [13, 14]. O'Dowd et al. [14] document some typical example of continuous growth over periods of up to 48 hours and calculated growth rates of the order of 0.8 nm hour$^{-1}$ whereas Ehn et al. [13] reported an average growth rate over four events of 3 nm hour$^{-1}$. The O'Dowd et al. [14] events show, more or less, constant growth throughout the 48-hour period, even at night time, while the study here shows high growth rates during daylight hours as condensable vapours are produced. Perhaps the reason constant growth relates to the increased ability for some organic molecules to condense to larger particles leading to a scenario whereby the lower volatility organics are condensing to the smallest particles during daytime while a reservoir of more volatile particles are accumulating to become available at night time and when the growing particles get larger and the Kelvin effect lesser.

## 6. Conclusions

Three nucleation schemes involving iodine oxides were implemented in the modal aerosol model M7 to explore the feasibility of iodine oxides contributing to marine new particle formation and growth. The two nucleating species considered were OIO and $H_2SO_4$, each with a midday peak concentration of $6 \times 10^6$ molecules cm$^{-3}$, decreasing to zero at sunrise and sunset. A kinetic OIO self-nucleation scheme was found to increase the background aerosol population ($N = 300\,\text{cm}^{-3}$) by 65% for $r > 15$ nm, decreasing to 2% for $r > 50$ nm. Activation of OIO by $H_2SO_4$ vapours increased the aerosol population by 226% for $r > 15$ nm, decreasing to 0.5% for $r > 50$ nm. When the latter case was considered with an additional condensable low volatility vapour with a concentration of $1.2 \times 10^7$ molecules cm$^{-3}$, the largest increase in aerosol concentration was observed where the aerosol concentration increased by 615% for sizes

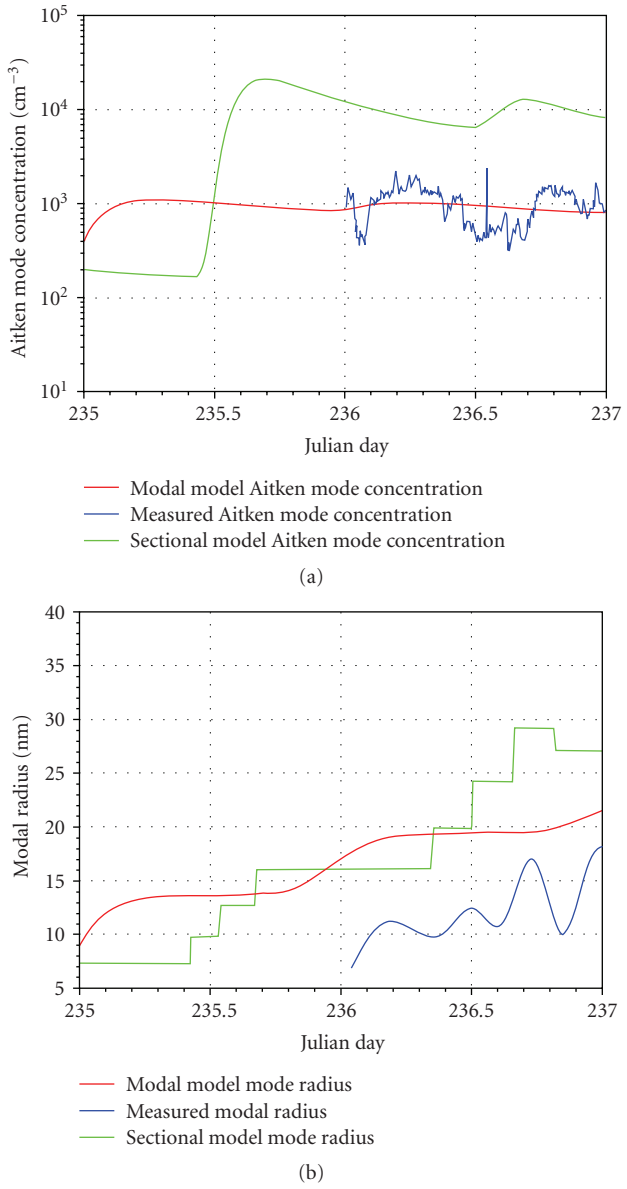


Figure 6: (a) Comparison of mode concentration and (b) mode radius between modeled and measured plumes.

$r > 15$ nm and by 15% for $r > 50$ nm. For the clean marine cases considered, where the total aerosol concentration was 300 cm$^{-3}$, after a nucleation burst *via* activation of OIO by $H_2SO_4$ vapours, and subsequent growth by a low volatility organic vapour, peak Aitken mode particle concentrations exceeded 3000 cm$^{-3}$, while the concentration at the end of two days of simulations at sizes $r > 15$, $r > 25$, $r > 35$, and $r > 50$ nm were 1585 cm$^{-3}$, 556 cm$^{-3}$, 230 cm$^{-3}$, and 126 cm$^{-3}$, respectively, suggesting that the combination of iodine oxide activation by sulphuric acid and subsequent growth by an organic vapour can significantly impact on the marine aerosol population number concentration. Changes of these magnitudes can have notable impact on marine stratiform cloud properties given the susceptibility of such clouds. A comparison case study analysis using the modal model and a sectional model displays reasonably good results. Despite the mode-jumping associated with modal models, the growth of the Aitken mode was predicted quite well and suggests that a modal model is suitable for large scale modelling applications.

## Acknowledgments

This work was supported by the European Commission under the EUCAARI Integrated Project and the MAP Specifically Targeted Research Project. In addition, the work was supported by Ireland's Higher Education Authority under the PRTLI4 programme: *Environment and Climate: Impact and Responses*.

## References

[1] IPCC, "Summary for policymakers," in *Climate Change 2007: The Physical Science Basis. Contribution of Working Group I to the Fourth Assessment Report of the Intergovernmental Panel on Climate Change*, S. Solomon, D. Qin, M. Manning et al., Eds., Cambridge University Press, Cambridge, UK, 2007.

[2] R. J. Charlson, J. E. Lovelock, M. O. Andreae, and S. G. Warren, "Oceanic phytoplankton, atmospheric sulphur, cloud albedo and climate," *Nature*, vol. 326, no. 6114, pp. 655–661, 1987.

[3] L. Pirjola, C. D. O'Dowd, I. M. Brooks, and M. Kulmala, "Can new particle formation occur in the clean marine boundary layer?" *Journal of Geophysical Research D*, vol. 105, no. 21, pp. 26531–26546, 2000.

[4] C. D. O'Dowd, J. L. Jimenez, R. Bahreini et al., "Marine aerosol formation from biogenic iodine emissions," *Nature*, vol. 417, no. 6889, pp. 632–636, 2002.

[5] C. D. O'Dowd, M. Geever, M. K. Hill, M. H. Smith, and S. G. Jennings, "New particle formation: nucleation rates and spatial scales in the clean marine coastal environment," *Geophysical Research Letters*, vol. 25, no. 10, pp. 1661–1664, 1998.

[6] C. O'Dowd, G. McFiggans, D. J. Creasey et al., "On the photochemical production of new particles in the coastal boundary layer," *Geophysical Research Letters*, vol. 26, no. 12, pp. 1707–1710, 1999.

[7] C. D. O.'Dowd and T. Hoffmann, "Coastal new particle formation: a review of the current state-of-the-art," *Environmental Chemistry*, vol. 2, no. 4, pp. 245–255, 2005.

[8] S. Pechtl, E. R. Lovejoy, J. B. Burkholder, and R. von Glasow, "Modeling the possible role of iodine oxides in atmospheric new particle formation," *Atmospheric Chemistry and Physics*, vol. 6, no. 2, pp. 505–523, 2006.

[9] A. Saiz-Lopez, J. M. C. Plane, G. McFiggans et al., "Modelling molecular iodine emissions in a coastal marine environment: the link to new particle formation," *Atmospheric Chemistry and Physics*, vol. 6, no. 4, pp. 883–895, 2006.

[10] H. Vuollekoski, V.-M. Kerminen, T. Anttila et al., "Iodine dioxide nucleation simulations in coastal and remote marine environments," *Journal of Geophysical Research D*, vol. 114, no. 2, Article ID D02206, 2009.

[11] E. Vignati, J. Wilson, and P. Stier, "M7: an efficient size-resolved aerosol microphysics module for large-scale aerosol transport models," *Journal of Geophysical Research D*, vol. 109, no. 22, pp. 1–17, 2004.

[12] M. Dall'Osto, D. Ceburnis, G. Martucci et al., "Aerosol properties associated with air masses arriving into the North

East Atlantic during the 2008 Mace Head EUCAARI intensive observing period: an overview," *Atmospheric Chemistry and Physics*, vol. 10, no. 17, pp. 8413–8435, 2010.

[13] M. Ehn, H. Vuollekoski, and T. Petäjä, "Growth rates during coastal and marine new particle formation in Western Ireland," *Journal of Geophysical Research*, vol. 115, Article ID D18218, 11 pages, 2010.

[14] C. O'Dowd, C. Monahan, and M. Dall'Osto, "On the occurrence of open ocean particle production events," *Geophysical Research Letters*, vol. 37, Article ID L19805, 2010.

[15] N. A. Fuchs, *Evaporation and Droplet Growth in Gaseous Media*, Pergamon, New York, NY, USA, 1959.

[16] H. Berresheim, T. Elste, H. G. Tremmel et al., "Gas-aerosol relationships of $H_2SO_4$, MSA, and OH: observations in the coastal marine boundary layer at Mace Head, Ireland," *Journal of Geophysical Research D*, vol. 107, no. 19, article no. 8100, 2002.

[17] H. Korhonen, K. E. J. Lehtinen, and M. Kulmala, "Multicomponent aerosol dynamics model UHMA: model development and validation," *Atmospheric Chemistry and Physics*, vol. 4, pp. 757–771, 2004.